Polymer Engineering and Science
Vol. 26 • No. 1 MID-JANUARY 1986

POLYBLENDS–'85

National Research Council of Canada
Industrial Materials Research Institute

Contents

1
PUBLISHER'S MESSAGE

2
Preamble/L.A. UTRACKI, Guest Editor

3
C.C. HAN, M. OKADA, Y. MUROGA, F.L. MCCRACKIN, B.J. BAUER, and Q. TRAN-CONG/Static and Kinetic Studies of Polystyrene/Poly(Vinyl Methylether) Blends

9
E. BENEDETTI, A. D'ALESSIO, M. AGLIETTO, G. RUGGERI, P. VERGAMINI, and F. CIARDELLI/Vibrational Analysis of Functionalized Polyolefins/PVC Blends

15
L.S. EGAN and M.A. WINNIK/Fluorescence Studies of Polymer Blends: Anchoring the Stabilizer Chain in Non-Aqueous Dispersions

28
D. ACIERNO, D. CURTO, F.P. LA MANTIA, and A. VALENZA/Flow Properties of Low Density/Linear Low Density Polyethylenes

34
L.A. UTRACKI, M.M. DUMOULIN, and P. TOMA/Melt Rheology of High Density Polyethylene/Polyamide-6 Blends

45
S. ENDO, K. MIN, J.L. WHITE, and T. KYU/Polyethylene-Polycarbonate Blends: Interface Modification, Phase Morphology and Measurement of Orientation Development During Cast Film and Tubular Extrusion By Infrared Dichroism

54
C.B. BUCKNALL and I.K. PARTRIDGE/Phase Separation in Crosslinked Resins Containing Polymeric Modifiers

continued on back cover

Published by Society of Plastics Engineers

Polymer Engineering and Science

Published by Society of Plastics Engineers

EDITOR—ROGER S. PORTER
Polymer Science and Engineering
University of Massachusetts
Amherst, Mass. 01003

GUEST EDITOR—L. A. UTRACKI
Industrial Materials Research Institute
National Research Council of Canada
75, Boul de Mortagne
Boucherville, Quebec
Canada J4B 6YA

ASSOCIATE EDITOR—RICHARD E. BALL
Western New England College
Springfield, Mass. 01119

ADVISORY BOARD

K. ABBAS
AB Bofors Plast

E. BAER
Case Institute of Technology

J. A. BIESENBERGER
Stevens Institute of Technology

D. M. BIGG
Battelle Columbus Laboratories

L. L. BLYLER, JR.
Bell Laboratories

L. J. BROUTMAN
Illinois Institute of Technology

E. S. CLARK
University of Tennessee

R. K. EBY
Johns Hopkins University

A. N. GENT
University of Akron

H. B. HOPFENBERG
North Carolina State University

J. F. JOHNSON
University of Connecticut

M. R. KAMAL
McGill University

R. P. KAMBOUR
General Electric Company

J. R. KNOX
Amoco Chemicals Corporation

S. MATSUOKA
Bell Telephone Laboratories

B. MAXWELL
Princeton University

C. L. MCCORMICK
University of Southern Mississippi

D. R. PAUL
University of Texas

D. H. RENEKER
National Bureau of Standards

C. E. ROGERS
Case Western Reserve University

R. SALOVEY
University of Southern California

N. S. SCHNEIDER
Army Materials and Mechanics Research Center

T. L. SMITH
IBM Research Center

M. TAKAYANAGI
Kyushu University

PUBLICATIONS COMMITTEE

D. W. RILEY, Chairman
Extrusion Engineers

R. P. BRADDICKS, JR.
Plastics Consultant

R. D. FORGER
Society of Plastics Engineers

L. H. DREXLER
AT&T Consumer Products

J. L. HULL
Hull Corporation

W. C. KUHLKE
Shell Chemical Co.

V. E. MALPASS
Ferro Corp.

M. A. MENDELSOHN
Westinghouse Electric Corp.

R. S. PORTER
University of Massachusetts

A. A. SCHOENGOOD
Society of Plastics Engineers

G. R. THOM
Regal Plastics Company

A. M. VARNER
Moldflow USA, Inc.

A. E. WHITNEY, JR.
Plastics Consultant

Copyright by Society of Plastics Engineers, 1986.

POSTMASTER: Send address changes to **Polymer Engineering and Science**, 14 Fairfield Dr., Brookfield Center, CT 06805. Telephone (203) 775-0471, TELEX #643-712. Reproduction in whole or in part without written permission is strictly prohibited.

Polymer Engineering and Science (ISSN 0032-3888) is printed at Waverly Press, Easton, MD 21601. Address changes, undeliverable copies, and orders for subscriptions should be sent to Circulation Manager, Society of Plastics Engineers, 14 Fairfield Dr., Brookfield Center, CT 06805. Published semimonthly except for June and December, when published monthly. Second-class postage paid at Brookfield Center, Conn., and additional entry offices. Accepted at special postal rate provided in P.M. Sec. 132.122.

Neither the Society of Plastics Engineers nor **Polymer Engineering and Science** is responsible for the views expressed by individual contributors, either in articles published in **Polymer Engineering and Science** or in technical papers presented at meetings of the Society.

Subscription rates for 1986. SPE members, 1 year—$95, 2 years—$175, 3 years—$225. Nonmembers (U.S. and North America), 1 year—$130, 2 years—$225, 3 years—$310. Corporate, Institutional, or Library, 1 year—$340. Postage charge for all subscriptions outside North America—$22 per year. Air delivery outside North America—$65 per year.

SOCIETY OF PLASTICS ENGINEERS
Business and Executive Offices, 14 Fairfield Dr., Brookfield Center, Conn. 06805

JANICE M. STRELEZ
Managing Editor

JEANNE M. CROTTY
Production Manager

JEANETTE M. PIASTUCH
Copy Editor

MICHAEL R. CAPPELLETTI
Circulation Manager

OFFICERS OF THE SOCIETY

RICHARD G. JOHNSON
President

GREG R. THOM
President-elect

JOHN R. KRETZCHMAR
First Vice President

BRUCE A. PETERSEN
Second Vice President

JACQUES DE CRAENE
Vice President for International Affairs

VIVIAN E. MALPASS
Secretary

LEONARD H. DREXLER
Treasurer

ROBERT D. FORGER
Executive Director and Publisher

POLYMER ENGINEERING AND SCIENCE is indexed by:—Chemical Abstracts—Engineering Index, Inc.

PUBLISHER'S MESSAGE

When you picked up this issue, you undoubtedly noticed a striking change at first glance. The former, staid cover has given way to one with a more modern, free-flowing design augmented by a more readable type. And in the coming months, we will make the type change inside the journals as well. We trust that the changes will make it more comfortable for readers to review and examine the contents of each issue.

In addition, publishing frequency in 1986 will be increased from 18 to 22 issues. Issues will appear semimonthly in all but June and December. As part of our new publication policy, the subsection POLYMER TOPICS will be published in the mid-issues for January, March, May, July, September, and November. The regular issues, which include papers covering a more-general range of subjects, will publish monthly, appearing, as in the past, near the end of each month.

The greatest change, however, will be in the introduction of the POLYMER PROCESSING AND RHEOLOGY subsection, which will appear quarterly in the mid-month of February, April, August, and October. Each will include offerings on processing—the acknowledged cutting edge of technology. In his mid-February editorial, Editor Roger S. Porter will tell you more definitively of his plans to cover this important area and his criteria for selecting papers for publication.

Because of its relevance to so many engineers and scientists, this new subsection will also be available through a separate subscription. Thus, in addition to being included within the 1986 volume of POLYMER ENGINEERING AND SCIENCE, the subsection can be purchased as though it were a separate journal of four issues.

We believe these changes, both physical and substantial, are positive and progressive, reflecting the constantly changing needs of the polymer field. We hope you agree.

Robert D. Forger
Publisher

PREAMBLE

The term "polymer" refers to plastics, rubbers, fibers, adhesives, binders, etc. Consequently, discussion on polymer alloys and blends should consider not only plastics blends but also those of other materials. Blending of rubbers is nearly as old as the rubber technology itself. Blending is a prevalent method of formulating general use adhesives and binders. However, since each of these fields is of comparable complexity and specificity, for reasons of current-day terminology they are seldom included in discussion of polymer alloys and blends. The papers presented in this volume confirm this observation; all but two discuss thermoplastic blends, and those two deal with thermosets.

The advantage of polymer blend technology is flexibility. The resin manufacturer does not have to produce an ever-increasing number of speciality products and the resin user does not have to overpay for performance not required in a specific application. Blending provides the means to accomplish both of these tasks. According to some market analysts, 50 percent of plastics are declared (i.e., materials specified as blends) or undeclared blends. It is estimated that 60 to 80 percent of linear low density polyethylene is being sold as alloys, that at least one-third of engineering resins are used in blends. In 1983, the value of declared blends (i.e., materials specified as blends) was about $2.1 billion or about 10 percent of all plastics. Polymer alloys, blends, and composites play an increasing role in automotive, business-machine, and electrical markets.

Blending frequently leads to improvement of processability, e.g. by reducing die pressure by a factor of 3 or 4. This rheological effect frequently leads to a morphology which may be highly desirable in one, but unacceptable in another application. In general, the most serious problem facing polymer blend technology is control of the morphology and interface properties related to this. Improvements in weatherability, low temperature impact, and dimensional stability are the most important problems to be solved. Over the years we have learned how to improve individual properties, viz. rigidity or toughness. Nowadays the challenge is to generate materials with the whole group of properties being simultaneously modified to match specifications, e.g., such as the blends for vehicle bumpers. This tendency will increase in the future as more and more emphasis is placed on high performance, engineering blends.

"Polyblends-'85" was the 13th symposium on polymers and plastics, the 6th one in the series on polymer alloys and blends organized and sponsored by the Industrial Materials Research Institute of the National Research Council of Canada. The previous five have been published in POLYMER ENGINEERING AND SCIENCE: **22**(2), **22**(17), **24**(2), and **24**(17). The two other symposia series are on modeling of plastics processing and on composites, published respectively in POLYMER ENGINEERING AND SCIENCE and in POLYMER COMPOSITES. The entire symposia are recorded and the tapes of the presentations and discussions are kept in the NRCC/IMRI library for a period of two years, available to anyone interested in the subject.

"Polyblends-'85" was the largest symposium on polymer blends organized by IMRI. With fourteen speakers from five countries and participants from eight, it had a stimulating international character. The 12 papers published in this issue with transcripts of discussions, as well as the text of the Panel and General Discussion on the future of industrial polymer blends, provide a comprehensive image of the meeting.

As organizer and chairman of "Polyblends-'85", I want to express my deep appreciation to the authors, speakers, and participants. It was a great meeting, and it was a pleasure to have you at the Institute.

L. A. Utracki
Guest Editor

Static and Kinetic Studies of Polystyrene/ Poly(vinylmethylether) Blends

C. C. HAN, M. OKADA, Y. MUROGA, F. L. MCCRACKIN, B. J. BAUER, *and* Q. TRAN-CONG

Polymers Division
National Bureau of Standards
Gaithersburg, Maryland 20899

A systematic study of static and kinetic phase behavior of deuterated polystyrene/poly(vinylmethylether) blends is presented in this paper. The static properties are studied by the small angle neutron scattering techniques and the kinetics of phase decomposition are studied by the temperature jump light scattering technique. This procedure provides detailed information about phase behavior with regard to both thermodynamics and kinetics

INTRODUCTION

The study of static and kinetic phase behavior provides not only a fundamental understanding of polymeric systems but also practical materials applications. This has long been recognized in the field of inorganic glasses and metallic alloys (1). In the polymer field, effort has been concentrated on the equilibrium studies of phase behavior (2–7). Although some kinetic studies have been carried out (8–13), so far relationships and subtleties between thermodynamics and kinetics have not been explored consistently. In this paper, we present a systematic study of the equilibrium phase behavior of deuterated polystyrene/poly(vinylmethylether) blends by the small angle neutron scattering (SANS) technique, and the phase separation kinetics by the temperature jump light scattering (TJLS) technique. Static properties, such as the spinodal temperatures and binary interaction parameters, χ, can be obtained from the static study and then used in the prediction of and comparison with kinetic results. The consistency and possibly the discrepancy between theories and experiments can be compared quantitatively in detail. An overall picture of phase decomposition kinetics and mechanisms may be developed.

BACKGROUND

Since the density-density correlation function in q-space is measured in a scattering experiment, it is natural to use the scattering technique to study the critical fluctuation of density or concentration before phase separation and even during phase separation. Although we have used neutron and light scattering in the static and kinetic studies separately, this is only dictated by the q-vector range needed (where $q = (4\Pi/\lambda)\mathrm{Sin}(\theta/2)$, with θ the scattering angle and λ the wavelength) in each experiment. In either case, the static structure factor $S(q)$, is measured except that the $S(q)$ is measured as a function of time after temperature jump into the two phase region in the kinetic studies. Also, because the grid size (q^{-1}, inverse of q-maximum) grows to a much larger length scale after phase separation is started, relative to the correlation length before phase separation, light scattering is chosen to provide the wavelength needed and the intensity (flux) necessary for fast kinetic measurements.

For a binary polymer blend, the concentration fluctuation length near the phase boundary may be described by the Ornstein-Zernike (14) form in the small q region which in turn gives a Lorentzian shape for the static structure factor.

$$S(q)/S(q=0) = \frac{1}{1 + q^2\xi^2} \tag{1}$$

deGennes has obtained $S(q)$ for binary polymer blends in one phase for all q-regions (15). This calculation is based on the random phase approximation together with the mean-field model. The structure factor $S(q)$ can be expressed as

$$\frac{K_N}{S(q)} = \frac{1}{\phi_A z_A v_A S_D(A)} + \frac{1}{\phi_B z_B v_B S_D(B)} - \frac{2\chi}{v_o} \tag{2}$$

with

$$K_N = N_A \left(\frac{a_A}{v_A} - \frac{a_B}{v_B}\right)^2 \tag{3}$$

here N_A is the Avogadro's number; a_i, v_i, ϕ_i, and z_i are respectively the scattering length, molar

volume, volume fraction, and the degree of polymerization of the i^{th} component; $S_D(i)$ is the Debye function of i^{th} polymer; χ is the binary interaction parameter, and v_o is the molar volume of a reference cell.

By expanding the Debye function up to the second moment, *Eq 2* can be expressed as

$$\frac{K_N}{S(q)} = \frac{2}{v_o}(\chi_s - \chi) + \frac{1}{18\phi_A\phi_B}(\overline{b^2}/v_o)q^2 \quad (4a)$$

with

$$\overline{b^2}/v_o = \phi_A\phi_B\left(\frac{b_A^2}{\phi_A v_A} + \frac{b_B^2}{\phi_B v_B}\right) \quad (4b)$$

and

$$\chi_s = \frac{v_o}{2}\left[\frac{1}{v_A z_A \phi_A} + \frac{1}{v_B z_B \phi_B}\right] \quad (4c)$$

where χ_s is the interaction parameter χ at spinodal temperature, T_s. *Equation 4* can be compared with *Eq 1* and gives the correlation length ξ as

$$\xi^2(T, \phi) = \frac{\overline{b^2}}{36}[\phi_A\phi_B(\chi_s - \chi)]^{-1} \quad (5)$$

Since the correlation length ξ normally expands from a few tens of Angstroms to a few hundreds of Angstroms in a convenient temperature range for binary polymer systems, small angle neutron scattering provides just this wavelength (q^{-1}) range with sensitivity when one of the polymers is deuterated. Therefore, the SANS technique is used in this study to provide all static information. We may notice that χ/v_o can be easily obtained from *Eq 2* as q approaches zero. Therefore, the same set of SANS measurements provides both ξ and χ/v_o as a function of T and ϕ in the miscible region.

By extrapolating ξ to its infinite value, one could obtain the spinodal temperature of the system for that volume fraction. Therefore, a complete phase diagram can be constructed in this fashion, as will later be demonstrated in the *Results* section. Once we have the phase diagram and the binary interaction parameter as a function of T and ϕ, we could proceed to study the phase separation kinetics.

We will not elaborate on the derivation of the kinetic theory in this paper, but we will mention the deGennes-Pincus results for polymers (16, 17) which uses the same linearization procedure originally proposed by Cahn-Hilliard (18–20). In this calculation, the concentration fluctuation grows exponentially with time in the initial state of phase separation as

$$\phi(q, t) = \phi(q, t = o)e^{R(q)t} \quad (6)$$

with

$$R(q) = q^2 D_c\left[\frac{\chi - \chi_s}{\chi_s} - \frac{R_o^2}{18}q^2\right] \quad (7)$$

for molecules A and B with the same chain length and diffusion coefficient D_c.

The rate of growth $R(q)$ has a strong q dependence. Actually, it peaks at q_m which can be obtained easily by setting $dR(q)/dq = o$ as

$$q_m^2 = \left(\frac{\chi - \chi_s}{\chi_s}\right)\Big/\left(\frac{R_o^2}{9}\right) \quad (8)$$

Since the field strength of scattered light, $E(q, t)$, is proportional to the local concentration ($E(q, t) \propto \phi(q, t)$), the scattered intensity can be expressed as:

$$I(q, t)/I(q, o) = \frac{\langle E(q, t)E^*(q, t)\rangle}{\langle E(q, 0)E^*(q, o)\rangle} = e^{2R(q)t} \quad (9)$$

therefore, measuring the scattering intensity as a function of time for all q's can provide the growth rate, $R(q)$, the q_m which corresponds to the most preferred grid size of separation, and other information which will be discussed later.

EXPERIMENTS

Anionically polymerized deuterated polystyrene (dPS) with $M_w = 4.35 \times 10^5$ and $M_w/M_n = 1.45$ was used as one component in this experiment. The other component is a cationically polymerized and fractionated poly(vinylmethylether) (PVME), with $M_w = 1.88 \times 10^5$ and $M_w/M_n = 1.32$. This molecular weight ratio was chosen to approximately match the contour length of both components. The same dPS and PVME were used for both static and kinetic study in order to enhance the scattering constrast in SANS experiment and to carry over all thermodynamic parameters to the analysis of kinetic results.

Small angle neutron scattering, (SANS), experiments were performed at the SANS facility at the National Bureau of Standards. The incident beam was monochromated by a velocity selector at wavelength $\lambda = 0.6$nm with a $\Delta\lambda/\lambda$ of 20 percent. A focusing collimation system was used to provide a q-range from 5×10^{-2} nm^{-1} to 1.2nm^{-1}. A two dimensional $x - y$ detector and laboratory computers were used for detection, data acquisition, and reduction. Collimation path length of 4.5m and a sample to detector distance of 3.6m were used throughout this study.

Temperature jump light scattering (TJLS) experiments were also carried out at NBS with a computer controlled light scattering photometer. Temperature jump was carried out with two independently controlled temperature blocks and a mechanically movable sample holder. The film sample of approximately 150μm was mounted on the sample holder and preheated in one temperature block before being mechanically pushed into the second block which is controlled at the desired temperature for phase decomposition measurements. Both temperature blocks are controlled by proportional-inte-

gral-differential controllers. A photomultiplier (PM) tube in the photon-counting mode was used as the detector, together with an identical PM tube and a light beam chopper to operate in the digital lock-in configuration.

A microcomputer is used to control the stepping motor driver which moves the goniometer arm with the PM detector, and also to control the digital lock-in circuit and data storage. Scattered intensity data at various scattering angles and times were then transferred to a super microcomputer for final analysis.

RESULTS AND DISCUSSION

Two kinds of SANS data were obtained for each volume fraction. First, a total detector count, I_{tot} was taken as a function of temperature during heating-cooling cycles (6). A constant heating or cooling rate of 0.5°C/min was used. A typical I_{tot} *vs.* T for two cycles of heating and cooling around the cloud point is displayed in *Fig. 1* for the 40/60 sample. (The notation of 40/60 indicates the weight fraction of dPS/PVME). The cloud point, T_c, is obtained by the linear extrapolation of intensities above and below the cloud point. We realize that this operationally defined cloud point may have some error besides its inherent difference from the binodal point due to polydispersity of the polymer sample (21). The second kind of SANS data was obtained and normalized as $S(q)$ for various temperatures below T_c which was obtained as described above. This structure factor, $S(q)$, at various temperature and volume fraction was then fitted according to *Eq 2* with a non-linear regression routine to obtain χ/v_o and the statistical lengths used in the Debye functions. This is demonstrated in *Fig. 2*. Then $\overline{b^2}/v_o$ and χ_s/v_o can be calculated according to *Eqs 4b* and *4c*. Finally, the correlation lengths were calculated according to *Eq. 5*.

If χ/v_o is linearly proportional to $1/T$, then from *Eq 5*

$$\xi^{-2} \propto \frac{T - T_s}{TT_s} \qquad (10a)$$

or

$$\xi^{-2} \propto |T - T_s| \quad \text{for} \quad |T - T_s| \ll T_s \qquad (10b)$$

In *Fig. 3*, χ/v_o for different ϕ's is plotted against $1/T$ to demonstrate this $1/T$ dependence. This is also used to justify the procedure of extrapolating ξ^{-2} against T as shown in *Fig. 4* to obtain the spinodal temperature, T_s, which is the temperature where $\xi \to \infty$ (or $\xi^{-2} \to o$). Actually, this procedure is redundant from the assumption that the polymer system follows a mean-field behavior where the correlation length obeys a power law dependence of reduced temperature as

$$\xi = \xi_o \left| \frac{T - T_s}{T_s} \right|^{-\nu} : \qquad \text{with } \nu = 1/2 \qquad (11)$$

Therefore, ξ^{-2} should be proportional to $|T - T_s|$. This assumption is checked and demonstrated in *Fig. 5*.

With the cloud points and spinodal points, the phase diagram is constructed and displayed in *Fig. 6*. We use this phase diagram to guide

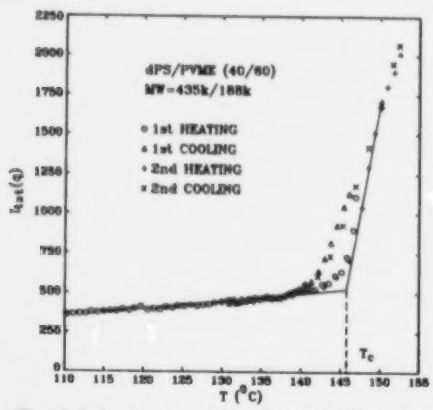

Fig. 1. Total detector count, I_{tot}, in a SANS experiment is shown as a function of temperature or heating and cooling cycles. The two temperature scanning rate is 0.5°C/min. This sample has a weight fraction of dPS/PVME = 40/60. The cloud point, T_c, is obtained as the break point of I_{tot} through linear extrapolation.

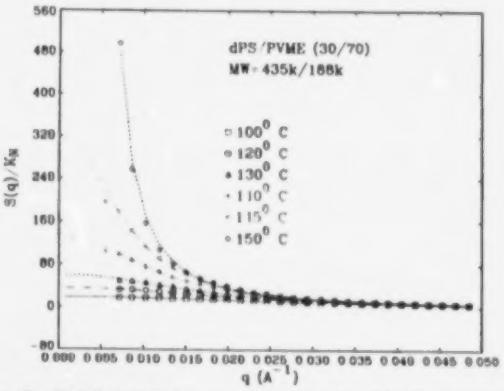

Fig. 2. SANS intensity profiles for the 30/70 sample at various temperatures. Lines are best fit according to Eq 2.

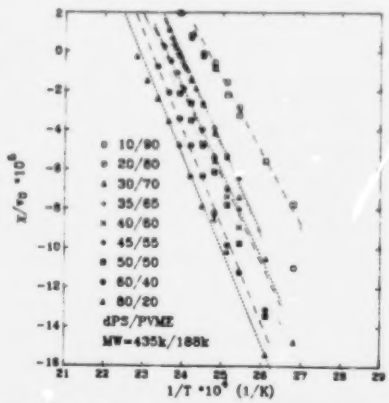

Fig. 3. Reciprocal temperature dependence of χ/v_o for samples of various compositions.

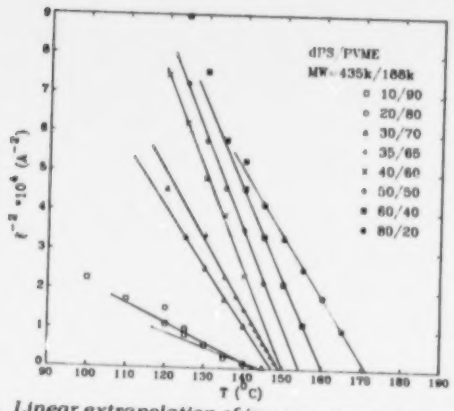

Fig. 4. Linear extrapolation of inverse square correlation length, ξ^{-2} vs. temperature for various compositions. The intercept at T-axis gives the spinodal temperature.

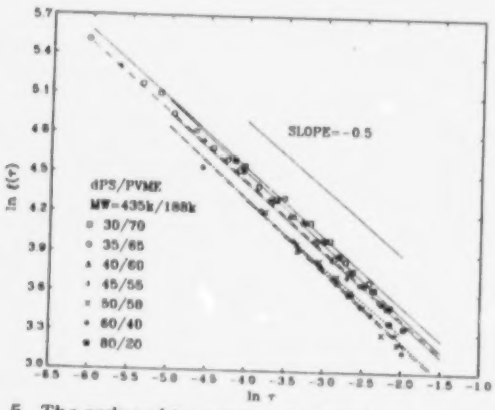

Fig. 5. The reduced temperature dependence of the correlation length, ξ, for various compositions. A solid line with slope of −0.5 is drawn for comparison. $\tau = |T - T_s|/T_s$.

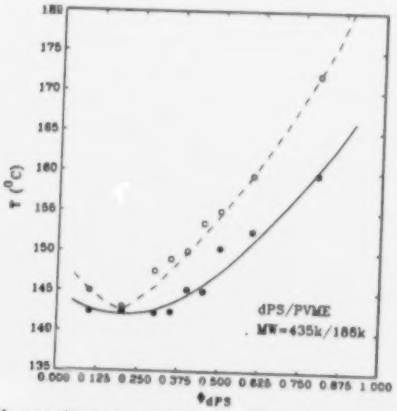

Fig. 6. Phase diagram of dPS/PVME blend with MW = 435 k/188k. Solid circles and open circles are cloud points and spinodal points, respectively.

our kinetic studies which will be discussed as follows. We are concerned mainly with the phase separation kinetics in the spinodal region.

By using the temperature jump light scattering (TJLS) technique, we make a temperature jump of desired depth into the spinodal region, then measure the scattered light intensity as a function of time over a q range of 2×10^{-3} nm^{-1} to 10^{-2} nm^{-1}. Since, in this case, the intensity is not normalized to an absolute scale, we use the notation $I(q)$ instead of $S(q)$ for all the TJLS results. We illustrate this study by showing the results for a 45/55 sample, which was preheated at 134°C and then jumped to a temperature of 156.02°C. The measured $I(q)$ at various times is plotted in *Fig. 7* to demonstrate the growth in the linear region. In this region, a peak is observed as predicted by *Eq 8*, which should not change as a function of time, and that is what we have observed. If we continuously observe this intensity growth, eventually the peak position, q_m, will shift toward a smaller q region as displayed in *Fig. 8*. This signifies the coarsening of the growing droplets which we shall discuss later. First, we need to check that we are indeed measuring the linear region of the spinodal growth predicted by the Cahn-Hilliard model. We will demonstrate this by examining the $I(q, t) = I(q, o)e^{2R(q)t}$ behavior in a semilogarithmic plot of $\ln I(q, t)$ *vs.* t for several q values in *Fig. 9*. $R(q)$ values can be obtained from the initial slope of these plots. In *Fig. 10*, $2R(q)/q^2$ values are plotted against q^2. According to *Eq 7*, these plots should give a straight line with intercept $D_c(\chi - \chi_s)/\chi_s$. It is clear that

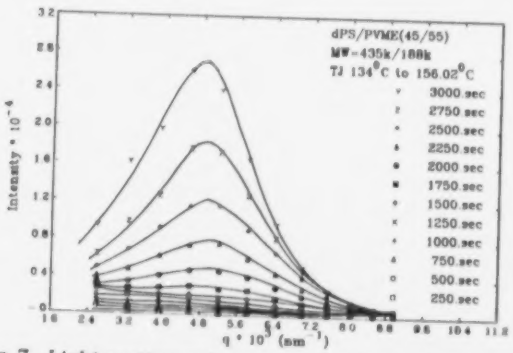

Fig. 7. Light scattering intensity profiles at various times during the early stage spinodal decomposition for 45/55 sample. Jump depth is about 5°C inside the spinodal region at 156.0°C.

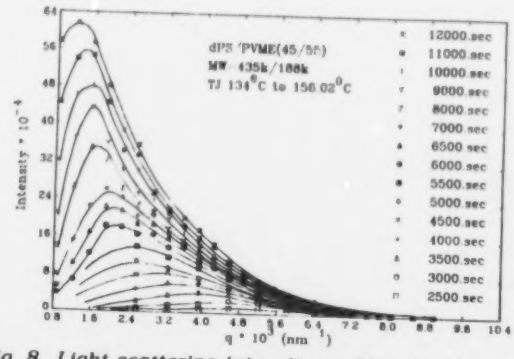

Fig. 8. Light scattering intensity profiles at later times for the same experiment as in Fig. 7.

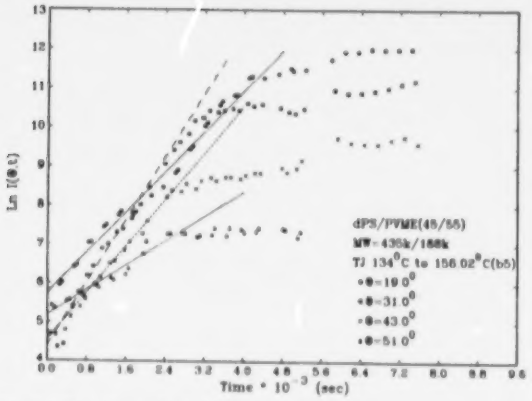

Fig. 9. Semilog plot of light scattering intensity vs. time for four different angles of the same experiment as in Fig. 7. The initial slope gives twice the growth rate, R(q), of the early stage spinodal decomposition.

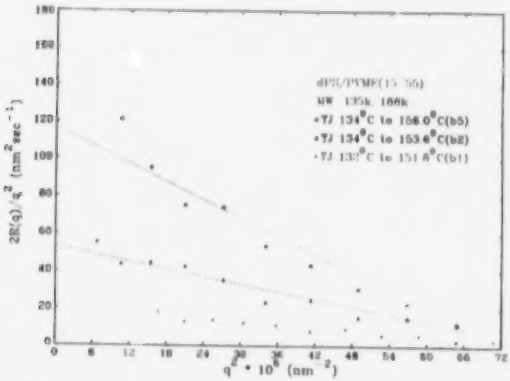

Fig. 10. 2 R(q)/q² is plotted against q² for several jump depths. Where R(q) is the initial growth rate as obtained in Fig. 9.

within experimental error, our results do show straight line behavior which is consistant with the linearized theory. Since $(\chi - \chi_s)/\chi_s$ should approach zero as T approaches T_s, the spinodal temperature can also be determined from kinetic experiments. This is demonstrated in *Fig. 11* for the 45/55 sample. The $D_c(\chi - \chi_s)/\chi_s$ values obtained from different jump depths are extrapolated against T. The spinodal temperature, T_s, obtained is 151.1°C which is within about 1 degree centigrade from that determined from static experiment. The last set of experimental data we present here is the q_m as a function of time. This is displayed in *Fig. 12* where $\ln q_m$ *vs.* $\ln t$ is displayed. As we have mentioned above, q_m should be unchanged in the initial stage of phase decomposition, then a coarsening process may take over. From our results of this 45/55 sample with about 5°C jump depth, the initial constant q_m can be clearly observed. The late stage coarsening seems to follow a t^{-1} power law. This power law exponent has been associated with growth mechanism in the hydrodynamic regime which is a surface tension driven process (22).

In this paper, we have presented a consistent

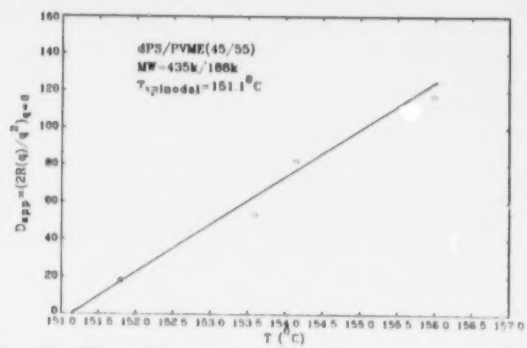

Fig. 11. The intercept of 2 R(q)/q² at q = o is plotted against jumped temperature. The intercept at T-axis is again the spinodal temperature, T_s.

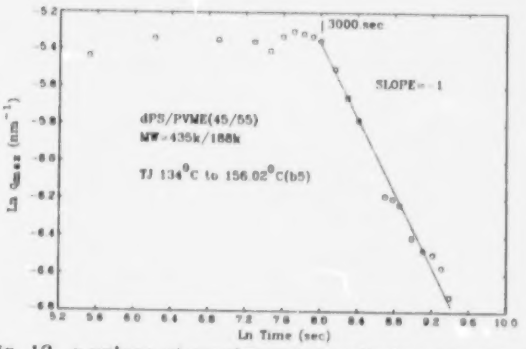

Fig. 12. q values at maximum intensity (q_{max}) is plotted as a function of time in a ln-ln scale. A constant q_{max} in the initial stage and a −1 slope in the later stage are observed.

procedure to study static and kinetic phase behavior of binary polymer blends. So far we have put our emphasis on procedure rather than results. Still, we can draw many conclusions from the data we have presented here. For example: we can obtain both cloud point curve and spinodal curve; the ϕ and T dependence of the binary interaction parameter, χ/v_o; the q-dependence of phase decomposition rate, $R(q)$, in the spinodal region; the preferred grid size (q_m^{-1}) during the phase separation. The exponential growth and the constant q_m in the initial stage can be explained readily by the linearized theory. The spinodal temperatures obtained from kinetic measurements are consistent with those from static measurements. Also, we have been able to observe the late stage growth which is proportional to time (or $q_m \propto t^{-1}$) for an off critical composition and about 5°C deep inside the spinodal region. This seems to be consistent with a surface tension driven coarsening mechanism.

Nevertheless, we have left many questions open and unanswered, such as the ϕ dependence of χ, the absolute magnitude of q_m, the sharp transition of q_m in time from initial stage to late stage coarsening process, the quench temperature dependence of D_c, the question of t^{-1} or $t^{-1/3}$ dependence of q_m in the late stage growth, and many other questions.

We do not pretend we understand the static and the kinetic behavior of phase separation for binary polymer blends at this time; we do think the procedure we have presented offers the potential to provide a clear understanding of this problem in the future. Meanwhile, we think more experimental data are needed, especially the molecular weight dependence of all properties. Theoretical improvement is also necessary.

ACKNOWLEDGMENT

This work was partially supported by the DARPA contract 4993.

REFERENCES

1. J. D. Gunton, M. San Miguel, and F. S. Sahni, in "Phase Transition and Critical Phenomena", Chap. 3, Vol. 8, C. Domb and J. L. Lebowitz, Ed., Academic Press, New York (1983).
2. (A) D. R. Paul and S. Newman, Eds., "Polymer Blends", Vol I and II, Academic Press, New York (1978). (B) O. Olabishi, L. M. Robeson, and M. T. Shaw, "Polymer-Polymer Miscibility", Academic Press, New York (1979).
3. T. Nishi, T. T. Wang, and T. K. Kwei, *Macromolecules*, **8**, 227 (1975).
4. T. Nishi and T. K. Kwei, *Polymer*, **16**, 285 (1975).
5. G. Hadziiannou and R. S. Stein, *Macromolecules*, **17**, 567 (1984).
6. H. Yang, M. Shibayama, R. S. Stein, and C. C. Han, *Polym. Bull.*, **12**, 7 (1984).
7. C. Herkt-Maetzky and J. Schelton, *Phys. Rev. Lett.*, **51**, 896 (1983).
8. T. Hashimoto, J. Kumaki, and H. Kawai, *Macromolecules*, **16**, 757 (1983).
9. H. L. Snyder and P. Meakin, *Macromolecules*, **16**, 757 (1983).
10. H. L. Snyder and P. Meakin, *J. Chem. Phys.*, **79**, 5588 (1983).
11. S. Nojima, Y. Okyama, M. Yamaguchi, and T. Nose, *Polymer J.*, **14**, 907 (1985).
12. T. Inoue, T. Ougizawa, O. Yasuda, and K. Miyasaka, *Macromolecules*, **18**, 57 (1985).
13. C. C. Han, M. Okada, Y. Muroga, B. J. Bauer, and Q. Tran-Cong, *SPE ANTEC Tech. Papers*, **31**, 306 (1985).
14. L. S. Ornstein and F. Zernike, *Proc. Acad. Sci.*, (Amsterdam), **17**, 793 (1914).
15. P. G. deGennes, *J. Physique*, **31**, 235 (1970).
16. P. G. deGennes, *J. Chem. Phys.*, **72**, 4756 (1980).
17. P. Pincus, *J. Chem. Phys.*, **75**, 1996 (1981).
18. J. W. Cahn and J. E. Hilliard, *J. Chem. Phys.*, **31**, 688 (1959).
19. J. W. Cahn, *J. Chem. Phys.*, **42**, 93 (1965).
20. K. Binder, *J. Chem. Phys.*, **79**, 6387 (1983).
21. (A) K. Kamide, S. Matsuda, T. Debashi, and M. Kaneko, *Polymer J.*, **16**, 839 (1984). (B) R. Koningsveld and H. A. G. Chermin, *Proc. R. Soc.* (London) A, **319**, 331 (1970).
22. E. D. Siggia, *Phys. Rev. A*, **20**, 595 (1979).

DISCUSSION: C. C. HAN

L. A. Utracki: I want to congratulate you for the progress you have made in the area of the dynamics of phase separation. In the past there were two mechanisms discussed: The spinodal decomposition, *SD*, leading to interconnecting domain structures and the nucleation and growth, *NG*, leading to discrete particle systems. I believe that you are operating within the region of the *SD* mechanism. You showed us two different exponents for the phase ripening: -1 and $-1/3$. Is it true that $-1/3$ should be observed for the *NG* mechanism?

C. C. Han: Yes. Let me first show you the diagram. This is 45 percent PS with 55 percent of PVME. We make a very, very shallow jump, just to about the spinodal temperature. On the scattering intensity curve we may see at low angle scattering a small peak. This we feel is related to nucleation and growth, but in this process you do not have time zero. Each nucleus formed will start a local growth of phase separation. Since we do not have time zero, we cannot say if the exponent is exactly $-1/3$ or not. However, we feel that the spinodal decomposition is more controllable, more important for generating a desired morphology. If we really understand the system we should be able to control not only the grid size, but also the interconnection, and the sharpness of phase separation.

R. E. Prud'homme: I would like to ask you for a clarification. What is the real meaning of extrapolation of χ-values to temperatures above the spinodal temperature. Under these conditions you have phase separation and the meaning of χ is lost. Usually, the interaction parameter is defined for homogenous mixtures.

C. C. Han: The χ represents the A-B interaction energy per unit volume. The interaction energy exists at any temperature. In homogenous systems this energy is attractive or slightly repulsive, insufficient to overcome the entropy of mixing contribution. But if you go above the spinodal temperature, χ is still a good measure of the driving force for phase separation. In short, the deeper you jump into the immiscible region the faster the phase separation will occur.

D. Froelich: You have been using fairly high molecular weight polymers. Do you have any idea what the molecular weight dependence of the phase separation kinetics is?

C. C. Han: There are some temperature jump experiments reported in the literature by Kawai and Hashimoto from Japan and by Meakin and Snyder from the USA. In both cases the authors used commercial PVME with a molecular weight of about $M = 60{,}000$. If you assume that the diffusion process goes by the reptation mechanism, then you should get M^{-2} dependence. The molecular weight of our sample was about $M = 2 \times 10^5$ and we had a linear region for about 3000 s. This means that they should have a linear region of approximately 5 min. Of course, this will depend on the depth of the jump in their experiment and also the *MW* of the other component. Looking at the reported data, I estimate that their linear region stretches to about 2 to 3 min which is consistent with this estimation within a factor of 2.

Vibrational Analysis of Functionalized Polyolefins/Poly(vinylchloride) Blends

ENZO BENEDETTI, ALDO D'ALESSIO, MAURO AGLIETTO, GIACOMO RUGGERI, PIERGIORGIO VERGAMINI, *and* FRANCESCO CIARDELLI

Centro CNR Macromolecole Stereordinate ed Otticamente Attive
Dipartimento di Chimica e Chimica Industriale
Università di Pisa
Via Risorgimento 35,56100 Pisa, Italy

Polyolefins functionalized with diethylmaleate were mixed with poly(vinylchloride) (PVC) in different compositions. Intermolecular interactions involving the carbonyl groups of the side chains of the functionalized polyolefins and methine hydrogens of PVC were investigated by means of infrared spectroscopy. The major flexibility of the ester groups attached to the backbone chains, with respect to polyesters, seems to increase the capability of such groups to interact with groups of more polar polymers, thus allowing prediction of easier miscibility, which however also depends on the starting polyolefin structure and functionalization degree.

1. INTRODUCTION

When high molecular weight polymers are mixed, the contribution of entropy change to the total free energy is negligible. Favorable intermolecular interaction is an indispensable requirement for lowering the free energy of mixing in order to attain compatibility.

The FT-IR spectroscopy has provided a substantial contribution to the understanding, at the molecular level, of the intermolecular interactions between different polymer chains. Over all, digital subtraction and addition techniques, where intermolecular interactions occur, may allow observation of considerable differences between the experimental infrared spectrum of the blend and of that synthesized by addition of the absorbance spectra of the pure components. These differences may be due to intermolecular interactions resulting in band shift and broadening, and also to changes in conformation (1, 2).

The plasticization of poly(vinylchloride) (PVC) by means of low molecular weight esters or polyesters has been the object of considerable investigation. In the case of PVC/low molecular weight plasticizer mixtures, particular attention has been given to the study of the PVC conformational changes induced by intermolecular interactions (3, 4).

In a previous investigation on a di-n-butylphthalate(DBP)/PVC system (5), it was evidenced that DBP gives rise to interaction with PVC mainly through a hydrogen bond between the carbonyl group of DBP and the methine hydrogen of PVC. It was shown that to a lesser degree, the β-hydrogens of PVC could also be involved and dipole-dipole interactions of the type C=O. . .Cl—C could not be excluded.

The carbonyl stretching vibration of poly(β-propiolactone) (PPL) do not show any change in frequency and broadness in the PPL/PVC immiscible blend (6), whereas in the poly(ϵ-caprolactone)(PCL)/PVC, compatible mixture, a shift towards lower frequencies and a broadness of this absorption with increasing PVC amount are observed (7, 8). Such a change in the carbonyl band feature of PCL has been attributed to a hydrogen bond with the methine hydrogen of PVC. When β-hydrogens, but no α-hydrogens are available, e.g., poly(vinylidene chloride), interactions still occur although not as strong as with PVC (9).

In the case of polyester/PVC blends, there is an optimum density of ester groups in the polymer chains (10) for achieving the maximum interaction with PVC. Too low —CH_2/COO— ratios ($x \leq 4$) result in immiscibility with PVC as the polyester chains are too rigid and cannot adopt the conformations required for specific interaction with the chlorinated polymer; too high —CH_2/COO— ratios ($x \geq 7$) also lead to

immiscible blends due to a too low concentration of carbonyl groups (11).

These results suggested the possibility of compatibilizing polyolefins with PVC provided mobile ester groups could be attached to the polyolefin chains in a proper concentration. Indeed such functionalization was achieved by reacting polyolefins like ethylene-propylene copolymer, atactic and isotactic polypropylene with diethylmaleate (12), and dibutylmaleate (13) in the presence of peroxides.

In the present note we describe new findings concerning functionalized polyethylene/PVC blends which are discussed with reference to previous results concerning propylene polymers.

2. EXPERIMENTAL

Functionalized high density polyethylene (FPE) was obtained by reacting the original polymer with diethylmaleate in the presence of dicumylperoxide at 200°C under nitrogen atmosphere. After reaction the polymer was fractionated by extraction with boiling *n*-heptane and toluene, in that order.

Films of the functionalized polyethylene and of its PVC mixtures were obtained by casting solutions in toluene/tetrahydrofuran(1:1) on KBr windows.

The spectra at room and high temperatures were run on a Perkin-Elmer model 180 spectrophotometer.

3. FUNCTIONALIZATION OF POLYOLEFINS

As described in a previous paper, isotactic polypropylene (IPP) and atactic polypropylene (APP) can be functionalized by reaction with an unsaturated functional compound in the presence of free radical initiators (12). Treating the polymer (in the melt) with diethylmaleate (DEM) and dicumylperoxide (DCP) at 200 to 225°C, a higher functionalization degree was obtained of the less rigid APP than that of the more sterically hindered IPP (see *Table 1*). Analogous results were obtained with ethylene-propylene copolymer (EP) and with high density polyethylene (PE) using the same reaction conditions.

In the case of EP, where the more reactive tertiary C—H bonds are less sterically hindered, a higher functionalization degree is obtained with respect to APP and IPP.

In the case of PE, despite the lack of tertiary hydrogens a rather high functionalization degree was achieved (*Table 1*), probably due to higher chain mobility.

Table 1. Functionalization Degree of Poly-α-Olefins Treated with Diethylmaleate and Dicumylperoxide at 200°C in Bulk.

Polymer	Degree of functionalization (weight %)
IPP	0.5
APP	3–8
EP	10–18
PE	20–22

IPP—isotactic polypropylene
APP—atactic polypropylene
EP—ethylene propylene copolymer
PE—polyethylene

The main reactions occurring during the functionalization process are schematically presented in *Scheme 1*, where the molecular structure and the chemical environment of the ester groups attached to the polymer chain for the functionalized ethylene-propylene copolymer (FEP) and polyethylene (FPE) are also presented. This *Scheme* does not take into account the degradation reaction of the macromolecular radical, which contributes not only to lowering the molecular weight, but also to generation of a different mechanism of functionalization with the introduction of the ester group at the end of the macromolecular chains (*Scheme 2*). Also, crosslinking is not considered as the polymers were completely soluble in boiling toluene at the end of the functionalization reaction (12).

Because of reaction conditions the propagation reaction of diethylmaleate is not considered, even if it cannot be completely excluded. IR spectra of starting and functionalized ethylene-propylene copolymer and high density polyethylene are reported in *Fig. 1*. In particular both functionalized polymers show a typically strong absorption centered at 1740 cm^{-1} associated with stretching vibration of C=O in the ester groups of attached maleate units, the functionalization degree resulting rather high for both polymers (*Table 1*).

4. VIBRATIONAL SPECTRA OF BLENDS

The polyolefins, functionalized with ester groups in the lateral chains, present remarkable commercial interest since the mobility of the ester groups outside the main chains should allow compatibilization even for a low degree of functionalization allowing retention of the mechanical properties of the original polymers.

In a previous work (14) we examined, by means of infrared spectroscopy, blends of ethylene-propylene copolymers, atactic and isotactic polypropylene, functionalized with diethylmaleate in the presence of dicumylperoxide, with PVC and PS. It was shown that intermolecular interaction occurs between carbonyl groups of the lateral chains and PVC.

The functionalized ethylene-propylene copolymer (FEP) in solution of *n*-heptane, tetrahydrofuran, carbon tetrachloride, 1,1,1-trichloroethane, and chloroform showed the shift of the carbonyl IR band toward lower frequencies compared with the *n*-heptane solution. The increases occur in the order $n\text{-}C_7H_{16}$ < THF < $CCl_3\text{-}CH_3$ < CCl_4 < $CHCl_3$, the maximum shift for chloroform suggesting that the methine hydrogen was mainly involved. However, interactions involving β-hydrogens or chlorine atoms had to be assumed to occur even if to a lower degree.

Scheme 1

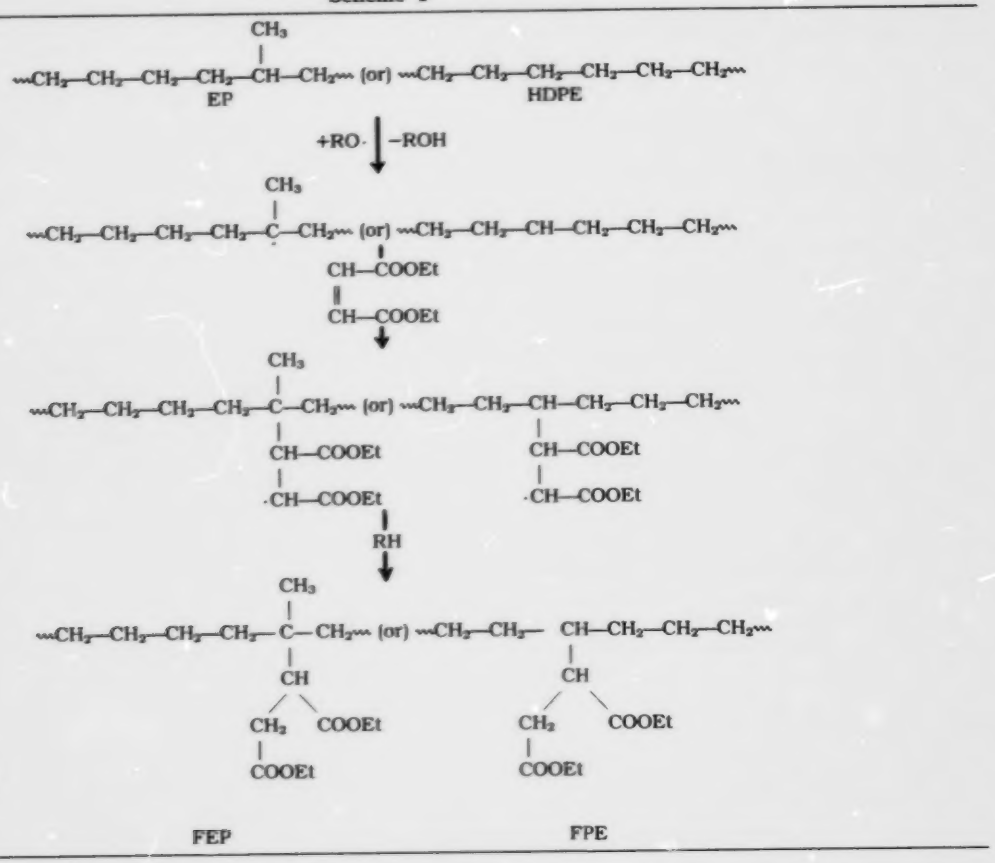

Scheme 2

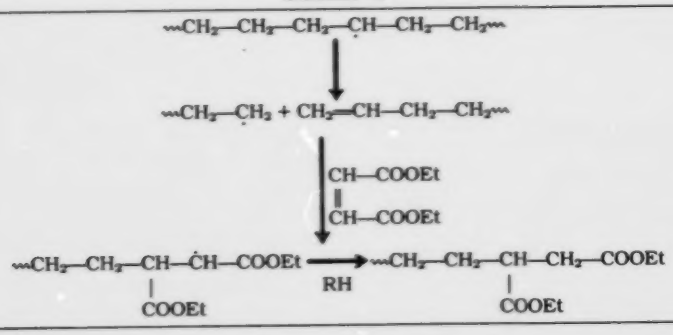

The minor changes in the carbonyl stretching vibration on going from the functionalized ethylene-propylene copolymers to atactic and isotactic polypropylene were interpreted as due to a gradual lack of compatibility because of major rigidity and lower functionalization of propylene homopolymers.

In this work it was observed that the carbonyl stretching band of functionalized high density polyethylene and its mixtures with PVC shifts towards lower frequencies and becomes broader with increasing PVC content as observed previously for FEP/ and FAPP/PVC mixtures (14) (*Fig. 2*).

The plot of the width at half-height of the C=O band *vs.* PVC percentage (*Fig. 3*) shows no change in the case of PPL/PVC, whereas for the PCL/PVC alloy, the S-shaped curve has been associated with interactions of the carbonyl group with PVC. Such interactions approach saturation at concentrations of approximately 1:4 molar ratio (7).

In the case of FEP/PVC and FPE/PVC mixtures, an intermediate trend is observed between PPL/PVC and PCL/PVC mixtures. This fact could indicate a limited compatibility; in particular, in addition to crystalline domains, shown by the splitting of the bands at 720 and

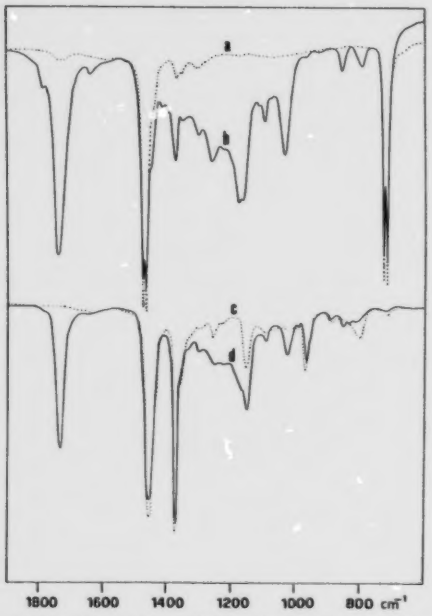

Fig. 1. Infrared spectra of (a) polyethylene, (b) functionalized polyethylene, (c) ethylene-propylene copolymer, and (d) functionalized ethylene-propylene copolymer.

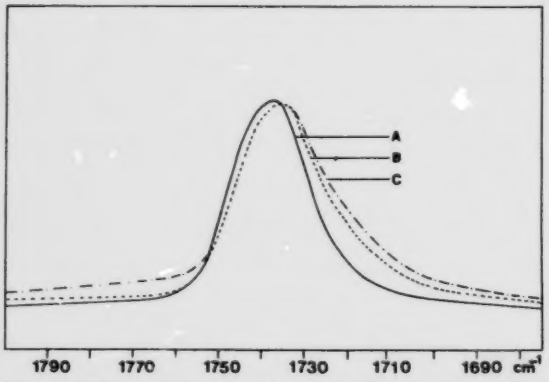

Fig. 2. Infrared spectra in the carbonyl stretching region of (A) functionalized polyethylene and functionalized polyethylene/PVC mixtures containing (B) 50, and (C) 75 weight percent PVC.

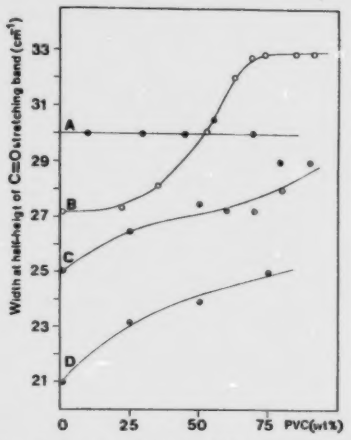

Fig. 3. Plots of the width at half-height of the carbonyl stretching vibration as a function of PVC concentration for (A) poly(β-propriolactone)/PVC, (B) poly(ε-caprolactone)/PVC, (C) functionalized ethylene-propylene/PVC, and (D) functionalized polyethylene/PVC mixtures.

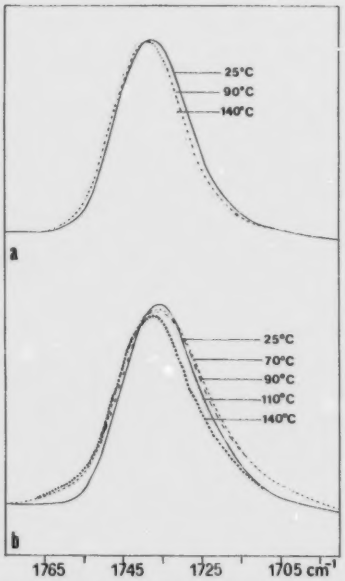

Fig. 4. Infrared spectra in the carbonyl stretching region of (a) functionalized polyethylene, and (b) funtionalized polyethylene/PVC mixture (25/75) at different temperatures.

1460 cm^{-1}, FPE contains amorphous domains where a higher concentration of the functional ester groups is expected. This can be deduced from the spectra of FPE and of the FPE/PVC (25/75 by wt.) mixture measured at different temperatures (*Fig. 4*). In the former, the changes of the shape of the carbonyl band are observable at about 90°C and in correspondence of the melting point of FPE (140°C) (*Fig. 4a*), when the splitting of the methylene rocking vibrations disappears. These shifts towards higher frequencies may be related to weak interactions of the ester groups in the same chain or in different chains which become weaker with increasing temperature. This seems to take place in two steps, one at 90°C still in the presence of the tridimensional order of the polyethylene segments in the crystalline domains and the other when this order disappears, corresponding to the melting point of the polymer.

For the FPE/PVC mixture, in which competitive interactions between the ester groups with themselves and with PVC occur, the behavior with changing temperature is more complex. The continuous shift to high frequencies is observed, at least as far as the band maximum position is concerned (*Fig. 4b*) and is not accompanied by a monotonic change of band broadness.

The different position of the carbonyl bands of FPE with respect to the FPE/PVC mixture at 140°C could be interpreted again on the basis

of interactions between ester groups of FPE and PVC giving no complete phase separation even at this temperature.

5. CONCLUSIONS

Polyolefins like polyethylene, ethylene-propylene copolymers, atactic and isotactic polypropylenes, functionalized with diethylmaleate give rise to molecular interactions with poly(vinylchloride) by means of a hydrogen bond involving the carbonyl of the ester groups in the lateral polyolefins chains and the methine hydrogen of PVC. These interactions may be responsible for the compatibility between samples of different polymers.

This kind of interaction has been evidenced on the basis of a progressive shift towards lower frequencies and broadening of the carbonyl band as a function of the PVC concentration. This very probably means an increase of the amount of CO groups, which are also in different environments, involved in the complexation, saturation being achieved with more than 50 percent by weight of PVC in the blend.

The higher polymer chains' rigidity, as in the case of atactic and above all isotactic polypropylene, is probably responsible for a phase separation in the corresponding blends with PVC even if the lower functionalization may also contribute to this effect. Mixtures of functionalized polyethylene with PVC show both crystalline and amorphous domains, these last containing a higher concentration of ester groups disposable for interaction with methine groups of PVC, thus suggesting a very modest effect, if any, of crystallinity on C=O band position. Indeed band shift is also observed at temperatures higher than the melting point.

ACKNOWLEDGMENT

Thanks are due to Dr. S. Speranza for experimental assistance in the functionalization of PE.

This work has been supported by the CNR Project "Chimica Fine e Secondaria" Sottoprogetto Bb.

REFERENCES

1. M. M. Coleman, J. Zarian, D. F. Varnell, and P. C. Painter, *J. Polym. Sci., Polym. Lett. Ed.*, **15**, 745 (1977).
2. F. J. Lu, E. Benedetti, and S. L. Hsu, *Macromolecules*, **16**, 1525 (1983).
3. D. L. Tabb and J. L. Koenig, *Macromolecules*, **8**, 929 (1975).
4. M. Theodorou and B. Jasse, *J. Polym. Sci., Polym. Phys. Ed.*, **21**, 2263 (1983).
5. E. Benedetti, F. Posar, A. D'Alessio, P. Vergamini, G. Pezzin, and M. Pizzoli, *J. Polym. Sci. Polym. Phys. Ed.*, **23**, 1187 (1985).
6. M. M. Coleman and D. F. Varnell, *J. Polym. Sci., Polym. Phys. Ed.*, **18**, 1403 (1980).
7. M. M. Coleman and J. Zarian, *J. Polym. Sci., Polym. Phys. Ed.*, **17**, 837 (1979).
8. D. F. Varnell, E. J. Moskala, P. C. Painter, and M. M Coleman, *Polym. Eng. Sci.*, **23**, 658 (1983).
9. A. Garton, P. Cousin, and R. E. Prud'homme, *J. Polym. Sci., Polym. Phys. Ed.*, **21**, 2275 (1983).
10. J. J. Ziska, J. W. Barlow, and D. R. Paul, *Polymer*, **22**, 918 (1981).
11. D. Allard and R. E. Prud'homme, *J. Appl. Polym. Sci.*, **27**, 559 (1982).
12. G. Ruggeri, M. Aglietto, M. Petragnani, and F. Ciardelli, *Eur. Polym. J.*, **19**, 863 (1983).
13. G. De Vito, N. Lanzetta, G. Maglio, M. Malinconico, P. Musto, and R. Palumbo, *J. Polym. Sci., Polym. Chem. Ed.*, **22**, 1335 (1984).
14. E. Benedetti, F. Posar, A. D'Alessio, P. Vergamini, M. Aglietto, G. Ruggeri, and F. Ciardelli, *Brit. Polym. J.*, **17**, 34 (1985).

DISCUSSION: E. BENEDETTI

R. E. Prud'homme: How do you explain the peak broadening effect as a function of addition of PVC?

E. Benedetti: An increase of the number of the carbonyl groups involved in the hydrogen bonds with the methine hydrogens of PVC, going towards a saturation, could explain the broadness of this absorption, analogously with that suggested for the PCL/PVC system. Of course, the effect is very complex considering the envelope of this band as constituted of many components.

R. E. Prud'homme: You mentioned that these measurements were done at room temperature. It seems to me that you should consider the influence of crystallinity which changes with composition. In cases I know quite well, poly(ε-caprolactone)/PVC, there is crystallinity up to 50 wt percent of PVC. At higher PVC content PCL becomes amorphous. The contribution to crystallinity is as large as the magnitude of the shift you reported.

E. Benedetti: In the case of these functionalized polyolefins there are long sequences of $-CH_2-$ groups but only a few functional ones. The trends of the width at half height of the carbonyl groups for the FEP/PVC and FPE/PVC mixtures as a function of PVC amount are compared with that of the PCL/PVC system in the molten state. Crystalline domains are present in the FPE/PVC blend, at room temperature, but they have to be related to the packing of the methylene segments, outside of the amorphous domains containing the major concentration of the functional groups.

R. E. Prud'homme: For PCL/PVC this is not so. In the PCL carbonyl group one can see very well the crystalline contribution, which disappears with increase of temperature above the melting point.

E. Benedetti: We have to consider that in the case of PCL the C=O groups are localized in the main chains and therefore are directly involved in the crystalline packing. In our functionalized polyolefins the ester groups are inserted in the

lateral chains, and because of their mobility and low content they probably scarcely affect crystallinity.

J. Bley: In the preparation of your functional polyethylenes you used peroxides at 200°C. In doing this, no doubt one must introduce crosslinking as well as oxidation. How do you differentiate this oxidation product from the functional group?

E. Benedetti: The C=O formed by oxidation is in a small amount because the functionalization reaction was carried out under N_2 atmosphere. After reaction we fractionated the polyethylene using *n*-heptane and toluene. The polymer fraction soluble in toluene was utilized in blends preparation.

J. Bley: If you fractionated the polymer you must have observed the insoluble, crosslinked fraction. Did you measure its C=O content?

E. Benedetti: No, we never observed crosslinked polyethylene; indeed the polymer after the functionalization reaction was completely soluble in boiling toluene.

L. A. Utracki: The miscibility in polymeric blends primarily depends on specific interactions. Both the conformational entropy and the dispersive heat of mixing play either a small or even a negative role. On the other hand, the specific interactions are evidenced by the IR or NMR peak shifts. Do you think it would be possible to quantify the specific interaction effects needed to secure miscibility by calculating energy involved in peak displacement?

E. Benedetti: Yes, we will attempt to relate these effects.

L. Z. Pillon: I have two questions: 1. How did you calculate the degree of functionalization, and 2. How did you prepare your samples?

E. Benedetti: We calibrated the C=O band absorbance, and then used the calibration curve to calculate the extent of functionalization. To your second question, the samples were prepared by solvent casting as described in the preprint.

Fluorescence Studies of Polymer Blends: Anchoring Stabilizer Chain in Non-Aqueous Dispersions

LUKE S. EGAN *and* MITCHELL A. WINNIK

Lash Miller Laboratories
Department of Chemistry and Erindale College
University of Toronto
Toronto, Ontario Canada M5S 1A1

and

MELVIN D. CROUCHER

Xerox Research Center of Canada
2660 Speakman Drive
Mississauga, Ontario, Canada, L5K 2L1

Non-aqueous dispersions of poly(vinyl acetate) stabilized by a surface layer of poly(2-ethylhexyl methacrylate) (PEHMA) were prepared. We modified the recipe for particle synthesis, using as a stabilizer a copolymer of EHMA containing a small amount of either phenanthrene (Phe) or pyrene (Py) groups. These fluorescent labels permit us to assess different aspects of stabilizer chain morphology and dynamics. In the particles labeled with Phe groups, the ability of oxygen to quench Phe fluorescence is used as a monitor of O_2 sorption at the stabilizer-particle interface. In these experiments, information about the location of the labels and the PEHMA polymer is obtained. In the particles labeled with Py, pyrene self-quenching and excimer formation serves as a sensor of conformational and mobility changes in the PEHMA polymer upon anchoring in the particle.

INTRODUCTION

One of the most powerful ways of studying complex systems involves introducing a sensor molecule into a specific environment so that its behavior can be interrogated. The sensor could be an isotopically labeled component to be examined by neutron or X-ray scattering, or a luminescent dye to be studied by fluorescence and phosphorescence spectroscopy. By covalently attaching the sensor to a component of one particular phase of a system, the sensor can serve as a molecular spy of phenomena occurring in its specific microenvironment.

Applications of fluorescence sensor techniques to polymer blend systems began some ten years ago. The original work by Frank (1) and Morawetz (2) focused on characterizing polymer compatibility with particular emphasis on the interface region between incompatible polymer pairs. In these experiments, a host of spectroscopic phenomena including excimer formation (1), energy transfer (2), and other fluorescence quenching (3) processes were exploited. In consequence, the information obtained has been both rich and varied.

In the last few years, novel methods based on fluorescence spectroscopy have been used to gain information on the spinoidal decomposition mechanism of polymer blend phase separation (4), epoxy cure kinetics (5), and free volume in polymer matrices (6). In a recent paper by Halary, *et al.* (4), it was demonstrated that polystyrene-poly(vinylmethylether) phase diagrams typically obtained by small angle neutron scattering (7) can be obtained by fluorescence spectroscopy using anthracene labeled polystyrene. The particular advantage of the fluorescence method is that one can gain easy access to a fluorescence spectrometer. Levy and Ames (5) describe preliminary results on the use of a unique viscosity-dependent fluorescence "self-probe" to monitor *in situ* epoxy cure kinetics. In these experiments, the observed increase in fluorescence from tetraglycidyldiaminodiphenyl methane epoxy as a function of cure time gave directly the cure kinetics.

Our contribution to this area has been in the

application of fluorescence techniques specifically to the study of polymer particles produced by dispersion polymerization (8, 9). In dispersion polymerization, a soluble monomer is polymerized in a solvent in which its homopolymer is insoluble. If this polymerization is carried out in the presence of a second soluble polymer, stable colloidal dispersions can be produced; the soluble polymer becomes anchored onto the particle surface. Its solvent swollen chains serve as a steric stabilizer (8) for the dispersion. Our previous efforts involved labeling the core of large (ca. 1 to 3 μm diameter) poly(methyl methacrylate) particles with fluorescent groups appropriate for elucidating the interior morphology of the particles (10). In the experiments described here, we look at the stabilizer chains and examine the consequences of anchoring these chains onto poly(vinyl acetate) particles, particularly as conformation and mobility of the chains are affected.

The specific systems we chose to investigate are nonaqueous dispersions [NAD] of poly(vinyl acetate) [PVAc] particles of mean diameter 0.3 μm, stabilized by poly(2-ethylhexyl methacrylate) [PEHMA]. In order to study the nature of the anchoring process, we prepared stabilizing polymers containing small quantities of a covalently bound fluorescent dye. Dispersion polymerization of vinyl acetate monomer in the presence of these copolymers yielded dispersions of particles selectively labeled with fluorescent groups within the PEHMA phase of the NAD. Experiments employing both steady-state and transient fluorescence techniques were then performed on labeled particles and stabilizers, and the results compared.

A simplified representation of the anchoring process is depicted in *Fig. 1*. Very little is known of the exact nature of the stabilizer chain attachment to the particle. It is thought that the morphology of the interface between particle core and stabilizer chains is controlled by the mechanism of particle formation. Particle formation in dispersion polymerization is itself only poorly understood (8). Therefore any experiment which can explore the interface between core and stabilizer polymers can provide information pertinent to the particle formation process.

CHOICE OF THE CHROMOPHORE

When designing fluorescence experiments for the study of complex polymer systems one of the most difficult decisions involves the choice of the appropriate fluorescent sensor. We employed phenanthrene (Phe) and pyrene (Py) chromophores in our studies. Phenanthrene was chosen because of its reluctance to form excimers, a factor which promotes simple (exponential) fluorescence decay behavior in polymeric systems (11). This feature is particularly useful in fluorescence quenching experiments where variations in the ability of certain solutes to reach different locations within a structure induce nonexponential components in the fluorescence decay curve. Pyrene, on the other hand, was employed because of its general tendency to form excimers (12). This property allows one to probe the interactions not only between pyrenes far removed from each other along a polymer chain backbone, but also between labels attached to different chains.

Oxygen quenching studies were performed on phenanthrene labeled systems. The special feature of this kind of experiment is that high-resolution information about the location of fluorescent labels can be obtained. Thus, since the labels are covalently bound to PEHMA, the information about probe location reflects the actual particle morphology. These experiments show very pronounced differences between the homogeneous solutions of stabilizer, and the model compound (phenanthrylmethyl pivalate) on one hand, and that of the particle-bound stabilizer on the other. The results demonstrate that a unique population of phenanthrene labels does not exist and are consistent with a model predicting a distribution of environments containing the fluorescent sensors and stabilizer chains. In considering results from oxygen quenching studies on core labeled colloids, we suggest that an interphase rather than a distinct interface exists between the stabilizing polymer and the PVAc core polymer. This result is a consequence of the detailed nature of the anchoring mechanism and it also supports our idea that the simple core-shell model is inadequate to describe the structure of most nonaqueous dispersions (10).

Studies on pyrene-labeled particles and pyrene-labeled free stabilizer reveal other kinds of information. It is known that excimer formation in solution between pyrenes attached to sites remote along a polymer backbone is extremely sensitive to the overall conformation of the polymer chain (13, 14). Furthermore, careful investigation of the kinetics of this process in a number of systems affords valuable insights into chain dynamics. We have taken advantage of this methodology. In our studies, the consequences of stabilizer chain anchoring, i.e., changes in chain conformation and dynamics, were determined by monitoring the differences between the luminescence behavior of the free and anchored stabilizers. The results indicate that the chains are concentrated in the stabilizer phase. In addition, it was found that the mobility of most of the pyrene sensors is severely restricted. Coupled with our interphase model for colloid morphology, these results lead us to envision the stabilizer phase as an overlapping network of PEHMA and PVAc chains in which the PEHMA is covalently anchored to PVA core polymer at one or more positions along the chain.

SPECTROSCOPY AND KINETICS

Fluorescence Quenching

For small molecules in fluid solution, the kinetics of fluorescence quenching by oxygen can be analyzed using the Stern-Volmer equation

$$I^0/I = \tau^0/\tau = 1 + k_q\tau^0[Q] \qquad (1)$$

In this equation, I^0, I, and τ^0, τ are the fluorescence intensities and fluorescence decay times in the absence and presence of quencher (Q), respectively, and k_q is the bimolecular quenching rate constant. *Equation 1* requires that the fluorophore have a unique fluorescence decay time (its decay must be exponential) and that the quenching process be described by a single rate constant k_q. One normally believes that a linear Stern-Volmer plot (I^0/I, τ^0/τ *vs.* $[Q]$) indicates that a single class of chromophore exists, and that all chromophores are all equally accessible to quencher.

The important parameter in *Eq 1* is k_q. Once its value is known and if quenching is diffusion controlled, k_q can be related, using the Smoluchowski equation (*Eq 2*), to the sum of the diffusion coefficients of the interacting species.

$$k_q = k_{diff} = \frac{4\pi N_A D \cdot pR}{1000}\ (M^{-1}s^{-1}) \qquad (2)$$

In *Eq 2*, $D = D_F + D_Q$ is the sum of the diffusion coefficients of chromophore and quencher, respectively, $R = R_F + R_Q$ is the sum of their interaction radii, N_A is Avogadro's number, and p is a factor describing the reaction probability per collision. Oxygen is known to quench most fluorophores with unit efficiency ($p = 1$) (14).

Certain considerations must be taken into account, however, when interpreting fluorescence quenching experiments on solutions of polymer bound dyes. Firstly, the concentration of quencher $[Q]$ inside and outside a polymer coil may not be equal. This is particularly true when there are specific interactions between Q and the polymer or when Q is a nonsolvent for the polymer. When present in high concentration, it may be excluded from the interior of the polymer coil. In addition, variations in quencher solubility must also be considered if condensed polymer phases are present in the sample. Secondly, the center-of-mass diffusion coefficient D_F is lower for a polymer bound chromophore. One often neglects polymer diffusion in interpreting k_q values, since the center-of-mass diffusion coefficient of the polymer is much smaller than that of Q. This neglect is not always warranted. For polymer bound phenanthrene groups, for example, the time scale of the fluorescence decay is 45 ns. During this time a quencher of $D_Q = 2 \times 10^{-5}$ cm^2/s would have a mean diffusion distance of approximately 14 nm. Local motions of the polymer with amplitudes of ca. 1 to 2 nm would contribute to the rate of the reaction. D_F in *Eq 2* would then describe the contribution of this motion to the quenching process.

Pyrene Excimer Formation

A simple model which describes the process of excimer formation between two polymer bound pyrene chromophores is shown below.

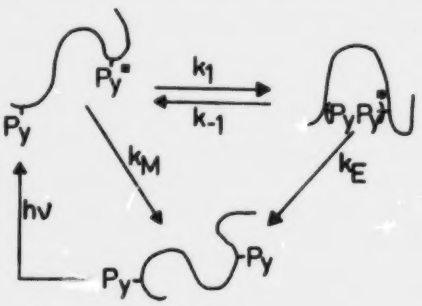

In this model, -Py and -Py* represent ground state and locally excited pyrene, respectively, and (PyPy)* represents pyrene excimer. k_1 is the first order rate constant for intramolecular excimer formation and k_{-1} describes the rate of excimer dissociation. The rate constants k_M and k_E are the reciprocal pyrene monomer and excimer (exponential) decay times, respectively.

This model makes specific predictions about the form of the monomer ($I_M(t)$) and excimer ($I_E(t)$) decay curves obtained from single photon counting (transient) fluorescence experiments (12, 13). At ambient temperatures, when k_{-1} is not too large, $I_M(t)$ and $I_E(t)$ are given by

$$I_m(t) = a_1\exp(-\lambda_1 t) \qquad (3)$$

and

$$I_E(t) = a_2\exp(-\lambda_1 t) + a_3\exp(-\lambda_2 t). \qquad (4)$$

Under these conditions and for this simple model, the experimental parameters should be identical for both experiments, and are directly related to the rate constants

$$\lambda_1 = k_1 + k_M \qquad (5)$$

$$\lambda_2 = k_{-1} + k_E \qquad (6)$$

The rate constant of interest to us is k_1. It can be calculated from *Eq 5* when the rate constant $k_M = 1/\tau_M$ for a suitable model compound is known.

The rate constant for excimer formation k_1 can also be determined from steady-state fluorescence measurements (15). In this case, the above model predicts that the ratio of excimer to monomer fluorescence intensity is of the form

$$\frac{I_E}{I_M} = \frac{\Phi_E^0}{\Phi_M^0}\frac{k_E}{k_M}\left(\frac{k_1}{k_{-1} + k_E}\right) \qquad (7a)$$

$$\frac{I_E}{I_M} = \frac{\Phi_E^0}{\Phi_M^0}\frac{k_1}{k_M} \qquad (k_E > k_{-1}) \quad (7b)$$

In *Eq 7*, Φ_M^0 and Φ_E^0 are the quantum yields of the pure monomer and excimer species, respectively. For most pyrene-pyrene excimer systems at 20 to 25°C, k_E is determined to be about 10 times larger than k_{-1}. Thus the ratio I_E/I_M directly reflects the magnitude of k_1.

For all intramolecular pyrene excimer formation processes, a second order rate constant $k^{(2)}$ can be defined according to

$$k_1 = k^{(2)}C_{eff} \tag{8}$$

where C_{eff} is the effective concentration of unexcited pyrenes in the neighborhood of the excited species. Perico and Cuniberti point out that for diffusion-controlled processes, both k_1 and $k^{(2)}$ are proportional to T/η where T is the temperature and η is the solvent viscosity (14a). Thus, changes in the magnitude of I_E/I_M, which can now be rewritten as

$$\frac{I_E}{I_M} \propto \frac{\Phi_E^0}{\Phi_M^0}\tau_M(T/\eta)C_{eff} \propto k_1 \tag{9}$$

can provide information about the behavior of k_1 as well as on the ratio C_{eff}/η.

A further degree of complexity arises when stabilizers and stabilizer-labeled colloids are considered. In principle, all possible chromophore pairs indicated in *Fig. 1* are capable of forming an excimer. Notice that for the anchored stabilizer chains, both interstabilizer and intrastabilizer chain excimers ought to be formed. For proximate labels, one expects large values of k_1 and short decay times (13). For well separated pyrenes, however, small values for k_1 and long decay times are predicted. Clearly, a unique rate constant k_1 cannot describe excimer formation in these kinds of systems. Rather one must consider a model in which a distribution of rate constants for excimer formation and a distribution of fluorescence decay times exists.

Preparation and Characterization of the Particles

A typical two step, "one-shot" synthesis of an NAD containing Phe labels in the stabilizer is described below. All materials employed were purified by standard methods (distillation and recrystallization) prior to use. In the first step, a deoxygenated solution of 2-ethylhexyl methacrylate (0.102 mole), AIBN (0.0019 mole), phenanthrylmethyl methacrylate (0.0004) mole in isooctane (80 ml) was stirred mechanically for 24 h at 75°C. After purification by repeated reprecipitation, the labeled PEHMA was dried in vacuo. The reaction yielded ca. 15 g of stabilizer (St-Phe), and GPC analysis showed no detectable residue of low molecular weight UV absorbing impurities.

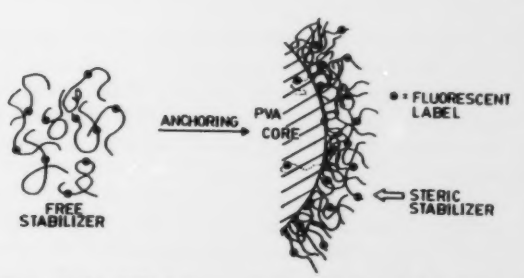

Fig. 1. A simplified representation of the stabilizer chain anchoring process in a non-aqueous dispersion polymerization.

The second step consisted of stirring a deoxygenated mixture of 5.6 g of St-Phe, vinyl acetate (19.2 g, 0.22 mole), and benzoyl peroxide (0.004 mole) in 40 ml of isooctane at 75°C for 17 h. Stirring was continued for 2 h at 90°C and the reaction mixture then cooled to room temperature. The resulting milky-white dispersion (C-Phe) was subjected to a series of five centrifugation/redispersion cycles. This procedure served to purify the particles and also to gradually exchange the solvent to cyclohexane. A small amount of this dispersion was freeze-dried, yielding a fluffy white powder and the remainder kept in the dispersed state for use in luminescence experiments. These particles dissolve in good solvents for PVAc (ethyl acetate, chloroform, etc.) to form homogeneous solutions. An unlabeled colloidal dispersion and two containing pyrene in the stabilizer phase (C-PyH and C-PyL) were prepared using the same procedure as described above.

The stabilizer chromophore content was calculated from the UV spectrum of a solution of St-Phe in ethyl acetate. St-Phe was found to contain 0.41 mole percent of phenanthrylmethyl methacrylate units. Colloid composition was determined from the 200 MHz ^{1}H NMR spectrum of a $CDCl_3$ solution of freeze-dried particles. Interestingly, the percentage stabilizer in C-Phe was determined to be only 6.5 wt. percent. Assuming complete conversion of monomer and total attachment of stabilizer, particles composed of 22.6 percent stabilizer and 77.4 percent w/w PVAc ought to have been produced.

GPC analyses in ethyl acetate provided estimates of polymer molecular weights. St-Phe was found to have a molecular weight of 51,000 with respect to polystyrene standards. From this value it was calculated that St-Phe contains, on average, 1.0 phenanthrene groups per stabilizer chain. The particles themselves gave a broad distribution of molecular weights when their solutions in ethyl acetate were analyzed by GPC. The apparent molecular weight was found to range between 1000 and 1,000,000, with a peak maximum at 107,000 in the differential refractive index detector. Also, the peak maximum (from a UV detector) of the signal due to anchored stabilizer was observed to shift to a molecular weight of 107,000 relative to polystyrene. This shift provides evidence that in the dispersion polymerization step, the stabilizer chains become covalently bound or grafted to

the PVAc core polymer. This is also consistent with the observation that C-Phe remains in a dispersed state in cyclohexane at temperatures up to 160°C; well above the T_g of PVAc. We suggest, therefore, that many of the fluorescent labels are located at or near the interface between the PVAc and PEHMA phases.

DSC measurements on C-Phe indicated that the thermal properties of the PVAc phase of the particles is very similar to that of bulk PVAc. Mean particle diameters $\langle D \rangle$ and size dispersity factors $\langle S \rangle$ (16) were measured using a Coulter submicron particle analyzer. For C-Phe, $\langle D \rangle$ and $\langle S \rangle$ were found to be 316 nm and 1.03, respectively.

Steady-state fluorescence spectra were complicated by the presence of a parasitic fluorescence created during particle synthesis, due to the initiator employed. This emission was observed both from samples of labeled (C-Phe) and unlabeled colloid (ULC). It is characterized by a peak maximum at 322 nm, blue shifted from phenanthrene fluorescence, and extends out to 500 nm. The fluorescence decay from ULC was dominated by a component with a lifetime of 1.2 ns. The fact that the intensity of fluorescence from a deoxygenated sample of ULC in cyclohexane remains practically unchanged when the sample is purged with oxygen establishes that the fluorescent impurity in question is located within the core of the PVAc particles.

The fluorescence spectra of deoxygenated dispersions of C-Phe and ULC in cyclohexane are shown in *Fig. 2*. Also shown in this *Figure* is the corrected C-Phe fluorescence spectrum (*c*); it was obtained by subtracting the contribution due to the impurity emission from the uncorrected C-Phe spectrum. This spectum is, in fact, very similar to that of the corresponding phenanthrene labeled stabilizer and model compound. Time-dependent fluorescence decay profiles were generated using the time-correlated single photon counting technique (17). These data were analyzed employing the nonlinear least squares iterative reconvolution method (18).

Oxygen Quenching Studies

When samples of PheMP, St-Phe, and C-Phe are exposed to air or their solutions are saturated with oxygen, the fluorescence intensities and decay times of the samples decrease. These phenomena are due to oxygen quenching the Phe^{*1} excited state. One normally analyzes these data in terms of the Stern-Volmer *Eq 1*. One plots I^0/I or τ^0/τ as a function of quencher concentration $[Q]$. In well behaved systems, such plots yield a y-intercept of unity and a slope equal to $k_q\tau^0$. When τ^0 is known, the magnitude of the bimolecular quenching rate constant k_q can be determined.

Compared in *Fig. 3* are the results of steady-state and transient fluorescence quenching studies on PheMP, St-Phe, and C-Phe. The solid

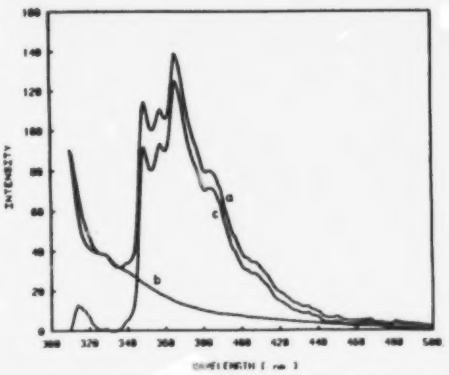

Fig. 2. The uncorrected (a) and corrected fluorescence spectrum (c) of a cyclohexane dispersion (5.0 mg/ml) of C-Phe at 23°C (λ_{ex} = 295 nm). Curve b is from ULC particles in cyclohexane.

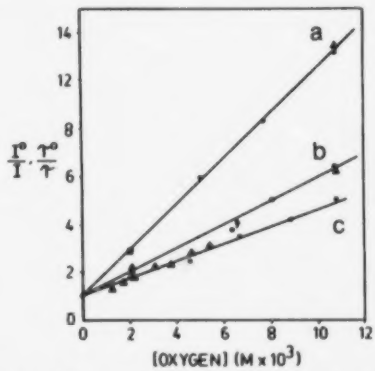

Fig. 3. Plots of τ^0/τ and I^0/I vs. oxygen concentration for samples of phenanthrylmethyl pivalate model compound (a), St-Phe (b), and C-Phe (c) in cyclohexane at 23°C. (●) and (▲) represent the steady state and transient decay data, respectively. The transient data for C-Phe are plotted as $\tau^0/\langle\tau\rangle$ vs. $[O_2]$.

lines through the points represent the best fits to the data. The linearity of these plots indicate that the Stern-Volmer law is obeyed and suggests that unique values of k_q and τ exist. The similarity between the steady-state and transient data for PheMP and St-Phe shows that no static quenching between Phe^* and oxygen occurs.

When the data are fit to *Eq 1*, we find that the rate constant for oxygen quenching of PheMP ($k_q = 2.02 \times 10^{10}\ M^{-1}s^{-1}$). We note that the rate constant for quenching of phenanthrene labels attached to St-Phe ($k_q = 1.15 \times 10^{10}\ M^{-1}s^{-1}$) is approximately a factor of two smaller than that for PheMP. The diffusion coefficients (D) calculated from *Eq 2* for these experiments are 4.7×10^{-5} and 2.7×10^{-5} cm^2/s, respectively. The reduced value of D for the St-Phe system reflects simply the fact that polymer bound phenanthrene diffuses slower than PheMP in solution. Note that if the contribution to D from local motions of the polymer (St-Phe) were zero, then the value of D obtained ought to have been exactly half that found for oxygen quenching of PheMP. These results, however,

do not prove that polymer motion makes a contribution to quenching, as other factors, such as a reduced oxygen diffusion coefficient inside the polymer coil would have the same effect.

The steady-state quenching data (I^0/I) for C-Phe also conform to *Eq 1*. This is gratifying in view of the complex nature of the colloidal materials. From the slope of the plot, a quenching rate constant equal to $0.81 \times 10^{10}\ M^{-1}s^{-1}$ is calculated. This quenching rate constant corresponds to $D = 1.91 \times 10^{-5}\ cm^2/s$. The fact that it is less than the value for St-Phe suggests that the oxygen concentration, or oxygen mobility in the stabilizer domain of the particle, is reduced over that of the solution as a whole.

A deeper insight into this phenomenon is revealed upon examination of the transient fluorescence decay traces from oxygenated samples of St-Phe and C-Phe in cyclohexane, shown in *Fig. 4*. Notice that as the oxygen concentration is increased, the plots of log I *vs.* time for both samples become increasingly steep. If the short component ($\tau = 1.2$ ns) is ignored, we find that when the $[O_2] = 0$, the C-Phe decay is exponential. In the presence of oxygen, however, the decays become increasingly nonexponential.

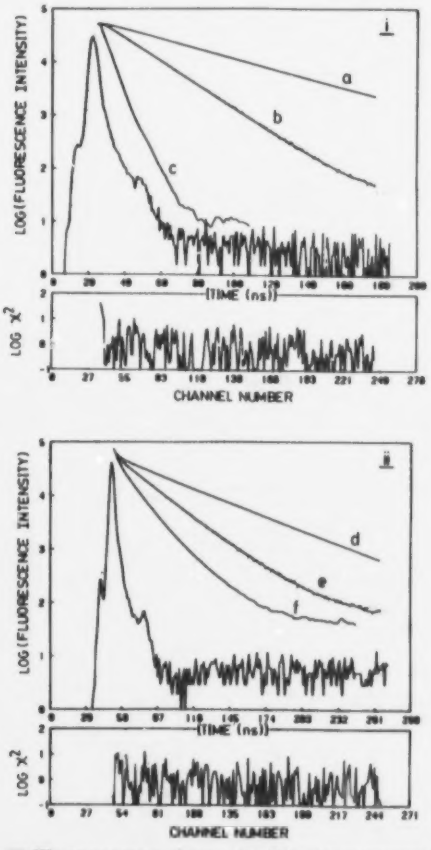

Fig. 4. (i) Fluorescence decay profiles of nitrogen (a), air (b), and oxygen (c) saturated samples of St-Phe (3.0 mg/ml) in cyclohexane at 23°C. (ii) Fluorescence decay curves from cyclohexane dispersions of C-Phe (10 mg/ml) containing 0 (d), 2.08 × 10^{-3} M (e), and 5.40 × 10^{-3} (f) M oxygen.

This implies that phenanthrene labels are located in a distribution of environments; each characterized by its own oxygen concentration and quenching rate constant. This behavior is very different from that for oxygenated and deoxygenated samples of St-Phe where the decay profiles remain exponential.

In order to analyze the kinetics of oxygen quenching of C-Phe, from the transient decay data, average decay times $\langle\tau\rangle$ were calculated. By definition, the average decay time $\langle\tau\rangle$ is given by

$$\langle\tau\rangle = \frac{\int_0^\infty tI(t)dt}{\int_0^\infty I(t)dt} \qquad (10)$$

where $I(t)$ describes the form of the fluorescence decay and t is the time. $I(t)$ was found by fitting the C-Phe decay data to a sum of three exponential components, (*Eq. 11*).

$$I(t) = a_1\exp(-t/\tau_1) + a_2\exp(-t/\tau_2) + a_3\exp(-t/\tau_3) \qquad (11)$$

The contribution due to the parasitic short component was removed by fitting the decay data to *Eq 11* and fixing the decay time of the first component at $\tau = 1.2$ ns. We do not ascribe significance to the values of the individual parameters (the second and third components), but rather we use them to calculate mean decay times $\langle\tau\rangle$ via *Eq 12*.

$$\langle\tau\rangle = \frac{a_2\tau_2^2 + a_3\tau_3^2}{a_2\tau_2 + a_3\tau_3} \qquad (12)$$

The decay parameters characterizing the fluorescence decay profiles of PheMP, St-Phe, and C-Phe are shown in *Tables 1* and *2*. Also listed in *Table 2* are the mean decay times $\langle\tau\rangle$ calculated using *Eq 12*. Values of $\tau^0/\langle\tau\rangle$ *vs.* $[O_2]$ are plotted in *Fig. 3*. The fact that these data fall on the line defined by the steady-state results supports the legitimacy of treating the decay data as we did. However, because a distribution of quenching rate constants exist, the data in the plot for C-Phe in *Fig. 3*, and the value of k_q obtained from it, represent an average of all the quenching events. We suggest that some of the labels are quenched with a k_q similar to that of the free stabilizer, and others, buried in the interphase, with a much smaller quenching rate constant.

Table 1. Fluorescence Decay Times from Oxygen Quenching Studies of PheMP and St-Phe in Cyclohexane at 23°C. λ_{ex} = 295 nm.

Condition	$[O_2]$ (*M*)	Fluorescence Decay Time (ns)	
		PheMP	St-Phe
nitrogen	0	46.59	46.65
air	2.08×10^{-3}	16.14	21.57
oxygen	10.8×10^{-3}	4.04	7.59

Table 2. Fluorescence Decay Parameters from Oxygenated and Nitrogen Purged Dispersions of C-Phe in Cyclohexane at 23°C. The Short Component (τ_1 = 1.2 ns) for Each Decay Curve Was Used as an Input Parameter in the Curve Fitting Routine. λ_{ex} = 295 nm.

[Oxygen] ($M \times 10^3$)	τ_2	τ_3	$A1$	$A2$	$A3$	$\frac{A3}{A2 + A3}$	τ
0	—	45.6	0.044	—	0.021	—	45.6
1.40	8.3	36.2	0.121	0.014	0.076	0.84	35.1
1.73	8.2	31.4	0.158	0.024	0.082	0.77	29.8
2.08	19.5	29.0	0.437	0.121	0.088	0.42	24.4
2.70	14.4	24.0	0.204	0.039	0.053	0.58	21.1
3.13	12.9	24.2	0.377	0.114	0.089	0.44	19.6
3.78	11.1	22.6	0.434	0.098	0.149	0.60	19.8
4.64	12.0	23.9	0.501	0.206	0.053	0.21	16.0
5.40	10.1	21.5	0.348	0.129	0.036	0.22	14.4

This analysis would be more rigorous if the parasitic fluorescence with τ = 1.2 ns (and not susceptible to oxygen quenching), were not present. However, it is clear that a single population of phenanthrene labels does not exist within C-Phe particles. In other experiments involving oxygen quenching in PVAc particles labeled in the core with phenanthrene (CLC-Phe), we have found that the fluorescent groups are less susceptible to quenching (19). Nevertheless, a detailed analysis of the non-linear Stern-Volmer plots indicated that a significant fraction of the phenanthrene groups in the core-labeled particles are readily quenched. The others seem to be located in an environment where they are protected from quenching by oxygen. We interpret this result to imply that there is a substantial interphase region consisting of PEHMA and PVAc chains. In this region Phe* groups can be quenched by O_2 but at a rate significantly slower than those on the stabilizer chains protruding into the solvent.

Pyrene Labeled Particles

Previous work in our research group has shown that the kinetics of excimer formation between two pyrene labels covalently attached to the ends of a polymer chain can be described accurately employing the two-state excimer model described earlier (13). Ignoring polydispersity effects, this result is obtained because a unique rate constant k_1 describes the process of excimer formation (14b, 20). For randomly labeled stabilizers and colloids, however, the picture is more complicated (14a). Excimers may form both between pyrene pairs that are spaced close together and far apart along a stabilizer chain. In the colloidal systems, excimer formation might also occur between labels located on adjacent stabilizer chains. The kinetics of excimer formation in these kinds of systems should be much more complicated. One expects nonexponential fluorescence decays. One might resort to a model invoking a distribution of cyclization rates: the distribution of pyrene-pyrene separations leads to a distribution of excimer formation rate constants. Alternatively, one might focus on mean decay times ($\langle\tau\rangle$) for the system and use these to calculate mean rate constants ($\langle k_1\rangle$) for excimer formation.

Stabilizer-labeled dispersions containing a low (C-PyL: 0.81 mole percent) and a high (C-PyH: 2.80 mole percent) pyrene loading were prepared. From UV and HPLC measurements we calculated that on average the stabilizers St-PyL and St-PyH contain approximately 2 and 7 pyrenes per chain, respectively (19). NMR measurements indicate that C-PyL and C-PyH contain 6.9 and 8.5 wt. percent stabilizer. The average particle diameters of C-PyL and C-PyH were found to be 266 and 240 nm, respectively.

Figure 5 shows the UV spectra of clear ethyl acetate solutions of C-PyH (0.825 mg/ml) and model compound, PyMP (1.22×1^{-5} *M*). Notice that the spectrum of C-PyH is significantly broader than that of PyMP. Similar effects have been observed in comparing the UV spectra of polyesters bearing pyrenylmethyl groups and the corresponding model compounds (21). These effects have been attributed to pyrene-pyrene interactions of the polymer bound chromophores. The degree of chromophore aggregation, of course, reflects the local concentration of pyrene within the polymer coil.

The UV spectra of solutions of C-PyL, St-PyL, and St-PyH in ethyl acetate show the same characteristic absorption peaks as for PyMP and C-PyH. However, after normalizing the spectra at 342 nm, one observes that the broadness of the peaks vary. In order to characterize the broadness of the five spectra, the width at half height ($W_{1/2}$) of the absorption bands centered at 342 nm were measured. The values of $W_{1/2}$, relative to that for PyMP are presented in *Table 3*.

The value of $W_{1/2}$ for St-PyH is greater than the value for St-PyL. This is expected since St-PyH has a higher pyrene loading and thus a higher local concentration (C_{eff}) of labels. Note also that for both systems, $W_{1/2}$ increases upon stabilizer anchoring. This result suggests that during the dispersion polymerization of C-PyL and C-PyH, the stabilizer chains become interconnected. If this were not the case, then upon dissolution in ethyl acetate, the anchored stabilizer chains would become evenly distributed throughout the solution and, therefore, would yield UV spectra identical to those of the respective free stabilizers.

The most interesting observation concerning

the data in *Table 3*, however, is that $W_{1/2}$ for C-PyL is greater than the value for St-PyH. Thus, the local concentration of pyrene groups in the dissolved C-PyL colloid sample (which contains 2 pyrene labels per stabilizer chain) is greater than the local concentration in St-PyH (which contains 7 labels per chain). In other words, the stabilizer chains in the dissolved C-PyL sample, perhaps by virtue of grafting to PVAc, must be more concentrated locally than for isolated St-PyH chains in ethyl acetate. We expect that in the native colloidal state, the stabilizer chains are concentrated to an even greater extent.

Normalized steady-state fluorescence emission spectra of C-PyH, St-PyH, and PyMP in deoxygenated cyclohexane at 23°C, excited at 345 nm are shown in *Fig. 6*. Note that no parasitic fluorescence is observed in these decays. At this excitation wavelength, the extinction coefficient of the impurity is zero. The fluorescence from the labeled polymers and the model compound, at short wavelengths, are very similar. This structured emission is due to the $S_1 \rightarrow S_0$ transition of monomeric pyrene species (12). The feature that distinguishes these spectra is the broad structureless emission centered at 470 nm, observed in the spectra of C-PyH and St-PyH. This emission is due to pyrene excimer. The absence of pyrene excimer in the fluorescence spectrum of PyMP is due to the low pyrene concentration in the sample. The fact that excimer emission is observed for C-PyH and St-PyH shows that pyrene groups can indeed associate when they are covalently attached to both free and anchored stabilizer chains.

The fluorescence spectrum of PyMP was subtracted from the spectra of the labeled polymers yielding the resolved excimer bands. The difference spectra for C-PyH are presented in *Fig. 7*. The intensities of excimer emission (I_E) for both excimer bands were calculated by numerical integration. Dividing I_E values by the total integrated area of the PyMP spectrum (I_M) yields the excimer to monomer intensity ratios (I_E/I_M), listed in *Table 4*. Also presented in *Table 4* are I_E/I_M values for samples of C-PyL and St-PyL. If

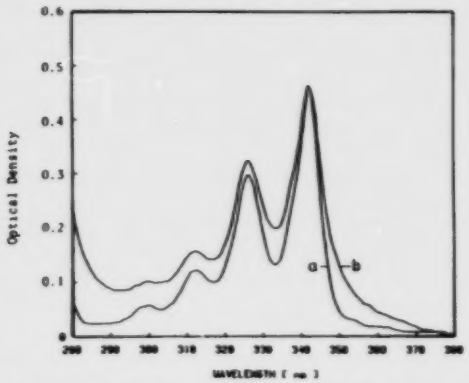

Fig. 5. Ultraviolet absorption spectra of ethyl acetate solutions of phenanthrylmethyl pivalate (a, 1.22×10^{-5} M) and C-PyH (b, 0.83 mg/ml) at 25°C. The spectra are normalized at 343 nm.

Table 3. Relative Spectral Broadening Factors ($W_{1/2}$) for the UV Absorption Peaks Centered at 343 nm for C-PyL, C-PyH, St-PyH, and St-PyL.

Sample	$W_{1/2}$
PyrMP	1.0
St-PyL	1.11
St-PyH	1.17
C-PyL	1.25
C-PyH	1.35

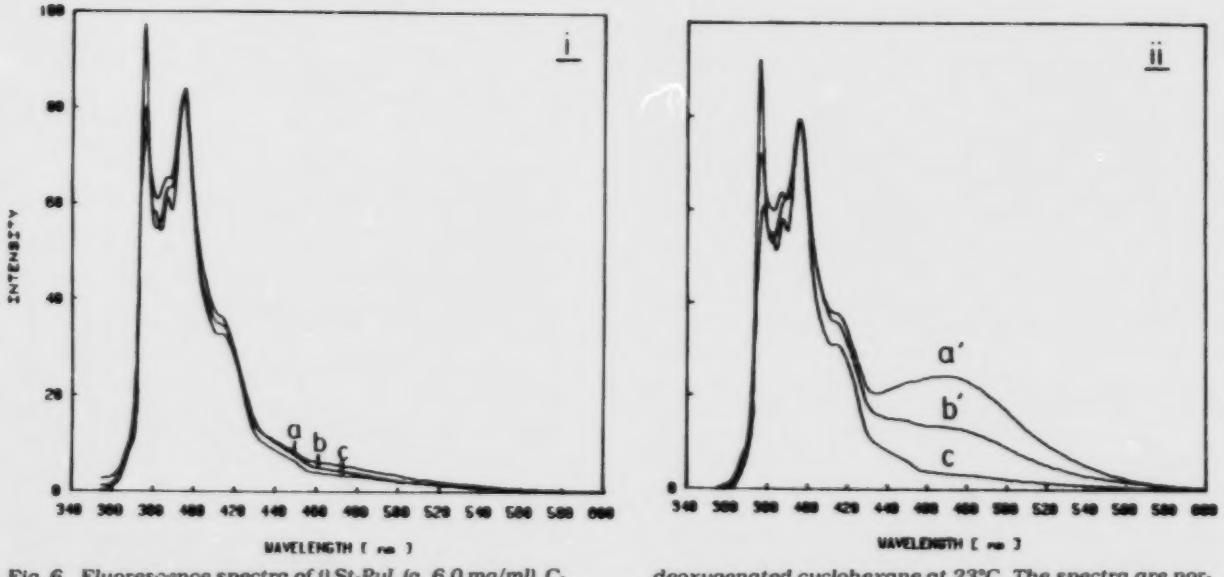

Fig. 6. Fluorescence spectra of i) St-PyL (a, 6.0 mg/ml), C-PyL (b, 11.0 mg/ml), and pyrenylmethyl pivalate (c, 1.2×10^{-4} M); ii) St-PyH (a', 3.1 mg/ml), C-PyH (b', 2.0 mg/ml) in deoxygenated cyclohexane at 23°C. The spectra are normalized at 396 nm. $\lambda_{ex} = 345$ nm.

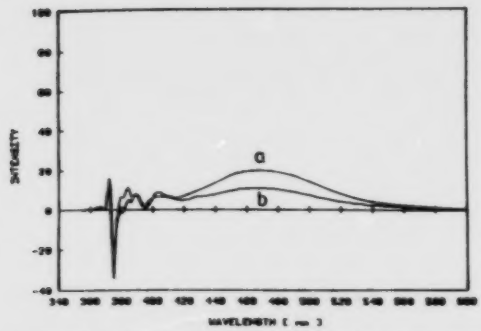

Fig. 7. Resolved excimer emission bands for samples of St-PyH (a) and C-PyH (b). Obtained by subtracting the normalized fluorescence spectrum of pyrenylmethyl pivalate (PyMP) from the fluorescence spectra of St-PyH and C-PyH (Fig. 5).

Table 4. Ratios of Excimer to Monomer Fluorescence Intensity (I_E/I_M) for Pyrene Labeled Stabilizers and Colloids.

Sample	I_E/I_M ∝ $\langle k_1 \rangle$	Average number of Pyrene labels per stabilizer chain
St-PyH	0.513	7
C-PyH	0.250	7
St-PyL	0.079	2
C-PyL	0.049	2

k_1 in *Eq 9* is replaced by the average quantity $\langle k_1 \rangle$, then according to our model, these data provide estimates of the mean rate constants for excimer formation.

The important observation to be made from the data in *Table 4* is that anchoring both St-PyL and St-PyH causes I_E/I_M to decrease by a factor of about 2. *Equation 9* predicts that both the mean rate constant for excimer formation $\langle k_1 \rangle$ and C_{eff}/η also decrease by a factor of 2. This prediction is at odds with the results from the UV absorption experiments; there we find a substantial increase in C_{eff} upon anchoring the stabilizer chains. In order to account for the reduction in the ratio C_{eff}/η upon stabilizer anchoring, one might conclude that the viscosity in the vicinity of individual stabilizer chains increases by an amount 2 times greater than the corresponding increase in C_{eff}. Intuitively, this explanation seems quite reasonable. However, if it were correct in detail then similar trends in $\langle k_1 \rangle$ upon anchoring the stabilizers ought to be obtained from the fluorescence decay data. These, however, also indicate that the average rate constant for excimer formation increases upon stabilizer anchoring.

Pyrene monomer fluorescence decay profiles from samples of St-PyH, C-PyH, and PyMP in deoxygenated cyclohexane at 23°C are presented in *Fig. 8*. Notice that the fluorescence from PyMP decays exponentially. The emissions from St-PyH and C-PyH, however, are clearly nonexponential. This is also true for the St-PyL and C-PyL monomer decay profiles. These results support our model invoking a distribution of rate constants for excimer formation in the pyrene-labeled colloidal systems.

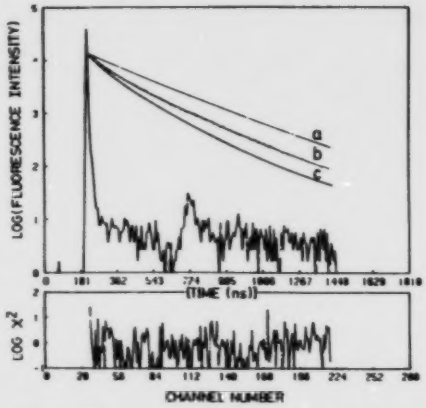

Fig. 8. Fluorescence decay profiles ($I_M(t)$) of samples of pyrenylmethyl pivalate (a, 2.2×10^{-6} M), St-PyH (b, 1.5 mg/ml), and C-PyH (c, 12.4 mg/ml) in deoxygenated cyclohexane at 23°C. $\lambda_{ex} = 345$ nm.

As was done in the oxygen quenching studies on phenanthrene-labeled particles, we chose also to fit our time-dependent pyrene fluorescence decay data to a sum of three exponential components (*Eq 11*). Values of $\langle \tau \rangle$ were calculated employing *Eq 12* (22). Using a modified form of *Eq 5*,

$$1/\langle \tau \rangle = \langle k_1 \rangle + k_M \qquad (13)$$

estimates of the mean rate constant for excimer formation were calculated.

The characteristic decay times and pre-exponential factors for the curves in *Fig. 8*, and those from samples of St-PyL and C-PyL are listed in *Table 5*. For example, the fluorescence decay from C-PyH is characterized by decay times of 28.9, 128.9, and 240.5 ns. According to our model which predicts a distribution of excimer formation rate constants, these values are attributed to pyrene-pyrene pairs whose separations cover a broad range of distances; those that are closely spaced yield short decay times and those that are far removed yield long decay times. Notice also that even the long decay times in the C-PyH samples are significantly shorter than the decay time of PyMP. This suggests that all the pyrene labels in C-PyH are involved in excimer formation. Excimer formation is defined here as any bimolecular process of the form

$$Py^* + Py \rightarrow (Py\text{-}Py)^* \rightarrow 2Py$$

which shortens the fluorescence decay time or decreases the luminescence intensity of the excited species. In solution, where there is sufficient mobility, all excimer pairs can relax to the preferred excimer geometry and all have an equal probability of emitting (12). In constrained systems, it is possible for a Py^* to be quenched by contact with another Py without being able to reach the proper geometry for excimer emission to occur. The excitation en-

Table 5. Monomer Decay Times (ns) and Coefficients from Fluorescence Decay Profiles[a] of PyrMP and Pyrene Labeled Polymers. Deoxygenated Samples in Cyclohexane were Investigated. λ_{ex} = 345 nm.

Sample	τ_1	τ_2	τ_3	$A1$	$A2$	$A3$	$A3/\Sigma A'$ (%)
PyrMP	—	—	273.9	—	—	—	100
St-PyL	—	140.2	273 9	—	0.26	1.0	79.6
C-PyL	11.6	146.0	273.9	0.31	0.53	1.0	54.3
St-PyH	32.9	134.3	269.8	0.29	1.10	1.0	41.8
C-PyH	28.9	128.9	240.5	0.67	1.42	1.0	32.3

[a]All χ^2 factors are less than 1.38.

ergy is dissipated non-radiatively. We refer to this particular self-quenching process as involving non-emissive excimers.

Table 6 lists the mean decay times and mean rate constants, calculated from *Eqs 12* and *13*, respectively, using the data in *Table 5*. From these data one observes that the values of $\langle k_1 \rangle$ for St-PyH and C-PyH are greater than the values for St-PyL and C-PyL, respectively. Of interest, however, is the fact that $\langle k_1 \rangle$ increases when the stabilizer chains become anchored in the particle. While this result by itself is reasonable, it appears to contradict the steady-state data which indicate that $\langle k_1 \rangle$ decreases upon stabilizer anchoring.

We explain these conflicting results as follows. Excimer to monomer intensity ratios decrease upon stabilizer anchoring because the number of pyrene labels capable of achieving the emissive excimer geometry decreases; a certain fraction of the pyrenes are simply quenched (10). On the other hand, $\langle k_1 \rangle$ increases because the formation of both emissive and nonemissive excimers contribute to the reduction in the average pyrene decay time.

In order to account for these observations, we introduce a model that accommodates the possibility that only a certain fraction (γ) of the pyrenes which are quenched in the anchored stabilizer form emissive excimers.

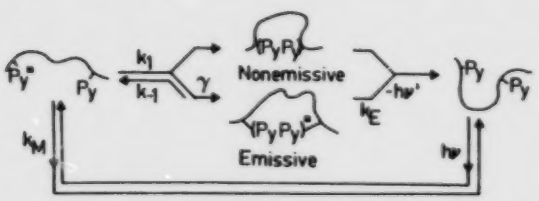

This model assumes that both emissive and non-emissive excimers form with the same average rate constant ($\langle k_1 \rangle$). For transient experiments, this model predicts for $I_M(t)$ an expression identical to that in *Eq 3*, where $\lambda_1 = \langle k_1 \rangle + k_M$. For steady-state data, however, the form of the ratio I_E/I_M is

$$\frac{I_E}{I_M} = \frac{\Phi_E^0}{\Phi_M^0} \frac{\gamma \langle k_1 \rangle}{k_M} \quad (k_E > k_{-1}) \qquad (7c)$$

The magnitude of I_E/I_M for pyrene-labeled stabilizer (St) relative to that for the corresponding colloidal (C) material can, therefore, be expressed as

Table 6. Mean Decay Times $\langle \tau \rangle$ and Mean Rate Constants $\langle k_1 \rangle$ for Pyrene Labeled Stabilizers and Colloids.

Sample	$\langle \tau \rangle$ (ns)	$\langle k_1 \rangle$ (sec^{-1})
PyrMP	273.9	—
St-PyL	258.4	2.19×10^6
C-PyL	243.4	4.57×10^6
St-PyH	217.7	9.43×10^5
C-PyH	185.1	1.75×10^6

$$\frac{I_E(St)/I_M(St)}{I_E(C)/I_M(C)} = \frac{\gamma(St)\langle k_1(St) \rangle}{\gamma(C)\langle k_1(C) \rangle} \qquad (14)$$

Because excimers formed from pyrene groups attached to flexible polymers are normally emissive, we assume that $\gamma = 1$ for solutions of St-PyL and St-PyH.

When the steady-state and transient data in *Tables 4* and *6* are treated using *Eq 14*, estimates of the γ factors for C-PyL and C-PyL can be obtained. Substituting the appropriate values of I_E/I_M and $\langle k_1 \rangle$ into *Eq 14* yields $\gamma = 0.28$ for both C-PyL and C-PyH. We attribute these small γ factors to the relatively small number of segments in the stabilizer phase that can undergo unrestricted motions. These results suggest that a large proportion of the pyrene labels, and stabilizer segments, are in a region of high segment density; presumably in the interphase. They have sufficient motional freedom to interact but not enough for the pyrenes to be able to form the most stable excimer geometry.

The fact that γ(C-PyL) = γ(C-PyH) suggests that the mechanism of stabilizer anchoring in the synthesis of these dispersions is similar. Finally, these results are consistent with our UV data which suggest that the stabilizer chains are concentrated in the steric barrier, and also with our model predicting an interphase region within individual colloidal particles.

CONCLUSIONS

In this paper, we examined the consequences of anchoring stabilizer chains to the surface of PVAc particles. Oxygen quenching experiments on particles labeled with phenanthrene in the stabilizer phase suggest that phenanthrene labels, and therefore stabilizer chains, are located in a distribution of environments of varying segment density and fluidity. The majority of labels exist near the surface of the particles, in

the stabilizer layer. The rest are in a region protected somewhat from oxygen. Oxygen quenching experiments (19) on PVAc particles labeled in the particle core with phenanthrene show that many of the labels are readily accessible to oxygen quenching. From this result we conclude that a significant portion of the labels (and PVAc chains) are located in a swollen environment, presumably intermixed with the anchored stabilizer chains. Thus, we infer that an extensive interphase rather than a distinct interface exists between the stabilizing polymer and the PVAc core polymer.

Experiments probing excimer formation in PVAc particles labeled in the stabilizer layer with pyrene yield information on stabilizer conformation and dynamics when these polymers are anchored in the particle surface. UV measurements monitoring the breadth of pyrene absorption bands for free and anchored stabilizers provided evidence that stabilizing chains become locally concentrated in the stabilizer layer. There are some indications that these polymers become interconnected as a result of graft formation during particle synthesis. Steady-state and transient fluorescence studies indicate that only a small portion of the pyrene labels (ca. 28 percent) and thus stabilizer chains are capable of sufficient diffusive motions to form excimers in the proper geometry for excimer emission to occur. The majority of the pyrene labels (ca. 72 percent) were found to form non-emissive excimers. These nearby chromophores are close enough to interact through very localized motion, but lack the mobility to form the geometry required for excimer emission. The predominance of non-emissive excimer formation provides strong evidence for high polymer segment density within the stabilizer layer, and for relatively restricted chain motion for chains in and adjacent to the interphase layer.

REFERENCES

1. C. W. Frank and M. A. Gashgari, *Ann. N.Y. Acad. Sci.*, **366**, 387 (1981).
2. (a) H. Morawetz, *Ann. N.Y. Acad. Sci.*, **366**, 404 (1981).
   (b) H. Morawetz, *Polym. Eng. Sci.*, **23**, 689 (1983).
3. A. Ledwith, *Pure Appl. Chem.*, **54**, 549 (1982).
4. J. L. Halary, J. M. Ubrich, J. M. Nunzi, L. Monnerie, and R. S. Stein, *Polymer*, **25**, 956 (1984).
5. R. L. Levy and D. P. Ames, *Org. Coat. and Appl. Polym. Sci. Proc.*, **48**, 116 (1983).
6. (a) R. O. Loutfy, *J. Polym. Sci., Polym. Phys. Ed.*, **20**, 825 (1982)
   (b) K. Y. Law and R. O. Loutfy, *Macromolecules*, **14**, 587 (1981).
7. Refer to the paper by C. C. Han, M. Okada, Y. Muroga, F. L. McCrackin, B. J. Bauer, and Q. Tran-Cong, in this issue.
8. K. E. J. Barrett, Ed., "Dispersion Polymerization in Organic Media", Wiley-Interscience, New York, (1975).
9. D. H. Napper, in "Colloid and Interface Science", M. Kerker, R. L. Rowell and A. C. Zettlemoyer, Eds., Vol. 1, pp. 413–430 New York, (1976).
10. (a) O. Peckan, M. A. Winnik, L. S. Egan, and M. D. Croucher, *Macromolecules*, **16**, 699 (1983).
    (b) M. A. Winnik, *Polym. Eng. Sci.*, **24**, 87 (1984).
11. (a) D. A. Holden, D. Ng, and J. E. Guillett, *Brit. Polym. J.*, 159 (1982).
    (b) D. Ng and J. E. Guillet, *Macromolecules*, **15**, 724 (1982).
12. J. B. Birks, "Photophysics of Aromatic Molecules", Ch. 7, Wiley-Interscience, New York, (1971).
13. M. A. Winnik, A. E. C. Redpath, K. Paton, and J. Danhelka, *Polymer*, **25**, 91 (1984).
14. (a) C. Cuniberti and A. Perico, *Europ. Polym. J.*, **16**, 887 (1980).
    (b) C. Cuniberti and A. Perico, *J. Polym. Sci., Polym. Phys. Ed.*, **15**, 1435 (1977).
15. J. R. Lackowitz, "Principles of Fluorescence Spectroscopy", pp. 260–275. Plenum, New York, (1983).
16. Size dispersity factors reflect the broadness of the particle size distribution and are calculated from the equation $a = (\langle S \rangle - 1)^{1/2}\langle D \rangle$, where a is the standard deviation of the mean particle size. $\langle S \rangle$ values less than 1.02 denote a monodisperse sample.
17. W. R. Ware, In "Creation and Detection of the Excited State", A. A. Lamola, Ed., Vol. 1, Part A, Ch. 5 Marcell Dekker, New York, (1971).
18. J. N. Demas, "Excited State Lifetime Measurements", Ch. 8 and 9 Academic Press, New York, (1983).
19. L. S. Egan, M. A. Winnik, and M. D. Croucher, to be published.
20. G. Wilemski and M. J. Fixman, *J. Chem. Phys.*, **80**, 866 (1980).
21. S. Tazuke, H. Ooki, and K. Sato, *Macromolecules*, **15**, 400 (1982).
22. A similar treatment was employed by Bauer, *et al.* in studies of the photophysics of pyrene adsorbed on silica particles; R. K. Bauer, P. de Mayo, K. Odaka, W. R. Ware, and K. C. Wu, *J. Phys. Chem.*, **87**, 460 (1983).

NOMENCLATURE

- I^0 = Fluorescence intensity in the absence of added quencher.
- τ^0 = Fluorescence decay time in the absence of added quencher.
- I = Fluorescence intensity in the presence of added quencher.
- τ = Fluorescence decay time in the presence of added quencher.
- k_q = Bimolecular quenching rate constant.
- $[Q]$ = Quencher concentration.
- k_{diff} = Diffusion controlled rate constant.
- N_A = Avogadro's number.
- D = Sum of the diffusion coefficients of the interacting species ($D_F + D_Q$).
- p = Reaction probability per collision.
- k_1 = Rate constant for pyrene excimer formation.
- k_{-1} = Rate constant for pyrene excimer dissociation.
- k_M = Reciprocal pyrene monomer decay time.
- k_E = Reciprocal pyrene excimer decay time.
- $I_M(t)$ = Time dependence of pyrene monomer emission.
- $I_E(t)$ = Time dependence of pyrene excimer emission.
- A, λ = Fluorescence decay parameters.
- τ_M = Pyrene model compound fluorescence decay time.
- $\Phi_M{}^0$ = Quantum yield of pure pyrene monomer emission.
- $\Phi_E{}^0$ = Quantum yield of pure pyrene excimer emission.

$k^{(2)}$ = Second order rate constant for excimer formation.
C_{eff} = Effective concentration of pyrene species.
η, T = Solvent viscosity and temperature.
$\langle\tau\rangle$ = Average fluorescence decay time.
$W_{1/2}$ = UV resolution factor.
γ = Fraction of quenched pyrenes that form emissive excimer.

DISCUSSION: LUKE EGAN

J Bley: You stated that these fluorescence techniques are powerful methods to study polymer blends morphology. You have shown that to identify the interactions on the outside or inside of the particles, the fluorescence quenching method can be used. On your graph you indicated that the half-life times are very short, of the order of nanoseconds. The question is: in preparing these blends and studying the morphology, what time scale are you using if the lifetime is so short?

L. Egan: With our instrument, called a "time-correlated single photon counter" we can measure phenomena occurring on time scales ranging from 0.5 to 1000 ns, with good accuracy. In the oxygen quenching studies, the fluorescence decay from excited phenanthrene groups was measured. In the absence of oxygen, phenanthrene has a fluorescence lifetime of 46 ns. Thus, the characteristic time scale of the experiment is 46 ns. The distance (X_{av}) over which a quencher can diffuse during the lifetime of the excited state can be estimated from the equation ($X_{av} = (2Dt)^{1/2}$), where t is time and D is a diffusion coefficient. For example, the distance oxygen can travel on average, in 46 ns, in a solution where $D = 2 \times 10^{-5}$ cm^2/s, is approximately 13.5 nm. Thus the excited phenanthrene is sensitive to and can report information about a rather large surrounding environment.

J. Bley: My question was not clear. You indicated that preparations and purifications also provide time for exposure to air. This time is obviously much longer than nanoseconds.

L. Egan: You are right. There is a second time scale that is important. It is the time scale for oxygen to diffuse into the particle when the dispersion is first exposed to air or oxygen. When we do the experiments we start by deoxygenating the sample. What we observe is that the samples come to equilibrium during the few seconds that gas is bubbled into the sample cell.

L. A. Utracki: You have been saying that these methods are very precise, very useful to study morphology of polymer blends. Nevertheless, you showed the behavior of dispersions of poly(vinyl acetate) particles in organic solvents, not exactly a polymer blend. Furthermore, on the basis of kinetic constants obtained from your experiments, one can conclude that there are only two types of traps: the readily accessible, located on the surface of the particles, and the somehow less accessible, located in the solvent-swollen shell of the particle. In short, your statement can be interpreted as saying that the interior of the particles are inaccessible to your probes, it is opaque. If so, this is equivalent to admission that the oxygen quenching method is not applicable to polymer blends. Could you please summarize shortly your point of view regarding the applicability of other fluorescence techniques to the study of polymer blends.

L. Egan: Let me address your opening comment first. One can define a polymer blend as an intimate mixture of two or more polymeric components: these components can be miscible on a molecular level, or can exist as distinct phases within the bulk material. From our studies we concluded that the morphology of our PVAc particles is more complicated than that predicted by the "core-shell" model; there also exists a substantial interphase region composed of both core and stabilizing polymer. Then on a molecular level distance scale, I suggest that our colloidal particles are, in fact, blends because some of the polymer is intimately mixed and the rest presumably exists as pure homopolymer in separate phases. Whether oxygen quenching as a technique is applicable to the study of more classical blends depends upon three factors: the lifetime of the excited state of the dye, the solubility of O_2 in each phase, and its local diffusion coefficient.

R. E. Prud'homme: Did you say that when the labels are in the core of the particles the labels are not accessible to oxygen quenching?

L. Egan: What I was trying to say was that if we have a core of poly(vinyl acetate) with a little bit of phenanthrene groups in it, we find using a simple kinetics model that assumes two distinct populations of fluorophores (one accessible and one inaccessible) that about 50 percent of these groups are inaccessible to oxygen quenching. I should have been more careful about how I used the term "inaccessible". In fact, although we do not report here the data obtained from oxygen quenching studies on the core-labeled particles, it was found that the lifetime of the inaccessible phenanthrenes was slightly reduced (ca. 5 percent) by the addition of oxygen at room temperature. Thus the phenanthrenes that I refer to as inaccessible are actually slightly quenched and the assumption that we have accessible and absolutely inaccessible populations in the particles is indeed an approximation. At 50 and 90°C, which is well above the T_g of pure PVAc, much larger changes

in the lifetime of the "buried" labels are observed upon the addition of oxygen.

L. A. Utracki: If I may enlarge on your statement. Observing the quenching of 50 percent of the phenanthrene groups could tell you something about the volume of particle swollen if the placement of the phenanthrene groups in the mass of PVAc particle is random. Even if the reactivity ratios of vinyl acetate and phenanthrylmethyl methacrylate were the same, due to immiscibility of the two components one should expect expulsion of the phenanthrene groups towards the surface. One could probably examine this phenomenon by following the particle swelling kinetics using quenching methods.

L. Egan: You are right. The distribution of phenanthrenes in the PVAc phase of the particles may not be random and thus it is not entirely correct to say that 50 percent of the PVAc phase is swollen with solvent. One might also get at this problem using staining techniques in conjunction with electron microscopy on crosslinked PVAc particles.

C. C. Han: What is the polydispersity of your particle size?

L. Egan: For the particles stabilizer labeled with phenanthrene, 80 percent of the particles have diameters between 200 and 370 nm with a mean value of 314 nm. For the unlabeled system, 80 percent of the particles have diameters between 235 and 335 nm with a mean of 295 nm. The reason for the broadened distribution in the fluorescently labeled particles is not clear.

C. C. Han: So it is fairly polydispersed. How does this affect your data analysis? Polydispersity will also give you a distribution of the swollen *vs.* not-swollen portion of the particles. This must be taken into account in the decay analysis. You used one short decay time plus two long ones. What would happen if instead you used three or four long components?

L. Egan: We worried about this problem. Using a computer, we generated synthetic decay functions having up to ten exponential terms. We found that as long as the parameters used in generating the decay vary smoothly, we could fit practically all of our complex decay functions to double exponential functions. Also, the mean lifetimes calculated from, for example, the ten and two exponential functions are identical. In this work, we are dealing primarily with mean lifetimes and so we feel that fitting the long components of our decays to double exponential functions is adequate. Nonetheless, we are currently trying to prepare monodisperse distributions of particles.

C. C. Han: If you have monodispersed particles then you can easily do scattering experiments to characterize the core-shell structure.

Flow Properties of Low Density/Linear Low Density Polyethylenes

D. ACIERNO

Istituto di Ingegneria Chimico-Alimentare
University of Salerno
Salerno, Italy

and

D. CURTO, F. P. LA MANTIA, *and* A. VALENZA.

Istituto di Ingegneria Chimica
University of Palermo
Palermo, Italy

Rheological data have been collected both in shear and non-isothermal elongational flow on three different types of blends, made from one low density polyethylene sample and three linear low density polyethylene samples.

In addition to the flow curves, data are presented on the extrudate-swell phenomenon, on the instability arising in capillary flow and on the tensile behavior in the molten state.

INTRODUCTION

The rheological behavior of polymer blends has in recent years been widely studied in view of the growing interest in such systems and in view of the relevance to processing (1–16). Of course, the flow properties of blends may heavily depend on the mutual compatibility in the molten state of the parent polymers, which in turn should depend on their structure.

Following a rather complete study of the rheology of high density polyethylene/low density polyethylene blends, HDPE/LDPE, (13–15) the aim of this work is to present a set of data on blends obtained by melt mixing linear low density polyethylene, LLDPE, and low density polyethylene samples. From a fundamental point of view it is interesting to evaluate the influence of LLDPE short chain branches, and from an applications viewpoint the data are of great importance because of the possibility of employing such blends in the preparation of improved films without drastic changes in processing equipment and conditions.

Data have been collected both in shear and (non-isothermal) elongational flow on three different types of blends, made from one low density polyethylene sample and three linear low density polyethylene samples. Particular emphasis has been given to the more relevant aspects of the applications, and thus, in addition to the viscosity curves, data are presented on the extrudate-swell, on the instabilities arising in capillary flow, and on the tensile behavior in the molten state.

EXPERIMENTAL

Three samples of LLDPE, polymerized with 1-butene as comonomer and already characterized both from a physico-chemical and a rheological point of view (17), and one sample of LDPE also previously considered (18) have been employed in the preparation of blends.

In the following the samples will be indicated as LD and LL instead of LDPE and LLDPE. The nomenclature of the LL samples will comprise the approximate indication of the melt flow index (*MFI*). The main physico-chemical characteristics of the samples are listed in *Table 1*.

The density, ρ, was measured at 23°C, according to the ASTM-D-1505/68 method. The melt flow index, *MFI*, was evaluated according to the ASTM-D-1238/73 method, procedure B, with a CEAST apparatus. The weight average molecular weight, M_w, and the dimensionless polydispersity, $\beta = M_w/M_n$, were determined by GPC in o-dichlorobenzene, ODCB, at 135°C, with a Waters instrument.

Blends from each LLDPE and LDPE have been prepared at various LDPE content, φ. In all cases the polymers have been mixed for about 20 min at 20 rpm and 210°C in a Brabender Plasticorder equipped with a cam mixer. The torque values have been recorded at the end of the mixing runs.

Rheological measurements in shear flow were carried out in the low shear rate region with the aid of a rotational viscometer in a cone and plate mode (Rheotron, Brabender) and in the high shear rate region with the aid of a constant rate capillary viscometer (Rheoscope 1000, CEAST). For the former apparatus, cone and plate were 5 cm in diameter and the cone angle was 2°; for the latter apparatus a flat entry capillary with D = 1 mm and L/D = 40 was used in most of the cases. For one type of blend (LL0.5/LD) three different capillaries were used in order to evaluate the entrance and exit effects: the diameter was always 1 mm and the length to diameter ratios were 40, 20, and 10. All the above tests were performed at 180°C.

Extrudate samples, cooled to room temperature, about 5 cm long, were cut for diameter measurements which were made by means of a micrometer after solidification of the samples.

The swelling ratio, B, has in all cases been evaluated as (19):

$$B = \frac{D'}{D}(\rho v_m)^{1/3} \qquad (1)$$

where D' is the diameter of the extruded samples, D the die diameter, ρ is the density of the polymer at room temperature, and v_m the specific volume at the extrusion temperature.

Visual observation of the collected samples has been done in order to evaluate the critical parameters, i.e., the shear rate and the shear stress at which the extrudates appear irregular, even only superficially. In most cases this corresponds to the sharkskin in the LD rich samples or to the periodical swelling accompanied by pressure fluctuations in the LL rich samples.

Non-isothermal elongational experiments were carried out, also with the aid of the Rheoscope 1000, equipped with the tensile module. In this mode the extruded monofilament passes through a pulley system and is then drawn by two counter-rotating rolls, the rotational speed of which can be continuously varied with a linear acceleration of 1 rpm/s.

The melt strength, *MS*, the force in the molten filament at breaking, is directly read. The breaking stretching ratio, *BSR*, can be calculated as the ratio between the drawing speed at break and the extrusion velocity at the die. The extrusion temperature was 180°C. The capillary employed was the one with an L/D = 10 and the tensile system was situated 25 cm below the die.

RESULTS AND DISCUSSION

Let us first discuss the entrance and exit effects in the capillary, studied for the LL0.5/LD blends, containing the most viscous linear low density polyethylene.

Figure 1 represents the end correction or Bagley's factors, e, evaluated in the usual way (20), as a function of the shear stress τ. One notices that the correction factors of the blends lie between the values of the parent polymers: at low shear rates the e values for the blends are similar to those of the LL0.5 sample rather rapidly increasing with τ as evident especially for the LD rich blends.

On the basis of the above results and of the large L/D ratio used, one may hypothesize that neglecting e values for the other blends (LL1/LD and LL4/LD) should imply minor errors in viscosity evaluations and, as will be apparent in the following, should be of no consequence in the qualitative observations of the present work.

Before presenting and commenting on the viscosity curves let us also say, again with reference to the capillary data, that the Rabinowitch correction to the shear rate has also been performed (21).

The viscosity data are reported in *Figs. 2* to *4* as a function of the shear rate. One may observe that in the low shear rate region, the low density

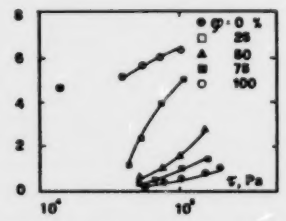

Fig. 1. End correction factor as a function of the shear stress.

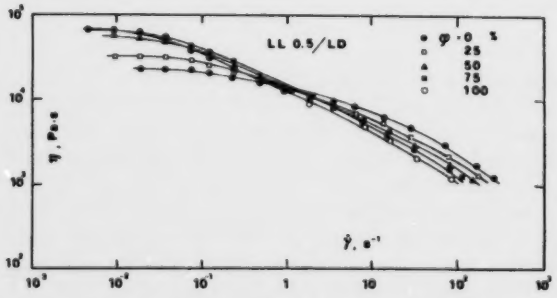

Fig. 2. Flow curves for the LL0.5/LD blends.

Table 1. Physico-Chemical Properties of the Raw Materials.

Resin	Sample code	Density (kg/m³)	M.F.I. (g/10 min)	$M_w \cdot 10^{-3}$	M_w/M_n
LDPE	LD	925	0.27	310	7.3
LLDPE	LL0.5	922	0.53	167	4.7
LLDPE	LL1	924	1.10	136	4.2
LLDPE	LL4	938	4.30	87	4.3

polyethylene has values larger than those of all the linear low density polyethylene samples. However, due to the typically different dependency of the viscosity on the shear rate for the two polymers, the flow curves cross at different $\dot{\gamma}$ values. For LL4/LD this occurs at the shear stress at which the irregularities appear. As for the blends, one may say that in the low shear rate region their viscosity values are mostly between those of the pure polymers. The observations at higher $\dot{\gamma}$ values were rather difficult.

To better elucidate the composition dependence, the viscosities have been also plotted *vs.* φ on a semilogarithmic scale, at constant stress values (see *Figs.* 5 to 7). The behavior of LL0.5/LD and LL1/LD qualitatively is similar. In both cases, at low stresses the LD has higher viscosity than the LL samples with the values for the blends in between. The variation of η is neither linear nor exponential with φ; in both cases the opposite is also true at the highest stresses, i.e., LD has the lowest viscosity and no simple dependency with φ is seen. In the intermediate τ region the viscosities of the parent polymers are similar and a maximum is present at about φ = 75 percent. As for the LL4/LD system only two cases are present and again a synergistic effect is evident at high stress, when the viscosities of the parent polymers are similar while intermediate viscosity values are shown by the blends at lower stresses when LD has a significantly higher viscosity. Similar observations have previously been made with regard to the

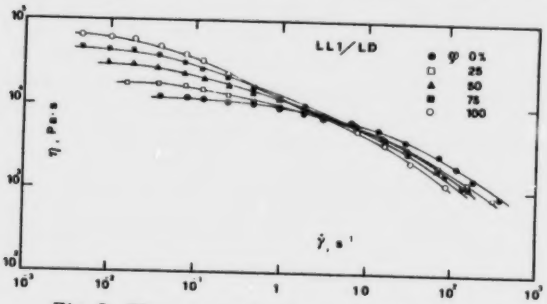

Fig. 3. Flow curves for the LL1/LD blends.

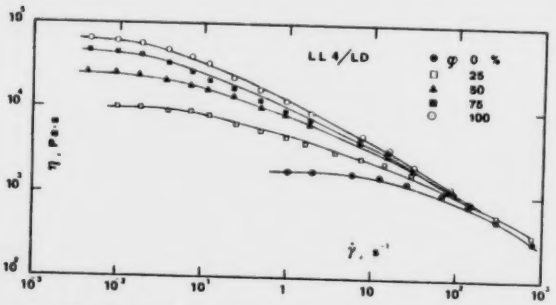

Fig. 4. Flow curves for the LL4/LD blends.

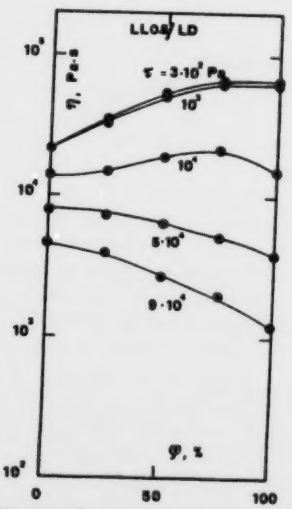

Fig. 5. Viscosity as a function of the composition for the LL0.5/LD blends at fixed constant stress.

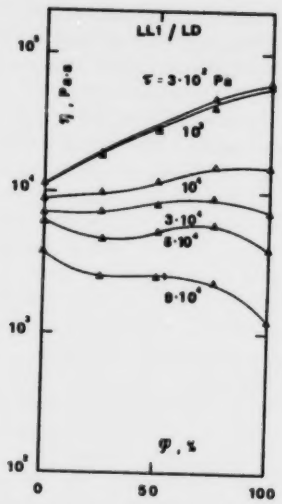

Fig. 6. Viscosity as a function of the composition for the LL1/LD blends at fixed constant stress.

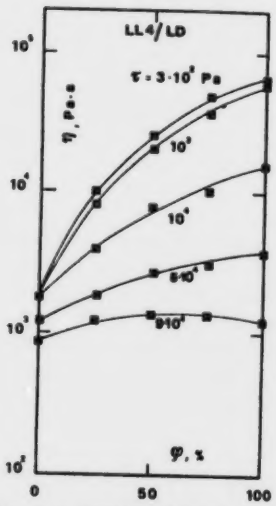

Fig. 7. Viscosity as a function of the composition for the LL4/LD blends at fixed constant stress.

high density polyethylene/low density polyethylene systems (13). We must recall also that the torque values recorded during the preparation of the discussed blends, and reported in *Fig. 8*, show a synergistic effect only in the case of values similar to those of the parents (17).

The swelling results which should not be considered of course as truly rheological data are, however, indicative of elastic effects in the polymer. In particular, *Fig. 9* represents B *vs.* φ at two different τ values for all the systems. All the blends show B values larger than the parent polymers and the effect is of increasing importance going from the LL0.5 to the LL4.

Figure 10 and *11* summarize the results on the appearance of irregularities in the extrudate. More particularly, *Fig. 10* represents the critical shear rate as a function of the blend composition for the three systems. It is evident that a primary role is played by the component present with a high concentration and thus for $\varphi = 25$ percent the $\dot{\gamma}_c$ values are mostly the same as those of the pure LL samples while for $\varphi = 75$ percent, the $\dot{\gamma}_c$ are very similar to the value corresponding to the pure LD. *Figure 11* represents then the critical shear stress as a function of composition. In such a case, observations similar to the ones above can be made although the differences are much smaller. It is, incidentally, well known that τ_c does not depend strongly on the type of polymer.

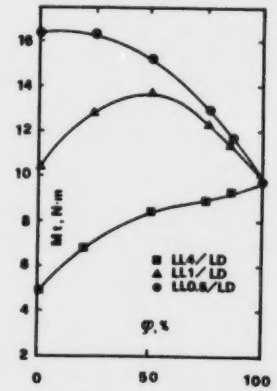

Fig. 8. Torque values as a function of the composition.

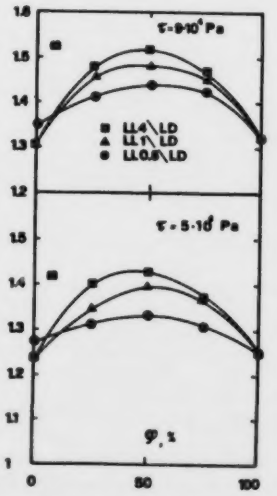

Fig. 9. Extrudate-swell as a function of the composition at two fixed constant stress.

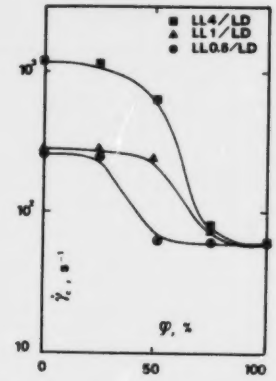

Fig. 10. Critical shear rate as a function of the composition.

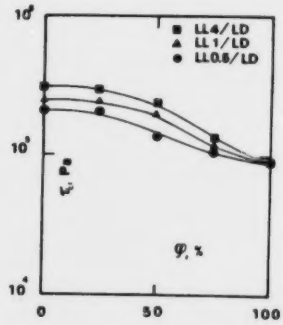

Fig. 11. Critical shear stress as a function of the composition.

Finally, regarding the non-isothermal elongational tests, *Fig. 12* shows the melt strength values, *MS*, as a function of the flow rate in the capillary, for all systems. When the low density sample (which has a *MS* value in all cases much higher than those of the pure LL samples) is mixed with LL0.5 or LL1, the blends exhibit a large increase in melt strength. At some composition, *MS* for the blends is even larger than for pure polymers. The same is not true for the LL4/LD, in which blends have intermediate *MS* values. The above data are replotted in *Fig. 13* as melt strength *vs.* the composition at a constant flow rate.

Figure 14 represents the breaking stretching ratio, *BSR*, data as a function of the flow rate, again for all systems. As is already well known, one observes that the LL samples have a much higher extensibility than LD. An antagonistic

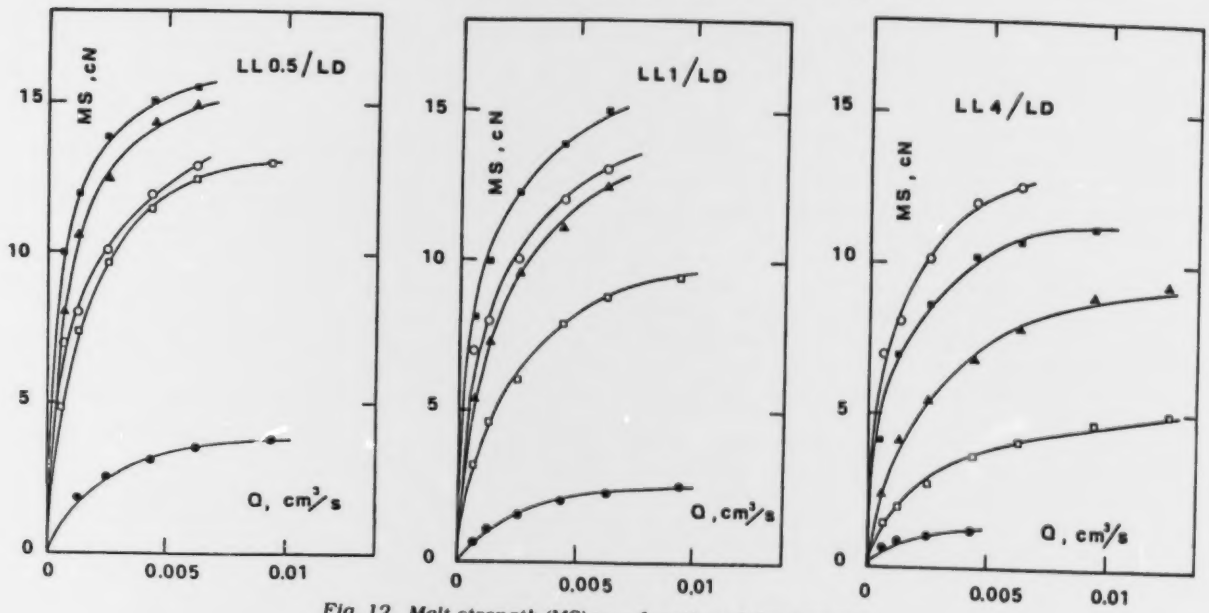

Fig. 12. Melt strength (MS) as a function of the flow rate.

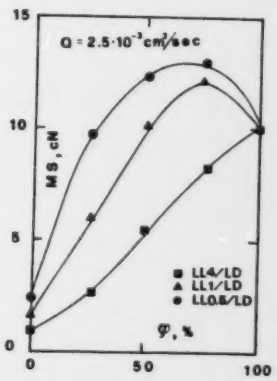

Fig. 13. Melt strength as a function of the composition at given flow rate.

effect is now present for the blends containing LL0.5 and LL1, and the minimum in the *BSR* can be better seen in *Fig. 15*. As expected, the minimum appears at the composition where a maximum was present in the *MS-φ* plot. For the LL4/LD system although an evident decrease of the *BSR* with the LD content is present, the values are always larger than those corresponding to the pure low density polyethylene sample.

CONCLUSION

From the full body of rheological data presented, one may conclude that the blend LL4/LD containing about 25 percent of linear low density polyethylene is the most interesting in view of the substituting of the low density poly-

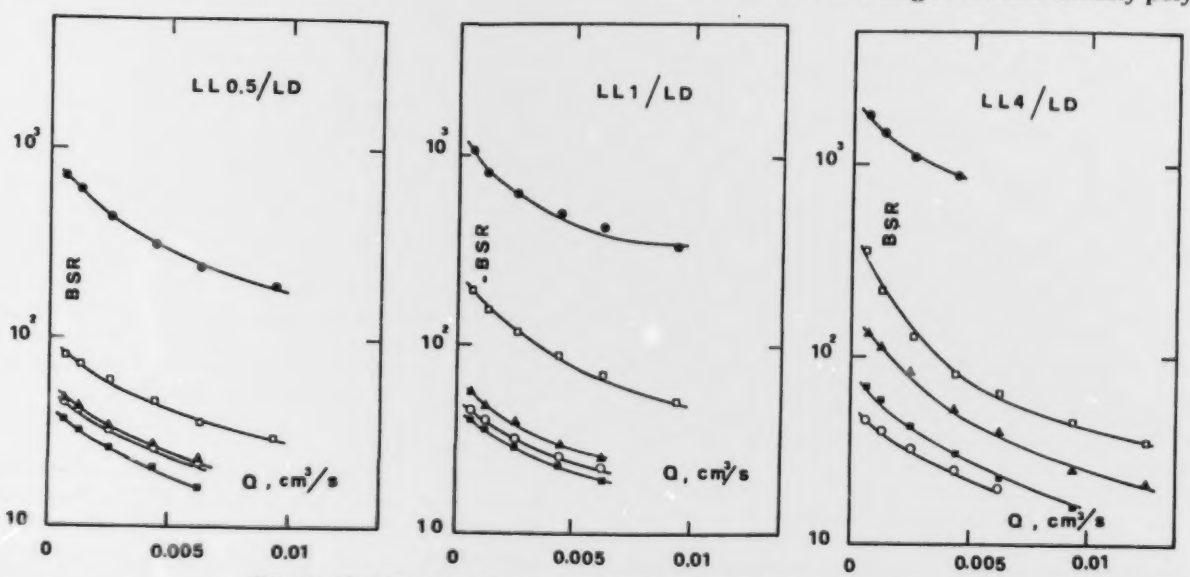

Fig. 14. Breaking stretching ratio (BSR) as a function of the flow rate.

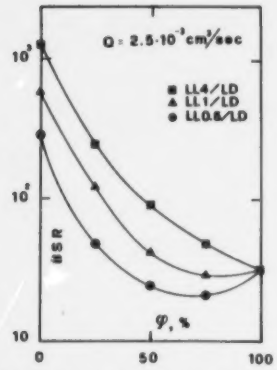

Fig. 15. Breaking stretching ratio as a function of the composition at given flow rate.

ethylene in the production of films by film blowing. It shows a similar shear viscosity, at the shear rates usually found in production, a melt strength only slightly lower, and a breaking stretching ratio larger than that of the LD sample. This should allow the production of thinner films without a too much larger consumption increase, somehow expected also because of the necessary rise of die temperature. Some preliminary results indicate that these blends also present interesting mechanical properties (17, 22).

ACKNOWLEDGMENT

This work has been carried out with the financial support of "Progetto Finalizzato del C.N.R. Chimica Fine e Secondaria."

Thanks are due to "Istituto per la Chimica e la Tecnologia dei Materiali Polimerici" for allowing use of the Rheotron and of the Rheoscope 1000 and to CEAST for allowing use of the tensile module.

REFERENCES

1. J. A. Manson and L. H. Sperling, "Polymer Blends and Composites," Plenum Press, New York (1976).
2. D. R. Paul and S. Newmann, Eds., "Polymer Blends," Academic Press, New York (1978).
3. O. Olabisi, L. M. Robeson, and M. Shaw, "Polymer-Polymer Miscibility," Academic Press, New York (1979).
4. A. P. Plochocki, *J. Appl. Polym. Sci.*, **16**, 987 (1972).
5. A. P. Plochocki, *Trans. Soc. Rheol.*, **20**, 287 (1976).
6. L. A. Utracki and M. R. Kamal, *Polym. Eng. Sci.*, **22**, 96 (1982).
7. F. P. La Mantia, D. Acierno, and D. Curto, *Rheol. Acta*, **21**, 452 (1982).
8. L. A. Utracki, Proceedings of IUPAC, Amherst, Mass., July 12–17, 1982.
9. L. A. Utracki, *Polym. Eng. Sci.*, **23**, 602 (1983).
10. M. M. Dumoulin, C. Farha, and L. A. Utracki, *Polym. Eng. Sci.*, **24**, 1319 (1984).
11. A. P. Plochocki, *Polym. Eng. Sci.*, **22**, 1153 (1982).
12. L. A. Utracki and M. M. Dumolin, *SPE ANTEC Tech. Pap.*, **28**, 51 (1982).
13. D. Curto, F. P. La Mantia, and D. Acierno, *Rheol. Acta*, **22**, 197 (1983).
14. F. P. La Mantia, D. Curto, and D. Acierno, *Acta Polym.*, **35**, 71 (1984).
15. D. Acierno, F. P. La Mantia, and D. Curto, *Polym. Bull.*, **11**, 223 (1984).
16. A. Valenza, F. P. La Mantia, and D. Acierno, *Europ. Polym. J.*, **20**, 727 (1984).
17. D. Acierno, D. Curto, F. P. La Mantia, A. Valenza, and A. Brancaccio, Proceedings of "Future Trends in Polymer Science and Technology, Polymer Commodities or Specialities" Capri, Italy, October 8–12, 1984.
18. F. P. La Mantia and D. Acierno, *Polym. Eng. Sci.*, to be published.
19. R. A. Mendelson and F. L. Finger, *J. Appl. Polym. Sci.*, **17**, 797 (1973).
20. E. B. Bagley, *J. Appl. Phis.*, **28**, 624 (1957).
21. B. Rabinowitch, *J. Phys. Chem.*, **A145**, 1 (1929).
22. F. P. La Mantia and D. Acierno, *Europ. Polym. J.*, in press.

NOMENCLATURE

e = Bagley's correction factor.
v_m = Specific volume at the extrusion temperature.
B = Swelling ratio.
BSR = Breaking stretching ratio.
D = Capillary diameter.
D' = Extrudate diameter.
L = Capillary length.
M_n = Average number molecular weight.
M_w = Average weight molecular weight.
MFI = Melt flow index.
MS = Melt strength.
Q = Flow rate.
$\dot{\gamma}$ = True shear rate.
$\dot{\gamma}_{app}$ = Apparent shear rate.
$\dot{\gamma}_c$ = Critical shear rate.
η = Viscosity.
ρ = Density at room temperature.
τ = Shear stress.
τ_c = Critical shear stress.
φ = LDPE content.

DISCUSSION: D. CURTO

L. A. Utracki: Could you please explain what are the *BSR* and *MS* and how are they measured? Are they related to each other?

D. Curto: The *BSR* is a ratio of two velocities, the highest stretching velocity at break divided by the melt velocity in the die. The *MS* is given by the force at break. The instrument gives us directly both the velocity and the force at break. We note that as *BSR* increases *MS* decreases. Both are very important processing parameters.

D. Froelich: Apparently you measured the Newtonian viscosity at low rate of shear. Did you try to plot these as a function of composition to see what type of dependence they follow?

D. Curto: In *Figs. 5* to *7* the curves relative to $\tau = 3 \cdot 10^2$ Pa correspond to the Newtonian viscosity as a function of the composition. In all cases neither a linear nor a logarithmic rule is obeyed.

Melt Rheology of High Density Polyethylene/Polyamide-6 Blends

L. A. UTRACKI, M. M. DUMOULIN, *and* P. TOMA

National Research Council Canada
Industrial Materials Research Institute
75 de Mortagne
Boucherville, Quebec, Canada J4B 6Y4

Commercial high density polyethylene and polyamide-6 (PA) resins were melt blended in the Brabender Plasticorder twin-screw extruder. The blends containing zero to 30 wt percent of polyamide-6 were examined in dynamic and steady state shear at 150, 200, and 250°C. The rheological test results are discussed in terms of morphology of the samples as observed under scanning electron microscope. Microscopy of the extrudates has shown a temperature dependent movement of the polyamide in the capillary during the extrusion and that fibrillation of the PA phase in the extensional field occurred at all temperatures.

INTRODUCTION

Polyethylene, PE, and polyamide, PA, are two polymers of great industrial importance. The former is the most widely used plastic while the very attractive properties of the latter are responsible for its ever increasing application. Nylon fibers have been used in the textile industry for years, and it is this application that led to early attempts to produce polyamide blends [1]. Polyethoxylated compounds such as poly(ethylene glycol) were blended with polyamides to produce fibers with durable antistatic properties [2, 3]. Work in this direction is still underway as indicated by recent attempts to reduce static charges in nylon fibers by blending with poly(ethylene glycol) [4] and N-acetyl polyethyleneimine [5]. Other blends involving polyamide were studied with the objective of improvement of impact properties.

It is well known that in semi-crystalline thermoplastics the presence of crystalline regions reduces chain mobility and therefore increases molecular relaxation times. The amount of strain that the polymer can absorb before break is then reduced. Incorporation of elastomer particles in the polymer matrix often helped to dissipate energy under impact conditions. In the case of polyamide, a modified polyolefin has been used for such purposes. High notched Izod impact strengths were reported for blends of polyamide-6,6 with poly(ethylene-g-maleic anhydride) [6]. The same principle was applied to blends of poly(ϵ-caprolactam) or polyamide-6, PA-6, with polypropylene, PP, or polystyrene, PS [7]. The use of maleic anhydride-grafted, PP or styrene-methacrylic acid copolymer, respectively, induced formation of a graft polymer between the polyamide and the modified PP or PS.

Blending of polyamides with polyolefins leads to thermodynamically immiscible two-phase systems. Braun and Eisenlohr [8] have used dynamic testing and microscopy to show the presence of two phases in blends of low density polyethylene, LDPE, with PA-6. Separation of the constituents by extraction did not indicate any grafting during processing. The thermal and mechanical properties of a similar system were reported [9] and lead to the same conclusions. Similarly, Liang, *et al.* [10] have observed the incompatibility of PP with PA-6 and, consequently, the difficulty of dispersing one into the other. Hinrichsen and Green [11] have studied the rheological behavior of polyamide blends and observed a negative deviation in the shear viscosity of blends of two PA-6 resins.

The aim of this work has been to improve the barrier properties of polyethylene films. For this reason, only low-PA content blends were studied. In Part I, Kamal, Jinnah, and Utracki [12] studied the oxygen and water vapor permeability through polyethylene/polyamide blends containing up to 30 wt percent of PA. Three types of polyethylenes (LDPE, LLDPE, and HDPE) were blended with three types of polyamide (PA-6,6, elastomer modified PA-6,6, and PA-6). Of the nine types of blends, the best results (reduction of oxygen permeability by a factor of 3.6) were obtained for the HDPE/PA-6 blend. In

Part II, Dumoulin, Toma, and Utracki [13] reported on the steady state viscosities and morphology of HDPE/PA-6 blends.

In this third part of the studies, we wish to complete the steady state flow studies and compare these results with the dynamic data. Further illustration of the effect of shear/elongational flow on blend morphology will be shown.

EXPERIMENTAL

Materials

The properties of the two commercial resins are given in *Table 1*. Blends were prepared using the Brabender Plasticorder twin-screw extruder. A temperature gradient was maintained in the barrel of the extruder, the entrance region being kept at 220°C and the die at 250°C. The screw speed was set at 30 rpm. Four compositions containing 0, 10, 20, and 30 wt percent of PA-6 in HDPE were prepared. In the following text, these samples will be identified by the symbols: HDPE, 10PA, 20PA, and 30PA, respectively. The extrudate was obtained in the form of a ribbon which was quenched in cold water, dried, and then granulated. Prior to testing, the materials were dried under vacuum for 24 h at 85°C to avoid the plasticizing and hydrolyzing effects of humidity on PA-6.

Rheological Tests

The steady state and dynamic flow properties of all materials were measured at three temperatures: 150, 200, and 250°C. The steady state shear viscosity was measured in the Instron Capillary Rheometer, Model 3211, ICR, using two sets of capillaries of different diameters (d = 0.762 and 1.27 mm). The data were systematically corrected according to the Bagley and Rabinowitsch procedures [13–16]. The Rheometrics Mechanical Spectrometer, RMS, Model 605, was used for the dynamic tests. The constant strain rate elongational viscosity was measured for HDPE at 150°C using the Rheometrics Extensional Rheometer, RER.

Microscopy

To study the morphology of the HDPE/PA-6 blends the extruded strands were collected, fractured under liquid nitrogen, and then observed under the Scanning Electron Microscope, SEM, JEOL Model JSM-35CF. In addition, micrographs were also taken on fracture surfaces from which PA-6 has been removed by treatment with 88 percent formic acid.

Table 1. Resin Properties.

Property	HDPE	PA-6
Density (kg/m^3)	961	1130
Melting point (°C)	134	219
Zero-shear viscosity, η_0 ($\times 10^{-3}$ Pa.s) at 250°C	>50	1.0
Supplier	Union Carbide	DuPont

RESULTS

The results of viscosity *vs.* deformation rate measurements are presented in *Figs. 1* to *4* as the extensional, η_e, shear, η, and dynamic, η', viscosities as functions of, respectively, the extensional strain rate, $\dot{\epsilon}$, shear rate, $\dot{\gamma}$, and the frequency, ω. It has been observed [17] that data obtained at different temperatures superimpose if plotted as η/η_0 *vs.* $\dot{\gamma}\eta_0$, where η_0 is the zero-shear viscosity. A reference temperature was selected (250°C) and the data in *Figs. 1* and *4* have been superimposed using a shift factor, a_T, defined as

$$a_T = \eta_0(T)/\eta_0(250°C) \qquad (1)$$

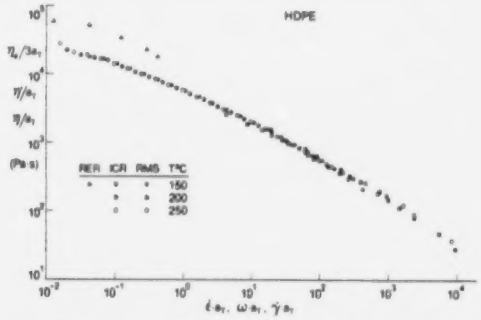

Fig. 1. Reduced viscosities: shear, η/a_T, elongational, η_e/a_T, and dynamic, η'/a_T, vs. respective reduced deformation rates: $\dot{\gamma}\cdot a_T$, $\dot{\epsilon}\cdot a_T$ and $\omega\cdot a_T$ for HDPE.

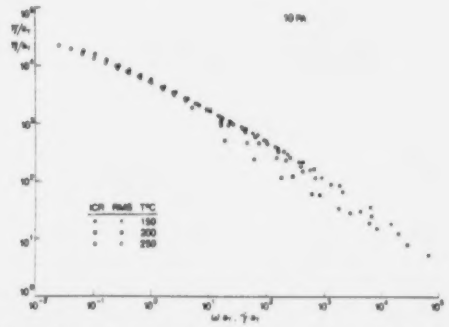

Fig. 2. Reduced viscosities: shear, η/a_T and dynamic, η'/a_T, vs. reduced shear rate, $\dot{\gamma}\cdot a_T$, and frequency, $\omega\cdot a_T$, for 10PA.

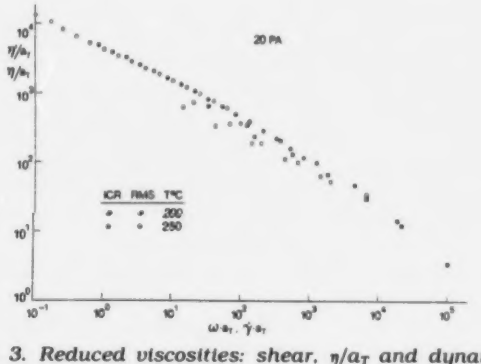

Fig. 3. Reduced viscosities: shear, η/a_T and dynamic, η'/a_T, vs. reduced shear rate, $\dot{\gamma}\cdot a_T$, and frequency, $\omega\cdot a_T$, for 20PA.

In *Figs. 1* to *4*, data measured at three temperatures using different rheometers are superimposed by dividing the viscosity values and multiplying the deformation rates by the same shift factor a_T. *Figures 1* to *3* show respectively the data for HDPE, 10PA, and 20PA while *Fig. 4* summarizes all the results, including 30PA. In *Fig. 5* a_T is plotted as a function of temperature for HDPE, 10PA, and 20PA.

As mentioned before, the capillary data were corrected using the Bagley procedure. In this method the pressure loss due to end effects, P_e, is evaluated and subtracted from the total pressure loss, P, in order to calculate the true shear stress, σ_{12}. *Figures 6* to *9* show the P_e *vs.* σ_{12} dependencies for HDPE, 10PA, 20PA, and 30PA, respectively. The results are summarized in *Fig. 10*.

The morphology of HDPE/PA-6 samples extruded through long capillaries with L/d = 40 to 60 is presented in *Figs. 11* to *15* as SEM micrographs taken under × 1000 (or × 500) magnification. In all cases the top micrograph (A) illustrates the central part of the extrudate, while the bottom one (B) that of the outside part. The conditions of sample preparation are summarized in *Table 2*. Finally, *Fig. 16A* shows the general view of the 30PA sample under a ×43 magnification while a detail of it can be seen in *Fig. 16B* for which the magnification was

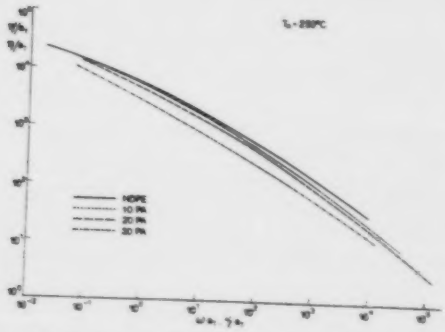

Fig. 4. Master curves for HDPE, 10PA, 20PA, and 30PA. The reference temperature T_R = 250°C was used.

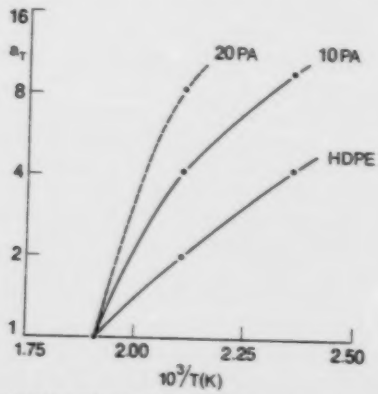

Fig. 5. Arrhenius plot of the shift factor, a_T, vs. absolute temperature, T.

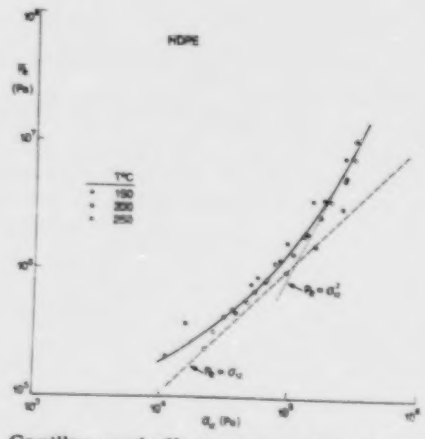

Fig. 6. Capillary end-effects pressure loss, P_e, vs. shear stress, σ_{12}, for HDPE.

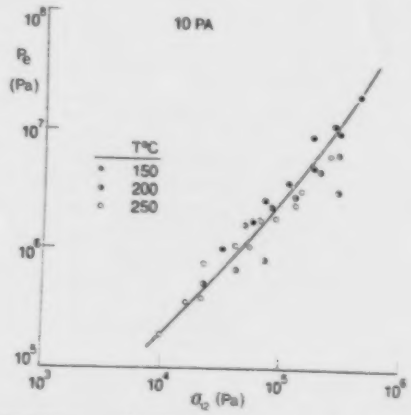

Fig. 7. Capillary end-effects pressure loss, P_e, vs. shear stress, σ_{12}, for 10PA.

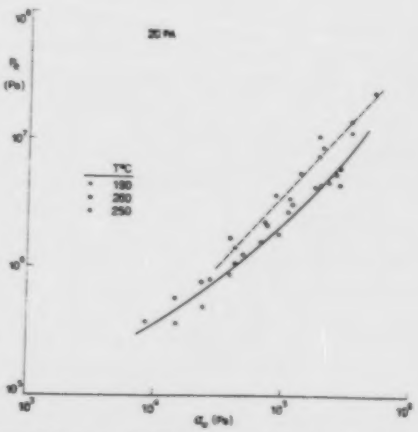

Fig. 8. Capillary end-effects pressure loss, P_e, vs. shear stress, σ_{12}, for 20PA.

×1000. The "tree-ring" structure postulated by Lin [18], indicating interlayer slip, is clearly visible.

DISCUSSION

In the following text, two related dependencies will be discussed, namely the correlation

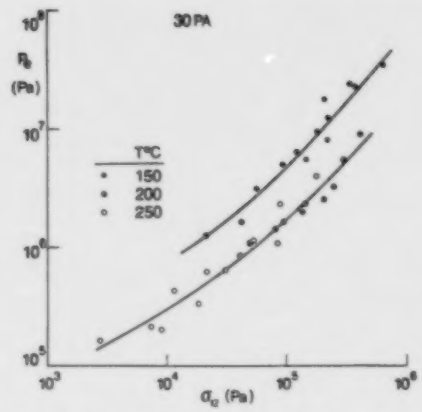

Fig. 9. Capillary end effects pressure loss, P_e, vs. shear stress, σ_{12}, for 30PA.

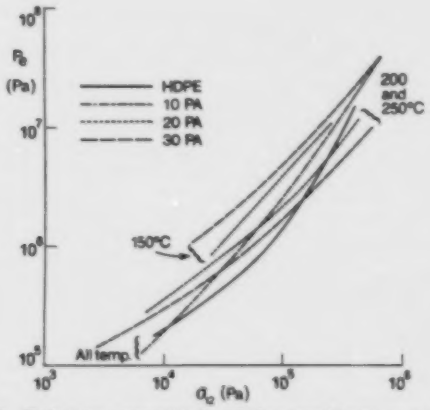

Fig. 10. Relative magnitude of the capillary end effects pressure loss, P_e, vs. shear stress, σ_{12}, for HDPE, 10PA, 20PA, and 30PA.

between rheological functions and the influence of the temperature and deformation field on morphology of the HDPE/PA-6 blends.

Rheological Results

As reported earlier [13], the influence of PA-6 concentration, c, on steady state (capillary) viscosity, η, is very sensitive to temperature. At 150°C, the dispersed PA-6 phase acts as a solid filler causing an increase of η with c. At 250°C, the low-viscosity PA-6 melt migrates to the wall causing a reduction of η with c. At 200°C, these two effects nearly compensate, resulting in η which is nearly independent of c.

To construct the master-plots in *Figs. 1* to 4, the shift factor, a_T, had to be computed. For this purpose the dynamic viscosity data, η', were used, superimposing the 150 and 200°C onto 250°C curve, as required by the Vinogradov-Malkin, *et al.* [17] method, by the same amount in the vertical and horizontal directions. Determined in this manner, a_T was subsequently used to shift the steady state, η, and elongational, η_e, viscosities.

As shown in *Fig. 1*, the use of a shift factor

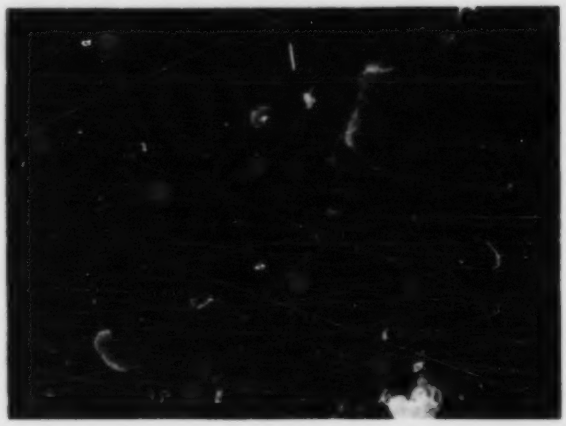

(A)

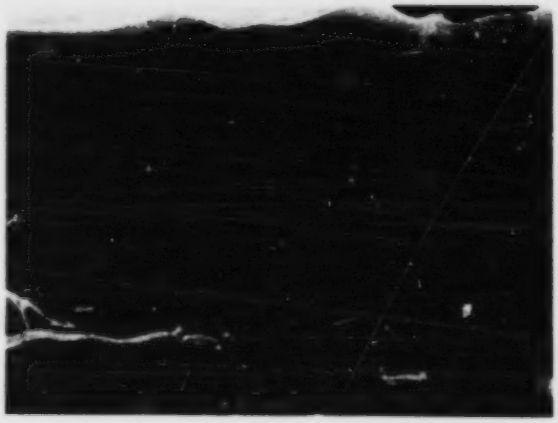

(B)

Fig. 11. SEM micrograph of 10PA extruded at 200°C and 1230 s^{-1}; (A) center and (B) outside of the extrudate under a ×1000 magnification.

defined by *Eq 1* does indeed allow construction of a master curve for HDPE within the six decades of deformation rates, implying that (1) the Vinogradov-Malkin method is applicable, and (2) that the Cox-Mertz rule is not obeyed but rather the theoretically more sound prediction that $\eta = \eta'$ at $\dot{\gamma} = \omega$. This is in accord with our previous observations [19–21]. Furthermore, it can be seen that the elongational viscosity, η_e, is about 6 to 8 times larger than the shear viscosities, $\eta = \eta'$, indicating an effect of strain hardening for this relatively high molecular weight HDPE. This again is in agreement with earlier publications [22, 23].

Upon addition of an increasing amount of PA-6 to HDPE, it becomes increasingly difficult to obtain a common master curve for dynamic and capillary flows, especially at $T \geq 200$°C. In all cases the dynamic results give reasonably good superposition. These data also coincide with the capillary results at 150°C but are higher than those obtained at 200 and 250°C. The most likely reason for this behavior is the migration of the dispersed phase reported in *Figs. 11* to

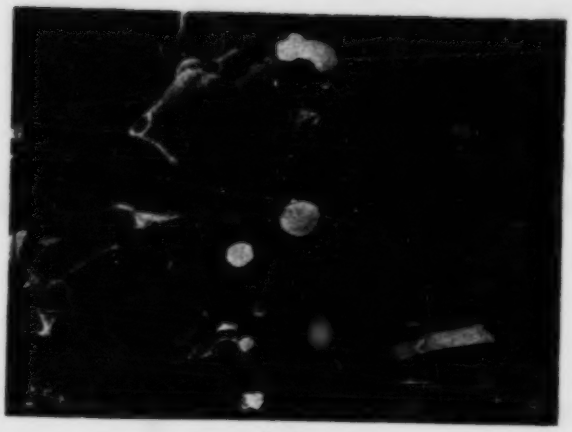

(A)

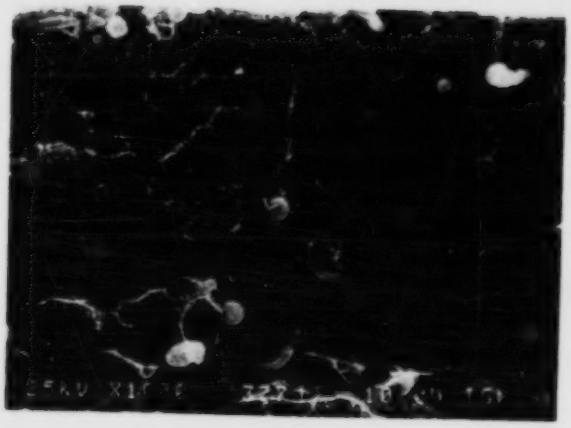

(B)

Fig. 12. SEM micrograph of 20PA extruded at 150°C and 1110 s^{-1}; (A) center and (B) outside of the extrudate under a ×1000 magnification.

(A)

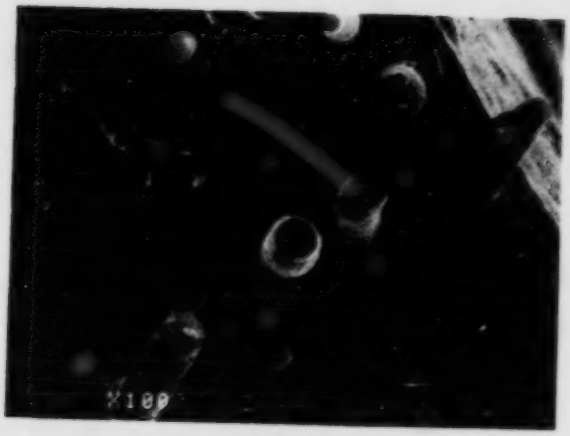

(B)

Fig. 13. SEM micrograph of 20PA extruded at 250°C and 12 s^{-1}; (A) center and (B) outside of the extrudate under a ×1000 magnification.

15. At 150°C, higher concentration of PA-6 is observed in the center, while at 250°C the opposite is true. Apparently, the presence of molten PA-6 near or at the capillary wall has a much more pronounced effect on the shear viscosity than the decrease of its solid concentration at 150°C. The steady state flow, which frequently leads to drastic changes in system morphology, is a singularly unreliable method for assessing the properties of multiphase systems [24–27]. However, since shear fractionation must also take place during processing, one is obliged to study the steady state behavior, relating to morphological changes.

The summary of data in *Fig. 4* must be looked at keeping in mind that the reference temperature was arbitrarily selected as T_R = 250°C. Consequently, the data are reduced to the plot of the liquid/liquid blends, for which η decreases with PA-6 concentration. The opposite effect observed at lower temperatures is hidden in the a_T *vs.* $1/T$ plot in *Fig. 5*. As indicated there, it is possible to determine two regions of the activation energy of flow, E_a, above and below 200°C. In the lower temperature region $E_a = 26 \pm 1.5$ (kJ/mol) for both HDPE and 10PA, in a fair agreement with the published [28] value of 27.8 kJ/mol, i.e., in this region, addition of the PA-6 "filler" does not significantly affect E_a. This is in contrast to the higher temperature region where, for HDPE, E_a is nearly identical to that given above, but upon addition of PA increases dramatically.

The dynamic tests also allow determination of the storage modulus, G', as a function of ω. The G' *vs.* ωa_T for HDPE, 10PA, and PA-6 is plotted in *Fig. 17* using the same values of T_R and a_T as those employed in constructing *Fig. 4*. As expected G' (HDPE) > G' (PA-6) in the full range of experimental variables. The curves for HDPE and 10PA cross at $\omega a_T \simeq 0.2$; at lower frequencies G' (10PA) > G' (HDPE), at higher the reverse is true. The storage moduli for blends with higher concentration of PA-6 were higher. Reproducibility of these data was poor. It should be noted that the initial slope for G' of

(A)

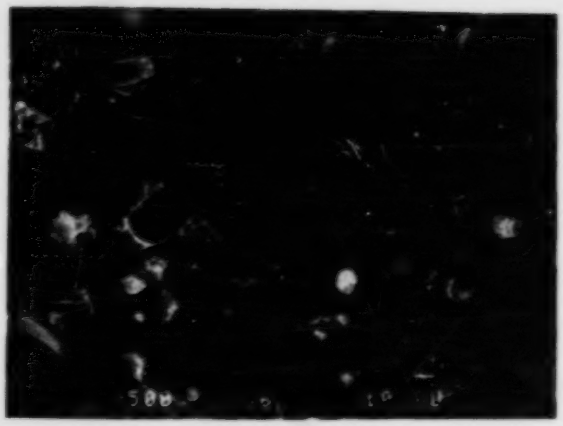

(B)

Fig. 14. SEM micrograph of 30PA extruded at 150°C and 370 s^{-1}: (A) center and (B) outside of the extrudate under a ×500 magnification.

(A)

(B)

Fig. 15. SEM micrograph of 30PA extruded at 250°C and 116 s^{-1}: (A) center and (B) outside of the extrudate under a ×1000 magnification.

PA-6 ($\partial \log G'/\partial \log \omega$) = 2. At temperatures below the melting point of PA-6 (T_m = 219°C) the blends should behave as a polymeric composite, filled with solid (but deformable) particles. If so, then it is expected [24–27] that G' and P_e will increase while the extrudate swell decreases with "filler" concentrations. This indeed is the case (see *Fig. 10*).

The detailed analysis of P_e *vs.* shear stress, σ_{12}, in *Figs. 6* to *9* reveals that for HDPE the dependence is universal, independent of T and capillary diameter. For 10PA a similar observation can be made, although the data at 150°C seem to be systematically higher than those at the higher temperatures. For 20PA and 30PA there is a definite dichotomy of results; at 150 and 250°C, the end correction, P_e, plot *vs.* σ_{12} forms, two dependencies with P_e (150) > P_e (250). The data at 200°C are intermediate: at lower shear stress, PA-6 domains behave as solid particles following the results obtained at 150°C, whereas at high shear stress the data fall neatly into the realm of the 250°C blend behavior. The difference between the solid-like and liquid-like behavior increases with concentration.

Table 2. Extrusion Conditions for SEM Samples Presented in *Figs. 11* to *16*.

Fig. No	Sample	Extrusion Conditions			Comments**
		T (°C)	L/d*	$\dot{\gamma}$ (s^{-1})	
11	10Pa	200	60	1230	FF
12	20Pa	150	40	1110	FF
13	20PA	250	60	12	FF
14	30PA	150	40	370	FF
15	30PA	250	60	116	AT
16***	30PA	250	40	1110	FF,

* L/d is the capillary length-to-diameter ratio.
** FF stands for freeze fractured while AT indicates additional formic acid treatment to remove PA-6 phase.
*** magnification ×43 and ×1000 for A and B micrographs, respectively.

For polymer blends the extrudate swell, B, may show either a positive or a negative deviation from the log-additivity rule (28–31). In a recent paper, Romankievich, *et al.* [32] report that for HDPE/PA-6 at 240 to 270°C, B as a function of PA-6 content reaches a maximum

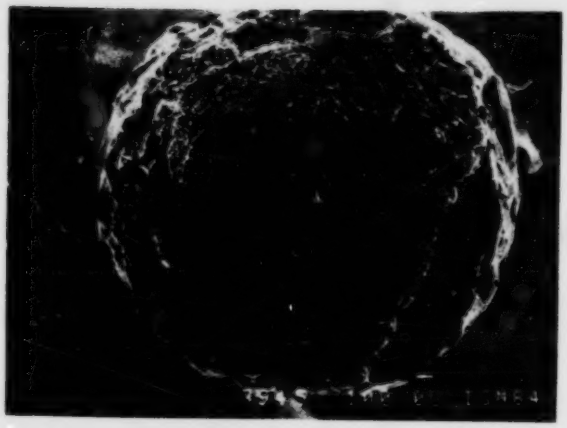

(A)

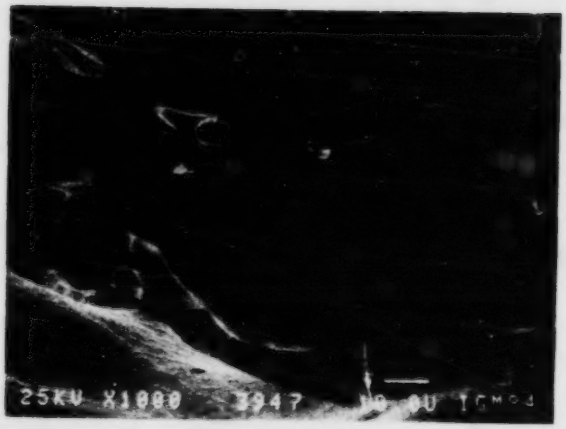

(B)

Fig. 16. SEM micrograph of 30PA extruded at 250°C and 1110 s^{-1}; (A) general view (B) details of the extrudate under, respectively, a ×43 and ×1000 magnification.

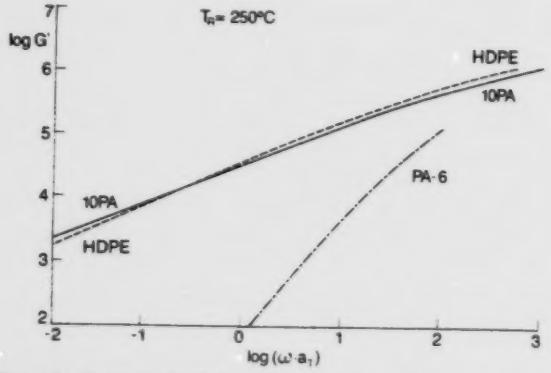

Fig. 17. Storage modulus, G', vs. reduced frequency, ωa_T, for HDPE and 10PA at 150, 200, and 250°C and for PA-6 at 250°C. The reference temperature T_R = 250°C.

at about 40 wt percent. For the system studied here, the presence of PA-6 also brings about an increase in B when the extrusion is performed at 250°C although the dependency between B and the composition does not seem to be regular. Once again the situation is reversed when the temperature is decreased to 150°C in which case the addition of PA significantly lowers B.

To summarize: the constant stress dynamic and capillary viscosities at 250°C show the positive deviation from the log-additivity rule, PDB, at low stresses ($G'' < 3.10^3$Pa) and negative deviation, NDB, at higher stresses ($G'' \geq 10^4$Pa). Similarly, measures of the blend elasticity: G', P_e, B at low deformation rates are PDB type and at higher rates NDB. The latter observation could be theoretically expected [33–34] since, even for emulsions and suspensions in Newtonian liquids, the elastic deformation of droplets or rotation of particles provides mechanisms for energy storage and recovery.

Morphology

Turning now to SEM results, it can be stated that during capillary flow several shear-induced effects on blend morphology were noted. Before examining these in detail, it should be stressed that there was no attempt made to stabilize the blend interphase. Due to large differences in the chemical structure of the monomers, immiscibility and relatively high interfacial tension should be expected, leading to coalescence of domains at temperatures above T_m of PA-6. However, under the dynamic test conditions, at strains $\gamma \leq 10$ percent, the viscoelastic response of the system was reasonably stable and reproducible, indicating little coalescence if any.

A different situation existed during capillary flow. Four shear-induced effects have been identified:

(1) A shear-induced segregation of polymer domains is apparent in *Figs. 11* to *15*. Comparing the SEM of the central part (photo A) with that of the rim (photo B) one notices differences in concentration of the dispersed phase (PA-6) in all cases. For low c (e.g., *Fig. 11*) domain segregation and shear stress dependent dispersion was observed. For samples 20PA and 30PA the effects were more complex. Here, at 150°C (namely, *Figs. 12* and *14*), the concentration of PA-6 was higher in the center than at the rim, while at 250°C (namely, *Figs. 13* and *15*) the reverse was true.

Migration of solid particles and liquid droplets in shear flow has been theoretically and experimentally studied by Mason, *et al.* (e.g., see [35]). In suspensions, presence of the particle-depleted layer near the capillary wall has been frequently demonstrated. In Newtonian systems, where viscosities of the two liquids are similar, there is an increasing tendency of deformable droplet to migrate toward the axis as droplet radius, flow rate, and radial position increase. In viscoelastic systems, the direction of the radial migration depends on both the shear stress and first normal stress difference [36]. Shear fractionation (in respect to molecular weight) was proposed by Busse [37], and experimentally demonstrated by Schreiber, *et*

al. [38, 39]. The authors argued that the effect is due to minimization of free energy of the systems. The long, entangled molecules, capable of storing more elastic energy, i.e., increasing their free energy, move toward the center of the stream where the rate of deformation and the stress field are low. In that argument, there is the unvocalized assumption that viscosity and elasticity are changing in a similar manner.

In the case of the HDPE/PA-6 system at 150°C the solid particles of PA-6 are observed to be forced away from the wall. On the other hand, at 250°C, the lower viscosity PA-6 melt tends to encapsulate the HDPE stream, in accordance with Han's observations [36].

(2) A stress-induced fibrillation was observed at all temperatures for $c > 10$ wt percent. At low concentration and low rates of shear the effect occurs only near the rim. It is important to note that the average diameter of the fibrils is quite comparable to the average size of the original droplets, while their volume is many times larger, i.e., the fibrillation is associated with a specific shear-induced coalescence. Fibrillation during melt extrusion of polyethylene blends with PA, polyacetal or polyethylene terephthalate has been reported [32, 40–42], but the mechanism observed for the HDPE/PA-6 blends is different from the simple "droplet spinning" proposed by Tsebrenko, *et al.* [43]. Furthermore, as shown in *Figs. 12* and *14*, fibrillation also takes place at temperatures $T < T_m$. This resembles the hydrostatic extrusion of polymers reported during the last few years (e.g., see [44, 45]). Whether the fibrillation occurs with or without coalescence, its mechanism is clearly extensional. For freely converging flow of homogeneous melt, Cogswell [46] derived the following relation between the extensional viscosity at the entrance to the die and the shear viscosity on the die wall:

$$\eta_e/\eta = 2 \tan^{-2} \alpha \qquad (2)$$

where α is the half-angle of convergence given by the ratio of the respective deformation rates:

$$\alpha = \text{arc tan } (2\dot{\epsilon}/\dot{\gamma}) \qquad (3)$$

It is interesting to note that from *Eqs 2* and *3* it follows that in the process, the energy dissipated in shear $\eta\dot{\gamma}^2 = 2\eta_e\dot{\epsilon}^2$, i.e., the entrance pressure loss due to extensional flow is a significant part of the total effect. In a recent work [47] $\alpha = 20.6 \pm 1.6°$ was computed for HDPE. Using this value, one finds: $\dot{\epsilon} = 0.188\ \dot{\gamma}$, $\eta_e = 14.156\eta$, and $\sigma_{11} = 2.660\sigma_{12}$, where σ_{11} and σ_{12} are the extensional and shear stress, respectively. A theory of free convergence flow for multiphase systems has not been developed. However, it is accepted that shear stress is the same across the interface, whereas deformation rate changes inversely with viscosity. Since, during capillary flow at 150°C, the shear stress of the matrix (see *Fig. 1*) changes from 20 to 300 kPa the available extensional stress is $\sigma_{11} = 50$ to 800 kPa. To test if PA-6 can be deformed under these conditions the dumbbell shaped samples were tested using the Instron Universal Tensile Tester, Model 1125, equipped with the constant temperature chamber. At 150°C the yield stress for PA-6 was found to be $\sigma_y \simeq 15$ kPa and the stress required for steady state straining $\sigma = 12$kPa, independent of the straining rate. This is much less than the stress available in the capillary entry region, σ_{11}, calculated for the convergent capillary entrance flow.

(3) Dynamic dispersion/coalescence. To quantitatively describe the extent of dispersion, the ratio D/D_o was used where D is the average diameter of particles of the dispersed phase in the 250°C extrudate and D_o is the same parameter in the starting blend used in capillary flow tests. As shown in *Fig. 18*, at the lowest rate of $\dot{\gamma} = 11.2$ (s^{-1}) this ratio is about 0.9. As $\dot{\gamma}$ increases to 1120 (s^{-1}), the ratio drops to about 0.3 in the center and 0.5 on the sides of the extrudate, indicating a progressive improvement of the dispersion with the increase in shear stress. In addition to the reduction of particle size, a radial movement of the dispersed phase was also observed. The data in *Fig. 18* refer only to low c blends in which fibrillation was not visible.

(4) The shear-induced interlayer slip is exemplified by *Fig. 16A* where a tree-ring structure is visible. The detail in *Fig. 16B* shows a clear interphase separation. This type of structure was theoretically predicted by Lin [18], who derived the following relation for immiscible blends with interlayer slip factor β_{12}:

$$1/\eta = \beta \sum w_i/\eta_i;\ i = 1,2 \qquad (4)$$

where

$$\beta = 1 - (\beta_{12}/\sigma_{12})(w_1w_2)^{1/2} \qquad (5)$$

In *Eqs 4* and *5*, w_i stands for weight fraction, n_i is the viscosity of pure ingredients ($i = 1$ and 2) while σ_{12} is the shear stress on the wall.

The dependencies (*Eqs 4* and *5*) predict a negative deviation from the log-additivity rule.

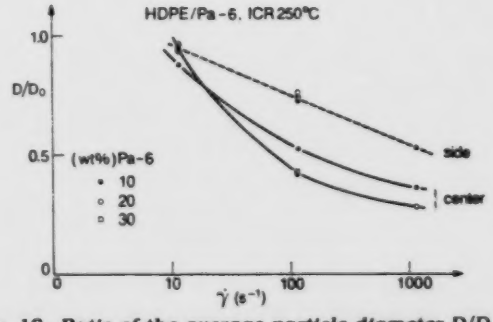

Fig. 18. Ratio of the average particle diameter D/D_o vs. the shear rate $\dot{\gamma}$. D_o and D are respectively the average PA-6 particle diameter before and after extrusion.

as those observed and reported [13] for HDPE/PA-6 capillary flow at 250°C. During the present studies, 32 extruded samples were observed under SEM. The tree-ring structure was observed only for 30PA strands extruded at 250°C at $\dot{\gamma} = 11$ to 1100 s^{-1}.

CONCLUSIONS

HDPE/PA-6 blends are immiscible. The studies conducted at temperatures below and above the melting point of PA-6 lead to the following conclusions:

1. The time-temperature shift allows superposition of the dynamic viscosities of all samples containing 0 to 30 wt percent of PA-6 in the full range of temperatures, $T = 150$ to 250°C, on their respective master curves.
2. In the case of HDPE, a good superposition was obtained for the capillary data using the shift factors determined for dynamic data. The capillary results for blends showed some scattering, the upper limit being determined by the dynamic viscosity master curve with a number of data points (especially those measured at 200 and 250°C) falling below.
3. Capillary flow introduces extensive morphological changes in the blends, dependent on concentration of the dispersed phase, temperature, and deformation rate.
4. Four types of morphological changes were identified: (i) shear segregation, causing the lower viscosity material to migrate toward the wall, (ii) fibrillation of the dispersed phase associated with coalescence at all temperatures, (iii) dynamic coalescence/dispersion, and (iv) interlayer slip in the material (data from two families of capillaries having different diameters indicated no slip on the wall!).
5. Dynamic tests are more reliable than steady state flow for the characterization of multiphase systems. However, the use of capillary viscometry should not be overlooked since it is more likely to depict the behavior of the material under true processing conditions.
6. The deformability in flow of the dispersed phase, not reported before, at temperatures below the melting point, may have important commercial consequences. Some of these will be discussed in a subsequent paper of this series.

ACKNOWLEDGMENT

The authors would like to acknowledge the careful work of Mr. Pierre Sammut for collecting rheological data and Mr. Michel Thibodeau for the SEM results.

REFERENCES

1. S. P. Hersh, *J. Appl. Polym. Sci., Appl. Polym. Sym.*, **31**, 37 (1977).
2. E. E. Magat and D. Tanner (to E. I. DuPont de Nemours & Co.), U. S. Pat. 3, 329, 557, July 4, 1967.
3. S. P. Hersh, *Polym. Plast. Technol. Eng.*, **3**, 29 (1974).
4. G. R. Bhat and S. P. Hersh, *J. Appl. Polym. Sci., Appl. Polym Sympos.*, **31**, 55 (1977).
5. Y. Sano, M. Miyamoto, Y. Kimura, and T. Saegusa, *Polym. Bull.*, **6**, 163 (1981).
6. S. Y. Hobbs, R. C. Bopp, and V. H. Watkins, *Polym. Eng. Sci.*, **23**, 380 (1983).
7. F. Ide and A. Masegawa, *J. Appl. Polym. Sci.*, **18**, 963 (1974).
8. D. Braun and U. Eisenlohr, *Kunststoffe*, **65**, 139 (1975).
9. M. Tokarzewska and Z. Bryla, *Polimery*, **24**, 46 (1979).
10. B. Liang, J. L. White, J. E. Spruiell, and B. C. Goswami, *J. Appl. Polym. Sci.*, **28**, 2011 (1983).
11. G. Hinrichsen and W. Green, *Kunststoffe*, **71**, 99 (1981).
12. M. R. Kamal, I. Jinnah, and L. A. Utracki, NRCC-IMRI "Polyblends-'84" Symposium, April 17, 1984, Boucherville, Canada.; *Polym. Eng. Sci.*, **24**, 1337 (1984).
13. M. M. Dumoulin, P. Toma, and L. A. Utracki, *S.P.E. ANTEC Tech. Papers*, **31**, 534 (1985).
14. E. B. Bagley, *J. Appl. Phys.*, **28**, 624 (1957).
15. B. Rabinowitsch, *Z. Phys. Chem.*, **A145**, 1 (1929).
16. L. A. Utracki and M. M. Dumoulin, *Polym. Plast. Technol. Eng.*, **23**, 193 (1984).
17. G. V. Vinogradov, A. Ya Malkin, N. V. Prozorovskaya, and V. A. Kargin, *Dokl. Akad. Nauk SSSR*, **154**, 980 (1964).
18. C.-C. Lin, *Polym. J.*, **11**, 185 (1979).
19. L. A. Utracki and R. Gendron, *J. Rheol.*, **28**, 601 (1984).
20. L. A. Utracki, The 9th Intl. Congr. Rheol., Acapulco, Mexico, 8–13 October, 1984; Proceed., **3**, 567 (1984).
21. L. A. Utracki, Proceed. Polymer Proc. Inst. Seminar on LLDPE, Teaneck, N. J., Jan. 15–16, 1985; Adv. Polym. Technol., **5**, 141 (1985).
22. L. A. Utracki, M. R. Kamal, and M. M. Al-Bastaki, *S.P.E. ANTEC Tech. Papers*, **30**, 917 (1984).
23. L. A. Utracki and J. Lara, Proceed. Table Ronde Intl. "Ecoulements élongationnels", Mülhouse-La Bresse, France, Jan. 23–28, 1983.
24. L. A. Utracki and B. Fisa, *Polym. Compos.*, **3**, 193 (1982).
25. B. Fisa and L. A. Utracki, *ibid.*, **5**, 36 (1984).
26. L. A. Utracki, *Rubber Chem. Technol.*, **57**, 55 (1984).
27. L. A. Utracki, The 9th Intl. Congr. Rheol., Acapulco, Mexico, 8–13 Oct., 1984; Proceed., **3**, 467 (1984).
28. L. A. Utracki and M. R. Kamal, *Polym. Eng. Sci.*, **22**, 96 (1982).
29. L. A. Utracki, *ibid.*, **23**, 602 (1983).
30. L. A. Utracki, and G. L. Bata, *Mater. Technol.* (Paris), **70**, 223, 282 (1982).
31. L. A. Utracki, *Polym. Plast. Technol. Eng.*, **22**, 27 (1984).
32. O. V. Romankievich, K. V. Yakovlev, S. E. Zabello, T. I. Zhila, and V. S. Rudchuk, *Khim. Volok.*, **1**, 21 (1984).
33. N. A. Frankel and A. Acrivos, *J. Appl. Mech.*, **44**, 65 (1970).
34. S. J. Choi and W. R. Schowalter, *Phys. Fluids*, **18**, 420 (1975).
35. H. L. Goldsmith and S. G. Mason, "The Microrheology of Dispersions" in Rheology Theory and Applications, Ed. F. R. Erich, Vol. 4, pp 85–250 Academic Press, New York, NY, (1967).
36. C. D. Han, "Multiphase Flow in Polymer Processing", Academic Press, New York, NY, (1981).
37. W. F. Busse, *Phys. Today*, **17**, 32 (1964).
38. H. P. Schreiber and S. H. Storey, *J. Polym. Sci. Polym. Letters*, **3**, 723 (1965).
39. H. P. Schreiber, *J. Appl. Polym. Sci.*, **18**, 2501 (1974).
40. W. Berger and C. Michels, *Faserf. Textilt.*, **26**, 390 (1975).
41. T. I. Zhila and V. I. Mazurenko, *Khim. Technol.*, **5**, 37 (1980).

42. A. P. Nikolaieva, A. A. Gierasimchuk, N. A. Skliar, O. V. Romankievich, and A.V. Yudin, *Khim. Technol.*, 3, 10 (1982).
43. M. V. Tsebrenko, A. V. Yudin, T. I. Ablazova, and G. V. Vinogradov, *Polymer*, 17, 831 (1976).
44. A. Cifferi and I. M. Ward, Eds., "Ultra High Modulus Polymers", Appl. Sci. Publishers Co., Barking, Essex, (1979).
45. A. E. Zachariades and R. S. Porter, Eds., "The Strength and Stiffness of Polymers", M. Dekker Inc., New York (1983).
46. F. N. Cogswell, *Polym. Eng. Sci.*, 12, 69 (1972).
47. A. M. Catani and L. A. Utracki, Proceed. Ann. Meet. Polymer Processing Society, Akron, OH., March 28–29, 1985; J. Polym. Eng., in press.

NOMENCLATURE

a_T = Shift factor.
B = Extrudate swell.
c = Polyamide-6 content.
d = Capillary diameter.
D/D_o = Dispersed phase diameter after and before extrusion.
E_η = Activation energy of flow.
G' = Storage shear modulus.
G'' = Loss shear modulus.
L = Capillary length.
P = Total pressure loss in capillary flow.
P_e = Capillary end effects pressure loss.
T = Temperature
T_m = Melting point.
T_R = Reference temperature.
w = Weight fraction.
α = Half-angle of convergence in capillary flow.
β = Parameter *Eq 4*.
β_{12} = Inter-layer slip factor.
$\dot{\epsilon}$ = Elongational strain rate.
γ = Shear strain in dynamic tests.
$\dot{\gamma}$ = Shear rate.
η = Steady state shear viscosity.
η' = Dynamic shear viscosity.
η_0 = Zero-shear viscosity.
η_e = Elongational viscosity.
σ_y = Yield stress.
σ_{11} = Elongational stress.
σ_{12} = Shear stress.
ω = Angular frequency.

DISCUSSION: L. A. UTRACKI, M. M. DUMOULIN, AND P. TOMA

H. P. Shreiber: The steady state data may be less reliable, but they give a more realistic assessment of the behavior during flow in an extrusion die, where the flow segregation must also occur.

M. M. Dumoulin: Yes, the capillary flow is very interesting but it is less useful as far as characterization of multiphase material is concerned. If you want to know the true rheological response of a given structure, a given morphology of polymeric blends or composites, you have to do dynamic testing.

H. P. Schreiber: Yes. It depends on the objectives.

D. Froelich: It is interesting to note that the temperature-frequency superposition works even below the melting point of one component in your blends, especially at the lower shear rates. The fact that you can apply the superposition both below and above the melting point data is rather surprising.

M. M. Dumoulin: Indeed we obtained good superposition but only with the dynamic data over the whole range of frequencies at low strain. Using the same shift factors determined for dynamic data we did not manage to superimpose the high strain capillary results. The superposition seems to depend not so much on rate of deformation as on strain and resulting modification of morphology.

J. M. Charrier: At the low temperature, 150°C, you observed what you called nylon fibrils. You used two terms: "drawn" and "coalescent" in explaining their formation. This was not clear to me since obviously the material was in the solid state.

M. M. Dumoulin: The glass transition temperature of poly(ϵ-caprolactam) is about 50 to 60°C. The crystallinity being about 40 percent, one may consider the PA-6 phase as a suspension of crystals in a viscous liquid. At the entrance to the capillary region there is a strong extensional field. We calculated the available elongational stress to be of the order of 50 to 800 kPa, which is higher than the value of 12 kPa, measured independently on a solid PA-6 sample at 150°C, as the value required to sustain a continuous drawing of the material. So, as far as drawing is concerned, I think that the mechanism is quite well understood. The fact that the drawing must be associated with a coalescence of the PA-6 domain is inferred from observation of the volume of the fibrils. Their diameter being approximately equal to that of the PA-6 particles in the blend as placed in the barrel and the length larger by at least one order of magnitude, leads to the conclusion that coalescence did occur. As a post factum one can justify this considering, on one hand, the crowding of flow lines at the entrance to the capillary and, on the other hand, the natural tendency of immiscible phases to grow.

R. Hoffman: Did you examine the morphological changes as a function of capillary length? Did you try to follow the kinetics of the process?

M. M. Dumoulin: Not really. We have used capillaries of different lengths. However, this was mainly in order to calculate Bagley's correction. We did see a general trend primarily where the shear segregation is concerned, but we did not examine carefully enough the variations of shape and size of PA-6 fibrils with the capillary length.

L. A. Utracki: We did measure the average particle size of PA-6 spherical particles (at low concentration) as a function of rate of shear. The average diameter in the granulated material, as loaded into the instrument, was about 4 μm. From this value the

diameter decreased to about 1.3 μm at $\dot{\gamma} = 10^3\ s^{-1}$. Capillary length had virtually no effect for capillaries with $L/d = 10$ to 40. On the other hand, the particles in the center of the stream were larger than those near the wall. This is illustrated in *Fig. 18* of the paper.

H. P. Schreiber: May I also mention that this paper warms the cockles of my ancient heart in that it constitutes the clearest demonstration of the migration of materials in the capillary flow. Leszek may remember that in the early sixties we were writing papers which showed redistribution of material in multicomponent polymer systems. Our interpretation at that time was that the materials which were least elastically deformable would migrate into the area of maximum deformability. In other words, the non-deformable particles would wind up at the capillary wall and the highly deformable material would migrate towards the center, where the profile is such that there is virtually zero shear rate. I think that your data tend to put a rather large check mark beside this idea, which pleases me no end.

Polyethylene-Polycarbonate Blends: Interface Modification, Phase Morphology and Measurement of Orientation Development During Cast Film and Tubular Extrusion by Infrared Dichroism

SHIGERU ENDO,* KYONSUKU MIN, JAMES L. WHITE, *and* THEIN KYU

Polymer Engineering Center
The University of Akron
Akron, Ohio 44235

The phase morphology and polymer chain orientation in polyethylene-polycarbonte blends is investigated. A blend with a dispersed polyethylene phase was found to exhibit phase growth under quiescent conditions. Addition of a styrene-(ethylene/butene) block copolymer controls the phase morphology and prevents phase growth. Melt spun tapes and tubular film have been prepared from polyethylene-polycarbonate blends. Orientation of the crystallographic axes of the polyethylene and the chain axis of the polycarbonate were determined by infrared dichroism. The addition of polycarbonate to polyethylene is found to decrease chain orientation at the same drawdown stress.

INTRODUCTION

Polyethylene (PE) and polycarbonate (PC) are both important commercial plastics. Their blends have received limited attention in the literature (1–3). The blends are incompatible and generally give coarse phase morphologies. They are superficially similar to the much studied polyethylene-polystyrene (PS) system in that they involve polyethylene and an aromatic glassy plastic. A major difference is the polarity of the polycarbonate results in larger interfacial tensions and hence to the coarser phase morphology.

This paper continues earlier investigations on the PE/PC and PE/PS systems (3, 4). It is well known that both substantial improvements in the properties of PE/PS blends are possible and morphologies made more fine grained by the addition of block and graft copolymers involving styrene, ethylene, and butene units (SEBS) (5–9). With the aromatic groups in PC, it is possible that such copolymers might act as interface modifiers in PE/PC blends as they apparently do in polyethylene-polyethylene terephthalate blends (10). We look to the influence of block copolymers of the SEBS type on phase morphology.

Also of concern to us is the measurement of orientation in polymers and blend systems. The study of orientation in different phases in a polymer blend has a topic of some interest (4, 11–15). Both uniaxial and biaxial orientation are of concern. Studies of uniaxial orientation in fibers and films have a long history. The characterization of biaxial orientation has only received substantial study in relatively recent years (14, 16, 19) largely using X-ray diffraction and birefringence. Little of this effort has used infrared dichroism (15, 20–22) and none have considered blends. We shall seek to apply this method in the present paper. Infrared dichroism measures the absorption of particular chemical groups. It is thus able to selectively detect orientation in the different types of polymers present and thus is quite suitable for studies of blends.

The development of orientation in melt spun fibers of blends have been investigated by Liang, *et al* (23) and by Min, et al (4). The latter authors used X-ray diffraction on polyethylene-polystyrene blends determined that orientation in polyethylene decreased with increasing level of polystyrene at fixed spinline stress or drawdown ratio. Liang, *et al* found using X-ray diffraction that in polypropylene-nylon-6 blends, the orientation of polypropylene is independent of spinline stress, but nylon-6 orientation decreased with polypropylene content. We look to

* Permanent Address: Ube Industries, Ltd., Research Laboratories, Chiba, Japan

the influence here of polycarbonate on the orientation of polyethylene.

Summarizing, in this paper we examine both the development of phase morphology in polyethylene-polycarbonate blends and the character of orientation in the individual phases of these blends. We first look at influences of annealing on the melt or phase morphology. We then turn to the continuous melt casting to form uniaxially drawdown tapes and use infrared dichroism to characterize the uniaxial orientation. We finally describe tubular film extrusion of the blends and the application of this same technique to determine biaxial orientation.

EXPERIMENTAL

Materials

The polyethylene used in this study was Chemplex 6186, and the polycarbonate a General Electric Lexan 101-111. The melts were blended together at 260°C in a Killion 3/4 inch screw extruder with a Koch static mixer. Blends were prepared with compositions PC/PE, 20/80, 40/60, 60/40, 80/20. Blends containing an additional 5 parts of styrene-(ethylene/butene) block SEBS copolymer (Shell Kraton G) were also prepared.

Annealing and Extrusion

The blends were annealed in the reservoir of an Instron capillary rheometer at 260°C and subsequently extruded through a die of diameter 1.27 mm (0.0501 in) and length-diameter ratio of 40. A die wall shear rate of 2.24 s^{-1} was used.

Drawdown (Spinning) of Tapes

The blends were extruded at 230°C through a slit die of dimensions 0.38 × 6.35 × 7.90 mm with drawdown onto a rotating take-up roll. Drawdown ratios were up to 240 and tensions were sensed with a Rothschild tensiometer.

Tubular Film Extrusion

Tubular films were prepared on a Killion 3/4 inch screw extruder with a tubular film attachment (inside diameter 3.04 cm and outside diameter of 3.17 cm). The extrusion temperature was 260°C. Drawdown ratios V_L/V_o were 4.1, 6.8, and 11.0. Blow-up ratios R_L/R_o, B, were 1.15 and 2. Bubble pressures were measured by U type manometer. The take-up tension was measured with a Rothschild tensiometer.

Scanning Electron Microscopy

The phase morphology of the blends was investigated using a JEOL U-3 scanning electron microscope. Fracture surfaces were prepared in liquid nitrogen. The samples were coated with a gold-palladium alloy before viewing to prevent charging in the electron beam.

Infrared Dichroic Measurements

Orientation in the blend tapes and films was investigated using infrared dichroic measurements with an IBM IR/32 Spectrometer.

The infrared bands used were for polyethylene (24) the 720, 730, 1303, 1352, and 1358 cm^{-1} band and for polycarbonate (25) the 889 and 1364 cm^{-1} bands. The polyethylene component 720 cm^{-1} band transition moment is parallel to the b-crystallographic axis and 730 cm^{-1} is dominated by a contribution parallel to the a-crystallographic axis. The transition moments for the polycarbonate have not been fully verified. Lunn and Yannis (25) suggest the 889 cm^{-1} is 70 ± 10° and 1364 cm^{-1} is 90 ± 10°.

The uniaxial orientation of the tapes was computed from the dichroic ratio defined by

$$D = \frac{A_1}{A_2} \tag{1}$$

where '1' is the machine and '2' the transverse directions. It may be shown that the Hermans-Stein orientation factor (26, 27) of a particular crystallographic axis is related to the dichroic ratio D through (20, 28, 29)

$$f_j = \frac{3\overline{\cos^2\phi_j} - 1}{2} = \frac{D-1}{D+2}\frac{D_o+2}{D_o-1} \tag{2}$$

where D_o is the maximum value of the dichroic ratio which is related to the angle α_j between the transition moment of a specific band and the j crystallographic axis by

$$D_o = 2\cot^2\alpha_j \tag{3}$$

In order to characterize biaxial orientation we measure the dichroic ratios D^0 and D^{45} at 0 and 45° tilting angles of the sample to the plane of the beam. This technique is due to Nomura, et al (15). These are related to the principal absorptivities A_{11}, A_{22}, and A_{33} by

$$D^0 = \frac{A_{11}}{A_{33}} = \frac{D_{13}}{D_{23}} \tag{4a}$$

$$D^{45} = \frac{2A_{11}}{A_{22}+A_{33}} = \frac{2D_{13}}{2D_{23}+1} \tag{4b}$$

where D_{13} and D_{23} are the biaxial dichroic ratios. We relate these to the White-Spruiell orientation factors (16) through the relationships (28):

$$\frac{A_{11}-A_{33}}{A_{11}+A_{22}+A_{33}} = \frac{D_{13}-1}{D_{13}+D_{23}+1} = \frac{a_\parallel^0 - a_\perp^0}{a_\parallel^0 + 2a_\perp^0} f_{aj} f_{ij}^B \tag{5a}$$

$$\frac{A_{22}-A_{33}}{A_{11}+A_{22}+A_{33}} = \frac{D_{23}-1}{D_{13}+D_{23}+1} = \frac{a_\parallel^0 - a_\perp^0}{a_\parallel^0 + 2a_\perp^0} f_{aj} f_{2j}^E \tag{5b}$$

where the D_{ij}^0 are maximum values of the di-

chroic ratios and

$$f_{1j}^{B} = 2\overline{\cos^2\phi_{1j}} + \overline{\cos^2\phi_{2j}} - 1 \qquad (6a)$$

$$f_{2j}^{B} = 2\overline{\cos^2\phi_{2j}} + \overline{\cos^2\phi_{1j}} - 1 \qquad (6b)$$

are biaxial orientation factors (12), $a_\parallel$ and $a_\perp$ are absorption coefficients parallel and perpendicular to the molecular axis and

$$f_{aj} = \frac{3\overline{\cos^2\alpha_j}}{2} - 1 \qquad (7)$$

where α_j is the angle between the j crystallographic axis and the transition moment. In applying *Eq 5* we take $a_\perp^0$ to be zero.

PHASE MORPHOLOGY OF THE EXTRUDATES OF THE BLENDS

The effect of the residence time on the phase growth of the blends which were kept in a reservoir of the capillary rheometer was observed. This study was carried out at residence times of 30, 60, and 90 min at 260°C.

The SEM photomicrographs of the cross sections of the extruded blends PC/PE = 40/60, 60/40, 80/20 are shown in *Figs. 1, 2,* and *3*. PC forms islands (dispersed domain) in a PE sea (continuous matrix) at the composition of PC/PE of 20/80 and 40/60. PC is the continuous phase and PE the dispersed phase when PC/PE is 80/20 or 60/40.

Phase growth is observed with increasing residence time when PC is the continuous phase. This the case for the 80/20 and 60/40 blends. PC/PE of 40/60 and 20/80 do not show phase growth. The observations are similar to those of Liang, *et al* (23) who observed phase growth in polypropylene nylon-6 blends when nylon-6 was the continuous phase but not when the polypropylene was. The coalescence of polyolefins in a polycondensate sea but not vice versa may be associated with the lower viscosity of the polycondensate matrix.

The effect of the SEBS block copolymer is observed clearly as may be seen in *Figs. 2* and *3*. It makes dimensions of the dispersed PE phase become smaller and retards phase growth. There is little effect when PE is the continuous phase. This is similar to the observations of Heikens and Barentsen (8) on PE/PS blends with a styrene-ethylene graft copolymer as compatibilizer.

The influence of the block copolymer would appear to be to control the interfacial tension. Decreasing interfacial tension stabilizes the system. This was argued by Liang, *et al* (23). The molecular mechanism needs further consideration. The polyethylene segment dissolves in the polyethylene component of the blend, the polystyrene segment may collect at the interface and associate with the phenyl rings in the polycarbonate. It is to be noted that polystyrene is not compatible with polycarbonate and the interactions must be more complex than in the PE/PS/SEBS system.

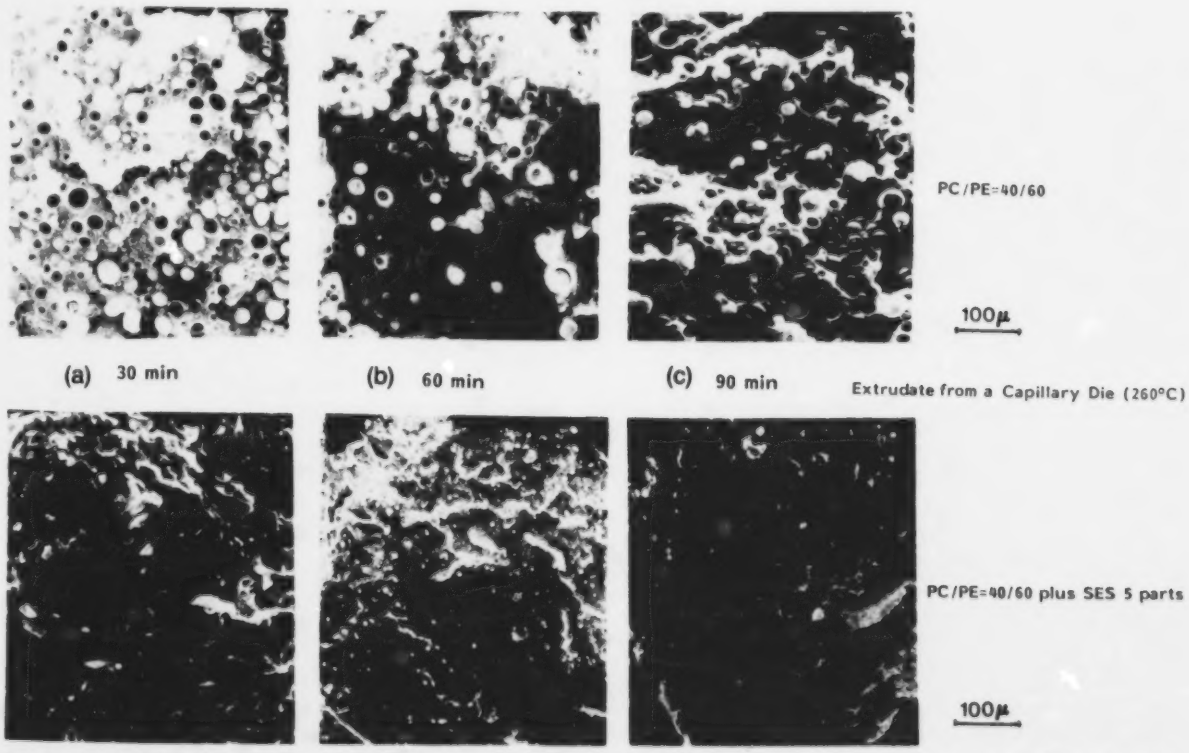

Fig. 1. SEM photomicrographs of PC/PE 40/60 and PC/PE/SEBS blends extruded from a die at $32Q/\pi D^3 = 2.44\ s^{-1}$ T = 260°C (a) 30 min, (b) 60 min, (c) 90 min.

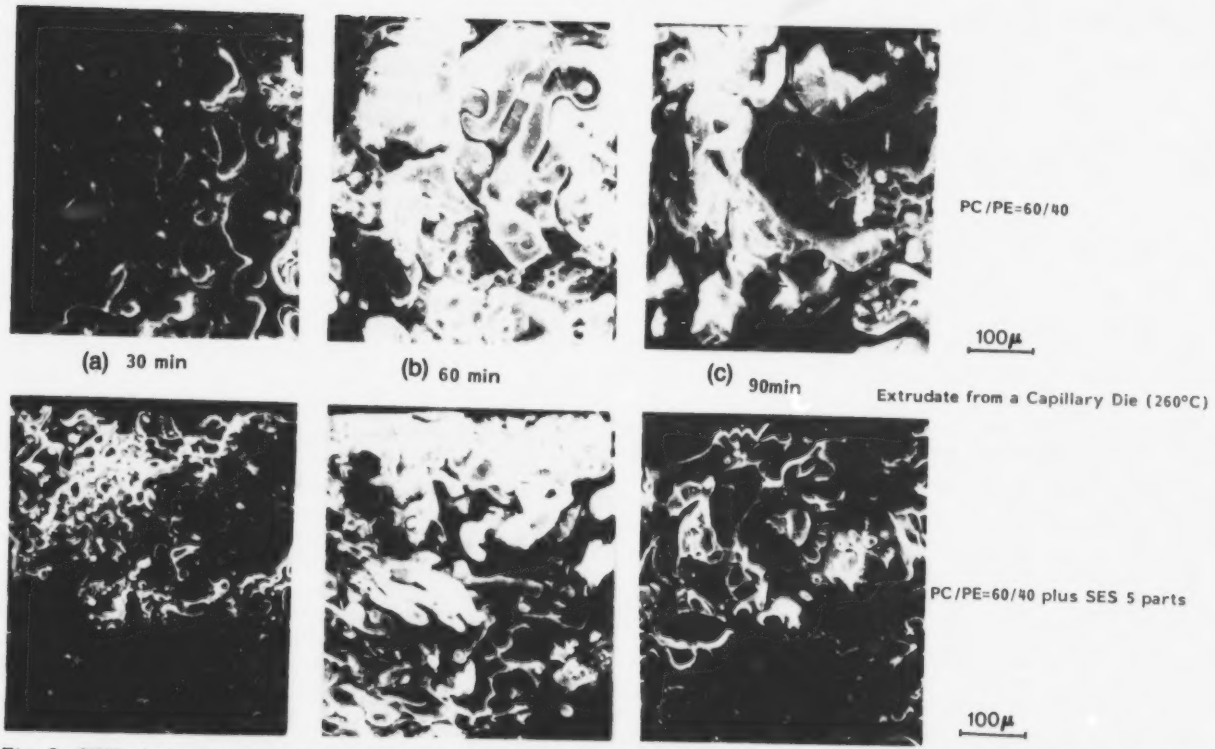

Fig. 2. SEM photomicrographs of PC/PE 60/40 and PC/PE/SEBS blends extruded from a die at $32Q/\pi D^3 = 2.44\ s^{-1}$, $T = 260°C$ (a) 30 min, (b) 60 min, (c) 90 min.

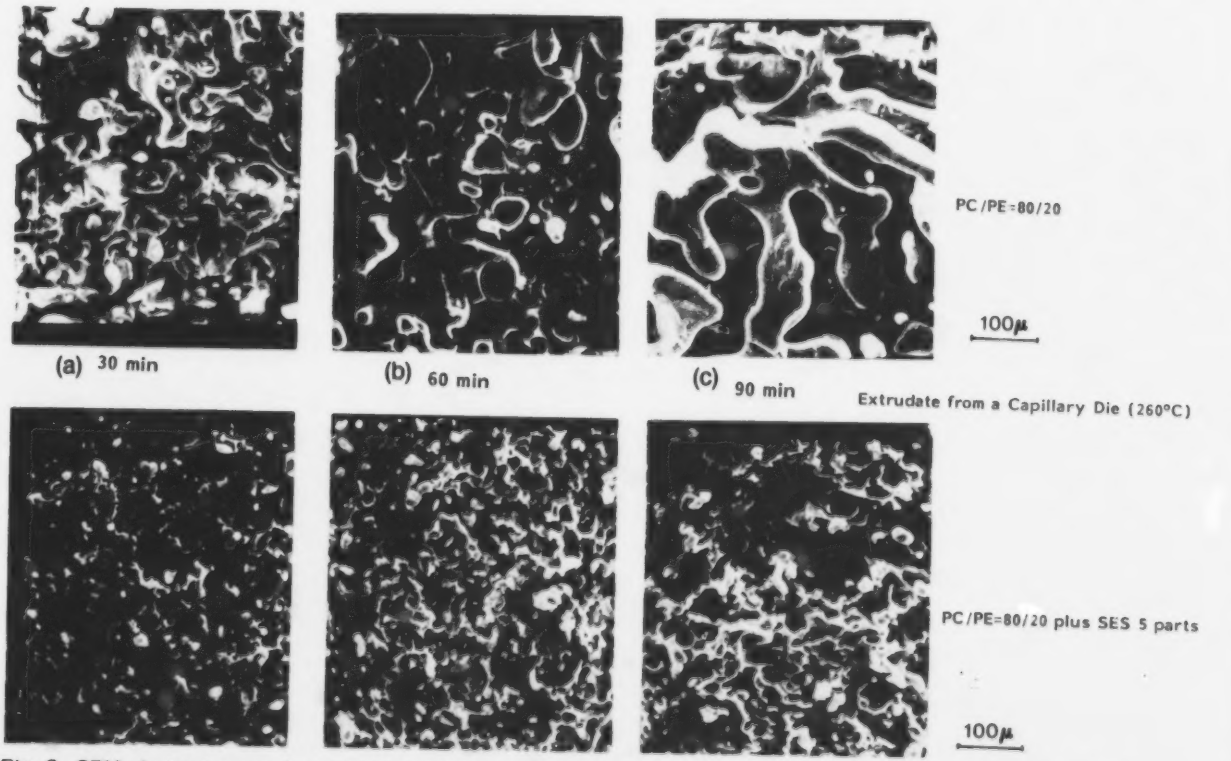

Fig. 3. SEM photomicrographs of PC/PE 80/20 and PC/PE/SEBS blends extruded from a die at $32Q/\pi D^3 = 2.44\ s^{-1}$, $T = 260°C$ (a) 30 min, (b) 60 min, (c) 90 min.

UNIAXIAL ORIENTATION IN EXTRUDED AND DRAWN DOWN TAPES

We first consider the pure polyethylene. The dependence of the orientation factors f_a, f_b, and f_c for the crystalline phase of polyethylene on drawdown ratio V_L/V_o is shown in *Fig. 4*. The results are basically similar to those obtained with wide angle X-ray diffraction for polyethylene fibers and films (18). The orientation decreases with increasing processing temperature.

The orientation factors f_a, f_b, and f_c for the crystalline regions of the polyethylene in the PE/PC blends are shown in *Fig. 5*. The data is presented as a function of drawdown stress. The correlation of orientation with spinline stress has been noted in various polymers (31, 32). The amorphous orientation factor of polyethylene is small and positive (see *Fig. 6*.)

The orientation of the pure polycarbonate phase is found small and positive. These are shown in *Fig. 7* as a function of drawdown stress. Here we have to take α to be 70° for the 889 cm^{-1} and 90° for the 1364 cm^{-1}. The orientation factors of the PE/PC blends will now be considered. The orientation of the PE crystalline phase decreases with increasing PC content when comparisons are made at constant drawdown ratio or spinline stress (see *Fig. 8*). The behavior is similar to that observed by Min, *et al* (4) who studied orientation in melt spinning of PE/PS blends using X-ray diffraction. It is the same as that found by Liang, *et al* (23) for the orientation of nylon-6 in blends with polypropylene. The orientation of the polypropylene is, however, independent of the spinline stress.

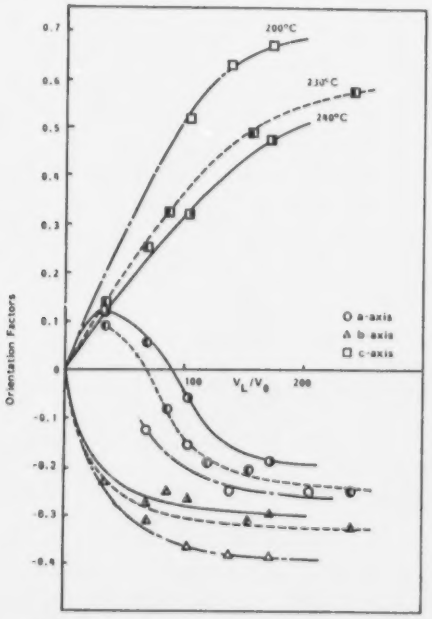

Fig. 4. Orientation factors for crystalline phase of PE as a function of drawdown ratio.

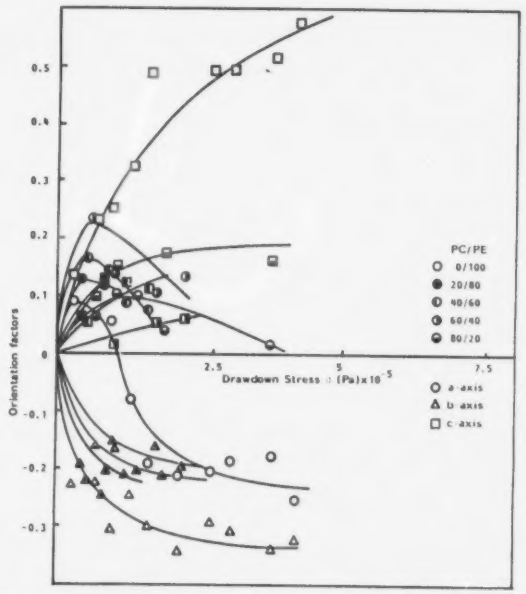

Fig. 5. Orientation factors for crystalline phase of PE in blends as a function of drawdown stress.

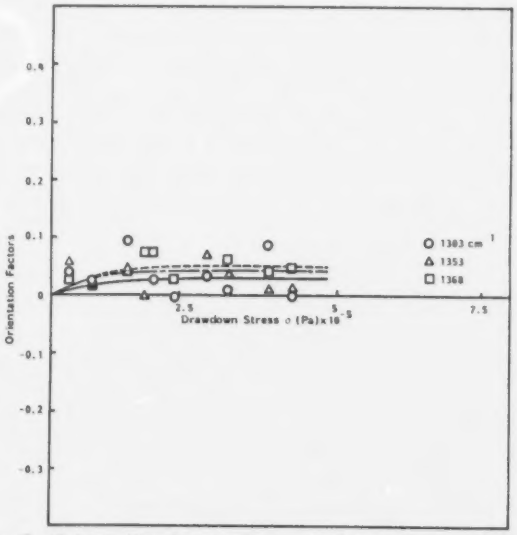

Fig. 6. Orientation factors for amorphous phase of PE as a function of drawdown stress.

The observation of orientation decreases in blends is probably due to a redistribution of stress among the components of the cross-section of the spinline. Without such redistribution of stress, voiding would occur. The material with the higher activation energy of viscous flow increases more rapidly in viscosity and takes up increasingly more stress. Thus the vitrifying polycarbonate in PE/PC blends and polystyrene in PE/PS takes up more and more of the stress. When the polyethylene crystallizes the stresses acting on it are lower and its orientation is lower. A similar argument was made by Min, *et al* (4). For the nylon-6/polypropylene blends, the latter component crystallizes

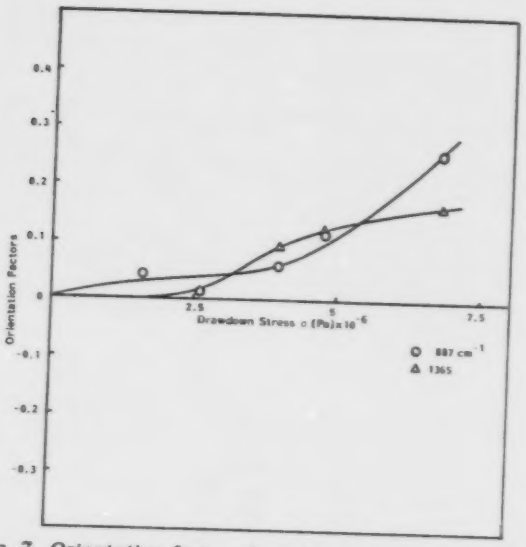

Fig. 7. Orientation factors for polycarbonate as a function of drawdown stress.

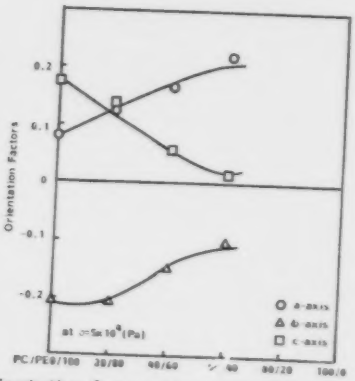

Fig. 8. Orientation factors for crystalline phase of PE vs. composition at constant drawdown stress in PE/PC blends.

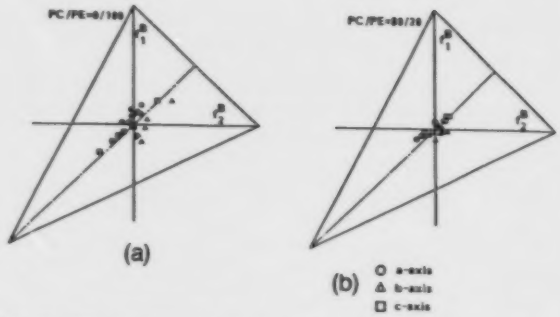

Fig. 9. White-Spruiell orientation factors for crystalline phase of HDPE in PE/PC blends. (a). PC/PE = 0/100, (b) PC/PE = 80/20.

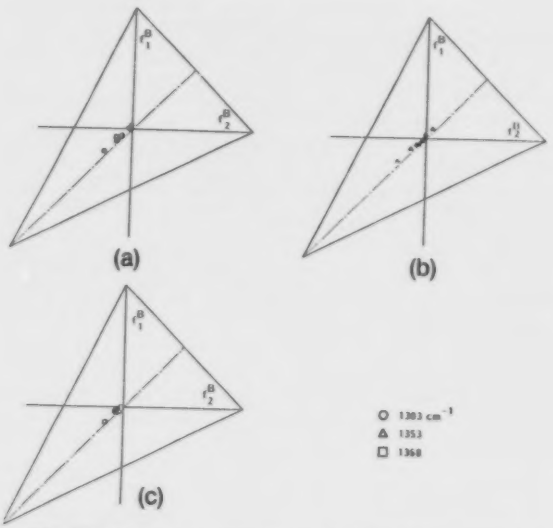

Fig. 10. White-Spruiell orientation factors for amorphous phase of HDPE. (a). 1303 cm^{-1} band, (b) 1353 cm^{-1} band (c). 1368 cm^{-1} band.

at about 90°C (31) but nylon-6 crystallizes after the fiber reaches the bobbin (33). The stress redistributes itself and concentrates on the crystallized polypropylene. There is little stress on the nylon-6 under the conditions in which it crystallizes. Thus the orientation of nylon-6 is greatly reduced by blending with polypropylene.

BIAXIAL ORIENTATION IN TUBULAR FILM EXTRUSION

We have plotted the orientation factors f^B_{1j} and f^B_{2j} determined from the tubular film in an isosceles triangle diagram of the type described by White and Spruiell (16, 19) in *Figs. 9* and *10*.

The orientation of both crystalline and amorphous phases are very small even in pure PE. Low orientations are generally found in tubular film extrusion because of the small stresses (18). This is accentuated by the high temperatures (260°C) necessary to form films for the blends. It was the lowest temperature at which blown films could be made in this blend system. However, it was found that the orientation decreases with increasing PC content as in the case of melt spinning.

CONCLUSIONS

There are two primary results of this paper. First, polyethylene dispersed in a polycarbonate melt exhibits phase growth and this phase growth is inhibited by an addition of SEBS block copolymers. This result is probably due to a reduction in the interfacial tension between the PE and PC by the SEBS.

The second important result is that the addition of PC to PE reduces the orientation in PE developed in film extrusion when determined at constant stress (or drawdown). The same phenomenon has been observed in polyethylene/polystyrene and nylon-6/polypropylene blends.

ACKNOWLEDGMENT

This research was supported by the Polymers Section of The Division of Materials of The National Science Foundation, through Grant No. DMR 8026051.

REFERENCES

1. A. F. Yee, *J. Mater. Sci.*, **12**, 757 (1977).
2. T. Kunori and P. H. Geil, *J. Macromol Sci. Phys., B18*, **93**, 135 (1980).
3. K. Min, J. L. White, and J. F. Fellers, *Polym. Eng. Sci.*, **24**, 1327 (1984).
4. K. Min, J. L. White, and J. F. Fellers, *J. Appl. Polym. Sci.*, **29**, 2117 (1984).
5. C. E. Locke and D. C. Paul, *J. Appl. Polym. Sci.*, **17**, 2791 (1973).
6. W. M. Barentsen and D. Heikens, *Polymer*, **14**, 579 (1973).
7. W. M. Barentsen, D. Heikens, and P. Piet, *Polymer*, **15**, 119 (1974).
8. D. Heikens and W. Barentsen, *Polymer*, **18**, 69 (1977).
9. G. R. Lindsey, D. R. Paul, and J. W. Barlow, *J. Appl. Polym. Sci.*, **26**, 1 (1981).
10. T. D. Traugott, J. W. Barlow, and D. R. Paul, *J. Appl. Polym. Sci.*, **28**, 2947 (1983).
11. S. Onogi, T. Asada, and A. Tanaka, *J. Polym. Sci., A-2*, **7**, 171 (1969).
12. S. T. Wellinghoff, J. L. Koenig, and E. Baer, *J. Polym. Sci. Polym. Phys. Ed.*, **15**, 1913 (1977).
13. D. E. Hubbell and S. L. Cooper, *J. Polym. Sci. Polym. Phys. Ed.*, **15**, 1143 (1977).
14. Y. Shimomura, J. E. Spruiell, and J. L. White, *Polym. Eng. Rev.*, **2**, 417 (1983).
15. S. Nomura, H. Kawai, I. Kimura, and J. Kagiyama, *J. Polym. Sci. A-2*, **5**, 179 (1967).
16. J. L. White and J. E. Spruiell, *Polym. Eng. Sci.*, **21**, 859 (1981).
17. K. Matsumoto, J. F. Fellers, and J. L. White, *J. Appl. Polym. Sci.*, **26**, 85 (1981).
18. K. J. Choi, J. E. Spruiell, and J. L. White, *J. Polym. Sci. Phys. Ed.*, **20**, 27 (1982).
19. M. Cakmak, J. E. Spruiell, and J. L. White, *Polym. Eng. Sci.*, **24**, 1390 (1984).
20. J. L. Koenig and S. W. Cornell, *J. Polym. Sci. A-2*, **5**, 301 (1967).
21. J. L. Koenig and S. W. Cornell, *J. Macromol Sci. (Phys.)*, **B1**, 279 (1967).
22. B. Jasse and J. L. Koenig, *J. Macromo. Sci.–Rev. Macromol Chem.*, **C17**, 61 (1979).
23. B. R. Liang, J. L. White, J. E. Spruiell, and B. C. Goswami, *J. Appl. Polym. Sci.*, **28**, 2011 (1983).
24. B. E. Read and R. J. Stein, *Macromolecules*, **1**, 116 (1968).
25. A. C. Lunn and I. V. Yannas, *J. Polym. Sci. Phys. Ed.*, **10**, 2189 (1972).
26. P. H. Hermans and P. Platzek, *Kolloid Z.*, **88**, 68 (1939).
27. R. S. Stein, *J. Polym. Sci.*, **31**, 327 (1958).
28. J. M. Preston and P. C. Tsien, *J. Soc. Dyers and Col.*, **66**, 361 (1950).
29. R. D. B. Fraser, *J. Chem Phys.*, **24**, 89 (1956).
30. J. L. White, *J. Polym. Eng.* (in press).
31. H. P. Nadella, H. M. Henson, J. E. Spruiell, and J. L. White, *J. Appl. Polym. Sci.*, **21**, 3003 (1977).
32. K. Oda, J. L. White, and E. S. Clark, *Polym. Eng. Sci.*, **18**, 53 (1978).
33. V. G. Bankar, J. E. Spruiell, and J. L. White, *J. Appl. Polym. Sci.*, **21**, 2341 (1977).

DISCUSSION: J. L. WHITE

Editors Comment—The presentation of the paper at the meeting, began by reviewing the contents of *Refs. 3* and *23* which are early work from our laboratories. Many of the questions refer to the earlier work as well as to the contents of the published paper.

A. P. Plochockt: Since you presented in the beginning the relations between the sizes and the concentration for three systems, could you comment on the range of the viscosity ratios of the two components in each blend and on the normal stress ratios. Were these ratios close to one or quite different from one?

J. L. White: This refers to work on polyethylene (PE) blends with polystyrene (PS), polycarbonate (PC), and nylon-6 already published in *Ref. 3*. The data is in *Fig. 1b* of that paper. PE had higher viscosity. The PC viscosity has a significantly lower η_0 but there is a cross-over at higher shear rates. The PS viscosity level was much lower. Nylon 6 had the lowest viscosity. The order of viscosity ratio at low shear rates is PE/N6 > PE/PS > PE/PC.

A. P. Plochockt: But were the ratios similar or different for each set of compositions? I think that making a blend one should attempt to keep the ratio of at least one function constant. The viscosity ratio is the simplest, but you may decide to keep the normal stress ratio or interfacial tension ratio constant, or whatever.

J. L. White: This is a very difficult thing to do. If you wish to compare materials as different as polyolefins, polycarbonate, styrenics, and nylon.

A. P. Plochockt: Most of the polyblends you studied were prepared in a combination of dispersive and distributive mixing, i.e., extruder and motionless mixer. Did you do any evaluation of blend morphology after mixing, but before extruding it through its capillary?

J. L. White: The photomicrographs where I compared PE, PC, nylon 6, and PS were taken from strands after the static mixer. All materials underwent the same kinematic history. (see *Ref. 3*).

R. E. Prud'homme: Several authors proposed that in order to optimize compatibilization behavior of two immiscible polymers, such as PE and PC. Certain requirements regarding the molecular weight of each block in the compatibilizing block polymer should be observed. What were the molecular weights of the different polymers you have used? Have you tried to optimize this important behavior?

J. L. White: No, but I would eventually like to. I imagine that what you are saying is true. We are at the state where we are looking at this phenomenon in many different systems. If you have a synthetic laboratory under your control, then you can do experiments like that, but if you are working with commercially available materials it is very difficult.

D. E. Henton: I understand that you are using SEM to characterize the domain sizes. I have a feeling that probably you are looking only from

one direction at these morphologies. If you would take SEM from two directions, you could see a more complete picture. You may have balls or logs.

J. L. White: We have made such experiments, and we discussed the balls/logs morphologies in our earlier papers. (Min, *et al J. Appl. Polym. Sci.*, **29**, 2117 (1984)). Whether you have balls or logs depends primarily on the viscosity ratio. If the dispersed phase has a much higher viscosity, then balls are formed. If the viscosity of the continuous phase is the same or lower, you may get logs.

D. E. Henton: That is true. But this means that it is important to know the molecular weight. So, when you see the end of this log you should know if this is a stump or if its a whole tree. This obviously will affect the blend viscosity. Depending on the type of dispersion the system will show different flow behavior. Previously you commented that one should go to simple system. But even a two component system is not simple due to the type and distribution of morphological structures. The only way out is to work with very low concentration of one component with significantly different viscosity.

J. L. White: There is always polydispersity in domain sizes. We generally evaluate the morphology in longitudinal and transverse directions (see *Refs. 3* and 4). The domain dimensions in the transverse direction usually vary by a factor of two. In the other direction the situation may be quite difficult, since sometimes these filaments can be quite long.

D. E. Henton: Regarding your SEBS compatibilize. Are you confident that it is the interfacial tension you are modifiying not possibly the viscosity ratio?

J. L. White: At that level of concentration you are primarily modifying the interfacial tension.

L. A. Utracki: I would like to make two comments. First, the ratio of viscosity not always works as Prof. White described, i.e., that higher the relative viscosity of the dispersed phase, bigger will be the tendency for ball structure. We prepared blends of polyethylenes and nylons. Extension through a capillary at temperatures significantly (by about 70°C) below the melting point of polyamide resulted in a log-structure. This will be discussed later during the symposium by M. Dumonlon. The mechanism obviously involves fusion and stretching of original balls in the convergent flow into the capillary.

J. L. White: This is a perverse example because you are describing a suspension of soft solid particles in a melt matrix in a strong elongational flow.

L. A. Utracki: Chacunà son gout. The second comment is regarding use of block polymers as compatibilizers. In principle two-block polymers of high-enough molecular weight should be used. There is a balance between the molecular weight and the required mass of block polymer required for mobilization of a given dispersion; higher *MW* lower *c*. At very high molecular weight levels, the copolymer will start forming micelles with itself, loosing the ability to compatibilize. The theory of this process was presented by J. Noolandi during our "Polyblends—83" symposium. The use of block polymers has been extensively discussed by the Liege group directed by Prof. P. Teyssie. The use of three-block polymers, on the other hand, can be much more complex. If for instance, the outer blocks were too large, the central block can be totally shielded and there will be no appreciable enhancement of compatibility. The effect of block polymers in principle is caused by an increase of thickness of the interphase layer.

J. L. White: This is in general correct. We see the same thing. Adding excess of SEBS we observed formation of a third phase. But coming back to the viscosity ratio, we observed the same tendency as that reported by Vinogradov and Tsebrenko, *et al.* There were also many studies dating back to G. I. Taylor, Henry Karam, and Stanley Mason, in which similar observations were reported for low molecular weight liquids.

R. E. Prud'homme: We cannot ignore the fact that there are optimum ratios of molecular weight between the homopolymers and copolymer blocks. If the block molecular weight is not large enough than there is no improvement in properties. This is not the academic but a very practical point.

J. L. White: I do not think that there is anyone who disagrees with you. All of us should do more studies using well characterized systems.

M. D. Whitmore: I do not understand if you are saying that the molecular weights of the block can be either too small or too large and they must be optimized in respect to the two homopolymers, or are you simply saying that they must be large enough to be useful?

R. E. Prud'homme: In the literature, there are numerous papers in which there are evidences that a minimum molecular weight of each block is required. if they are too small, there is no improvement of properties.

J. L. White: The situation is more complex

than that. There are numerous compatibilizers used to affect the interphase, which are more closely related to random than to block copolymers. For instance, there are reports on polystyrene/nylon-6 and EPDM/nylon-6 blends where maleic anhydride modified EPDM is used to control the interfacial tension. In our laboratory, we have recently been using what looks like a random poly(styrene-co-maleic anhydride) which has a similar effect in some polystyrene/nylon-6 blends.

D. Froelich: Concerning reduction of orientation of polyethylene by blending with polycarbonate. If you change the continuous phase by changing the composition, is your change reduced on orientation?

J. L. White: It seems a continuous function. We have not looked carefully enough whether there is a change in the rate. But it continues to change even after the phase inversion.

D. Froelich: But this may be due to the fact that your spinning is not isothermal.

J. L. White: Maybe the phrase "phase inversion" is not proper. Undoubtedly in many of these systems we have two continuous phases.

D. Froelich: May be a good way to test would be to measure the elongational flow of these blends involving isothermal conditions.

J. L. White: Yes, we have published studies of this in *Ref. 4*. Sometimes we find that the blend filament specimens shrink after being placed in an isothermal bath and it is very difficult to measure the elongational viscosity. (e.g., A. Santamaria and J. L. White, *J. Appl. Polym. Sci.* (in press)).

B. Amaduli: Have you measured the glass transition temperature and what is the compositional dependence of T_g?

J. L. White: Studies on these systems indicate that there is no miscibility. We did not measure T_g's of the ternary systems with block polymer present.

C. C. Han: When you add block polymer do you get a truly thermodynamically stable system, or are you simply slowing down the coalescence rate?

J. L. White: It is not clear. I am not sure if the system is thermodynamically stable.

C. C. Han: There is no evidence that you have to dissolve in the system, stir it in. The copolymer just disperses to the particular sites. But supposedly you will mix, stir in the copolymer very uniformly, and then leave the system above the transition point for a very long time, until degradation takes over. Would you see a time dependent coarsening?

J. L. White: This would be difficult to do quantitively, especially on a coarsened system.

L. A. Utracki: Work in this area has been carried out by Philip Teyssie and his group. These researchers demonstrated that the effect of a properly taylored block polymer in a polymer blend can be compared to that of a surfactant in an emulsion. One can over disperse the phases and after the agitation is stopped a coarsening to the level appropriate for a given concentration of the interfacial tension modifier will be obtained. The stability of blend is demonstrated to be as valid as stability of emulsion. According to J. Noolandi the block polymer increases the thickness of the interphase layer, preventing the coalescence. The thickness is related to the square root of the block molecular weight.

C. C. Han: I am familiar with that work on A + B polymers with A − B block polymer. But here the system is different, and I am not certain what answer one may get.

M. D. Whitmore: To answer this question, one must compare the free energy of that morphology with all other possible morphologies.

Phase Separation in Crosslinked Resins Containing Polymeric Modifiers

C. B. BUCKNALL *and* I. K. PARTRIDGE

School of Industrial Science
Cranfield Institute of Technology
Cranfield, Bedford, MK43 OAL, United Kingdom

An analysis is made of the thermodynamic and kinetic factors affecting phase separation in blends of di-, tri- and tetrafunctional epoxy resins, cured with either diaminodiphenylsulphone (DDS) or with dicyanodiamide (Dicy), and modified with either poly(ethersulphone) (PES) or carboxyl-terminated butadiene acrylonitrile (CTBN) rubber. The applicability and limitations of the solubility parameter approach in predicting compatibility in reactive blends are considered.

INTRODUCTION

In comparison with available information on miscibility in thermoplastic polymer alloys and blends, the study of phase separation in blends of reactive thermosetting resins with thermoplastics or elastomers is a relatively uncharted area. Nevertheless, the need for understanding of the phase separation processes taking place in thermosetting blends is the same as in their thermoplastic counterparts, since the resulting morphology is known to affect the optical and mechanical properties of the cured blends. Particular examples of commercially important blends of thermosetting resins with polymeric modifiers include (a) rubber-modified epoxies and acrylics, which are gaining applications as structural adhesives; (b) low shrinkage dough molding compounds based on unsaturated polyesters modified by 'low-profile' thermoplastic additives; and (c) most recently, high-temperature epoxy systems which contain a significant proportion of poly(ethersulphone) (PES) used as a processing aid in the manufacture of advanced carbon fiber-epoxy composites.

The only systematic study of phase separation in modified thermosets has been made by Gillham and co-workers (1, 2) using rubber-modified DGEBA-type epoxy resins. Most other studies of morphology and mechanical properties of rubber modified epoxies also report on the various aspects of phase separation between the rubber and the epoxy, but because the amount and type of rubber, hardener, and the curing regime used are almost invariably different in different investigations, it is not possible to exploit the existing information any further.

A previous paper (3) describes the phase separation behavior of blends of trifunctional and tetrafunctional glycidylamine epoxy resins with PES, using either diaminodiphenylsulphone (DDS) or dicyanodiamide (Dicy) as the hardener. The present paper extends the study to include the more widely used difunctional DGEBA-type epoxy resin and CTBN rubber as an additive. A scheme for comparing the relative compatibilities of individual components of the blends is put forward, based on theoretical values of the solubility parameter, δ.

EXPERIMENTAL

Materials

The structural formulae of the materials are shown in *Table 1*. A single batch of each component material has been used throughout.

Three different liquid epoxy resins were provided by Ciba-Geigy (UK) for this investigation: Epoxy II is the most commonly utilized diglycidyl-ether of Bisphenol A; Epoxy III is a molecularly distilled version of triglycidyl para-aminophenol resin, and Epoxy IV is tetraglycidyl 4,4′-diaminodiphenyl methane resin, which is the basis of most commercial high-temperature epoxy formulations. *Table 2* summarizes manufacturer's data on the properties of the liquid resins; an important feature is the low room temperature viscosity of Epoxy III.

The thermoplastic poly(ethersulphone) modifier is Victrex 100P, a low molecular weight grade of this amorphous, high-temperature engineering plastic. To facilitate the incorporation of this component into the resin blends, ICI (UK) provided the polymer specially milled to a fine powder with a maximum particle size of 6 μm. The degree of polymerization of the 100P grade

Table 1. Structural Formulae of the Components of the Blends.

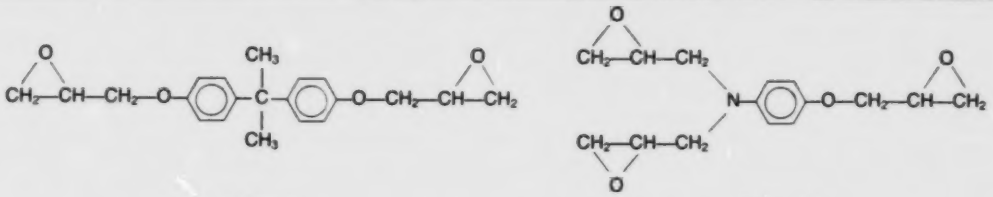

Epoxy II

Epoxy III

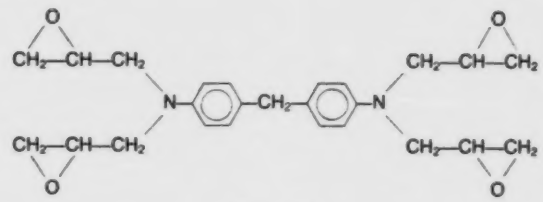

Epoxy IV

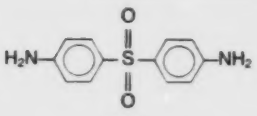

DDS

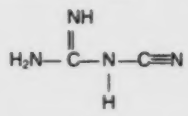

Dicy

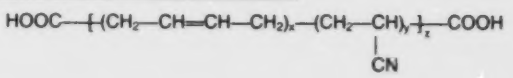

CTBN

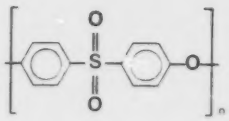

PES

Table 2. Comparison of Some Liquid Epoxy Resin Properties.

	Epoxy equivalent weight (g/gmol)	Specific gravity (kg/m³ at 20°C)	Viscosity (Pa.s at 25°C)
Epoxy II	190	1170	8–20
Epoxy III	95–107	1210–1230	0.55–0.85
Epoxy IV	133	1210	10–20*

* At 50°C.

is approximately 100; in about 80 percent of the molecules, one of the chain ends is terminated by an —OH group. The other modifier used in this study was a carboxyl terminated liquid reactive rubber, Hycar 1300X8, supplied by BF Goodrich (UK). This grade has molecular weight of 3320, carboxyl content 2.4 percent and acrylonitrile content 18 percent. The epoxy-modifier blends were cured with either 30 parts by weight of DDS per 100 parts of epoxy, or with 5 pbw of Dicy per 100 parts of epoxy, without an accelerator.

Methods

All of the blends were prepared by a hot-melt, one-step method without a pre-react stage. Poly(ethersulphone) does not dissolve readily in either Epoxy II or Epoxy IV resins and has to be added as a solution in methylene chloride. The solvent is immediately flashed off from the hot melt. This procedure was found not to affect the structure or properties of the cured blends in any way. The mixtures were carefully degassed and cured according to the following schedule, with either of the two hardeners:

7h at 93°C (200°F) 2h at 149°C (300°F)
16h at 121°C (250°F) 2h at 177°C (350°F)
4h at 200°C (392°F) (post-cure)

Different curing regimes were employed in several cases to check the effect of cure rate on phase separation. When curing the Epoxy III and Epoxy IV formulations, and particularly with the Dicy hardener, extreme care must be taken to avoid the initiation of an uncontrolled exotherm.

Phase separation in these systems was studied with the aid of dynamic mechanical analysis (DMA) over a temperature range between −90°C and the glass transition of the matrix resin, and by scanning electron microscopy (SEM) of the fracture surfaces of the cured blends. Identification of the individual phases in the electron microscope is made possible by the use of an osmium stain which can be attached to the unsaturated parts of the CTBN molecule and identified by X-ray microanalysis or, in the case

of the Dicy-cured epoxy-PES blends, the PES-rich phase can be identified by X-ray microanalysis since it is the only sulphur-containing molecule present (3).

Differential solvents can also be used as selective etching agents to aid phase identification. *Figure 1* illustrates the use of methyl ethyl ketone as a differential solvent for the thermoplastic phase in a thermosetting polyester containing poly(vinyl acetate) (4).

A DuPont DSC990 module was used with a 1090 temperature programmer unit in a limited study of the cure reactions of Dicy and DDS with the epoxy resins. Temperature scans were carried out between 200 and 340°C, at a constant heating rate of 10°C per min.

A detailed description of materials and methods used can be found in *Ref. 5*, together with the results of determinations of the mechanical properties of the cured blends.

THE SOLUBILITY PARAMETER APPROACH

The concept of the solubility parameter, δ, was developed by Hildebrand, who obtained the following expression from consideration of interactions between neighboring molecules:

$$\Delta H_m = (\delta_1 - \delta_2)^2 \phi_1 \phi_2 \qquad (1)$$

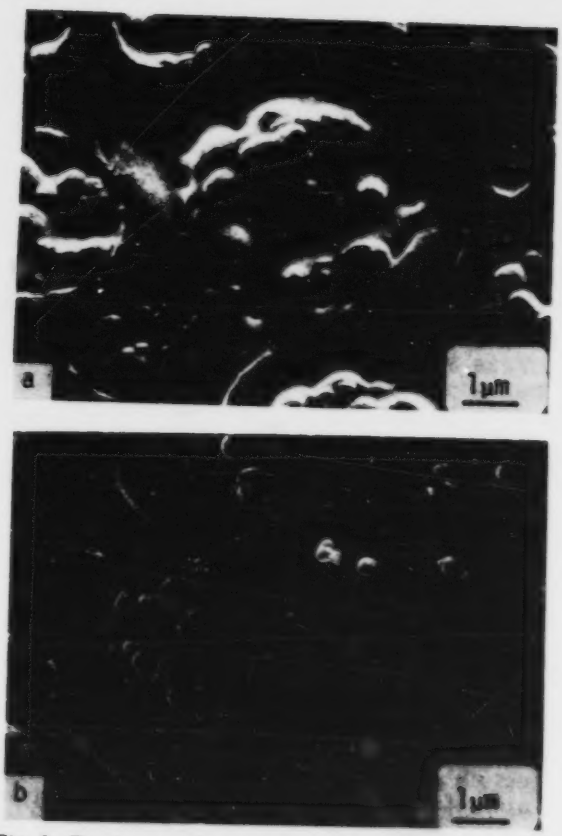

Fig. 1. Fracture surfaces of a cured blend of styrenated polyester containing 8 wt. percent of poly(vinyl acetate) (a) untreated, (b) etched with methyl ethyl ketone for 20 min.

where ΔH_m is the heat of mixing per unit volume of a two-component system and ϕ_i and δ_i are the volume fraction and the solubility parameter respectively of the components of the mixture. In the Flory-Huggins theories, the interaction parameter χ (6), responsible for the enthalpic contribution ΔH_m, has been related to the difference of δ_i of the polymer and solvent.

This theory predicts that two low molecular weight components with similar solubility parameters will be miscible because the negative entropic contribution to the free energy of mixing will tend to dominate. However, when considering mixtures of high molecular weight components, such as polymer-polymer blends, the combinatorial entropy of mixing is severely diminished and the enthalpy of mixing is the dominant factor in determining whether or not mixing occurs. The solubility parameter approach to the prediction of enthalpy of mixing, using experimentally determined or calculated values of δ (6), has been used with some degree of success in studies of polymer-solvent and polymer-polymer miscibility. However, it has obvious deficiences, particularly in dealing with specific interactions between molecular species. Interactions can in some cases give rise to exothermic mixing, a result that clearly cannot be predicted by *Eq 1*. Provided that these deficiences are recognized, the method is useful in examining the effects of chemical structure on miscibility. It is against this background that the solubility parameter approach is applied to polymerizing resin systems in the present work.

In this study, the solubility parameter values for each resin modifier and hardener were determined by calculation, to ensure a common basis for comparisons between them. The method used was that proposed by Fedors (7), which is similar to the better known method of Small (8). Both involve summation of constants representing chemical groups, but Fedors' method may be considered to be superior for two reasons: (a) the contributions of a much larger number of functional groups have been evaluated, and (b) the calculation requires only a knowledge of the structural formula of the compound, whereas Small's method depends upon an experimental determination of molar volume. The internal energy of varporization ΔE_v and the molar volume ΔV were calculated for each compound; the molar volume value having been corrected by the high molecular weight factor, which takes into account the number of main chain skeletal atoms in the smallest repeating unit of the particular polymer. The solubility parameter is then given by

$$\delta = (\Delta E_v / \Delta V)^{1/2} \qquad (2)$$

The method was found to give results in good agreement with reported measured values of solubility parameters of low molecular weight, non-polar compounds. *Table 3* shows the cal-

culated δ values for the epoxy resins, modifiers, and hardeners used in this study. Details of calculations can be found in *Ref. 5*.

OBSERVATIONS OF PHASE SEPARATION

Epoxy-PES system

Examination of a wide range of possible combinations of PES with the three epoxy resins and the two hardeners shows that the blends which exhibit distinct phase separation features, as observed by SEM of fracture surfaces of the cured blends, all contain (a) a significant weight proportion (>5 percent) of PES, (b) more than 20 percent by wt. of the total epoxy component in the form of Epoxy III, and (c) Dicy hardener. *Figures 2* and *3* are examples of typical morphologies of such blends. The spherical inclusions are uniformly distributed through the material. Increasing the PES concentration in the blend and the proportions of the trifunctional epoxy in the resin component generally results in increasing the average size of the nodules.

The observed range is between 0.2 and 8 μm in diameter and the total volume fraction of nodules is estimated to range between 10 and 90 percent in different compositions. X-ray microanalysis in the SEM shows that the nodules are the PES-rich phase. Considerations of volume fractions indicate that the nodules must also contain a significant proportion of epoxy resin. This conclusion is supported by the observation that the nodules are unaffected by methylene chloride.

With the DDS hardener, only samples consisting entirely of Epoxy III with PES exhibited nodular features large enough to be resolved by SEM. In cured Epoxy III/Epoxy IV/30 DDS/PES blends phase separation was indicated by the appearance of a new peak in the DMA spectrum, between the glass transitions in PES (210°C) and of the epoxy matrix (235 to 240°C). The size scale of the separation in these cases was too small to be resolved by SEM (3).

The final morphology of the cured blends is determined entirely by the composition of the blend; no effects due to variation in the imposed cure regime were found within the accessible cure rate range.

Table 3. Calculated Solubility Parameters, Molar Volumes, and Molecular Weights for Epoxy, Modifer, and Hardener Monomers (values correspond to 25°C).

Compound	δ (H)	Molar volume (cm^3/mole)	*M.W.*
Epoxy II	10.0	272	380
Epoxy III	10.9	180	300
Epoxy IV	11.0	285	530
Dicy	15.8	72	84
DDS	11.4	193	256
PES	11.3	157	236
CTBN	9.9	3127	3320

Fig. 2. Fracture surface of a cured sample of 50 Epoxy II/50 Epoxy III/5 Dicy/25 PES.

Epoxy-CTBN rubber system

The solubility parameter values in *Table 3* indicate that the particular grade of CTBN rubber used here would be expected to be more miscible with Epoxy II than with either Epoxy III or Epoxy IV. This prediction was borne out by experimental observation. Attempts to prepare 50 Epoxy III/50 Epoxy IV/30 DDS/CTBN blends by a single-step method resulted in an almost immediate apparent gross separation of the phases, although some limited intermixing was observed on examination of the cured sample.

By contrast, 100 Epoxy II/30 DDS/CTBN blends are initially miscible and on curing phase separate to form unusually large rubber particles, between 50 and 200 μm in diameter, and exhibiting a range of internal rubber particle morphologies. The same kind and size of rubber particles were observed in cured 75 Epoxy II/25 Epoxy III/30 DDS/CTBN blends. *Figures 4–6* show examples of these large rubber particles, revealed by SEM investigations of fracture surfaces of samples broken after first cooling in liquid nitrogen.

DSC RESULTS

Figure 7 shows DSC traces for Epoxy III cured with DDS and with Dicy. Under the conditions

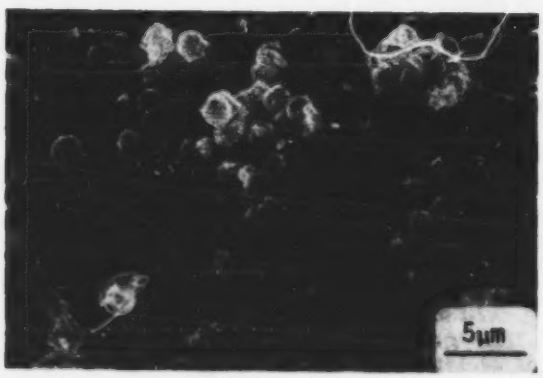

Fig. 3. Fracture surface of a cured sample of 80 Epoxy III/20 Epoxy IV/5 Dicy/14 PES.

Fig. 4. Large rubber particles in a cured sample of 75 Epoxy II/25 Epoxy III/30 DDS/10 CTBN.

Fig. 5. Large rubber particles in a cured sample of 75 Epoxy II/25 Epoxy III/30 DDS/18 CTBN.

of test, the total heat output is approximately the same with both hardeners, but the course of the reaction is clearly different. In the equivalent experiment carried out with Epoxy IV, the total heat output was 599 J/g in the case of Dicy cure and 476 J/g in the case of DDS cure. Qualitatively, the traces were identical to those obtained with the Epoxy III resin, showing that the mechanism of cure depends on the choice of the hardener and not on the epoxy resin.

DISCUSSION

It is know that co-polymerization occurs between Epoxy II and CTBN rubbers, the copolymer phase separating from the homopolymer as the molecular weights of both components increase. The phase separation mechanism is nucleation-and-growth (9). These systems are conventionally cured with triethylenetetramine, for several hours at 60 to 80°C, and rubber particle diameters are typically in the range 2 to 15 μm. The much larger particles observed in this study appear to be the result of the slow DDS cure, which would allow for an extended period of growth of the dispersed phase.

The incompatibility between Epoxy III, Epoxy IV, and the CTBN rubber grade used is indicated by the difference in their respective δ values. Lee, *et al* (10) found it necessary to use a more polar rubber and a two-step, pre-react method, in order to achieve a uniform dispersion of rubber particles in an Epoxy IV/DDS system.

The simple, one-component, solubility parameter concept is extremely limited when dealing with polar compounds with relatively high molecular weights. In general, the predictive capability of this approach can be improved by separating the components due to dispersion, polar, and hydrogen bonding forces (11, 12). The condition for miscibility of two compounds then becomes that corresponding individual components of their solubility parameters should be the same, a condition which is rarely met.

Despite the limitations of the method, the values of δ in *Table 3* provide a useful framework for discussion of miscibility between the starting components of the complex blends used in this investigation. On this basis low molecular weight Epoxy III, Epoxy IV, PES, and DDS with δ values between 10.9 and 11.4 would all be expected to be miscible, and this is found to be the case in practice. The one immiscible component of these blends is Dicy (δ = 15.8). This crystalline compound is employed as a latent hardener with epoxy resins, remaining inactive until it reaches its melting point in the epoxies at about 130°C.

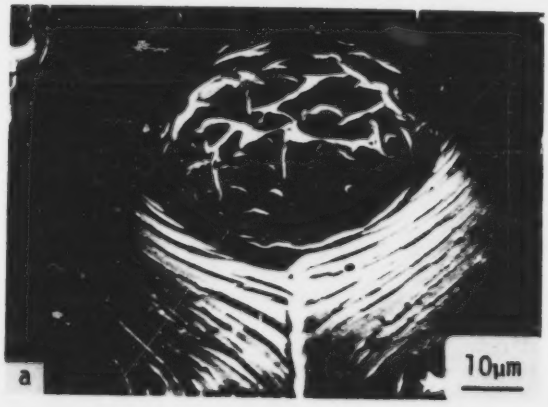

Fig. 6. Examples of composite rubber particle morphologies in (a) 75 Epoxy II/25 Epoxy III/30 DDS/18 CTBN, and (b) 100 Epoxy II/30 DDS/10 CTBN.

At the start of cure, the solubility characteristics of the molecular species present in the blends will change as a result of epoxy-hardener reactions, epoxy homopolymerization reactions (13), and probably reactions of both epoxies and hardeners with the terminal —OH group on the PES molecule. *Figure 8* indicates how the solubility parameter of the individual epoxies can be expected to change as a result of the reaction between the epoxy ring and the primary amine group of the DDS hardener, as a function of the number of reacted epoxy groups. In the case of Epoxy IV, the molecule reacts four times to form —NH—CH_2CHOH— linkages, and the diagram shows the solubility parameter of the resulting compounds (Epoxy IV) $(DDS)_x$ where $x = 1$ to 4. A similar calculation is carried out for Epoxy II and Epoxy III. Epoxies III and IV form isomers of slightly differing solubility parameters when $x = 2$; in these cases average values of δ are plotted. With all the three epoxies, the largest increase in the solubility parameter results from reaction of the first epoxy group on the molecule. This is a reflection of the increase in polarity due to the creation of new —OH groups. Subsequent reactions of the same molecule increase the value of δ further, but the percentage increase is smaller. In reality, the —OH groups thus formed would be expected to take part in the cure reaction (14, 15) and the final δ value for a cured system will then be lower than indicated in *Fig. 8*. It is difficult to comment on the equivalent values for the Dicy cure in the absence of detailed knowledge about the nature of the reaction products in the complex Dicy cure (16).

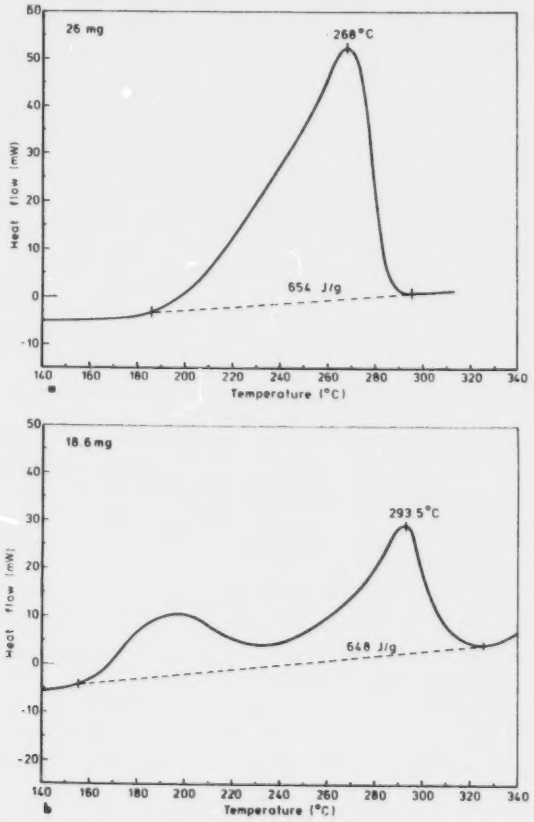

Fig. 7. DSC scans of (a) 100 Epoxy III/30 DDS, and (b) 100 Epoxy III/5 Dicy samples.

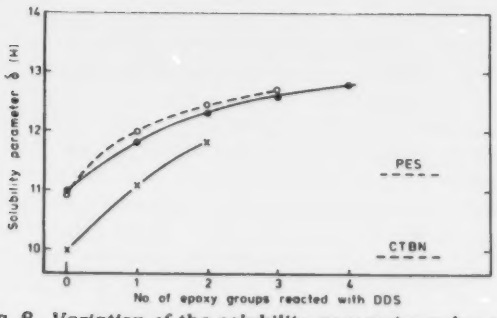

Fig. 8. Variation of the solubility parameter value with the number of reacted epoxy groups. ● Epoxy IV/DDS; ○ Epoxy III/DDS, × Epoxy II/DDS.

It can be stated that a thermodynamic drive for phase separation between Epoxy II and CTBN, and between Epoxy III/Epoxy IV and PES will be set up at an early stage in the epoxy curing reaction. Whether or not the phases actually separate will depend on (a) the existence of a nucleating mechanism, (b) molecular mobility, and (c) time to gelation under the conditions of cure.

Thermodynamic considerations alone fail to provide an indication of the observed differences in morphology of blends cured with the two different hardeners, and similarly show no reason for the marked differences between Epoxy III and Epoxy IV with respect to their interaction with PES (5). In view of the complexity of the system, and of the simplified treatment of the thermodynamic parameters, this lack of predictive capability is not surprising. Moreover, the differences between the action of the two hardeners are more likely to be due to their different cure kinetics, which are indicated by the DSC results, and consequent differences in the viscosity of the blends during the critical pre-gelation part of the cure cycle. *Figure 9* shows how the viscosity of Epoxy IV

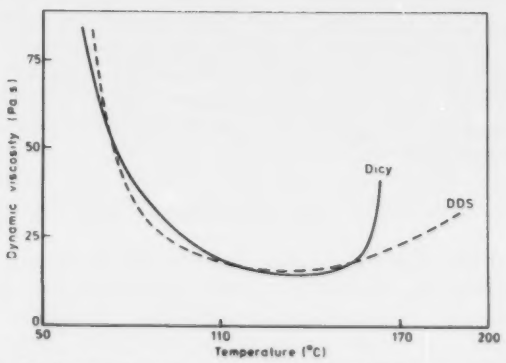

Fig. 9. Dynamic viscosity η^* of Epoxy IV resin during cure with DDS or Dicy (Rheometrics, frequency 10 rads/s, heating rate 2°C/min. Courtesy of Ciba-Geigy (UK) Ltd.).

alone changes during cure with Dicy or DDS at a heating rate of 2°C per min. Studies of chemoviscosity have been carried out for an unsaturated polyester system (17), but no data are available for the blends studied here. It is also possible that the presence of insoluble Dicy particles may provide a more effective nucleation mechanism for phase separation, accounting for the observation of nodular features in blends cured with Dicy, but not with DDS.

It is more difficult to account for the observed differences in the behavior of PES towards Epoxy III and Epoxy IV. The room temperature viscosity of Epoxy III is very much lower than that of Epoxy IV, but the difference is less pronounced at the temperature of cure. Also, Epoxy II, which is a low viscosity resin, behaves in the same way as Epoxy IV with respect to its interaction with PES.

It seems more likely that there exists some specific interaction between the PES molecule and the tertiary amine group present in the backbone of Epoxy III and Epoxy IV which is prevented from occurring, at the temperature of cure, by the conformation of the Epoxy IV molecule. Steric hindrance has been reported in studies of DDS cure of Epoxy IV (15, 18). Molecular models show that the Epoxy III molecule would be expected to be less hindered. The existence of a strong interaction between the PES and Epoxy III would account for most of the experimental observations of phase separations in these blends.

The complex blends studied in the present work are not particularly suitable for systematic studies of phase separation. Many of these blends contain four initial components and relatively little is known about their reaction products. Practical limitations resulting from the nature of the Dicy cure make it difficult to exploit the TTT-diagram representation put forward by Gilham and co-workers (1, 2) which would otherwise be a useful means of comparing the different systems.

Nevertheless, the above considerations of solubility parameters of initial blend components, and the way in which they can be expected to change in the course of the cure, help to explain experimental observations of phase separation in these complex blends. The same approach, applied to simpler model systems and supported by studies of cure kinetics and viscosity changes during cure, should therefore prove rewarding.

CONCLUSIONS

A simple one-component solubility parameter can be used to predict initial miscibility between low molecular weight components in blends of epoxy resins with polymeric modifiers. Without detailed knowledge of reaction products, the thermodynamic approach cannot be pursued any further. Final morphology of cured blends is governed by the kinetics of cure and its effects on the mobility of phase separating species.

Observations of phase separation in blends of epoxy resins with PES could be explained by the existence of a strong specific interaction between the PES molecule and tertiary amine groups of the glycidyl amine epoxies.

ACKNOWLEDGMENT

The authors wish to thank Mr. P. Szekely for preparing the CTBN-epoxy blends and Ciba-Geigy (UK) Ltd. for the data in *Fig. 9*.

REFERENCES

1. L. T. Manzione, J. K. Gillham, and C. A. McPherson, *J. Appl. Polym. Sci.*, **26**, 889 (1981).
2. J. B. Enns and J. K. Gillham, *J. Appl. Polym. Sci.*, **28**, 2567 (1983).
3. C. B. Bucknall and I. K. Partridge, *Polymer*, **24**, 639 (1983).
4. C. B. Bucknall, P. Davies, and I. K. Partridge, *Polymer*, **26**, 109 (1985).
5. I. K. Partridge, PhD Thesis, Cranfield Institute of Technology, Bedford, U.K. (1984).
6. O. Olabisi, L. M. Robeson, and M. T. Shaw, "Polymer-Polymer Miscibility," Ch. 2 and 3, Academic Press, London (1979).
7. R. F. Fedors, *Polym. Eng. Sci.*, **14**, 147 (1974).
8. P. A. Small, *J. Appl. Chem.*, **3**, 71 (1953).
9. J. E. Sohn, *Org. Coating Plast. Chem.*, **44**, 38 (1981).
10. B. L. Lee, C. M. Lizak, C. K. Riew, and R. J. Moulton, BF Goodrich Internal Report ("Rubber Toughening of Tetrafunctional Epoxy Resin") (1982).
11. M. T. Shaw, *J. Appl. Polym. Sci.*, **18**, 449 (1974).
12. D. G. Peiffer, *J. Appl. Polym. Sci.*, **25**, 369 (1980).
13. T. E. Munns and J. C. Seferis, *J. Appl. Polym. Sci.*, **28**, 2227 (1983).
14. E. T. Mones, C. M. Walkup, J. A. Happe, and R. J. Morgan, UCRL-87821 14th National Society for the Advancement of Material and Process Engineering Technical Conference, Atlanta, Georgia, Oct. 12–14 (1982).
15. A. Gupta, M. Cizmecioglu, D. Coulter, R. H. Liang, A. Yavrouian, F. D. Tsay, and J. Moacanin, *J. Appl. Polym. Sci.*, **28**, 1011 (1983).
16. S. A. Zahir, Ciba-Geigy Internal Report ("The Mechanism of the Cure of Epoxide Resins by Cyanamide and Dicyanamide") (1980).
17. K. W. Lem and C. D. Han, *J. Appl. Polym. Sci.*, **28**, 3207 (1983).
18. R. J. Morgan, J. E. O'Neal, and D. B. Miller, *J. Mater. Sci.*, **14**, 109 (1979).

NOMENCLATURE

DGEBA	= Diglycidyl-ether of Bisphenol A.
PES	= Polyethersulphone.
CTBN	= Carboxyl-terminated butadiene acrylonitrile.
χ	= Flory-Huggins interaction parameter.
δ	= Solubility parameter.
DDS	= Diaminodiphenylsulphone.
Dicy	= Dicyanodiamide.
DMA	= Dynamic mechanical analysis.
SEM	= Scanning electron microscopy.
ΔH_m	= Heat of mixing per unit volume.
ϕ	= Volume fraction.
ΔE_v	= Molar heat of vaporisation.
ΔV	= Molar volume.
H	= Hildebrand unit, 1H = 1 $(cal.cm^{-3})^{1/2}$.

DISCUSSION: I. K. PARTRIDGE

J. Bley: You mentioned that you have been using three epoxy resins: the regular glycidyl-ether type and the other glycidyl-amine types. You also said that the latter ones are becoming more important as they give higher crosslink density. Usually high crosslink density leads to more brittle behavior. How does the elastomer phase influence the crosslink density of the epoxy phase as opposed to the regular glycidyl-ether type?

I. K. Partridge: We believe that with both types of epoxy the thermoplastic is present only in the nodular inclusions and does not affect the crosslink density of the epoxy phase outside these inclusions. Because of their high crosslink density the glycidyl-amine epoxy resins form a very unyielding matrix. The toughening mechanisms operating in rubber-toughened polymers are based on the stress-concentrating effect of the rubber particles, enabling a local yielding in the matrix. If a matrix will not yield, there will be no toughness enhancement. I believe this to be the reason why only limited improvements to the toughness of these glycidyl-amine resins have been achieved.

R. E. Prud'homme: Have you considered the multi-dimensional solubility parameter approach? Would you gain anything by doing that?

I. K. Partridge: Yes, I think that one should gain something by this approach. The materials are polar and we also think that there exists a specific interaction between the Epoxy III and the PES. (The same interaction should occur between PES and Epoxy IV, but is probably sterically hindered.) Thus the use of a single-component solubility parameter is a gross approximation and one should consider the polar and hydrogen bonding interaction components of the solubility parameter as well. We do not have any data for them and did not use this approach.

L. A. Utracki: The use of the solubility parameter can be justified only if the phase separation occurs in either monomeric or very early in an oligomeric stage. The structure generated would be due mainly to the enthalpic effects, and it would remain virtually frozen at a later stage as a result of high viscosity and high reaction rate. With this proviso, the solubility parameter is a reasonable approach. The three-parameters solubility method, such as developed by Hansen, is rather elaborate and may not give you much better agreement. Finally, I would like to hear your opinion as to why in these epoxy systems of highly diverse structures the mechanical properties are nearly the same.

I. K. Partridge: This was a surprise to us as well. I believe this to be due to the fact that the inclusions have almost the same mechanical properties as the matrix. Then, unless there is a weak interface, the system is not really changed by containing such inclusions. Obviously in this particular case the interface region is weaker than the nodules, as I have never seen a fracture surface passing through a nodule, but the difference in strength must be very small, almost within the region of experimental scatter in the measurements of mechanical properties.

L. A. Utracki: Well, if this is the case, you could fill the epoxy with any high modulus solid and you should have the same mechanical properties.

I. K. Partridge: Only provided the material had the same shear modulus as that of the cured epoxy resin and if the interface were strong enough.

S. Y. Hobbs: I would like to make a comment in respect to the preceding discussion. In our laboratory looking at glassy-glassy blends, not epoxy but other systems, we found very similar situations where, if there is good adhesion between the phases, there is very little variation in properties depending on morphology. This is dissimilar to the system where you have glass beads or a mineral filler, because the stress concentration varies according to the relative magnitude of the moduli of the two phases. It is important to calculate the two moduli in order to predict where the maximum stress is located around the dispersed phase. If the dispersed phase is very hard, for example, the maximum stress occurs at the particle pole, whereas when the moduli are matched the critical stress is displaced toward the particle equator. This significantly increases the craze density and craze volume. That is why there should be a difference in mechanical behavior between epoxy filled with mineral particles and that containing polymeric particles as described in this paper.

A. E. Platt: Do you have any evidence that the poly(ether sulphone) is chemically incorporated into your matrix during the curing?

I. K. Partridge: No, I do not have any direct evidence of that. However, the terminal —OH group on the PES would be expected to take part in the epoxy cure reactions. We know that other polysulphones without the terminal —OH group had been found not to bind with epoxy.

A. E. Platt: Your methylene chloride etching appears to indicate some possibility of interpenetration or trapping.

I. K. Partridge: Rheovibron viscoelastic spectra indicate an interaction between the PES and Epoxy III. In this cured blend a new peak ap-

pears in the graph of tan δ against temperature, at a temperature between the glass transitions of the PES and the pure Epoxy III/DDS. This is in addition to the normal Epoxy III/DDS glass transition peak. No such additional peak is observed in a blend of PES with Epoxy IV. While this in itself is no proof of any actual chemical bonding, we believe that there is a strong association between PES and Epoxy III. We should probably do a more detailed NMR or IR spectroscopic study, but so far we have had neither the equipment nor the time to do it.

M. R. Kamal: Could you please detail the mechanical procedure used in preparation of your samples. To what extent may the mechanical behavior of your materials be affected by preparation of your samples?

I. K. Partridge: The curing was done in a stagnant, non-mixed system.

M. R. Kamal: You noted that PES inclusions did not seem to have any influence on the ultimate properties of the system. You concluded from this that the interface is strong. I was wondering if this does not mean the opposite; that the interface is very weak. If the microstructure and the interphase do not affect the mechanical properties this may be an indication that you are measuring only the matrix behavior. In some of your micrographs one could see the PES spheres just sitting unattached in the epoxy bowls.

I. K. Partridge: Our conclusion was that the combined PES/epoxy inclusions have about the same shear modulus as the epoxy itself and would not be expected to be effective toughening agents. (However, with these particular epoxies, only minimal toughness improvement is achievable, even with elastomeric CTBN-rubber inclusions). If the interface were particularly strong one might perhaps expect some improvement in the modified system over the pure epoxy; conversely a very weak interface might lead to a deterioration in properties of the modified resins. But we found the modified and the unmodified systems experimentally indistinguishable from each other in their fracture and yield properties.

Morphology and Mechanical Properties of Amine-Terminated Butadiene-Acrylonitrile/Epoxy Blends

E. BUTTA, G. LEVITA, A. MARCHETTI, *and* A. LAZZERI

Study Centre of Mechanical and Technological Properties of Macromolecular Systems, CNR, Department of Chemical Engineering University of Pisa Via Diotisalvi,2-56100 Pisa, Italy

Morphology and mechanical properties of (amine terminated butadiene acrylonitrile rubber/diglycidyl ether of bis-phenol-A epoxy resin) blends of different compositions, cured in wide range of temperatures, are described. Curing at low temperature promoted formation of homogeneous materials with poor fracture resistance. On the contrary, at high temperature tough heterogeneous blends were obtained. Such blends showed phase inversion above 20 percent of rubber. The volume fraction of precipitated phase, determined on SEM micrographs, was higher than the amount of added rubber. A fracture mechanism to account for this is proposed. Extensive voiding and interface damage were observed in the low temperature cured materials. Such phenomena did not contribute to the fracture energy.

INTRODUCTION

The deformation behavior of highly cross-linked polymers is characterized by the absence of crazing and little yielding. As a consequence the fracture energy of these materials is very low, ranging on an average below 100 J/m^2. However, in the case of epoxy resins, a certain degree of plasticity is retained and this explains why they are considered tough thermosets. There are, in fact, formulations whose fracture energy can be as high as 500 J/m^2 (1), a value close to that of brittle thermoplastic glasses. This value is, however, still too low for many practical applications and a major technological advancement was achieved when McGarry and Willner (2) and Sultan (3) and McGarry (4) showed that the fracture energy of epoxy resins could be significantly increased by the addition of carboxyl terminated butadiene acrylonitrile rubbers (CTBN). The resulting materials were morphologically similar to the well known toughened thermoplastics.

Due to the importance of epoxy resins, many studies have been devoted to elucidating the effects of blend formulation, chemical nature of the rubber, cure conditions, and morphological parameters such as volume fraction and size of rubber particles (4–28). CTBNs have been most used so far and rubbers with different terminal functionalities have received less attention (21, 26, 29–31).

This paper describes the properties and morphology of blends obtained by adding different amounts of an amine terminated rubber (ATBN) to a bisphenol-A type epoxy resin followed by curing at different temperatures. The use of amine modifiers is attractive because of the high reactivity of the end groups towards the epoxide ring so that they can be regarded as co-curing agents. A variety of materials can be obtained, ranging from toughened rigid cross-linked systems to flexible thermoplastics. Only properties of toughened products are dealt with in this work.

MATERIALS AND EXPERIMENTAL TECHNIQUES

Materials

The epoxy prepolymer was a low molecular weight liquid diglycidyl ether of bisphenol-A, DGEBA (Epon 828 by Shell Co). The hardener was reagent grade piperidine. In order to have a constant amine in all formulations to epoxy group ratio, the amount of piperidine was varied depending on ATBN content. The reactive liquid rubber was a random acrylonitrile-butadiene

copolymer (Hycar 1300 × 21 by BF Goodrich) with an acrylonitrile content of 10 percent and an amine equivalent weight of about 1100. Details on sample preparation and cure schedules are in *Ref. 31*.

Testing

Impact tests were carried out with a Charpy pendulum (CEAST MK2) in accordance with DIN 53453. Stress intensity factors, K_{IC}, were measured by instrumenting the pendulum. The samples had a span to width ratio of 4. The critical stress intensity factor, K_{IC}, was calculated using the relationship:

$$K_{IC} = \frac{PcS}{BW^{0.5}}\left[2.9\left(\frac{a}{W}\right)^{1/2} - 4.6\left(\frac{a}{W}\right)^{3/2} + 21.8\left(\frac{a^{5/2}}{W} - 37.6\left(\frac{a}{W}\right)^{7/2} + 38.7\left(\frac{a}{W}\right)^{9/2}\right]\right. \quad (1)$$

The samples were sharply notched by introducing a razor blade into them at high temperature (~40° above T_g). The hardness (Rockwell, scale HRM) was measured in accordance with ASTM D785.

Morphology

SEM analysis was carried out with an ISI DS 130 microscope in samples impacted at room temperature or after immersion in liquid nitrogen. Fracture surfaces were gold coated.

Kinetics

Kinetics of phase separation were determined by measuring the intensity of light transmitted through thin layers (0.7 mm) of mixtures using a Reichert microscope equipped with a hot stage and inserting a light sensor into the eyepiece.

RESULTS

Morphology

In order to ensure the formation of a finely dispersed reinforcing phase, the liquid rubber must be soluble in the epoxy resin and phase separation must take place before setting. The solubility of these rubbers depends on many parameters, such as temperature, acrylonitrile content, and molecular weights of both resin and rubber. An increase in acrylonitrile content enhances the compatibility owing to a higher molecular polarity; contents of 10 to 30 percent are typically used. At room temperature ATBNs, like CTBNs, are not completely soluble in the epoxy prepolymer and two phase systems form upon mixing. Wang and Zupko (32) determined the phase diagrams of two CTBN/epoxy mixtures and showed that the epoxy phase contains almost no rubber whereas the rubber phase dissolves appreciable amounts of resin. These mixtures clarify when the temperature is raised above a critical value (cloud point) or if the rubber reacts with the resin.

From the single phase blends the rubber precipitates out when the molecular weight of the resin increases because the free energy of mixing, which is proportional to the molar volume of the mixture, becomes higher than the free energy required to create a new phase. It has been found (31) that the final morphology is strongly dependent on cure temperature and rubber content. Given a certain amount of ATBN, the lower the temperature the smaller the size of particles. Below a certain value of T_{CURE} no segregation was observed and the materials were optically clear. Internal friction and specific heat data, however, indicated also for the clear blends a two phase structure and suggested that the size of the rubber domains must be below the wavelength of light.

The temperature at which clear materials were obtained increased with increasing rubber content; the 10 percent blends were transparent when cured below 20°C whereas the 50 percent blends were still transparent at 60°C.

Curing at high temperature gave rise to the formation of large spherical domains dispersed in a crosslinked matrix. The morphology of samples of different compositions, all cured at 120°C, is illustrated in *Figs. 1* to 4. At 5 percent ATBN (*Fig. 1*) a limited number of particles, average diameter 5 μm, with a large center-to-

Fig. 1. SEM of 5 percent ATBN, T_{cure} = 120°C.

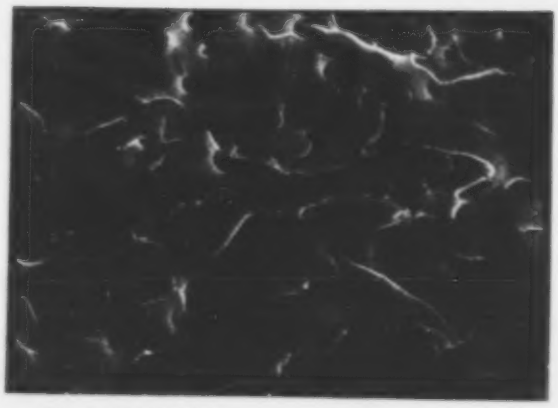

Fig. 2. SEM of 10 percent ATBN, T_{cure} = 120°C.

Fig. 3. SEM of 20 percent ATBN, T_{cure} = 120°C.

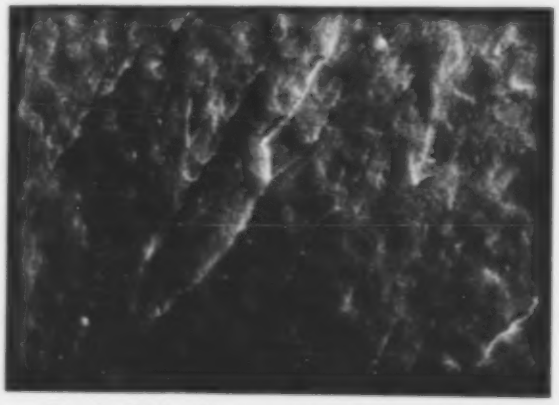

Fig. 4. SEM of 30 percent ATBN, T_{cure} = 120°C.

center distance separated. Increasing the amount of rubber to 10 percent (*Fig. 2*) caused the formation of a greater number of particles, almost the same size as at 5 percent, but with an average distance of about 2 diameters. The domains became bigger and more closely packed at 20 percent; the average distance was less than the particle dimensions. A further addition of ATBN (*Fig. 4*) brought about a dramatic change of morphology: the rubber phase disappeared, yet the materials remained opaque. This can be explained in terms of phase inversion, a phenomenon known to also occur in thermoplastic systems. The pattern in *Fig. 3* resembles an array of closely packed spheres so that a simple model can be considered. In a fact centered cubic lattice the minimum distance center-to-center is given by $D = 1.81\ R/(1-\phi)^{1/3}$, where ϕ is the volumetric fraction of the non-sphere component. The spheres touch one another when $D = 2R$ so that $\phi = 0.26$, which, taking into account the specific gravities of rubber and resin, corresponds to an ATBN content of about 23 percent by wt. This is an oversimplification for the rubber particles are neither closely packed nor have the same sizes. Nevertheless the model should be reasonably accurate as suggested by the pattern in *Fig. 3*.

Visconti and Marchessault (33), and Boisserie and Marchessault (34) showed that in the CTBN/DGEBA system phase inversion occurred at 28 percent CTBN. After inversion the continuous phase was rubbery and contained occlusions of resin. Bascom, *et al.* (14) also reported a transition from particulated to homogeneous blends at about 20 percent CTBN.

However, such high rubber contents are useless for most applications due to the loss in overall mechanical performance. The effects of cure temperature on morphology and kinetics of phase separation were therefore studied for blends with 10 percent of rubber. *Figure 5* shows plots of the absorbed light as function of reaction time at different temperatures. The phase separation was characterized by an induction period ranging from 0.5 to 7 h, in the temperature range 43 to 185°C, during which the mixture remained clear. According to Manzione, *et al.* (23) phase separation stops at gelation. The increase in absorbance observed after gelation has been attributed by Wang and Zupko (32) to localized changes in composition. The time lag reached a minimum at 80 to 100°C and it is unknown whether the trend in *Fig. 6* just parallels the dependence of gel times on temperature or results from specific interactions between rubber and resin. *Figure 6* also shows the equilibrium values of absorbed light which also depend on T_{CURE}. Conaghan and Rosen (35) showed that in a particulated system, given a certain amount of dispersed phases, the turbidity reaches a maximum for particles dimensions of 1 μm and strongly depends, below

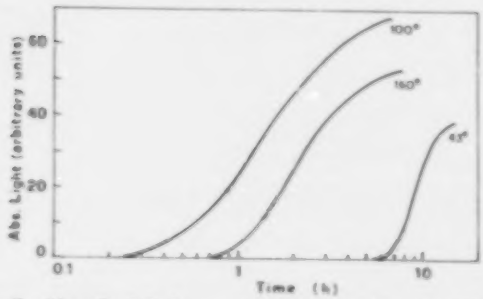

Fig. 5. Absorbed light vs. reaction time in 10 percent ATBN at different temperatures.

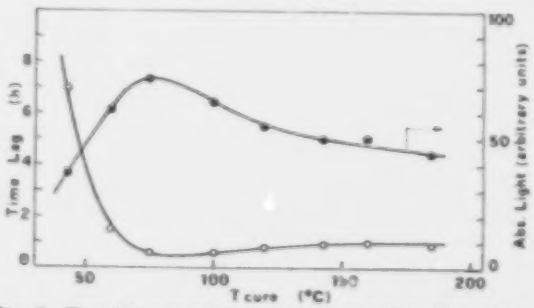

Fig. 6. Equilibrium values of absorbed light (●) and time lag of phase separation (○) vs. T_{cure} in 10 percent ATBN.

3 μm, on the refractive indexes of the two phases. Therefore the maximum in *Fig. 6* should not necessarily be attributed to a maximum in the amount of precipitated rubber.

These factors, along with the intrinsic nonlinearity of the light sensor utilized, have prevented the development of a kinetic model. It is, however, interesting to note that turbidity and kinetics are somehow related, as suggested by the occurrence of maxima and minima at the same temperature.

Figs. 3, and *7* to *12* show the change in morphology brought about by different cure temperatures. At low temperature no particles were observed, at high magnifications a pattern resembling a nodular structure was visible. At 60°C a large number of small particles formed, whereas at 160°C the number of particles was more than one order of magnitude smaller and the domains were larger. The influence of I_{CURE} on the number and size of particles is summarized in *Figs. 13* and *14*.

By measuring the area of each particle on a

Fig. 7. SEM of 10 percent ATBN. T_{cure} = 15°C.

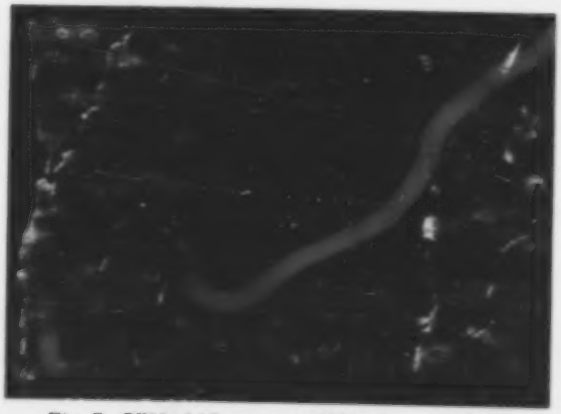

Fig. 8. SEM of 10 percent ATBN. T_{cure} = 60°C.

Fig. 9. SEM of 10 percent ATBN. T_{cure} = 80°C.

Fig. 10. SEM of 10 percent ATBN. T_{cure} = 100°C.

Fig. 11. SEM of 10 percent ATBN. T_{cure} = 140°C.

Fig. 12. SEM of 10 percent ATBN. T_{cure} = 160°C.

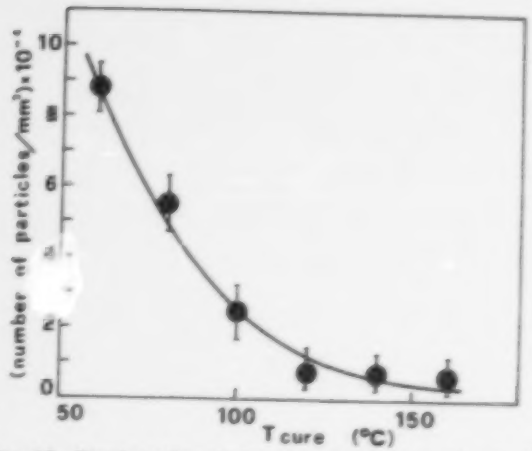

Fig. 13. Number of particles per unit area vs. T_{cure} in 10 percent ATBN.

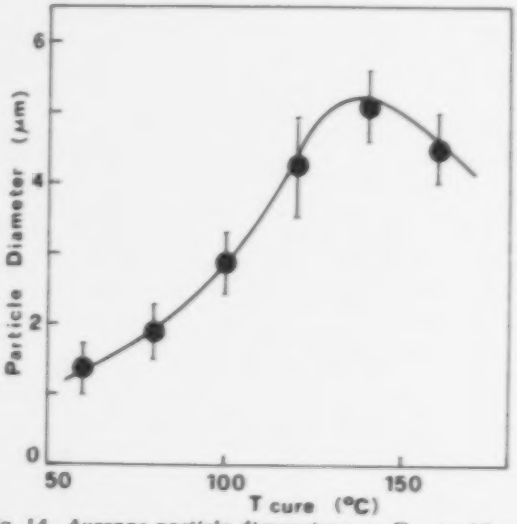

Fig. 14. Average particle dimensions vs. T_{cure} in 10 percent ATBN.

large number of SEM pictures the volume fraction, ϕe, of rubber was determined (e stands for effective as explained later on).

The dependence of ϕe on T_{CURE} is shown in *Fig. 15*, and it is worthwhile to note that its values were always higher than the volume of added rubber ($\phi g = 0.11$).

The phase separation and the morphology are controlled by thermodynamic and kinetic parameters. The driving force is the loss of compatibility due to the increase in average molecular weight during the polymerization. The resisting force is the high viscosity of the solution which controls the formation and growth of rubber particles (both quantities vary considerably with time). These parameters have been analyzed by Manzione, *et al.* (23) who proposed a morphology map that predicts the formation of many small particles at low temperature and of a limited number of large particles at high

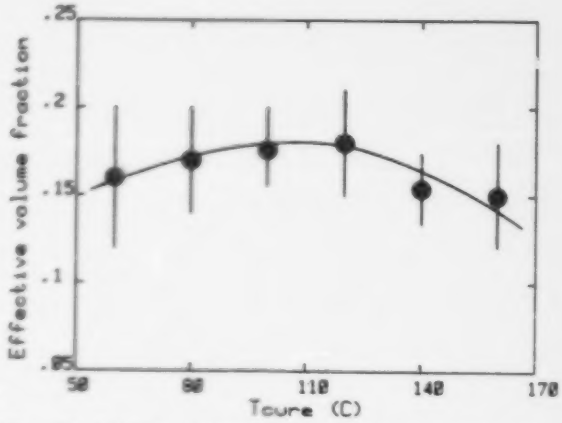

Fig. 15. Effective volume fraction of segregated rubber vs. T_{cure} in 10 percent ATBN.

temperature; experimental data from this work agree with this generalization.

However, a complication arises from the existence of convection currents within the liquid mass, which may promote the coalescence of the rubber droplets (phase separation starts before the step increase in viscosity at gelation). Such currents depend on the volume of castings, their geometries and characteristics of the ovens (still or circulating air). This can prevent data obtained on a small laboratory scale from being extended to large castings.

Mechanical Properties

The curing agent used in this work is a secondary amine and formulations based on this hardener are characterized by long pot lives. Setting takes place via a two step mechanism: 1) a tertiary amine is readily formed, and 2) which reacts with other epoxide rings as a Lewis base, particularly in the presence of hydroxyl groups. If the setting is made at room temperature, or below, the resin turns into a brittle solid and postcuring is needed to develop good mechanical properties. The crosslink density is not particularly high, as indicated by the large, more than two decades, drop in elastic modulus at T_g. Although all castings were postcured at the same temperature, the properties of the neat resin depended markedly upon T_{CURE}. Thus the mechanical characteristics of the matrix in the rubber modified systems will reflect this dependence, a point often neglected. Materials obtained at low temperature are more brittle than those obtained at high temperature as indicated by the critical parameter, K_{IC}, in *Fig. 16* (bottom). In fracture tests the crack grew in an unstable manner with a mechanism known as stick and slip. The fracture surfaces were substantially featureless except from river markings propagating from the root of the starter cracks and for curved lines that indicated the arrest position of the moving crack. The crack arrest occurred only in specimens within high a/W ratios since the amount of energy stored at

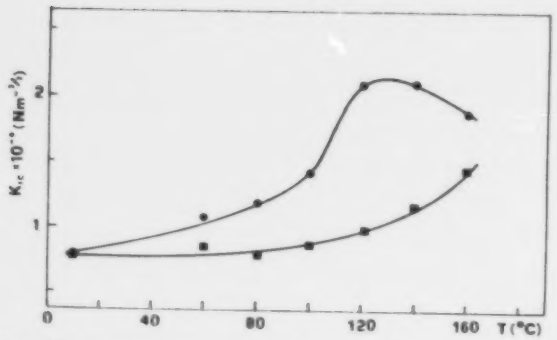

Fig. 16. Critical stress intensity factor, K_{IC}, vs. T_{cure} for (■) neat resin, (●) 10 percent ATBN.

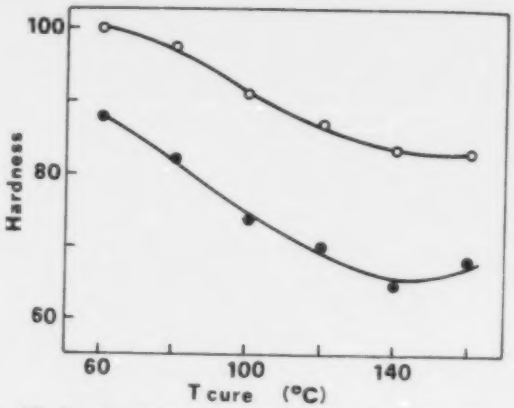

Fig. 17. Rockwell hardness (HRM) vs. T_{cure} for (○) neat resin, (●) 10 percent ATBN.

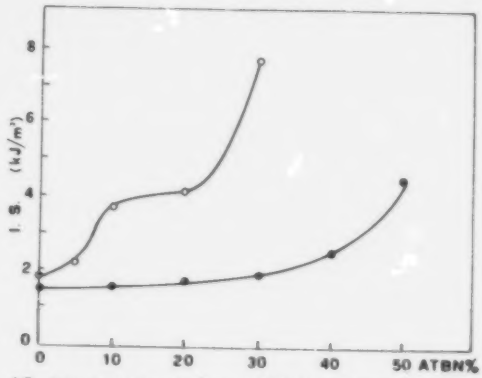

Fig. 18. Impact strength vs. ATBN content for (●) homogeneous and (○) heterogeneous blends.

the critical point was not sufficient to sustain the propagation throughout the samples. The temperature of cure can influence properties in several ways. Morgan and O'Neal (36) showed that DGEBA can crystallize when the resin is cured at low temperature. On subsequent heating for postcuring the small crystals melt, thus leaving numerous holes, which exert a weakening action. On the other hand, Gillham (37) has demonstrated that during the cure of epoxy resins two phenomena take place, i.e., gelation and vitrification. Gelation results from an increase in medium viscosity subsequent to branching reactions, whereas vitrification results from quenching these reactions due to a lack of molecular mobility. The degree of polymerization at vitrification increases with increasing T_{CURE}. When the materials are postcured, particularly above T_g, the crosslink reactions start anew and eventually go to completion. In this step cycle different network structures can result due to different extent of conversion attained at vitrification. A further complication is due to a possible volatilization of piperidine, particularly at high T_{CURE}. Oxidation of the hardener also occurs as indicated by the progressive darkening of castings as T_{CURE} was increased. Both phenomena can lead to less dense networks and then explain the decrease in T_g at high cure temperatures (31).

With similar argumentation, the decrease in hardness can be accounted for, *Fig. 17* (top). The hardness can be related, although not in a simple manner, to the yielding behavior and a progressive decrease in compressive yield stress was measured as T_{CURE} increased.

Like morphology, mechanical properties depend on both rubber content and cure temperature.* The effects of these parameters on the impact strength, *I.S.*, is shown in *Fig. 18*. The bottom curve refers to blends characterized by optical clarity, the top one to opaque blends (obtained at 120°C). The first thing to be noted is that, at least with ATBN, the right choice of cure conditions can be more important than the presence of rubber. Giving rise to the appropriate morphology, at 10 percent ATBN, can double the *I.S.*, an increase otherwise obtainable only with more than 40 percent ATBN. This constitutes a drawback for many practical applications in which curing at high temperature is not allowed. The second is that, in the case of heavily segregated materials, different toughening mechanisms are active, depending on the rubber content. Below 5 percent ATBN there is almost no improvement, the small increase in *I.S.* being attributable to the decrease in elastic modulus brought about by the presence of soft particles. The *I.S.* shows a definite increase at 10 percent ATBN and thereafter remains constant up to 20 percent of rubber. A similar trend was reported, in the same range of rubber concentrations, for both ATBN and CTBN either by measuring G_{IC} or falling weight *I.S.* (26, 29). It has been shown (31) that the matrices of 10 and 20 percent blends are substantially the same; the softening temperatures are almost unchanged and the decrease in modulus is due to the greater amount of soft particles.

A further step increase in *I.S.* occurs when the rubber content is above 20 percent; the *I.S.* of the particulated 30 percent blend is four times that of the corresponding clear material.

* Another parameter is the prereaction between epoxy resin and ATBN. In this study there was no prereaction.

Above this amount of rubber the materials are too soft for most applications. The deterioration of mechanical properties can be kept to a minimum by limiting the amount of rubber to 10 percent, which already yields materials with improved fracture resistance. The influence of T_{CURE} on the fracture toughness of 10 percent ATBN blends is shown in *Fig. 16* (top).

DISCUSSION

The presence of a particulated soft phase is the necessary condition to induce localized plastic deformations whose effects can be interpreted in terms of energy absorption (high energy release rate) or crack tip blunting (high critical stress intensity factor). Irreversible deformations can take place in both soft phase and matrix, with different consumption of energy.

Bascom and Hunston (19) were the first to report on the formation of rubber ligaments spanning the crack opening in toughened epoxy resins. These observations were turned by Kunz, *et al.* (38) into a quantitative model which predicts a linear dependence of the fracture energy, G_{IC}, on the amount of separated rubber. The model gives a realistic estimate of the contribution of the rubber to the rupture energy. However, the fracture energy of rubber/epoxy blends can largely exceed the values predicted by this model whose applicability should then be limited to formulations in which the contribution of other mechanisms is negligible.

Extensive particle voiding (formation of voids within the particles) was reported by Breuer, *et al.* (39) in rubber modified PVC and in ABS. It was shown that the intense stress whitening produced in tension originated from cavitation, mainly occurring in the particles located in the sheared zones. It was also suggested that particle voiding might be a general deformation mechanism for toughened polymers characterized by ductile matrices. The same mechanism was proposed by Kinloch, *et al.* (27, 28) for toughened epoxy resins.

Typical morphologies of 10 percent ATBN blends, displaying different fracture toughness, are shown in *Figs. 2, 8* to *12*; some features are worth noting.

1) Almost all the particles in the 60°C blend exhibit internal ruptures. The number of broken particles decreases as T_{CURE} increases; at 120°C about 2 percent of particles are broken and while none are at 160°C.

2) Voiding at the interface is also predominant in blends cured at low temperature. Internal and interface voiding are competing phenomena. This can be inferred by carefully examining the micrograph in *Fig. 9*. On an average, the particles bonded to the matrix are internally broken, while those detached are undamaged. The importance of these dilational processes lies in the possibility of relieving the triaxial stress field in the vicinity of the crack tip. The transition from triaxiality to biaxiality would enlarge the yielded zone and promote crack blunting. At this point the question arises as to whether interface or particle voiding takes place, in the present case, ahead of the crack tip or in the opening zone. In the first case a crack blunting mechanism should be active, whereas in the second case voiding should have little effect on toughness. Since K_{IC} of 10 percent ATBN blend cured at 60°C is very close to that of the neat resin cured at the same temperature, it must be concluded that the contribution of voiding is, in the present case, negligible.

There are, then, differences between the voiding reported here and that reported by Breuer, *et al.* (39). Such differences can be originated by different rubber properties or, more likely, by different deformation mechanisms. Unlike toughened PVC or ABS, the ATBN or CTBN blends deform homogeneously or with little tendency to necking**. In toughened PVC stress whitening, related to voiding, is particularly evident in zones yielded at low rates. The micrographs shown in this work were taken on fracture surfaces of impacted specimens on which no whitening was observed.

3) The particles formed at low temperature appear to be composite in nature. The presence of extraneous material, as particle filler, has been repeatedly reported in CTBN systems (18, 23, 26) and attributed to incorporation of epoxy resin. The subinclusions should have the effect of increasing the volume fraction of the rubber. However, data obtained analyzing a large number of fracture pictures did not show any major dependence of volume fraction upon T_{CURE}, *Fig. 15*. It was to be noted that epoxy resin can exist in the segregated phase as isolated particles, or be molecularly dispersed. The little dependence of ϕ_r on T_{CURE} can be accounted for by admitting that the subinclusions are progressively replaced by dissolved resin as T_{CURE} increases.

The fracture data obtained in this work do not agree with Kunz's model or with the linear dependence of G_{Ic} on rubber volume experimentally determined by Bucknall and Yoshii (18). The existence of subinclusions seems to exert a weakening action on the rubber and facilitates voiding. Low cure temperatures also seem to promote both the formation of weak interfaces and debonding. In other words, particles formed at low temperature are close to behaving as empty cavities. A close look at the particle morphology in *Figs. 19* and *20* confirms the above points.

Dissipative processes can also occur in the matrix, of the type shown to be active in toughened thermoplastics, i.e., crazing and localized shear yielding. Morgan, *et al.* (40) reported that coarse crazes can grow in amine cured epoxy

** There are formulations based on the addition of bisphenol-A to DGEBA that do show necking in tension. These materials are not considered here.

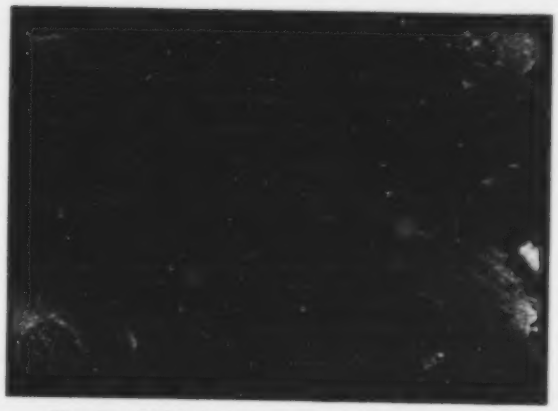

Fig. 19. SEM of 10 percent ATBN. T_{cure} = 60°C.

Fig. 20. SEM of 10 percent ATBN. T_{cure} = 160°C.

resins, though such structures were smaller and less numerous than those observed in thermoplastics. Crazing has been disregarded as a deformation mechanism by Yamini and Young (41), Mijovic and Koutsky (42), and Gledhill and Kinloch (43). Electron microscope studies suggest that, after setting, epoxy resins consist of highly crosslinked agglomerates surrounded by lower molecular weight material, so that localized crazing can be admitted. It should be clear, however, that in this context only crazing occurring on a large scale can be considered as an energy absorbing mechanism.

It is extremely difficult to demonstrate that presence of sheared zones on the fracture surfaces by using SEM analysis, particularly, as in this case, when the fracture plane deviates continuously and a pattern of shear bands cannot be unambiguously identified. Shearing occurs at constant volume and interface or particle voiding, on the contrary, bring about dilation. The most elegant technique to discriminate between these processes consists in measuring the volume change during the deformation. This method was applied by Bucknall and Clayton (44) to HIPS and by Bucknall and Yoshii (18) to CTBN/epoxy blends. In the latter it was found that increasing the amount of rubber had the effect of magnifying the importance of voiding. These results were obtained with creep measurements and the importance of shear yielding relative to voiding is expected to vary as the deformation rate increases. In their study on PC/PE blends Maxwell and Yee (45) observed a regular increase of $\Delta V/Vo$ with increasing $\dot{\epsilon}$ and concluded that the total amount of voiding increased with strain rate.

A striking feature of fracture surfaces of rubber/epoxy blends is that most particles appear at the bottom of circular cavities in the matrix; a number of explanations can be given to account for this. It is possible that the particles break into three pieces; two remain bonded to the original sites and the third is ejected during the fracture. Efforts to trap such fragments were unsuccessful however (46). It is also possible that, after failure, the half-particles just retract due to the vanishing of triaxial tensile stress, *Fig. 21a*. In this case the surface of the particles should lie below the fracture plane. The matrix can also flow under the action of the stress field generated in the vicinity of particles; this can generate the dark rings that encircle the particles on SEM micrographs, *Fig. 21b*. However, micrographs of fracture surfaces produced at low temperature have shown there is no retraction into the holes. After reheating the sample at room temperature, the matrix region around the particle was flatter and the dark ring less evident. Finally, the dark ring can be originated from a failure of the interface and an enlargement of the original diameter at the equator. This would leave a circular ditch around the particles, *Fig. 21c*. This conclusion is supported by micrographs taken using the Y-modulation technique. An example is given in *Fig. 22*, which shows the particle arrowed in *Fig. 10*; the annular depression around the particle shows up clearly.

An important parameter in toughened systems is the effective volume fraction, ϕe, of the soft phase. In rubber modified polystyrene a nominal 6 percent of rubber can give rise to more than 50 percent of separated phase (47). Different amounts of rubber can segregate in epoxy systems depending on blend formulation

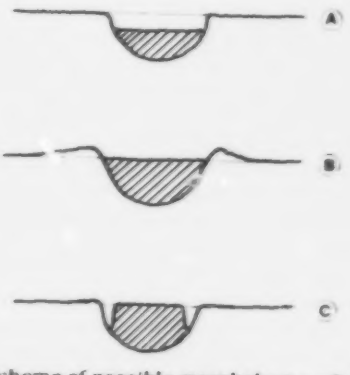

Fig. 21. Scheme of possible morphologies after failure.

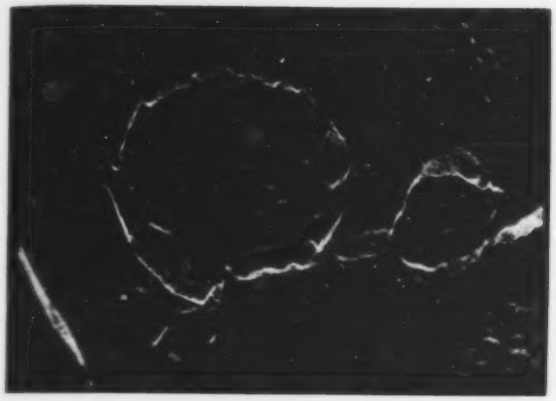

Fig. 22. Enlargement of the arrowed particle in Fig. 10.

Fig. 23. SEM of 10 percent ATBN, T_{cure} = 140°C.

and cure conditions and it was shown by Bucknall and Yoshii (18) and Manzione, *et al.* (24) that the fracture resistance strongly depends on ϕe. This parameter is, however, difficult to assess because its measure is affected by several errors. Kunz, *et al.* (26) obtained very different estimates of ϕe using TEM or NMR; and Sayre, et al. (25) showed that overestimates resulted from TEM analysis. The volume fractions shown in *Fig. 15* were determined on SEM images by using the relationship (48).

$$V_v = \int V_i/L^3 = \int \frac{A_x}{L^2}\frac{dx}{L} = A_A \qquad (2)$$

The calculated values were invariably higher than the value corresponding to the added rubber. The possibility of obtaining an increase of e due to the presence of subinclusions has been mentioned and there is also the possibility for the resin to dissolve molecularly in the particles as a consequence of copolymerization with the rubber (this resin would not show up with staining techniques based on osmium tetroxide). However, the examination of fracture surfaces indicated both a further source of errors and an interesting feature of the rupture processes. *Figure 23* shows a detail of the root of the starter crack in a sample cured at 140°C. The parallel lines in the upper part are those left by the blade when the crack was introduced at high temperature. In this region there are about 5300 particles/mm^2 whereas on the fracture region this figure increases to about 8000. Moreover, the particles cut by the blade appear smaller than those broken during the fracture. It must be concluded that the particles are not broken at random; they are approached on equatorial planes by the crack front owing to the stress concentration on these planes, as exemplified in *Fig. 24*.

The first consequence of this is the inapplicability of *Eq. 2*, based on statistical considerations. However, the volume fractions calculated by *Eq. 2* are those really active during the fracture processes. Two types of volume fractions then exist in the material: a geometric one

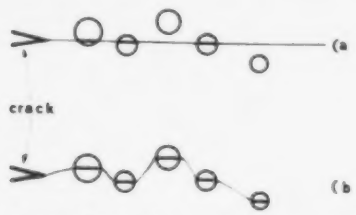

Fig. 24. Scheme of possible crack trajectories: particles broken a) randomly, b) on equatorial planes.

(whose value can already be different from the amount of added rubber as said before), and another, that can be termed effective since it represents the amount of rubber to be effectively broken.

The second consequence is that the fracture plane must continuously deviate, on a microscopic scale, thus increasing the amount of new surface to be created. Such continuous deviations can also lead to a multiplication of fracture planes and the numerous ridges on the fracture surfaces, *Fig. 25*, can result from the intersections of these planes. A multi-level fracture was also proposed by Bascom and Hunston (19) in piperidine cured CTBN/DGEBA blends. Approaching the particles on equatorial planes also increases the volume of the damaged zone around them, *Fig. 22*.

A comparison of data in *Figs. 14* and *16* suggests a strong dependence of K_{IC} on particle dimensions. Although the decrease in fracture toughness for samples cured above 140°C is probably non-related to the decrease in particle size above this temperature (diameters in the range 120 to 160°C are much too close, particularly taking into consideration the error bars) a dependence of K_{IC} on particle size can confidently be inferred. The effect of particle size on the deformation mechanisms of CTBN/DGEBA was studied by Sultan and McGarry (11). They showed that an enlargement of particles was paralleled by an increase of fracture energy. The dimensions reported in that work were smaller than those observed in this study, which is likely the consequence of the different

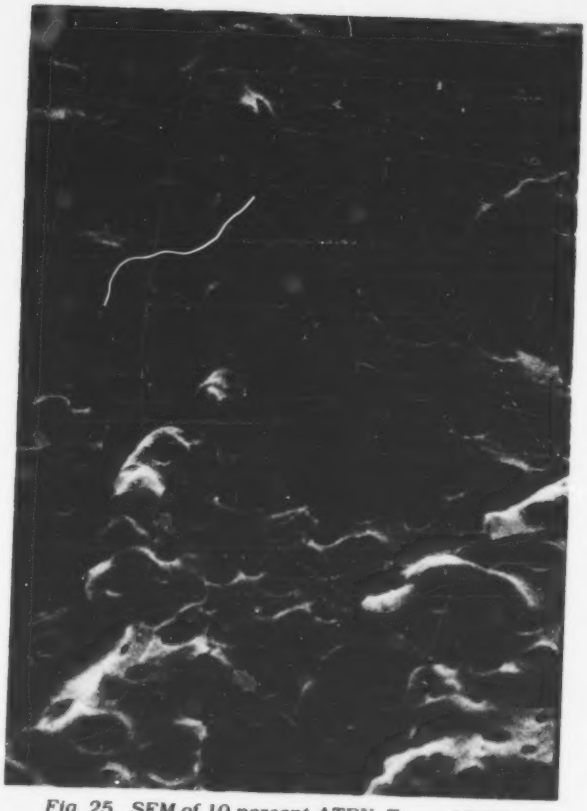

Fig. 25. SEM of 10 percent ATBN, T_{cure} = 120°C.

acrylonitrile content of the rubber (5). In the same study it was also shown that the activation energy for yielding was smaller for the epoxy with large particles and this can explain the dependence of hardness on T_{CURE} shown in *Fig. 15*. However, the parallel change in hardness of the unmodified resin suggests that the properties of the matrix are also to be carefully considered; any change of experimental parameters aimed at modifying the morphology of the segregated phase can alter the matrix properties. The enhanced toughness of the high temperature cured blends is also the result of the increased fracture resistance of the matrix.

It is known that the toughness of rubber modified polymers does not show a monotonic dependence on parameters such as degree of compatibility, volume fraction, or particle dimensions. For instance, the *I.S.* of HIPS reaches a maximum when the volume fraction of rubber is about 20 percent and deteriorates at higher values (47). The existence of such maxima can explain the plateau between 10 and 20 percent in *Fig. 18*. As the ATBN content increases there is parallel increase in *I.S.* due to the formation of a second phase whose efficiency reaches a maximum at 10 to 15 percent. At higher contents the *I.S.* should therefore diminish if it were not for the onset of phase inversion that brings about both a further increase in *I.S.* and a rapid deterioration of all the other mechanical properties.

ACKNOWLEDGMENTS

This work is dedicated to Prof. F. R. Schwarzl on the occasion of his 60th birthday and it was made possible by the financial support of the Progetto Finalizzato Chimica Fine e Secondaria of the CNR.

The authors wish to express their gratitude to Dr. A. Tonazzini (IEI) who kindly carried out image processing, to Prof. B. Pellegrini who courteously allowed use of the electron microscope, and to Mr. S. Ciucci for his patience in operating the microscope.

REFERENCES

1. D. C. Philips, J. M. Scott, and M. J. Jones, *J. Mater. Sci.*, **13**, 311 (1978).
2. F. J. McGarry and A. M. Willner, *MIT Res. Rep.*, R68-8 (1968).
3. J. N. Sultan and F. J. McGarry, *MIT Res. Rep.*, R69-59 (1969).
4. F. J. McGarry, *Proc. R. Soc. London*, **A319**, 59 (1970).
5. E. H. Rowe, A. R. Siebert, and R. S. Drake, *Mod. Plast.*, **47**, 110 (1970).
6. A. C. Soldados and A. S. Burhans, *ACS Adv. Chem. Ser.*, **99**, 531 (1971).
7. J. N. Sultan, R. C. Laible, and F. J. McGarry, *Appl. Polym. Symp.*, No. **16**, 127 (1971).
8. A. R. Siebert, and C. K. Riew, Proceed. of the 161th ACS, Org. Coat. Div. 552 (1971).
9. A. R. Siebert, E. H. Rowe, C. K. Riew, and J. M. Lipiec, 28th Annual Tech. Conf. SPI (1973) Sec. 1-A, p1.
10. H. H. Bowerman and W. J. McCarty, 28th Annual Tech. Conf. SPI Sec. 9-A, p1 (1973).
11. J. N. Sultan and F. J. McGarry, *Polym. Eng. Sci.*, **13**, 29 (1973).
12. A. D. S. Diggwa, *Polymer*, **15**, 101 (1974).
13. A. C. Meeks, *Polymer*, **15**, 675 (1974).
14. W. D. Bascom, R. L. Cottington, R. L. Jones, and P. Peyser, *J. Appl. Polym. Sci.*, **19**, 2545 (1975).
15. C. K. Riew, E. H. Rowe, and A. R. Siebert, *ACS Adv. Chem. Ser.*, **154**, 326 (1976).
16. W. D. Bascom, R. L. Cottington, and C. O. Timmons, *J. Appl. Polym. Sci.*, **10**, 165 (1977).
17. J. K. Gillham, C. A. Glandt, and C. A. McPherson, in "Chemistry and Properties of Crosslinked Polymers" by S. S. Labana, Academic Press (1977).
18. C. B. Bucknall and T. Yoshii, *Brit. Polym. J.*, **10**, 53 (1978).
19. W. D. Bascom and D. L. Hunston, Proc. Int. Conf. on Toughening of Plastics PRI London, p22.1 (1978).
20. R. Y. Ting and R. L. Cottington, *J. Appl. Polym. Sci.*, **25**, 1615 (1980).
21. A. Hussain and F. J. McGarry, *MIT Res. Rep.*, R80-2 (1980).
22. W. D. Bascom, R. Y. Ting, R. J. Moulton, C. K. Riew, and A. R. Siebert, *J. Mater. Sci.*, **16**, 2657 (1981).
23. L. T. Manzione, J. K. Gillham, and C. A. McPherson, *J. Appl. Polym. Sci.*, **26**, 889 (1981).
24. L. T. Manzione, J. K. Gillham, and C. A. McPherson, *J. Appl. Polym. Sci.*, **26**, 907 (1981).
25. J. A. Sayre, R. A. Assink, and R. R. Lagasse, *Polymer*, **22**, 87 (1981).
26. S. C. Kunz, J. A. Sayre, and R. A. Assink, *Polymer*, **23**, 1897 (1982).
27. A. J. Kinloch, S. J. Shaw, D. A. Tod, and D. L. Hunston, *Polymer*, **24**, 1341 (1982).
28. A. J. Kinloch, S. J. Shaw, and D. L. Hunston, *Polymer*, **24**, 1355 (1983).
29. V. S. Pircivanoglu, T. C. Ward, I. Yilgor, A. K. Banthia, and J. E. McGrath, *ACS Polym. Prep.*, **22**, No. 1, (1981).
30. G. Levita and E. Butta, *La Chimica e L'industria*, **66**, 233 (1984).
31. G. Levita, A. Marchetti, and E. Butta, *Polymer*, in press.
32. T. T. Wang and H. M. Zupko, *J. Appl. Polym. Sci.*, **26**, 2391 (1981).

33. S. Visconti and R. H. Marchessault, *Macromolecules*, **7**, 913 (1974).
34. C. Boisserie and R. H. Marchessault, *J. Polym. Sci. Polym. Phys. Ed.*, **15**, 1211 (1977).
35. B. F. Conaghan and S. L. Rosen, *Polym. Eng. Sci.*, **12**, 134 (1972).
36. R. G. Morgan and J. E. O'Neal, in "Chemistry and Properties of Crosslinked Polymers" by S. S. Labana, Academic Press (1977).
37. J. K. Gillham, *A.I.Ch.E.J.*, **20**, 1066 (1974).
38. S. Kunz, P. W. R. Beaumont, and M. F. Ashby, *J. Mater. Sci.*, **15**, 1109 (1980).
39. H. Breuer, F. Haaf, and J. Stabenow, *J. Macromol. Sci. Phys. Ed.*, **B14**, 387 (1977).
40. R. J. Morgan, E. T. Mones, and W. J. Steele, *Polymer*, **23**, 295 (1982).
41. S. Yamini and R. J. Young, *J. Mater. Sci.*, **15**, 1823 (1980).
42. J. Mijovic and J. A. Koutsky, *Polymer*, **20**, 1095 (1979).
43. R. A. Gledhill and A. J. Kinloch, *Polym. Eng. Sci.*, **19**, 82 (1979).
44. C. B. Bucknall and D. Clayton, *J. Mater. Sci.*, **7**, 202 (1972).
45. M. A. Maxwell and A. F. Yee, *Polym. Eng. Sci.*, **21**, 205 (1981).
46. D. L. Hunston, J. L. Bitner, J. L. Rushford, J. Oroshnik, and W. Rose, *Elast. Plast.*, **12**, 133 (1980).
47. E. R. Wagner and L. M. Robertson, *Rubb. Chem. Technol.*, **43**, 1129 (1970).
48. A. G. Guy, "Introduction to Material Science," McGraw-Hill, (1971).

DISCUSSION: G. LEVITA

H. P. Schreiber: In the micrographs the interfacial failure was quite evident. Low temperature cure seems to result in almost a lack of wetting between the cured phases.

G. Levita: It is difficult to respond to your comment since we are talking of two miscible liquids to start with. During the curing phase separation takes place, but why the interphase properties should so depend on the curing temperature I do not know.

H. P. Schreiber: Could you tell us how one could go about measuring the interface interactions in your systems to quantify this effect?

G. Levita: No, I do not see how to do it.

I. K. Partridge: It is possible that this is a secondary effect which has little to do with relative strength of the interphase.

L. A. Utracki: How much reaction takes place inside the dispersed particles?

G. Levita: We could answer this question by measuring the amount of swelling. We did not do it. But why?

L. A. Utracki: The question was inspired by one of your graphs in which you indicated that the curing temperature was below the glass transition temperature, T_g. In numerous publications on this subject it has been stated that there is no reaction at $T \leq T_g$ (on the usual time scale of the experiment). In short, if there is epoxy trapped in the glassy domain this material should be eliminated from consideration of matrix properties.

G. Levita: There are two types of epoxy present within the particles. The first is a molecular dispersion or solution. There is no way to detect it by any fractographic techniques; this material is copolymerized with the rubber. The second type is present in a form of dispersed domains in structures sometimes called "the salami structure." We did not see this structure in our systems, probably because the rubber used had very low acrylonitrile content.

L. A. Utracki: The system is dynamic in the sense that during the temperature scan there is polymerization, co-polymerization, and complex phase separation taking place simultaneously. It would be very interesting to be able to characterize these processes separately, to determine the reaction constants and then to mathematically model the complete system. It is obvious that the morphology and properties will depend on the temperature profile. Without this, it will be very difficult to understand the system.

G. Levita: I agree.

The Effect of Rubber Particle Size on the Impact Properties of High Impact Polystyrene (HIPS) Blends

S. Y. HOBBS

Polymer Physics and Engineering Branch
Corporate Research and Development
General Electric Company
Schenectady, New York 12301

The impact fracture of nominally identical high impact polystyrene resins having different and well-characterized rubber particle size distributions is discussed. A numerical model for craze termination is presented and its predictions are compared with experimental data. An alternative explanation for the observed effect of particle size on fracture energy is considered.

INTRODUCTION

It is well known that the toughness of glassy polymers can be markedly improved by the addition of a dispersed rubber phase. In the case of high impact polystyrene (HIPS), energy dissipation is enhanced primarily by the development of large, stable craze fields in the matrix resin. The degree of toughness can be influenced by a variety of factors including the amount of rubber added, the type of rubber, the degree of crosslinking, the level of adhesion, and the rubber particle size (1). Because these variables are often strongly coupled it has been experimentally difficult to isolate and quantify their effects.

The effect of changing rubber particle size is of particular interest since this feature can be rather carefully controlled during the emulsion polymerization and can be characterized in considerable detail by a number of techniques (2). At this writing there is general agreement that there is a critical particle size below which the ability of a particular rubber to toughen a resin drops off markedly. For polystyrene, the critical diameter is 1 to 2 μm (3). More ductile resins can be toughened with smaller particles (4–6).

While it is usually assumed that "size" is equivalent to the number average particle diameter, the majority of papers fail to explicitly define this term or to detail how the measurements were made. As a result of these deficiencies, few quantitative models relating rubber particle size to properties such as impact strength have been proposed. Bucknall has suggested that particle size effects are manifested primarily in the termination step through the process of craze blunting (7). This position is supported by the results of creep experiments on specimens formulated with large and small particle rubbers (8). In contrast, Kramer has proposed that larger particles are more efficient in craze nucleation than small particles citing observations of crazing in films containing rubber particles with a range of diameters (9). There is additional evidence that the shape of the rubber particle size distribution may have an important effect in impact strength (10, 11).

In this study, the crazing process in HIPS is modeled numerically as a function of the particle size distribution and volume loading of rubber. It is assumed that "pinning" of individual crazes by large rubber particles controls the size of the craze field which develops prior to fracture and, hence, the measured toughness. The results are compared with experimental measurements of the impact strengths of HIPS resins having systematically varying and well-characterized particle size distributions. A detailed discussion of the determination of these distributions by scanning electron microscopy is presented. Morphological evidence supporting the conclusions drawn from the above comparisons is offered.

EXPERIMENTAL

Modeling

A bimodal distribution of particle sizes was used for the numerical modeling studies. Both the large and small particles were represented by monodisperse distributions to simplify the calculations although this assumption does not materially affect the results. The following assumptions were made:

1. All particles act as craze initiators.
2. The probability of initiation is independent of particle size.
3. Only the large particles are effective in terminating crazes.
4. Craze growth from a given particle is terminated only if the center of the particle of interest lies within a triangle bounded by large particles lying within a vertical distance $\pm R$ to the craze plane.
5. The material fails when the maximum craze length exceeds a critical value L^*.

The computations were carried out in two steps (5). Large particles centered on randomly selected x, y, and z coordinates were sequentially introduced into a cube having dimensions equal to those of a unit cube plus a guard layer of thickness H (see *Fig. 1*); H is an adjustable parameter slightly greater than the calculated interaction distance, θ, defined below. Overlapping particles were eliminated. After reaching the desired volume loading of large particles, small particles ($r = 0.1R$) were added in the same fashion until the desired overall volume fraction of rubber was obtained.

At this point, each particle in the unit cube was sequentially selected as a test particle and the nearest large particle neighbors forming a triangular perimeter lying within a vertical (Z) distance of $\pm R$ to the equator of the test particle were identified (see *Fig. 2*). This geometry was taken to satisfy the "pinning constraint" noted above. The average separation distance along the equatorial plane between the test particle and its three large particle neighbors was determined and averaged over all test particles to calculate the average interaction distance, θ. Statistically reproducible values of θ were obtained when the number of large particles was in excess of 200. Significantly, the separation distance was found to depend only on the volume fraction of large particles, V_L, and to be independent of the number of small particles present. This fact was used to reduce the computation time when the volume of small particles was high.

The computed normalized interaction distances, θ/R, are plotted as a function of the volume fraction of large particles in *Fig. 3*. θ/R is observed to drop precipitously as large particles are first introduced and then to decrease more slowly for V_L values above 0.1.

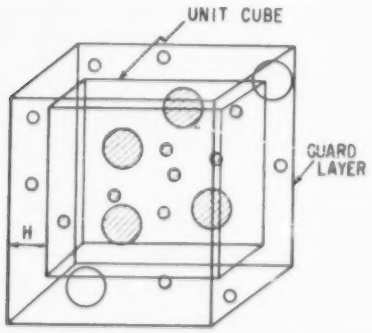

Fig. 1. Diagram showing partially filled unit cube and "guard layer".

Rubber Particle Size Measurements

Rubber particle size measurements were carried out on extracted samples using scanning electron microscopy. This technique was selected in preference to transmission electron microscopy and optical microscopy to avoid approximations associated with non-diametrical cutting and poor sampling statistics in the former and resolution limitations in the latter. The technique was found to produce accurate and reproducible results when the extraction was carried out with sufficient care. To establish the validity of the technique over a range of particle sizes, initial studies were carried out on

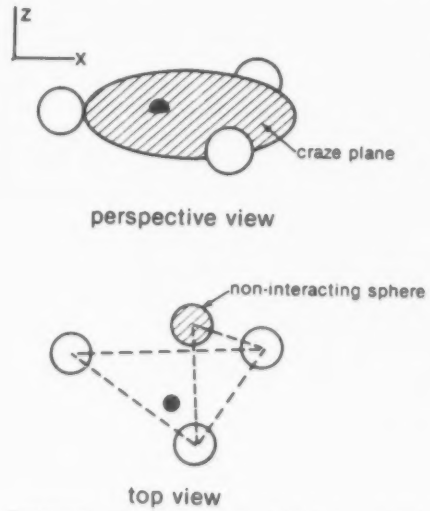

Fig. 2. Diagram showing geometrical constraints required for craze termination.

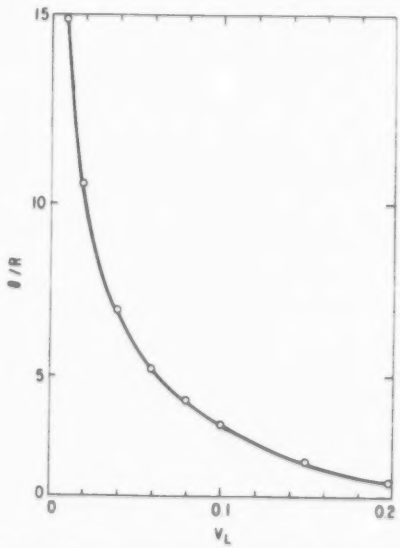

Fig. 3. Reduced interaction distance (θ/R) vs. volume fraction of large rubber particles.

FG 834, a Foster Grant HIPS resin having a broad rubber particle size distribution.

Rubber was removed from the HIPS following the procedure suggested by Keskkula and Traylor (12). Typically, 0.05 gm of the resin was dissolved in 10 ml of toluene to which 1 wt percent OsO_4 was added to fix the rubber and reduce extraction of polystyrene from interior occlusions. After dissolving the polystyrene, the rubber phase was separated by centrifugation at 15,000 rpm for thirty min. The water-white supernatent liquid was subsequently decanted off. The centrifuged rubber was washed with fresh toluene, centrifuged a second time, and redispersed in isopropanol by placing the sample in an ultrasonic cleaner for five min. A drop of the dispersion was placed directly on an SEM pedestal, dried, and sputtered with Au/Pd prior to observation. A typical micrograph taken of rubber particles extracted from FG 834 resin in this fashion is shown in *Fig. 4*. With the aid of a Zeiss MOP-3 image analyzer, a series of such micrographs were used to produce particle size histograms and to calculate number and volume average diameters. To avoid bias, all of the particles in a given micrograph were counted and 300 to 500 particles were measured to produce statistically reliable averages.

The centrifugation conditions were found to be an important variable. At lower rpms and shorter times the extractions were incomplete. This deficiency was not immediately recognized because the mother liquid appeared to be water white and free of suspended particles. In fact, the liquid contained a large number of particles of insufficient size to scatter light. These particles were readily visible in the SEM after evaporating a small amount of this phase on a pedestal (see *Fig. 5*). Improper counting of such particles produced large errors in the calculated number average particle size as shown by comparing the cumulative number fraction distribution curves in *Fig. 6*. The weight of suspended rubber could be calculated by partially summing the distribution curves for the extracted and supernatent phases in order to match the curve obtained under more rigorous centrifugation conditions. For the example shown, the weight fraction of suspended rubber was 1.8 percent. The supernatent liquid in subsequent extractions was carefully monitored to ensure that the extractions were quantitative.

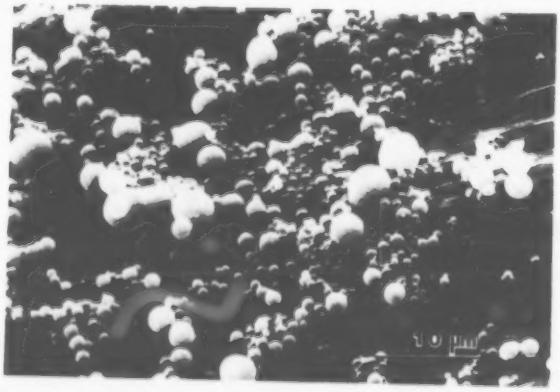

Fig. 4. Scanning electron micrograph. Rubber particles extracted from toluene solution of HIPS by high speed centrifugation.

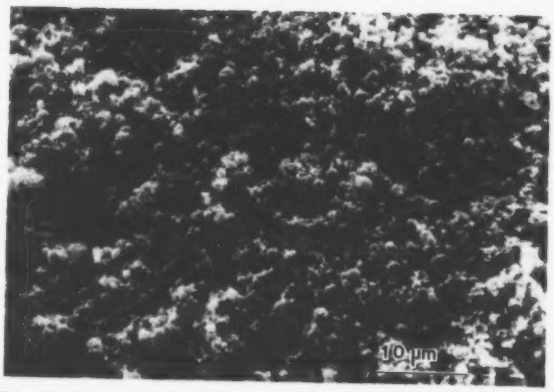

Fig. 5. Scanning electron micrograph. Small rubber particles separated from clear supernatent toluene after inadequate centrifugation.

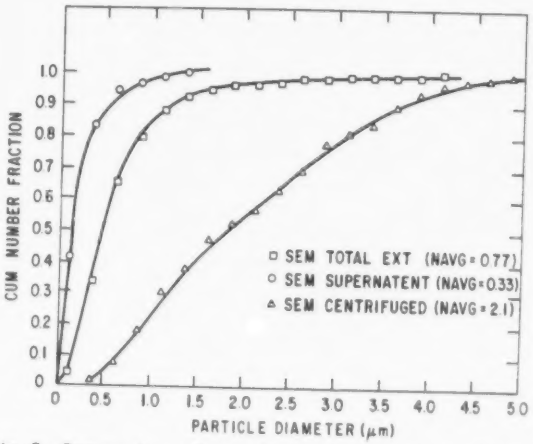

Fig. 6. Comparison of cumulative number fraction distribution functions for rubber particles in FG-834 obtained under different centrifugation conditions.

Elimination of osmium from the separation procedure produced some surface wrinkling of the rubber particles indicating that partial extraction of the occluded polystyrene had occurred. Significantly, however, this effect produced little change in the measured size distributions. Because of the extreme toxicity and handling concerns associated with organic osmium solutions, osmium was not used in subsequent extractions.

Blend Preparation And Testing

The blend studies were carried out on two Monsanto HIPS resins (Q-369 and Q-301) having comparable molecular weights, rubber morphologies (Salami), and other physical parameters (see *Table 1*) but differing markedly in

rubber particle sizes. The respective cumulative number and volume fraction distribution functions are reproduced in *Figs. 7* and *8*.

Blends of these resins were compounded by melt extrusion and injection molded into Izod test specimens. The weight fraction of rubber was held constant by the addition of atactic polystyrene homopolymer having a molecular weight equivalent to that of the HIPS resins ($\bar{M}_n$ = 80,000; $\bar{M}_w$ = 200,000). The Izod bars were notched with a fly cutter having a 10 mil radius and tested in three-point bend at a ram speed of 100 in/s using an MTS testing machine with a hydraulic actuator (13). The results are plotted in *Fig. 9* as a function of the relative amounts

Table 1. HIPS Resin Characterization Data

Resin	Q-301	Q-369
% Rubber	9.3	9.5
% Gel	20.7	24.2
Molecular Weight		
$\bar{M}_n$	100,000	74,000
$\bar{M}_w$	230,000	238,000
$\bar{M}_z$	400,000	436,000
% Mineral Oil	1.7	1.7
Particle Radius (μm)		
N_{avg}	0.48	0.81
V_{avg}	0.92	3.9
Notched Impact (ft-lb/in)	1.1	2.7

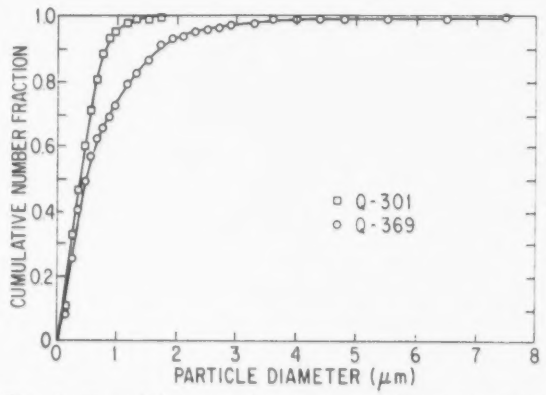

Fig. 7. Cumulative number fraction distribution functions for rubber particles in Q-301 and Q-369 resins.

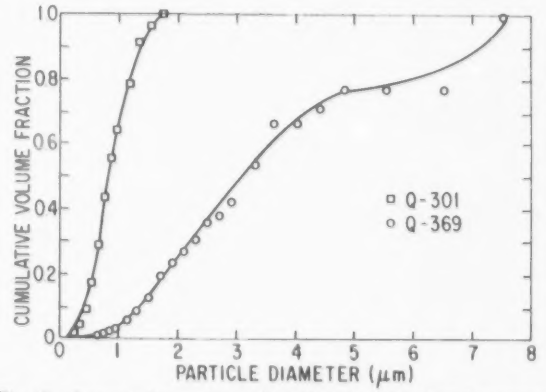

Fig. 8. Cumulative volume fraction distribution functions for rubber particles in Q-301 and Q-369 resins.

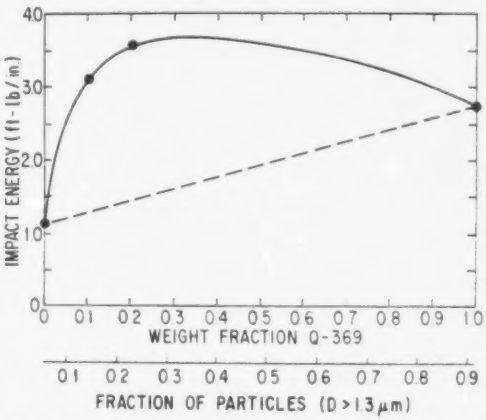

Fig. 9. Fracture energies for notched HIPS specimens broken in three point bending at 100 in/s.

of the two resins and as a function of the fraction of "large" (greater than 1.3 μm) particles in the blend.

RESULTS AND DISCUSSION

Examination of *Fig. 9* shows that at constant rubber concentration, small additions of large particle rubber initially cause a rapid rise in the notched impact energy. At higher concentrations, however, the impact energy decreases. This unusual behavior contrasts strongly with other physical properties which tend to closely follow the rule of mixtures. The impact strengths and moduli of blends of either of the HIPS resins with crystal polystyrene, for example, were found to increase linearly with rubber content. Moreover, the moduli of the mixed HIPS blends were found to be independent of the relative amounts of each resin present as long as the overall amount of rubber was kept constant. The unusual peaking in impact strength with particle size suggests that some critical process is involved.

The modeling results predict that the average interaction distance will fall off rapidly with the initial introduction of large particles (see *Fig. 3*). If one accepts the tenet that the growth of individual crazes is terminated or slowed beyond this distance, the probability of a craze reaching a length L^* will drop in a similar fashion. Thus, the number of stable crazes (and the dissipated energy) is expected to vary in proportion to the number of particles per unit interaction distance (NR/θ). From the experimentally measured particle size distributions, it is possible to calculate the total number of particles per unit volume and the fraction of those particles exceeding a given diameter at any Q-301/Q-369 composition. The corresponding θ/R values can be obtained directly from *Fig. 3*. From this information it is possible to estimate the variation in energy dissipation with composition as shown in *Fig. 10*. While the vertical scale is necessarily arbitrary, the shape of the plot is consistent with that observed experimen-

tally. The curve first rises sharply as the interaction distance drops precipitously and then falls off slowly as the number of particles per unit volume decreases with increasing particle size. A similar variation is observed even when the constraint that all particles are equally efficient in craze nucleation is relaxed as shown in the lower curve in *Fig. 10*.

Microscopic examination of transverse cross sections of both fractured specimens and specimens removed prior to failure showed that the number of crazes increased rapidly and their average length decreased as large rubber particles were introduced into the blend by the addition of Q-369. Representative photographs are presented in *Figs. 11* and *12*. The increased number of shorter crazes in the blends containing large rubber particles is consistent with the prediction of a "pileup" of crazes of length L_e when the average interaction distance is less than L^*.

It is perhaps surprising that the simplistic craze termination model presented above appears to account as well as it does for the observed variation in impact strength with rubber particle size in HIPS. While the predictions are to a large extent qualitative, the essential behavioral patterns of the HIPS blends (e.g., the non-linear rise in impact strength with the introduction of large particles; the maximum in the impact strength/composition curve) can be satisfactorily described. In spite of these successes, several deficiencies remain in this analysis:

1. The model makes no effort to explain the efficacy of large particles in terminating or retarding craze growth. Although it has been suggested that the presence of a particle having a large radius of curvature at the craze tip may reduce the local stress concentration and slow further growth, no explicit experimental evidence for such behavior was found in this work
2. The current model is largely qualitative in concept and predictive ability and requires further refinement and experimental documentation.
3. The model ignores the observation that craze nucleation efficiency may vary markedly with particle size. (Since it has been suggested that this variation alone may be enough to account for efficacy of larger rubber particles in improving impact strength, this hypothesis is considered more carefully below).

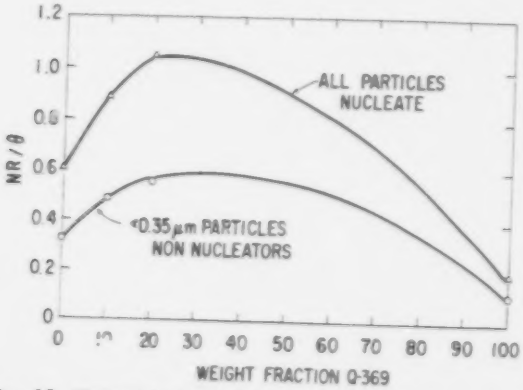

Fig. 10. Calculated variation in fracture energy with composition for Q-301/Q-369 blends.

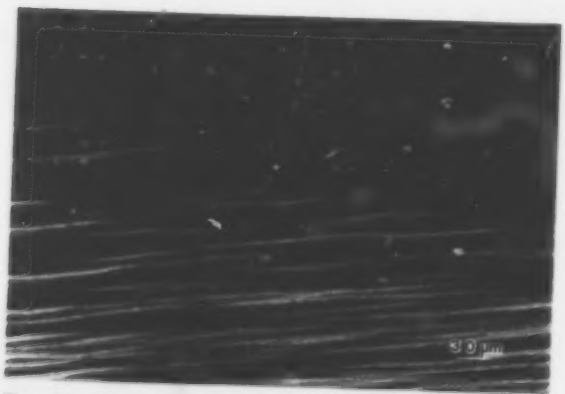

Fig. 11. Optical micrograph showing subsurface craze field at notch tip of broken Q-301 test specimen. Note low number of relatively long crazes.

Fig. 12. Optical micrograph showing subsurface craze field at notch tip of broken Q-369 test specimen. Note large number of short crazes.

Although the dimensions of the stress field around a spherical inclusion scale with the particle radius, the magnitude of the stress concentration at the interface is independent of size. Thus, *a priori*, small and large inclusions should be equally capable of nucleating crazes. Donald and Kramer have proposed that discrimination with respect to size arises from the need to establish a critical stress level over some distance (i.e., approximately 75 nm) from the particle surface (9). Following this argument a computer program was written to estimate the variation in craze length and absorbed energy with applied stress for the Q-301 and Q-369 resins used in the current study. The following assumptions were made:

1. The equatorial tensile stress σ_{ω} (14) was assumed to be the primary stress leading to craze initiation.

2. Craze initiation was assumed to occur when the tensile stress concentration at a distance of 75 nm from the particle surface reached the craze initiation stress for the matrix. The stress was calculated using Goodier's model for spherical inclusions.
3. Crazes were assumed to remain constant in thickness and grow in an annular fashion at a rate which was exponential with respect to the applied stress.
4. The energy absorbed was taken to be a linear function of the craze volume.
5. Reasonable choices were made for the various fixed parameters used in the calculation (e.g., craze thickness, growth rate constants, etc.) although their exact values were not critical since only comparative results were of interest.
6. The number of particles/unit volume in each resin and their respective sizes were obtained directly from the measured distribution functions shown in *Figs. 7* and *8*.

The relative energies dissipated as the result of craze initiation and growth in the two resins, calculated on the basis of the above assumptions, are plotted as a function of the externally applied stress in *Fig. 13*. A value of 4500 psi was used for the craze initiation stress of the polystyrene matrix. The corresponding changes in the maximum craze length with energy are shown in *Fig. 14*. At low stress levels the resin containing large rubber particles (Q-369) is able to absorb the largest amount of energy because crazes are initiated earlier. As the stress increases, however, a substantially larger number of crazes develops in the resin with smaller rubber particles (Q-301) since the number of particles rises with R^{-3}. The ultimate fracture energy is predicted to be significantly greater in the latter case. Moreover, the absorbed energy is expected to fall monotonically with increasing particle size. In addition, the longest crazes and the broadest distribution of craze lengths are predicted to occur in the resin containing the largest rubber particles. None of these features are consistent with the observations made in this study.

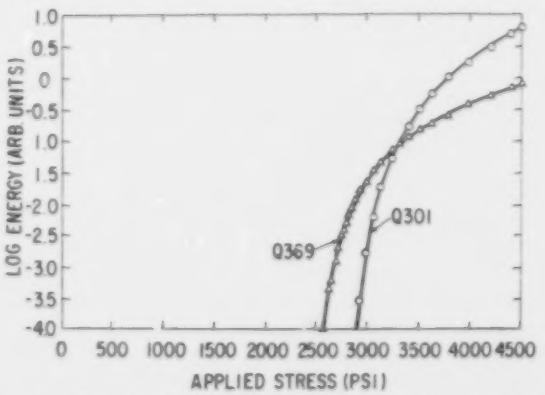

Fig. 13. Calculated energy dissipation resulting from initiation and growth of crazes in Q-301 and Q-369 resins.

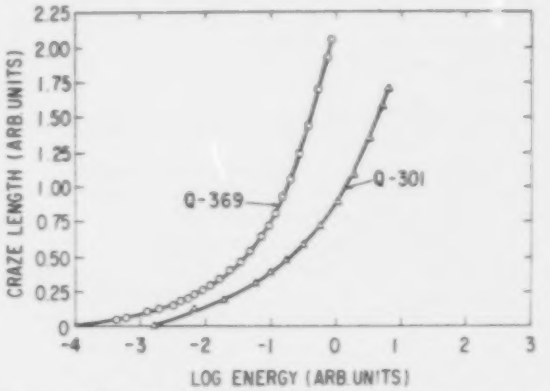

Fig. 14. Calculated variation in maximum craze length with absorbed energy for Q-301 and Q-369 resins.

CONCLUSIONS

1. A numerical model relating craze termination to rubber particle size in HIPS has been developed. The assumptions that large rubber particles retard craze growth, that the average craze length is related to an interaction distance, θ, and that failure occurs when a critical craze length is reached are inherent in the model.
2. The model predicts a non-linear rise in fracture energy with the addition of large rubber particles to a resin containing predominantly small rubber particles followed by a more gradual drop in fracture energy as the overall number of particles falls with increasing average radius. These predictions are supported by notched impact data on HIPS blends having sharply different and well-characterized particle size distributions.
3. The deficiencies in relating fracture energy solely to the process of craze termination are cited and the need for further experimental data is noted.
4. The concept that differences in nucleation efficiency alone can account for observed variations in impact energy with rubber particle size is briefly addressed and shown to be lacking in several important respects. Significantly, however, such differences can be accommodated in the termination model without markedly changing the results.

REFERENCES

1. C. B. Bucknall, "Toughened Plastics", Applied Science Publishers, Ltd., London (1977).
2. A. D. T. Gordon and T. D. Pendle, *Rubber Chem. Technol.*, **56**, 664 (1983).
3. J. Silberberg and C. D. Han, *J. Appl. Polym. Sci.*, **22**, 599 (1978).
4. C. F. Parsons and E. L. Suck, *ACS Adv. Chem. Ser.*, **99**, 340 (1971).

5. S. Y. Hobbs, R. C. Bopp, and V. H. Watkins, *Polym. Eng. Sci.*, **27**, 380 (1983).
6. R. Braglia and T. Casiraghi, *J. Mater. Sci.*, **19**, 2643 (1984).
7. C. B. Bucknall, ibid., pp. 205 ff.
8. C. B. Bucknall, D. Clayton, and W. E. Keast, *J. Mater. Sci.*, **7**, 1433 (1972).
9. A. M. Donald and E. J. Kramer, *J. Appl. Polym. Sci.*, **27**, 3729 (1982).
10. A. Sugio, *et al.*, US Pat. 4,448,931 (1984).
11. F. Brandstetter, *et al.*, US Pat. 4,446,277 (1984).
12. H. Keskkula and P. A. Traylor, *Polymer*, **19**, 465 (1978).
13. S. Y. Hobbs and C. F. Pratt, *J. Appl. Polym. Sci.*, **19**, 1701 (1975).
14. J. N. Goodier, *ASME Trans.*, **55**, 39 (1933).

NOMENCLATURE

R = Rubber particle radius.
H = Thickness of "guard layer".
N = Number of particles/unit volume.
L^* = Critical craze length for initiating fracture.
$\bar{M}_n$ = Number average molecular weight.
$\bar{M}_w$ = Weight average molecular weight.
N_{avg} = Number average particle size.
V_{avg} = Volume average particle size.
V_L = Volume fraction of "large" particles.
L_o = Average craze length at time of termination.
σ_{ee} = Equatorial tensile stress.

DISCUSSION: S. Y. HOBBS

I. K. Partridge: Did you measure the total effective volume of your rubber particles in the two materials?

S. Y. Hobbs: The issue is, that the resins we used were normalized according to gel fraction rather than to rubber fraction. This is a major issue when one deals with small particles having a core/shell structure, where the bound polystyrene in the outer layer forms a major part of the gel. In the systems we used, which both had salami-type rubber particles, there was very strong correlation between the amount of rubber and the amount of gel in these two systems. So, this was not an issue in the experiment.

I. K. Partridge: But if you keep the total rubber content constant and change the dispersion, the effective volume should change introducing differences in performance.

S. Y. Hobbs: I guess I do not follow that. The gel content was very similar. The particles were quite complex containing polystyrene inclusions, but the total effective volume was very similar.

I. K. Partridge: I agree that small rubber particles are ineffective as craze initiators, but I object to you equating those to non-nucleators. We have just done extensive work which shows that rubber particles as small as 0.2 μm do initiate crazes but at a low rate.

S. Y. Hobbs: That is a very important point. During an impact experiment, when one can dump energy into the system very quickly and failure may occur prematurely, the small rubber particles may never have time to develop crazes. I did not know how to account for this kinetic behavior in the relatively crude model I proposed. Therefore, I chose to assume that small particles are ineffective initiators for the conditions used in our experiments, and to use this to illustrate that observation is not inconsistent with the craze termination model.

I. K. Partridge: Can you see an extension of your model to account for the observation that the stress concentration factors you measured are greater than the theoretical predicted maximum value of two?

S. Y. Hobbs: No, there is no way of doing that. Both models discussed are very crude and many people will not agree with the assumptions made. The purpose was to test the concept. It seems that the termination process may better explain the behavior than only the nucleation. Most likely it is some combination of these two which should be used.

L. Piche: Is there a relation between this type of behavior and what is found for dislocations in metals? Would a model like that of Lücke and Granato be applicable?

S. Y. Hobbs: We have not looked into this in any great detail. Of course we borrowed the idea of pinning and used the metallographic terms to describe the process. It is probably a somewhat different mechanism since in metals you do not have crazes, and craze growth mechanism does not occur. There is one thing which is important to point out from a practical point of view, in terms of adjusting these particle size distributions. There are reasons for the use of small rubber particles, e.g., for gloss. It may be advantageous to make a small particle resin with very high gloss and dope it with a small number of large particles retaining a good gloss while achieving substantial improvement in the impact strength.

H. P. Schreiber: Does the styrene matrix play any role in defining what is meant by a "small" rubber particle?

S. Y. Hobbs: I am sure it does. But we looked at one particular PS molecular weight. If one makes a Noryl, where you blend poly(phenylene oxide) with polystyrene and essentially change the matrix ductility, one can shift the required minimum particle size to a lower and lower level. So, in fact, matrix ductility is a factor influencing the choice of particle sizes. There is no reason to believe that it should not show this maximum behavior. In fact, in some of the

Noryls that GE makes commercially we see this, but it is displaced to smaller particle sizes.

D. E. Henton: We also know that the swelling index and the graft level are very important as well. Have you been characterizing those two in your resins?

S. Y. Hobbs: We did measure the relative swell of the rubber particles in the two systems. They were very comparable. We took this as an indication that the graft level is probably comparable as well. How do you measure the graft level? We did try to keep most of the parameters constant (these are listed in *Table 1* of the paper) and vary only the particle sizes.

D. E. Henton: Do you think that maybe the difference in determining particle size using different techniques was due to extraction of the occlusions because of different solvents used?

S. Y. Hobbs: In the original solvent extraction procedure that we used (pioneered by Keskkula and Traylor) one introduces osmium to the extracting solvents. The idea is that Os will be picked up by the rubber, preventing penetration of the extracting solvent into the internal occlusions and thereby preventing extraction of the internal styrene. When we repeated the procedure in the absence of Os, yes, some of the particles appeared to have wrinkled surfaces, indicating that some of the interior styrene has been extracted. However, when we measured the distribution functions, the results were within the experimental error. So, by using appropriately short extraction times and still getting the extraction completed we were able to dodge this Os issue, reduce the toxicity, and obtain reliable particle size measurements.

Effect of Rheological Parameters on Phase Morphology of Polyblends: a Route to Computer Aided Design and Development of Industrial Polyblends

A. P. PLOCHOCKI

Stevens Institute of Technology
Castle Point
Hoboken, New Jersey 07030

Set of procedures employing melt viscoelasticity functions for selecting components and composition of the binary polyblends and estimating minor phase domain size is introduced and illustrated with examples. The procedures intended for Computer Aided Manufacture of the polyblends (CAMOBLE) are based on shear stress dependent viscoelasticity ratios, and the selection of the composition exploits stress dependent synergism of the viscoelasticity functions. Also used is auxilary procedure for composition selection is based on verified blending laws accounting for interaction and shear effects. Evaluation of the performance characteristics ("mechanical properties") is illustrated with a modified Kerner model.

INTRODUCTION

Development of polyblends or polyalloys is currently based on trial-and-error and/or statistical procedures (1–5). Progress in developing the theory of polyblends and a vast amount of experimental data accumulated within the last 30 years (6–10) open possibilities for development of polyblends/polyalloys with desired morphology, in a manner similar to metallic alloys or to compound design in organic chemistry. The enormous databases of component-polymers material functions and complexity of description of the mixing processes (11–16) can be only handled using computers. A possibility seems to emerge, therefore, for a type of "computer aided manufacturing" (CAM) [17] of polyblends/polyalloys of required phase morphology. The basic model for the CAM could start with rheology criteria (which are known to control the type and fineness of the morphology) the viscosity ratio, η_r, elasticity ratio $(\psi_1)_r$, or $(N_1)_r$ with the interfacial tension, $\nu_{1,2}$ and, possibly, elongational viscosity, λ_r. Since the relationship between morphology and properties in polyblends is reasonably well established (9) the criteria of creation phase morphology could be employed for prediction of polyblends/polyalloys processability and performance. Alternatively, it may be feasible to start with a set of desired properties of a polyblend/polyalloy and compute the rheological properties required for "candidate" component-polymers.

In the present communication a first elementary step in this direction will be taken by demonstrating:

- the stress dependence of the rheological criteria which govern phase morphology formation in polyblends
- the way in which the criteria could be derived and used for predicting the type and fineness of phase morphology
- an example of stress dependent characteristic domain size, $\langle d \rangle$, for a polyblend of disperse morphology as compared with a polyblend of synergistic composition
- the feasibility of accounting for influence of the mixing process on phase morphology formation. Such a procedure would require a knowledge of stress fields in the mixer. From that information, the ranges of η_r, $(N_1)_r$ could be established giving an insight into domain sizes range.

The scope of the approach is necessarily restricted by the scarcity of information on: interfacial tension in the stress field (during melt flow), significance of the elongational viscosity ratio, λ_r (especially with respect to the relaxation time, τ_r and/or elastic strain, γ_r ratios (1)), dependence of crystallization on morphology (6, 19) and role of the mixing process (14, 18).

BACKGROUND

CAM benefits are numerous. One may use computer generated information to select components and compositions, to control com-

pounding and pelletizing operations, to design processing and finishing steps, to predict profitability, and to help the quality assurance personnel (17). One may visualize such a model for a polyblend as a sequence of programs supported by its own data-base built over viscoelasticity ratio functions, *M*, *MWD*, and other pertinent characteristics. The programs would predict effects of changes in: composition, mixing (compounding) parameters and processing conditions on morphology, processability, and performance. Phase morphology in polyblends is specified qualitatively by the type (disperse or stratified) and quantitatively, by domain size distribution and intensity of segregation (8, 13, 20).

In the following text the term "CAMOBLE" will be used to identify "Computer Aided Manufacture of Polymer Blends."

Thermodynamics

Multicomponent polymer systems consist of miscible or immiscible polyblends. Since there are few polyblends of commercial importance which belong to the former category, we will concentrate on the latter, microheterogeneous systems. The phase morphology of these, in contrast to metal alloys, is determined by thermodynamics and melt rheology of the phases and of the interface. The diffusion controlled formation of phase morphology (nucleation, spinodal decomposition, and Oswald ripening (6, 21–23)) is usually slow in relation to rate of industrial processes. However, thermodynamics of polyblends or polyalloys has to be employed in CAMOBLE mostly through relations between the thermodynamic functions (free energy of mixing, excess volume, characteristic parameters) and melt rheology of mixing and processing flows. Notable exceptions are in directly relevant thermodynamical characteristics: interface behavior and specific volume. The latter is of particular importance because its pressure dependence (*Fig. 1*) is coupled with responses in melt rheology functions (apparently, with a transition in phase morphology (24, 30).

An equation of state, developed by Simha and co-workers for multicomponent polymer systems (26), can be used in CAM programs. Thermodynamics of polymer/polymer interface do not as yet seem to be developed to the extent which would permit its application to the CAM of polyblends (25).

Melt rheology of polymers should be incorporated as:

1. a specific "CAM compatible" database;
2. rheological description of the polyblends; and
3. as a set of CAM oriented rheological criteria governing formation of morphology in polyblends.

The rheology of polyblends or polyalloys (No. 2 above) may in turn, be incorporated (in the decreasing order of physical consistency) via:

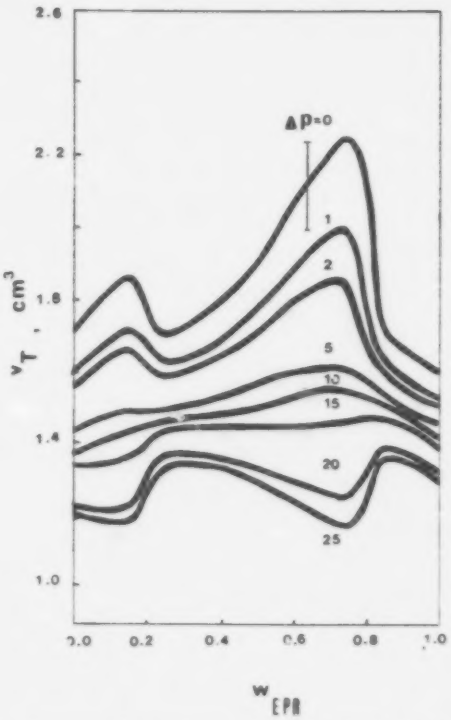

Fig. 1. Pressure dependence of the specific volume, v_T (T = 463K) synergism in i-PP/EP polyblends, vertical bar on the "O" (atmospheric pressure) curve indicate the confidence interval (30).

2.1. Rigorous treatment of multiphase system rheology with constitutive equations involving interface stress/rate of strain tensors (27);

2.2. Quasi continuum approximation (QCA) involving mixing laws, e.g., as introduced by Bogue in the form of the quadratic blending rule for relaxation spectra (H) of two component blend:

$$H = (w_1)^2 \cdot H_{11} + 2w_1 \cdot w_2 \cdot H_{12} + (w_2)^2 \cdot H_{22} \quad (1)$$

subsequently generalized to the "blending rule" integral type constitutive equation (28). In the memory function contributions of component polymers are embodied in characteristic relaxation time ($\tau^*_{1,2}$):

$$\tau^*_{1,2} = \frac{\tau_1 \cdot \tau_2}{1 + a\sqrt{\tau_1 \cdot \tau_2 \cdot \Pi_d}} \quad (2)$$

with $\Pi_d^{1/2}$ – the time averaged 2nd invariant of the rate of deformation tensor, **D**. In a "simplified" form (which neglects contributions of components polymers) QCA approach is the most widely pursued to date (6);

2.3 Suspension approximation very successful in accounting for minor phase size

distribution effects but developed for shear flow only (29);

OUTLINE OF CAM POTENTIALS FOR POLYBLENDS

The underpinning assumption of the procedure which we propose is in the continuity of (shear) stress across the interface (7). This leads to the notion of inherent shear rates ("ISR"—i.e., shear rate within a phase—*Fig. 2*) and to organization of the database of component polymers material functions: viscosity, η, elasticity, N_1, and (in a future development) elongational viscosity, λ in the form of stress dependent characteristics. The ISR concept is a useful tool in selecting the level of stress during melt mixing and in processing flows. The stability of polyblends' morphology as well as the "strength" of the interface depend on the amount of shear in the phases, which is proportional to the ISR. For convenience ISR may be expressed as $\Delta\dot{V} = \dot{\gamma}_2 - \dot{\gamma}_1$.

The database of material functions is subsequently used for computer aided generation of viscosities, η_r, and elasticities, $(N_1)_r$, ratio functions which might be generated at selected levels ($\Delta\dot{V}$) of ISR. In the next step the procedure utilizes an estimate of interfacial tension, $\nu_{1,2}$ at the stress level of interest together with an estimate of the minor phase domain size, $\langle d \rangle$, for prediction of the phase morphology type. The dispersed type morphology is formed, at a set of $\nu_{1,2}$ and $\langle d \rangle$ values, only if the elasticity of the minor phase is higher than that of the matrix. Alternatively, stratified morphology will ensue (31, 32). Subsequently, the minor phase domain size could be evaluated as a function of stress. Thereby it should be possible to simulate quantitative changes in phase morphology (e.g., $\langle d \rangle$) caused by different stress levels during mixing and/or processing. This analysis forms a basis for selecting components of a polyblend by CAMOBLE: it is possible to simulate a large number of binary polyblends with respect to the type and fineness of phase morphology and their dependence on melt flow *prior* to actual mixing and processing.

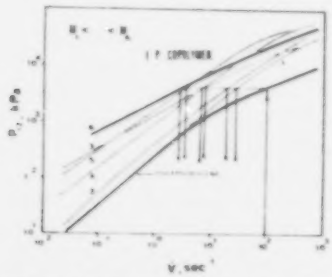

Fig. 2. Concept of the inherent shear rate (ISR) illustrated with flow curves (reduced to 260°C) for components of the i-PP/EPDM blends: 1–6 flow curves for EP copolymers of increasing $\bar{M}$: $\bar{M}_1 < \ldots < \bar{M}_6$. At the stress level of $p_{12} = 5$ MPa the difference in ISR between i-PP and EPDM #6 amounts of $\Delta\dot{V} = 100\ s^{-1}$ (Data courtesy S. Miller after (24).

The next step in CAMOBLE is selection of the composition. The selection may be based on synergistic ("particular rheology"—PRC) compositions (1, 9b). Localization of PRCs and evaluation of their dependence on the rate of deformation (synergistic η, N_1) or pressure (synergistic V_T) might be based on the generalized "mixing rules" (28, 33, 34). Calculated PRC should subsequently be verified by experimental data from the "discrete composition sampling" procedure (DCS) (1, 9b). Of course the final selection of a composition depends on the anticipated processing technique and intended application(s) of the polyblend.

If a high performance plastic is the objective of CAMOBLE, then the composition selection part of CAM would have to incorporate performance characteristics of component polymers and models for the morphology-composition dependence of the polyblends' characteristics (see Dickie in (9a)).

On the other hand, CAMOBLE directed toward processability improvement or incorporation of large amounts of particulate fillers would have to incorporate a model for the stress dependence of the "synergistic rheology" PRC or a model of the pressure dependence of the "synergistic specific volume" PRC (24, 30).

In the procedure outlined below we follow the conclusions of numerous studies into polyblends melt rheology (7, 8, 35, 36), that the "size controlling" factor in phase morphology formation is that of η_r. The role of η_r can be generalized by accounting for its stress dependence. The type of phase morphology can be predicted on the basis of the ratio of components elasticity, $(N_1)_r = f(p_{1,2})$ as well as $\nu_{1,2}$ and $\langle d \rangle$ estimates. It can be assumed that the morphology of a polyblend could be either of the disperse or stratified type (Van Oene (31) and (20, 24)). In spite of such a crude assumption which has to be further simplified because of limited availability of the data on interface tension and its stress dependence (10), CAMOBLE allows estimation of the stress dependent domain size, $\langle d \rangle$. Yet, due to these limitations, CAMOBLE appears to be inapplicable either to polyblends of exceptionally large interface (14, 27) or to miscible blends (7, 8).

The database of melt rheology and melt properties of component polymers, together with computer generated characteristics of the polyblends, assembled at the "screening" stage of CAMOBLE are also useful in setting up an industrial melt mixing process and/or in predicting changes in phase morphology during processing (1, 9b, 12).

Algorithms of "CAMOBLE"

Viscosity and elasticity functions of the component polymers and of the polyblends are used

in a convenient, logarithmic parabola approximation, truncated to "generalized" power laws (11, 1) which correlate stresses with inherent shear rates (ISR):

$$\text{—shear stress: } p_{12} = p_{12}^{\circ} \cdot \dot{\gamma}^{n} \tag{3}$$

$$\text{—principal normal stress difference: } N_1 = N_1^{\circ} \cdot \dot{\gamma}^{m} \tag{4}$$

where $\eta^{\circ} \equiv p_{12}^{\circ}$ and $N_1^{\circ} \equiv \psi_1^{\circ}$ are viscosity and elasticity parameters taken at standardized [1] $\dot{\gamma}^{\circ} = 1\ s^{-1}$. In multiphaseous melts only the stress field is continuous, nevertheless, convenient *Eqs 3* and *4* could still be used—defining:

$$S = p_{12}/\eta^{\circ} \quad \text{and} \quad q_i = 1/n_i, \tag{5}$$

one can write: $\dot{\gamma}_i = S_i^{q_i}$ (where $i = 1,2$) and the viscosity ratio at a constant shear stress: $p_{12} = (p_{12})_1 = (p_{12})_2$ is given by:

$$\eta_r = 1 + \Delta\dot{V} \cdot S_1^{-q_1} \tag{6}$$

where 1, 2 are the indices of the component polymers, minor and matrix, respectively, with $\Delta\dot{V}$ = difference in ISRs. The ratio of the first normal stress difference coefficients: $(\psi_1^{\circ})_r = (\psi_1^{\circ})_1/(\psi_1^{\circ})_2$, at ISRs with difference in $\dot{\gamma}_i$ equal to $\Delta\dot{V}$ becomes:

$$(\psi_1)_r = (\psi_1^{\circ})_r \cdot (S_2^{q_2} - \Delta\dot{V})^{(m_1-2)} \cdot S_2^{q_2(2-m_2)} \tag{7}$$

It follows from definition of ψ_1 that the elasticity ratio depends strongly on shear rate:

$$(\psi_1)_r = (N_1)_r \cdot (\dot{\gamma}_2/\dot{\gamma}_1)^2 \tag{8}$$

Hence, in representing the effects of normal stresses on morphology formation $(\psi_1)_r$ yields results biased by η_r^2 effects (ratio of squared ISRs). For this reason, use of the normal stress ratio function $(N_1)_r$ is preferred.

Van Oene's criterion for disperse $\langle - \rangle$ stratified phase morphology transition (9, 24, 31) is:

$$\langle d \rangle \leqq 6[(\nu_o)_{1,2} - \nu_{1,2}]/\Delta N_1 \tag{9}$$

where:

$$\Delta N_1 = (N_1)_1 - (N_1)_2 = (N_1)_2[(N_1)_r - 1] \tag{10}$$

$(N_1)_r$ in *Eq 10* can be expressed as:

$$(N_1)_r = (N_1)_1/(N_1)_2 = (N_1^{\circ})_r(\eta_1^{\circ})^{-z_1}(\eta_2^{\circ})^{z_2} p_{12}^{(z_1-z_2)} \tag{11}$$

where: $z = m \cdot q$

Equation 9 specifies the flow regime in which phase "1" remains dispersed in phase "2" with mean characteristic domain diameter, $\langle d \rangle$. Symbols $(\nu_o)_{1,2}$ and $\nu_{1,2}$ designate the interface tension under quiescent and steady flow conditions, respectively. Once the components of the polyblend are selected with respect to the resultant phase morphology at an admissible level of $\Delta\dot{V}$ one may proceed with estimation of the minor phase domain size and with selecting the composition of the polyblend.

The traditional and the least realistic approach to the characteristic size $\langle d \rangle$ estimate is based on the stability of a droplet in emulsion of two Newtonian liquids (8, 35). From equilibrium of viscous (shear) and interface tension forces it follows that:

$$\langle d \rangle = \frac{k^{+} \cdot \nu_{1,2}}{p_{12}^{q_2} \cdot \eta_2^{(1-q_2)} \cdot \eta_r(p_{12})} \tag{12}$$

where k^{+} is a material constant. This approach is still being pursued (e.g., (35)) even though more realistic treatments, e.g., involving a viscoelastic matrix with the relaxation time criterion of stability, are available (9a, 37). For our purpose, we have selected Schowalter, Chaffey and Brenner (SCB) (38) approach, successfully applied to binary blends of amorphous polymers [39]. From SCB constitutive equation for an emulsion with elastically deformable minor phase, the normal stress function for the polyblends is derived. From the function, in turn the characteristic size of the minor phase may be shown to depend on shear stress:

$$\langle d \rangle = \frac{40 \cdot N_1 \cdot \nu_{12} \cdot (\eta_r + 1)^2}{(19\eta_r + 16)^2 \cdot (\eta_1)^2 \cdot \dot{\gamma}^2 \cdot w_1} \tag{13}$$

Here, parameters without subscript refer to the polyblend while subscript 1 refers to the minor phase. *Equation 13* yields an estimate of the stress dependent characteristic size which could be used in CAMOBLE (*Fig. 3*).

Composition of a polyblend, as stipulated before, should be selected with respect to the synergistic (PRC) compositions. It could be accomplished by computer simulation of the stress *and* composition dependence of the polyblend viscoelasticity which would lead to localization of the synergistic melt rheology composition(s). At present, the feasibility of such a simulation via a "mixing rule" was verified only for shear viscosity (33, 34).

In the introductory treatment of CAMOBLE the composition and stress dependence of melt

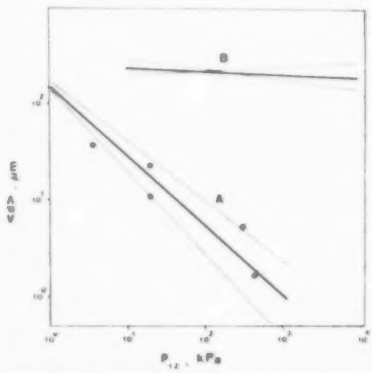

Fig. 3. Computer generated stress dependence of the (minor component) domain size $\langle d \rangle$: bold line – mean $\langle d \rangle$, thin lines – $\langle d \rangle$ confidence limits established from the confidence limits of the viscosity and elasticity functions. (Tables 1 and 2 in (1)). Datapoints: $\langle d \rangle$ estimated from turbidity measurements (45) A – HDPE/LDPE polyblend at 80/20 composition and 463 K, B – i-PP/HDPE polyblend at 25/75 (synergistic!) composition 463K (19).

viscosity may be simulated by the Carley-Crossan equation (33) (*Eq 14*). Once the synergistic composition is localized, specifics of its melt flow dependence are evaluated with the (redefined) Kasajima equation (34) (*Eq 15*). The corresponding algorithms are:

$$\ln \kappa = x_1^3 \ln \kappa_1 + x_2^3 \ln \kappa_2 + 3 x_1^2 x_2 \ln \kappa_{12} + 3 x_1 x_2^2 \ln \kappa_{21} + 3 x_1^2 x_2 \ln \left(\frac{2\bar{M}_1 + \bar{M}_2}{3}\right) + 3 x_1 x_2^2 \ln \left(\frac{\bar{M}_1 + 2\bar{M}_2}{3}\right) + x_1^3 \ln \bar{M}_1 + x_2^3 \ln \bar{M}_2 + \ln (x_1 \bar{M}_1 + x_2 \bar{M}_2) \quad (14)$$

where $x_{1,2}$—molar fractions, $M_{1,2}$—molecular mass of the components, $\kappa_i = \eta_i \cdot (v_T)_i$ is the kinematic viscosity, and v_T—specific volume at a temperature T; and:

$$(\eta^o)^q = p_{12}^{(1-q_2)} \cdot (\eta_1^o)^{q_1 w_1^+} \cdot (\eta_2^o)^{q_2 (1-w_1^+)} \quad (15)$$

where: $w_1^+ = w_1 \cdot \Phi$, Φ – interaction parameter

$$\Phi = \frac{q \cdot \ln S - q_2 \cdot \ln S_2}{w_1 \cdot (q_1 \cdot \ln S_1 - q_2 \cdot \ln S_2)} \quad (16)$$

TENTATIVE RESULTS OF THE PROPOSED CAM FOR POLYBLENDS (CAMOBLE)

Performance of the selected elements of CAMOBLE was tested on an available database consisting of standardized viscosity and elasticity characteristics at 463K presented with pertinent confidence limits for HDPE/LDPE ("d"), i-PP/LDPE ("a") and i-PP/HDPE polyblends (1, 19).

The following elements were studied: standardized viscoelasticity with respective η_r and $(N_1)_r$ ratios, size of domains—stress dependence, localization, and stress dependence of rheosynergistic compositions; localization and pressure dependence of v_T synergism. Three systems were considered: low $\nu_{1,2}$ disperse polyblends ("d", "a" – "PL" (1)), high η_r disperse polyblend ("PEP" (24)), and a synergistic (stratified) polyblend of low $\nu_{1,2}$ (19). In *Figs. 4* to *6* stress dependence of the viscosity and elasticity ratios at arbitrary differences in ISRs are presented for "d", "a" and "PL" polyblends. The upper limits of the experimental data are marked with "▼". In contrast to the accepted notion of constant η_r (7, 8, 35)) it was found that computer generated, stress dependent viscosity ratios for "d" and "a" polyblends increase at medium and low stresses 4 to 7 times, only to decrease to the level corresponding to 3 to 4 times of the initial value of η_r at higher stresses.

It is worth underscoring that the stress sensitivity of η_r decreases with $\Delta\dot{V}$ increase. Elasticity ratios differ significantly in the patterns of the stress dependence on comparing polyblends "d" and "a". While the ratios for HDPE/LDPE system are similar to the viscosity ratios, for i-PP/LDPE the elasticity ratios change 4 orders of magnitude and almost monotonously increase with stress. It seems reasonable to assume, therefore, that the flow-dependent phase morphology in both polyblends would be significantly different. Whether the differences are quantitatively limited to a change in $\langle d \rangle$ or are qualitative (change in the type of morphology e.g., transition between disperse $\langle - \rangle$ stratified)

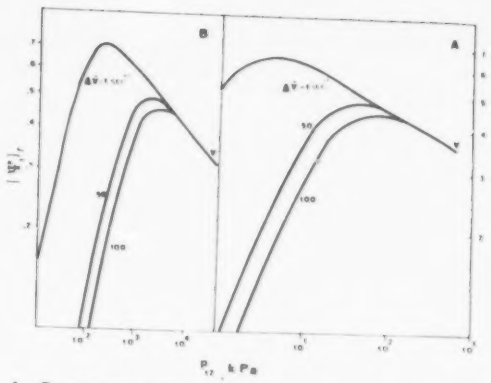

Fig. 4. Computer generated stress dependence of melt viscosities (A) and elasticities (B) ratios at inherent shear rates (ISR) differences of 1, 50, and 100 1/s. HDPE/LDPE polyblend ("d") (1) at 463K).

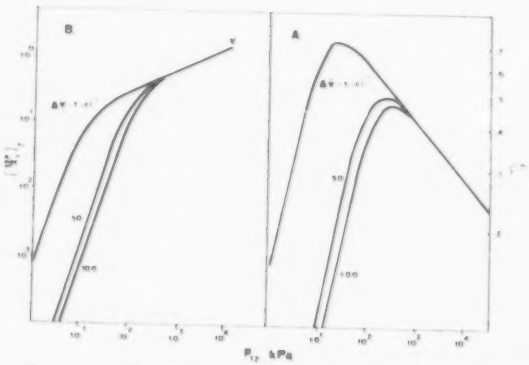

Fig. 5. Stress dependence of the melt viscosity (A) and elasticity (B) ratios at arbitrary differences in ISR, i-PP/LDPE polyblend ("a") – (1) at 463K).

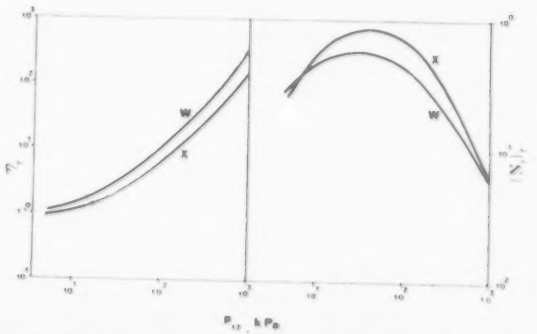

Fig. 6. Computer generated curves of stress dependent viscosity and elasticity ratio for i-PP/LLDPE polyblends (463K). Data courtesy S. S. Dagli (30).

it could be resolved by referring to interfacial tension and to mean domain size, as stipulated by Van Oene criterion *Eq 9*.

The computer simulated stress dependence of the minor phase size $\langle d \rangle$ is illustrated with *Fig. 3* for HDPE/LDPE (A) (1) and i-PP/HDPE (B) (1, 19) polyblends. Characteristic $\langle d \rangle$, estimated from the mean values of the material functions are given with bold lines. Thin lines represent upper and lower bounds of the size estimate $\langle d \rangle$ corresponding to the confidence limits of the melt viscoelasticity functions for component polymers and their blends. There is a striking difference in the pattern of $\langle d \rangle$ stress dependence. It follows from the fact that (B) represents a synergistic rheology (PRC) composition (19). It has been demonstrated (24) that at PRC "core-sheath" and/or "stratified" (*Fig. 7*) morphologies are fairly common. It is possible, therefore that the multiphase "emulsion" flow mechanism is replaced here by e.g., macrolaminar (telescopic) shear, and *Eq 9* is no longer valid.

Composition selection for a polyblend is significantly facilitated if the synergistic concentration(s) are known (1). Those "particular rheology compositions" (PRC) are computer simulated by evaluating ψ_1 at a nominal shear rate, $\dot{V}$ level using *Eqs 3* and 4 and the definition of ψ_1 with subsequent polynomial fit to the composition. Thereby CAMOBLE makes it possible to localize the composition of melt elasticity synergism (PRC) (9b) and to follow the dependence on $\dot{V}$ (*Fig. 8*) or stress. At low $\dot{V}$ = (10 to 60 s^{-1}) PRC is at $w_1 = 0.4$ LDPE and its amplitude is within the range of 300 to 1400 [Pa. s^2].

Increasing the flow rate to $\dot{V} = 100\ s^{-1}$ shifts PRC to $w_1 = 0.2$ LDPE and lowers its amplitude to 15 to 80 [Pa. s^2]. The effectiveness of "mixing rules" in direct computer simulation of viscosity—composition dependency from viscosities of the component polymers is illustrated with *Fig. 9*—only the Carley (curve "1") mixing rule which incorporates structure (M_i; x_i) and rheothermodynamics interactions (x_{12}, x_{21}, etc.) terms (*Eq 14*), accounts for the synergistic behavior. Carley's rule is "deficient", however, in that it incorporates η_i at a level of $\dot{V}$.

In order to study the shear *stress* dependency

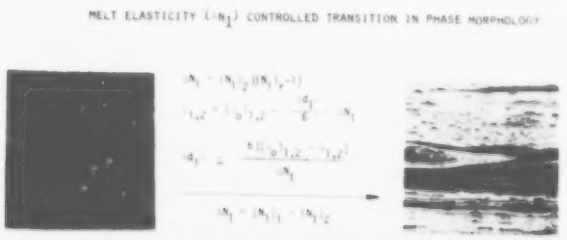

Fig. 7. Transition in the phase morphology type: from disperse (left) to the stratified (right) induced by the change in sign of the principal normal stress difference: At the shear stress level at which matrix elasticity becomes greater than $(N_1)_i$, minor phase no longer preserves droplet shape and stratifies.

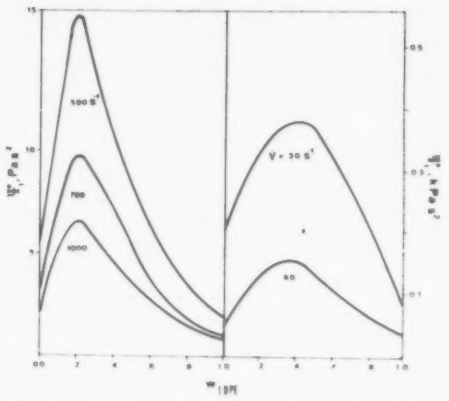

Fig. 8. Melt elasticity (ψ_1) synergism and its dependence on V·HDPE/LDPE polyblend, 463K ("d", (1)); computer generated curves from the elasticity functions of component polymers and of the polyblends.

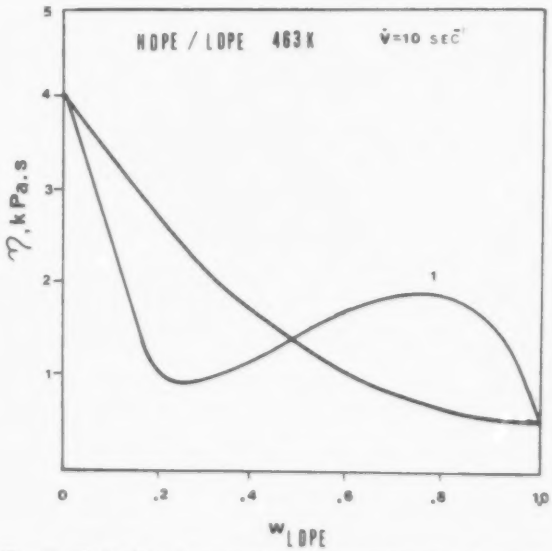

Fig. 9. Calculated composition dependence of shear viscosity (η) HDPE/LDPE polyblend at $\dot{V} = 10\ s^{-1}$ and 463K. Comparison of Carley (1) and Kasajima (2) mixing rules in predicting synergism. Simulation performed with data from (1).

of viscosity synergism one may follow the approach of Kasajima, *et al.* (34). Computer simulation will then be restricted to the composition and stress dependence of the "interaction factor", Φ, and of "effective concentration", w_1^+ (*Fig. 10*). Synergistic compositions are observed at $w_1 = 0.4$ and 0.8. Sensitivity of synergism toward stress is higher for the $w_1 = 0.8$ composition. Disagreement with *Fig. 9* follows from computing the viscosities at the same level of $\dot{V} = 10\ s^{-1}$. From *Figs. 10* and *11* it is evident that the interaction factor, Φ, is more sensitive an indicator of the synergism than w_1. The Φ factor is computer simulated in *Fig. 11* as a function of shear stress with w_1 as the parameter. $\Phi = f(p_{12})$ indicates not only the sign of the composition synergism but also reflects its stress sensitivity. The latter is obviously impor-

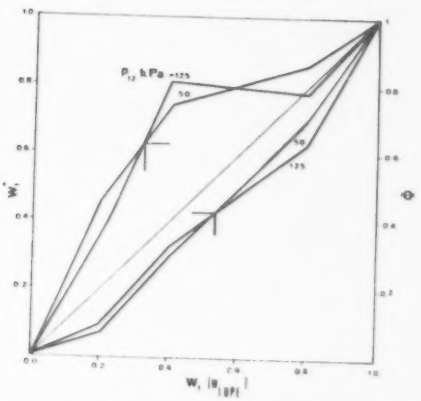

Fig. 10. Composition and stress dependence of shear viscosity synergism for the HDPE/LDPE polyblend. Synergistic compositions localized from computer generated parameters of the Kasajima's mixing rule at two levels of shear stress; w_1^* – stress dependent minor component fraction, and Φ interaction parameter (data for "d" polyblend (1)).

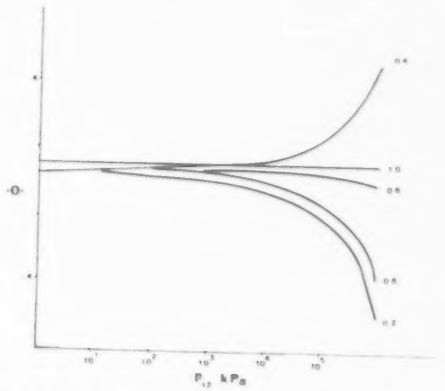

Fig. 11. Stress dependence of the melt flow interaction parameter (Φ) for a range of the HDPE/LDPE polyblends, differing in composition, w_1. Curves from Kasajima mixing rule manifest stress dependence of the synergism and indicate possibility of viscosity synergism at w_1 = 0.4 and 0.6 composition range. (Note that elasticity synergism—Fig. 8—was observed at w_1 = 0.2 and 0.4).

tant for predicting processability of a polyblend. CAMOBLE may be extended to performance characteristics of the polyblends. It is illustrated with storage modulus, G', — composition dependency in *Fig. 12*. Here the Faucher (40) algorithm was employed and the resulting G', Poisson ratio and the difference of the calculated and experimental moduli, $\Delta G'$, are plotted together with the composition dependence of (measured) radius, R_o of HDPE spherulites. Although traces of G' and experimental curves for R_o are similar, the simulation fails in the vicinity of PRC (Maximum on $\Delta G'$—composition curve). Phase morphology, specific to the synergistic composition, seems to be preserved in solid polyblends. At PRC, therefore, the composition dependence of modulus cannot be described with the Kerner/Faucher model. A similar observation of "preserved morphology" was made upon analyzing the composition dependence of density for i-PP/EPR and PE/PS polyblends (34, 41).

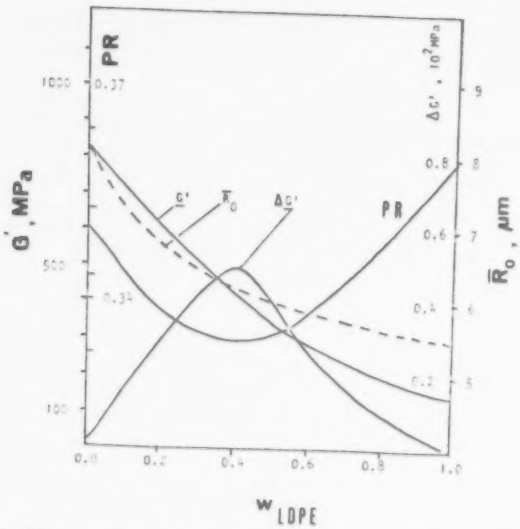

Fig. 12. Composition dependence of modulus, G', and Poisson ratio, PR, computer generated using Kerner-Faucher model (40) compared with the composition dependence of $\Delta G'$ (the difference between calculated and experimental moduli) and of HDPE spherulites radius (Ro) (LALS data courtesy L. Makaruk); "d" polyblend, 293K (1).

CONCLUSIONS

A "computer aided manufacturing" (CAM) type procedure for preparing polyblends of specific type of phase morphology and domain size is shown to yield reasonable results. The procedure (CAMOBLE) based on stress dependent ratios of component polymers' melt viscoelasticity implicitly involves interface and thermodynamic interaction effects. Those are incorporated in Van Oene's criterion for the type of morphology and Carley's mixing-with-interaction rule, respectively. In this aspect CAMOBLE prevails over statistical ("black box") techniques (2–5) and over the semiempirical blending rule approaches employed in specifying relationships between melt rheology and MWD in homopolymers (18, 42, 43). Major shortcomings of the latter are neglecting effects of the interface and the assumption of a homogeneous melt (uniformity of shear rate) (28).

With CAMOBLE it is possible to gain an insight into formation and permanence of phase morphology in polyblends, concomitant to mixing and processing if only:

1. component-polymers rheology and thermodynamics are specified over a sufficiently wide range of stresses (p_{12}, p_{11}), and
2. a realistic estimate of the stresses distribution in mixing and processing equipment is available.

Further development of CAMOBLE into a comprehensive CAM for polyblends and polyalloys would require an expanded database con-

sisting of reliable material functions in the appropriate format (1), interface tension *and* its melt flow dependence as well as of kinetics of phase formation-decomposition (7, 8, 21–23, 36, 37). The last element of the database is of particular importance for blends of crystallizable and/or liquid crystal polymers.

The trend in the direction of engineering and, in particular, computer aided engineering (CAE) of polyblends and polyalloys is evident not only from recent publications but also from initiation of inter-laboratory research programs on the dependency of phase morphology of polyblends on melt flow (44).

NOMENCLATURE

"a" = Designation of i-PP/LDPE polyblends (1).
a = Adjustable constant of a memory function (28).
CAE = Computer Aided Engineering.
CAM = Computer Aided Manufacture (17).
D = A rate of strain tensor.
$\langle d \rangle$ = Mean (characteristic) size of the minor phase domain, μm.
"d" = Designation of HDPE/LDPE polyblend (1).
DCS = Discrete composition sampling, a procedure for composition selection in polyblends (1).
EP = Ethylene-propylene copolymer (random, rubbery).
G' = Storage (shear) modulus, Pa.
H = Relaxation time spectrum, Pa (41, 42).
i-PP = Isotactic polypropylene.
i = Component index (subscript), here i = 1 – minor phase i = 2 – matrix.
ISR = Inherent shear rate (= $\dot{\gamma}$i), s^{-1}.
j = (Second) component (subscript) index.
k^+ = A constant in *Eq 12* grouping standardized material characteristics.
m = Power law (elasticity) exponent.
$\bar{M}$ = Molecular mass.
MWD = Distribution of molecular mass, usually ($\bar{M}w/\bar{M}n$).
n = Power law (viscosity) exponent (11).
N_1 = Primary normal stress difference, Pa.
o = Superscript "standardization" (here at $\dot{\gamma}^o = 1\ s^{-1}$ (11).
p_{ij} = Stress (p_{12} – shear, p_{11} – elongation), Pa.
P = Pressure, Pa.
PR = Poisson ratio.
PRC = Particular rheology (synergistic) composition.
"PL" = i-PP/LLDPE polyblend (30).
PS = Polystyrene.
q = Reciprocal of the power law (viscosity) exponent.
r = Subscript "ratio" or "relative" as in $(N_1)_r$.
S = Ratio of stress to the standardized viscosity, dimensionless.
t = Time, s.
T = Temperature, K (°C).
$\dot{V}$ = "Nominal" shear rate (i.e., calculated for a polyblend with the assumption of the uniform shear rate field), sec^{-1}.
v_T = Specific volume at temperature T, cm^3g^{-1}.
w_i = Mass fraction.
w_i^* = Shear adjusted w_i ($w_i^* = \Phi \cdot w_i$) (34).
z = Ratio of the power law exponents, m · q = $m/n = z$.
x_i = Molar fraction.
Δ = Difference in material functions or rheological parameters, e.g., ΔN_1.
η = Shear viscosity, Pa·s (poises).
γ = Shear strain.
$\dot{\gamma}$ = Shear rate, s^{-1}.
κ = Kinematic shear viscosity, m^2s^{-1} (or stokes).
$\nu_{1,2}$ = Interfacial tension, dynes cm.
λ = Elongation viscosity, Pa·s (poises).
Φ = Interaction coefficient (*Eq 16*, (34)).
Ψ_1 = Elasticity (first normal stress difference coefficient) Pa·s^{-2}.
τ = Relaxation time, s.
+ = Superscript "characteristic", e.g., τ^+.

REFERENCES

1. A. P. Plochocki, *Polym. Eng. Sci.*, **22**, 1153 (1982).
2. G. C. Derringer, *J. Appl. Polym. Sci.*, **18**, 1083 (1974).
3. W. Spendley, *et al.*, *Technometrix*, **4**, 441 (1962).
4. B. I. Raktoe, A. Hedayad, and W. T. Federer, "Factorial Designs", Wiley, New York (1981).
5. J. A. Cornell, "Experiments with Mixtures", Wiley, New York (1982).
6. L. A. Utracki, Ed., a) "Polyblends '83", *Polym. Eng. Sci.*, **24** (2) (1984); b) "Polyblends '84", *Polym. Eng. Sci.*, **24** (17) (1984).
7. C. D. Han, "Multiphase Flow in Polymer Processing", Academic Press, New York (1981).
8. V. N. Kuleznev, "Mixtures of Polymers", Khimya, Moscow (1980).
9. D. R. Paul and S. Newman, Eds., "Polymer Blends", a) vol. 1, p. 353 ff; b) vol. 2, p. 319 ff., Academic Press, New York (1978).
10. S. Wu, "Polymer Interface and Adhesion", Dekker, New York (1982); see also (9), vol. 1.
11. J. M. McKelvey, "Polymer Processing", Wiley, New York (1962).
12. P. Machowski and A. P. Plochocki, *Polimery*, **22**, 82 Warsaw (1977).
13. Z. Tadmor and C. G. Gogos, "Principles of Polymer Processing", Ch. 7, 11, Wiley, New York (1979).
14. R. Chella and J. M. Ottino, *IEC Fundam.*, **24**, 170 (1985).
15. J. R. A. Pearson "Mechanics of Polymer Processing", Elsevier, Amsterdam (1985).
16. Z. Tadmor, a talk on the "Effects of Mixing History on Phase Morphology in Polyblends", 1st Workshop of the Polymer Processing Institute program, Castle Point, August 1985.
17. B. Flachsbart, G. Peters, and J. McDonald in "Encyclopedia of Computer Science and Engineering", 2nd ed., p. 267ff. Van Nostrand Reinhold, New York (1983).
18. J. L. White see comments in discussion.
19. A. P. Plochocki, *Trans. Soc. Rheol.*, **20**, 287 (1976).
20. S. Y. Hobbs, *J. Macromol. Sci.*, **C19**, 221 (1981).
21. D. L. P. McMaster in ACS "Advances in Chemistry," **142** (1975).
22. G. N. Avgeropulos, F. C. Weissert, P. H. Biddison, and G. G. A. Bohm, *Rubber Chem. Technol.*, **49**, 93 (1978).
23. J. J. Elmendorp and R. J. Malcke, "*A Study in Polymer Blending Microrheology*" Unpublished, Sept. 1982.

24. A. P. Plochocki, *Polym. Eng. Sci.*, **23**, 618 (1983).
25. L. A. Utracki, private communication, 1984.
26. R. Simha, *Polym. Eng. Sci.*, **22**, 74 (1982).
27. J. C. Slattery in "Handbook of Multiphase Systems", Gad Hestroni, Ed., p. 1-224-273, McGraw Hill, New York (1982).
28. R. Racin and D. C. Bogue, *J. Rheol.*, **23**, 263 (1980).
29. R. J. Farris, *Trans. Soc. Rheol.* **12**, 281 (1968).
30. A. P. Plochocki, S. S. Dagli, and H. Emmanuilidis, ACS Ann. Meeting, Symposium on Composites, Miami, paper #151 (1985).
31. H. Van Oene, *J. Colloid Interface Sci.*, **40**, 448 (1972) and letter to the author (2/8/78).
32. L. Valsamis, Commun. to the author, May 1, 1985.
33. J. F. Carley, and S. C. Crossan, *Polym. Eng. Sci.*, **21**, 249 (1981).
34. M. Kasajima, A. Suganuma, D. Kunii, and K. Ito, Proceedings Intl. Conf. Polymer Processing, MIT, Cambridge, (1980).
35. K. Min, J. L. White, and J. F. Fellers, *J. Appl. Polymer Sci.*, **29**, 2117 (1984) and in [6b], p. 1327.
36. J. Lynggae-Jorgensen, communique at 56th Annual Meeting Soc. Rheol., VPI, Blacksburg, March 1985.
37. H. P. Grace, *Chem. Eng. Commun.*, **14**, 225 (1982).
38. W. R. Schowalter, C. E. Chaffey, and H. Brenner, *J. Colloid Interf. Sci.*, **26**, 152 (1968).
39. C. S. Martinez and M. C. Williams, *J. Rheol.*, **24**, 421 (1980).
40. J. A. Faucher, *J. Polym. Sci.*, **12-A2**, 2153 (1974).
41. D. Heikens, *Kem. Ind.*, **31**, 165 (1982).
42. J. M. Dealy, "Rheometers for Molten Plastics", Van Nostrand Reinhold, New York (1982).
43. F. N. Cogswell, "Polymer Melt Rheology", Halsted/Wiley, New York (1981).
44. A. P. Plochocki "Melt Rheology of Polyblends", Interlaboratory (IUPAC) Program . . ., Communique at the 56th Annual Meeting, Society of Rheology Blacksburg, February 1985.
45. A. P. Plochocki, *Adv. Polym. Technol.*, **3**, 405 (1984).

DISCUSSION: A. P. PLOCHOCKI

L. A. Utracki: The term "Computer Aided Design" is used in plastics engineering in reference to complex analysis of injection molding or extrusion processes usually leading to designing of a mold, screw, or a die. The use of this term in the context of formulation of polymer blends may be misleading. My second comment concerns the use of several empirical or semi-empirical relations valid in limited ranges of independent variables for the purpose of predicting the blend morphology. This just cannot be generally valid. During the compounding or processing, the ranges of deformation stresses and strains are very large. For example, the power law may be adequate to describe the flow through a die, but it is insufficient to provide a base for development of morphology inside the extruder. Do you have any evidence that the proposed method provides an approximation to morphology of the blend?

A. P. Plochocki: Admittedly, most of the approximations I used are semi-empirical, but they work in many cases. My understanding is that for a well-designed mixer, even a distributive mixer, the designer should at least be able to get a feeling as to the range of operating stresses. I am not saying that there are only shear stresses. Maybe in some mixers the most important type are the extensional stresses. But, at any rate, it seems possible, and I know a number of at least dispersive types of mixers where estimation of the range of stresses is possible. Once we have the range, then we can conceivably think of a range of sizes to be generated. If somebody could develop such a program it would be worth thousands of dollars. But what I have been trying to do is to provide a guiding procedure, which conceivably may be employed. Tadmor (16) expressed the opinion that the field of stresses can be calculated in dispersive mixers. In distributive mixers, in which the cutting of the flow lines takes place, this is possible only for a very simple geometry and low number of passes. Besides, I think that the proposed method may be useful for processors of the polyblends. These people are processing different blends on different pieces of equipment. A method unifying their experience and providing guidance for future operation would be of great use.

J. L. White: I have been considering how to attack this problem. The task which you set up to accomplish is impossibly complex and difficult to achieve. Rheological properties of the blend will depend on the phase morphology which in turn will depend on the mixing condition and thermodynamics, etc. However, what one could do is make a significant start. For example, look at the effect of polydispersity in homopolymers. There is enough experimental data in the literature to make predictions from the molecular weight distribution regarding the shape of the relaxation spectra, the shape of the flow curve, the form of the first normal stress, and to a reasonable extent, what the extrudate swell will be. One could make up a sort of CAD-package with that sort of information, containing those correlations. Using the GPC data as input, one could provide predictive programs for rheological dependencies. This should work, since we have a backlog of data from twenty years of experience. But I think to try to do it now for blends is impossibly difficult. You could start with polydispersity of homopolymers and gradually build up to blends.

A. P. Plochocki: The comment is excellent and was in fact my starting point. It was not a question of ambition which forced me to go into blends, but simply that on a number occasions I had to select blend components and on the basis of these experiences I developed certain procedures presented during my talk. In the 60's there were some attempts to do what Prof. White proposed. However, since then little work seems to have been carried out in this field.

H. P. Schreiber: One of the significant items of progress that we have made in the last twenty years has been the more incisive realization as to the subtlety of the viscoelastic melt and solid

state responses to the micromorphology of the polymeric systems. That micromorphology is critically dependent on shear history, on thermal history, and the interaction thermodynamics of the constituents. Unless those factors are included in parametric or constitutive approaches to predictive programs, you are bound to fall short of your goal. In a sense I am echoing what both Utracki and White were saying before me. You may find a particular system which mixed in a particular tool will yield predicted behavior, but this will be rather an accidental happening, from which one could not extrapolate to other systems, mixers, or processes. Sounds rather depressingly pessimistic, but this is how I feel about it.

D. Froelich: One other way to simplify the problem would be to use a simple mixer in which the stress field would be well-defined.

A. P. Plochocki: I cannot but agree. But we have a dichotomy between science and processing. I am trying to approach the problem of commercial blend preparation and processing which is not waiting for science to catch up with it.

A Structure-Oriented Computer Simulation of the Injection Molding of Viscoelastic Crystalline Polymers Part I: Model with Fountain Flow, Packing, Solidification

P. G. LAFLEUR* *and* M. R. KAMAL**

Department of Chemical Engineering McGill University Montreal, Canada H3A 2A7

A realistic simulation of the injection molding process should be capable of describing moldability parameters, such as pressure drop in the delivery system and cavity and melt-front progression during cavity filling, as well as predicting the characteristics of the final product, such as residual stresses and crystallinity distributions. After a brief review of the existing models for the mathematical modeling of the injection molding process, a new model, that meets the above requirements, is proposed.

INTRODUCTION

Injection molding is a process whereby a solid thermoplastic material is heated until it reaches a state of fluidity. It is then transferred under pressure into a closed hollow space (mold cavity) and then cooled in the mold until it again reaches a solid state, conforming in shape and dimensions to the mold cavity. Injection molding is accomplished in an injection molding machine which consists of two basic components: the injection unit and the clamping unit. The injection unit serves to heat the raw material to a molten state and to transfer it under pressure into the mold, which is held by the clamping unit. The injection molding process can be divided into three major stages: filling, packing, and cooling.

During the filling stage the pressure in the mold rises slowly, as the molten, non-Newtonian, compressible polymer spreads to fill the empty cold cavity. The flow is unsteady, and the polymer starts cooling as soon as it touches the cold walls of the mold. Polymer flow into the cavity does not cease when the melt reaches the outer boundaries. It is desirable to introduce more polymer into the cavity during the packing stage, in order to compensate for shrinkage during cooling. Here, the viscous polymer is compressed and the cavity pressure rises to a peak. Cooling, however, through heat exchange with the solid walls of the mold, causes the molding to solidify. Thus, in the cooling stage, a continuous decrease in cavity pressure is observed.

The physical properties of injection molded articles are markedly affected by the temperature, pressure, and velocity fields that prevail in the mold cavity during the molding cycle. The resin properties, mold geometry, and molding conditions interact to produce the thermomechanical history experienced by the resin, which determines the microstructure distribution and, therefore, the ultimate properties of the molded article. *Figure 1* shows a schematic representation of the important interactions during plastics processing.

In order to quantitatively analyze the behavior of a fluid as it interacts with a processing system, it is necessary to formulate and solve the equations which describe the process. The modeling process involves writing the general conservation (mass, momentum, and energy) equations that a system must obey, along with the constitutive equations which describe the properties of the material being processed. The conservation equations must be solved subject to certain constraints, the boundary conditions, which typically describe factors such as the geometry of the system and forces or deformations imposed at or by the boundaries. Generally, such mathematical formulations are too complex to admit simple analytical solutions and require numerical solutions.

A realistic simulation of the injection molding process should be capable of describing moldability parameters, such as pressure drop in the delivery system and cavity and melt-front progression during cavity filling, as well as predicting the characteristics of the final product, such as residual stresses and crystallinity distributions. After a brief review of the existing models for the mathematical modeling of the injection molding process, a new model, that

* Present address: National Research Council of Canada, Industrial Materials Research Institute, 75 de Mortagne Blvd., Boucherville, Quebec, Canada J4B 6Y4.
** To whom all correspondence should be addressed.

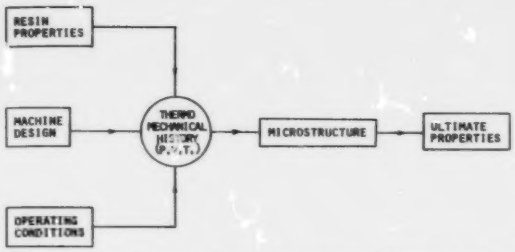

Fig. 1. Components of the plastic processing system.

meets the above requirements, will be proposed. The theoretical predictions will then be compared with experimental results.

GENERAL BACKGROUND

A number of studies have been proposed for the simulation of the injection molding process with varying degrees of complexity, depending on the mathematical formulation of the flow equations, the nature of the constitutive equation and other assumptions relating to material properties, and the technique used for the treatment of the resulting system of equations.

The analysis of mold filling in injection molding, started with the work of Spencer and Gilmore (1) in the early 1950's. One-dimensional rectangular flow was studied by Ballman, *et al.* (2) and Staub (3). More recently, Harry and Parrott (4) considered a one-dimensional quasi steady-state flow analysis coupled with an energy balance equation. Lord and Williams (5, 6) made a significant contribution by considering all the components of a fully one-dimensional non-isothermal flow. A similar model was presented by Thienel and Menges (7) using a different solution technique.

In order to study a more representative one-dimensional flow, a number of analyses were presented in the radial filling of a center-gated disc mold. The model of Kamal and Kenig (8, 9) proposed an integrated mathematical treatment of the filling, packing, and cooling stages of the injection molding cycle. For the analysis of the filling stage, equations of continuity, motion and energy were simplified, taking into account a one-dimensional creeping flow. Similar simulations were done by Berger and Gogos (10), Wu, Huang, and Gogos (11) and Stevenson (12).

An analytical solution for a two-dimensional flow in a rectangular cavity was presented by Kuo and Kamal (13) and Kamal, Kuo, and Doan (14). Ryan and Chung (15) used a conformal mapping technique to solve a similar set of equations. A combined finite element/finite difference method for the solution of arbitrary two-dimensional flow was presented by Hieber and Shen (16). A modified version with an improved numerical scheme for the solution of the pressure field has been provided by Shen (17).

Van Wijngearden and Dijksman (18) analyzed the non-isothermal two-dimensional flow into a rectangular cavity, taking into account the orientation and corrective effect due to the formation of a solid layer at the walls.

None of the above models take into account the viscoelastic nature of polymeric materials, and the fountain effect due to the transient free surface flow in the cavity is neglected. Isayev and Hieber (19) have included a viscoelastic constitutive equation in their analysis in order to calculate the shear and normal stresses in the cavity. Tadmor (20) presented a semi-quantitative model to describe molecular orientation in injection molding, in which the effects of the fountain flow were considered. The flow was analyzed in two parts: a fully developed flow away from the flow front, and a planar stagnation flow in the vicinity of the flow front.

Two numerical analyses of the flow front have been reported. A finite difference scheme based on the Marker-and-cell technique by Huang, *et al.* (21) and a finite-element technique by the Cornell Injection Molding Group (22). These investigations have provided details on the velocity, temperature, and pressure fields of the front.

Relatively little experimental or theoretical work has been carried out with regard to the packing stage. Spencer and Gilmore (1) derived an equation to calculate the maximum pressure in the cavity, combining an equation of state with an empirical relationship for the filling time. In their analysis of semi-circular mold cavities, Kamal and Kenig (8, 9) considered the packing stage as the non-isothermal flow of a compressible material. Kuo and Kamal (13) presented an analytical treatment of the packing stage, using a Spencer-Gilmore equation of state for a two-dimensional flow in a rectangular cavity. A numerical solution of the same basic equations was presented by Chung and Ryan (23), using different boundary conditions from those suggested by Kuo and Kamal (13). Chung and Ide (24) introduced the dependence of viscosity on shear rate in the analysis.

The packing models are based on the analysis of compressible flow. The numerical solution of the resulting equations requires a considerable amount of computer time. In an attempt to simplify the analysis of the packing stage, Deterre (25) decoupled the flow and the compressibility equations. Incompressible flow is used to calculate the pressure field and the change in specific volume is calculated with an equation of state.

The last part of the molding cycle, the cooling stage, is analyzed as a transient cooling problem of a stationary volume of polymer melt. The model of Kamal and Kenig (8, 9), mentioned previously, considered a two-phase process. The heat conduction equations were solved for both the melt and solid with standard boundary conditions. Latent heat effects were taken into consideration. The pressure was calculated using an equation of state. The effect of pressure

drop in the energy equation was introduced by Dietz (26) to establish a cooling model for the heat transfer in a crystallizing polymer under varying pressures.

Dietz, White, and Clark (27) developed a simplified algorithm, which couples the cooling model to a stress relaxation equation to calculate residual stresses. The constitutive equation used was a linear viscoelastic Maxwell model. The same approach was used by Greener and Pearson (28) for a different constitutive equation, the Marruci model (29). Isayev and Hieber (19) analyzed the residual stresses and the birefringence in a rectangular cavity using the viscoelastic model of Leonov (30).

MATHEMATICAL FORMULATION

General Approach

The injection molding process can be fully described in terms of the equations of conservation of mass, momentum, and energy. In the treatment of injection molding, the process will be divided into three stages: filling, packing, and cooling. Each stage of the process is governed by a set of initial and boundary conditions. Solutions usually involve simplifying assumptions, in order to render the treatment practical and to reduce computing costs. Even though the treatment deals with the three stages separately, they are not independent of each other, since the conditions prevailing at the end of one stage become the initial conditions of the next stage.

In order to simplify the geometry of the system, a fan gate mold has been designed, and the analysis is restricted to two-dimensional motions in a plane. Therefore, the hydrodynamic and energy equations will be developed for a two-dimensional Cartesian coordinate system.

The equations of conservation of mass, momentum, and energy for the laminar flow of an incompressible fluid in a two-dimensional coordinate system are the following.

Continuity:

$$\frac{\partial \rho}{\partial t} + \frac{\partial}{\partial x}(\rho u) + \frac{\partial}{\partial z}(\rho w) = 0 \tag{1}$$

Motion:

$$\rho\left(\frac{\partial u}{\partial t} + u\frac{\partial u}{\partial x} + w\frac{\partial u}{\partial z}\right) = -\frac{\partial p}{\partial x} - \left(\frac{\partial \tau_{xx}}{\partial x} + \frac{\partial \tau_{xz}}{\partial z}\right) + \rho g_x \tag{2}$$

$$\rho\left(\frac{\partial w}{\partial t} + u\frac{\partial w}{\partial x} + w\frac{\partial w}{\partial z}\right) = -\frac{\partial p}{\partial z} - \left(\frac{\partial \tau_{xz}}{\partial x} + \frac{\partial \tau_{zz}}{\partial z}\right) + \rho g_z \tag{3}$$

Energy:

$$\rho C_p\left(\frac{\partial T}{\partial t} + u\frac{\partial T}{\partial x} + w\frac{\partial T}{\partial Z}\right) = -\left(\frac{\partial q_x}{\partial x} + \frac{\partial q_z}{\partial z}\right) - \left(\tau_{xx}\frac{\partial u}{\partial x} + \tau_{zz}\frac{\partial w}{\partial z}\right) - \tau_{xz}\left(\frac{\partial u}{\partial z} + \frac{\partial w}{\partial x}\right) + \left(\frac{\partial \ln v}{\partial \ln T}\right)_p\left(\frac{\partial p}{\partial t} + u\frac{\partial p}{\partial x} + w\frac{\partial p}{\partial z}\right) \tag{4}$$

A two-dimensional representation of the problem was employed in order to take into consideration the "fountain flow", which occurs near the front of the advancing melt. This effect is considered to be important in injection molding.

Constitutive Equations

The equations of continuity, motion, and energy are expressed in terms of the stress tensor. In order to use these equations to determine velocity distributions, it is necessary to express the various stresses in terms of velocity gradients and fluid properties, using a rheological constitutive equation. Unfortunately, no constitutive equation that can represent the full range of flow and deformation encountered in the injection molding process is available. Thus, one must learn the art of rheological compromise. It is necessary to examine the flow kinematics of the injection molding process and judge which elements are most crucial to the predictive specifications of the model. In order to predict the development of normal stresses and transient phenomena, a viscoelastic model is essential. In the injection molding process, polymer melt elements are subjected to both shear and elongational stresses. Shear stresses are generally predominant; however, elongational stresses are significant whenever unsteady flow, where the polymer chains are subjected to accelerations and decelerations, takes place. Because of the predominance of the shear stresses during the filling stage, inelastic models are sufficiently accurate when pressure drop or flow rate relations are needed. However, to predict microstructure and orientation distributions, the complete stress field must be calculated. In the present work, the White-Metzner (31) modification of the Maxwell model, utilizing the Oldroyd derivative in contravariant form, has been employed.

$$\overset{s}{\tau} + \lambda(II)\frac{d\overset{s}{\tau}}{dt} = \eta(II)\,\dot{\Delta} \tag{5}$$

where both η and λ are functions of the second invariant of the flow field. The usual assumption is to relate λ to η through a modulus G so that

$$\lambda = \eta/G \tag{6}$$

The interesting feature of this model is the

prediction of viscosity as a function of the second invariant in steady shear flow. For the injection molding process, where the shear rates are relatively high, the power-law relationship has been used in the present work to calculate the shear dependent viscosity used in the White-Metzner model. This relationship can be written as follows:

$$\eta = K\,[\mathrm{II}/2]^{n-1/2} \tag{7}$$

The same approach was suggested by Middleman (32) and used by Deiber and Schowalter (33) in the modeling of the flow of viscoelastic fluids through porous media.

For a two-dimensional flow, the independent components of stress for the White-Metzner model are:

$$\tau_{xx} + \frac{\eta}{G}\left[\frac{\partial \tau_{xx}}{\partial t} + u\frac{\partial \tau_{xx}}{\partial x} + w\frac{\partial \tau_{xx}}{\partial z} - 2\frac{\partial u}{\partial x}\tau_{xx} - 2\frac{\partial u}{\partial z}\tau_{xz}\right] = 2\eta\frac{\partial u}{\partial x} \tag{8}$$

$$\tau_{zz} + \frac{\eta}{G}\left[\frac{\partial \tau_{zz}}{\partial t} + u\frac{\partial \tau_{zz}}{\partial x} + w\frac{\partial \tau_{zz}}{\partial z} - 2\frac{\partial w}{\partial x}\tau_{xz} - 2\frac{\partial w}{\partial Z}\tau_{zz}\right] = 2\eta\frac{\partial w}{\partial z} \tag{9}$$

$$\tau_{xz} + \frac{\eta}{G}\left[\frac{\partial \tau_{xz}}{\partial t} + u\frac{\partial \tau_{xz}}{\partial x} + w\frac{\partial \tau_{xz}}{\partial z} - \frac{\partial u}{\partial z}\tau_{zz} - \frac{\partial w}{\partial x}\tau_{xx}\right] = \eta\left[\frac{\partial u}{\partial z} + \frac{\partial w}{\partial x}\right] \tag{10}$$

The second invariant of the rate of deformation tensor is

$$\dot{\Delta}:\dot{\Delta} = 4\left(\frac{\partial u}{\partial x}\right)^2 + 2\left(\frac{\partial u}{\partial z} + \frac{\partial w}{\partial x}\right)^2 + 4\left(\frac{\partial w}{\partial z}\right)^2 \tag{11}$$

The equations of mass, momentum, and energy coupled with the constitutive equations can be used to describe the unsteady flow of a non-isothermal polymer melt. However, in applying the energy equation to a crystallizing polymer, it is necessary to recognize the presence of two phases in the system: a melt and a solid phase. Therefore, a general formulation involves the application of the energy equation to both the solid and melt phases while allowing the thermal properties to vary continuously with temperature and pressure. Thus, following Dussinberre (34), no distinctions are made between the melt and solid phases, except in the differences that exist between their properties.

Thermal Effects

The functional variations of thermal conductivity and density with temperature and pressure can be obtained experimentally. The specific heat, C_p, is a function of the experimental conditions at which it is evaluated, especially the cooling rate. For semi-crystalline polymers, C_p increases up to the region of the melting point. In practice, where there is a melting range, C_p exhibits a sharp maximum and decreases to values that are lower than those just below the melting range. The area above the heating baseline, in the region of the melting range, is equal to the product of the crystalline volume fraction and the heat of fusion.

Assuming that the specific heats of the melt and the solid are independent of the cooling process, within the solidification range, the latent heat of solidification is included in the specific heat as follows (35):

$$C_p = C_p' + \frac{d\lambda}{dT} = C_p' + \lambda_{pc}\frac{dx}{dT} \tag{12}$$

where λ_{pc} is the heat of fusion of the pure crystal, X is the degree of crystallinity, as a weight fraction, and C_p' is the baseline heat capacity. The term λ_{pc} reflects the changes in sample enthalpy as a result of changes in crystallinity. Thus, it is essential to follow the development of crystallinity in order to calculate the specific heat at any desired temperature. Therefore, a realistic heat transfer model should include a crystallization kinetics equation to follow the development of crystallinity.

The change in crystallinity, as a function of time during isothermal crystallization, has generally been described by the Avrami equation (36) as:

$$X_R(t) = [1 - e^{-Z_c t^{n'}}] \tag{13}$$

where X_R is the weight percent crystallinity at time, t, n' is an integer depending on the shape of the growing crystallite, and Z_c is a rate constant depending on the nucleation and growth rates at a given temperature.

Crystallization during polymer processing occurs non-isothermally. Therefore, non-isothermal crystallization should be studied in terms of polymer characteristics and cooling conditions, to estimate the crystallinity of the polymer. The influence of the level of stress on the crystallization process is neglected, due to the lack of models regarding stress effects on crystallization kinetics. The development of crystallinity with time will be followed by employing the equation of Nakamura, *et al.* (37), based on the Avrami equation, which was modified to apply to the non-isothermal process under certain assumptions. The fundamental equation was written on the basis of iso-kinetic conditions in the following form.

$$X_R(T) = [1 - \mathrm{EXP}\{\int K_A(T(\lambda))d\lambda)^{n'}\}] \tag{14}$$

where $X_R(t)$ is the degree of phase transformation at time, t, $K_A(T)$ is a parameter related to the crystallization rate constant of the Avrami equation, $Z(T)$, by the relation $K(T) = [Z(T)^{1/n'}]$, and n' is the Avrami exponent. From this model, non-isothermal crystallization can be

analyzed in terms of data from isothermal crystallization.

COMPUTATION

Computational Method

The filling stage of the injection molding process is represented by a free surface unsteady flow of a hot non-Newtonian compressible melt into an empty cold cavity, which is held at a temperature below the solidification temperature of the polymer. Polymer flow into the cavity does not cease when the melt reaches the outer boundaries of the cavity. An additional amount of material is introduced into the cavity during the packing stage. After filling and packing are completed, cooling of the plastic continues by virtue of the lower temperature of the mold. Cooling without flow continues until the plastic has reached a sufficient level of solidification. In view of the above, injection molding involves unsteady-state flow problems coupled with heat transfer, heat transfer being present during the three stages of the process. The equations of conservation of mass, momentum, and energy, described previously, with the appropriate simplifying assumptions can fully represent each stage of the injection molding process, forming a system of multiple, simultaneous, coupled, non-linear partial differential equations which can be solved by a numerical technique.

There are two powerful numerical methods for the solution of systems of partial differential equations: finite-differences and finite-elements. In this model a finite-difference method was selected for two reasons. Firstly, whenever straight wall boundaries are involved (simple geometry), the finite-difference is simple and straightforward in principle. Secondly, the incorporation into the model of a viscoelastic constitutive equation and a kinetic crystallization equation contribute to increase the degree of complexity.

One of the best known finite-difference techniques to solve free surface transient problems is the Marker-and-Cell (M.A.C.) method. This technique has been developed by researchers at Los Alamos Scientific Laboratory (38). A good review of the method was presented by Browne (39), and several publications using the M.A.C. technique for viscous flows are reported in the literature (40–42). The technique is outlined as follows. The region of interest is divided into cells, and particles are placed in those cells, which initially contain fluid. Initial velocities, pressures, and temperatures are specified for each fluid cell, together with appropriate boundary conditions. Finite-difference forms of continuity, momentum, and energy equations are solved iteratively to obtain, for some small interval of time later, new values of velocity, pressure, and temperature. Each particle is then moved by allotting to it an average of the velocities in surrounding cells and then multiplying this velocity by the time interval to obtain the displacement in both magnitude and direction. All cells are then examined and reflagged as full, empty or surface, so that a new configuration of the fluid (shape of the melt front) is determined. This process is repeated as often as is necessary to obtain the required flow information.

The set-up of the M.A.C. method comprises three main parts. The first part is to submit general information, such as the properties of the fluid, the number of cells, time step, marker particles density, and other parameters pertaining to the problem. The second part concerns the set-up of the cells. The input information concerning the system boundaries is used to flag all the cells in the system. If there are no particles in the system, all interior cells are flagged as Empty cells (EMP cells); if some of the cells contain particles, they are flagged as full or surface cells (FUL, SUR cells). The third part is to set-up the marker particles. The particles that will represent the fluid flow are created, and the coordinates of the particles are stored for future reference.

After this preliminary organization, one is ready to proceed to the first time cycle. The fluid flow is advanced through a series of time cycles, each of finite length Δt. Each time cycle consists of recalling the information from the previous cycle, reflagging all the cells, calculating the new variables, and moving the marker particles accordingly. The process is repeated until the flow front reaches the end of the cavity. *Figure 2* gives an outline of the computational procedure of the M.A.C. technique. Representation of the flow field in the M.A.C. method of calculation employs two coordinate systems. The primary one covers the entire domain of interest with a rectangular grid of cells, each of dimensions Δx, Δz. The field variable values describing the flow field are directly associated with these cells. Their points of definition, relative to a cell, are shown in *Fig. 3*. In addition to the primary coordinate system of finite-difference cells, there is a coordinate system of

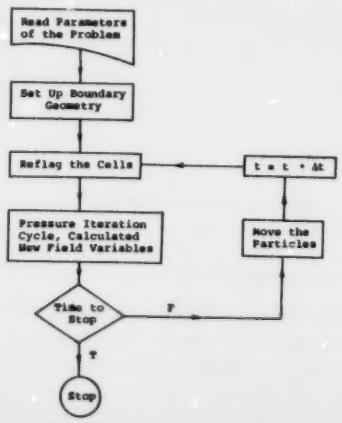

Fig. 2. Outline of the computational procedure.

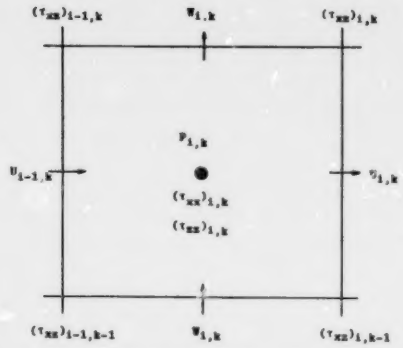

Fig. 3. Field variables and their points of definition.

particles, whose motions describe the trajectories of fluid elements. The particles delineate the fluid surface locations and determine the configuration of each cell as an empty, full or surface cell. The cell network is surrounded by a frame of boundary cells (BUN); these may also contain particles, in which case they are either inflow or outflow boundaries or they may be empty, representing rigid walls that may be free-slip or no slip.

The solution of the finite-difference approximations is carried out in the region of the rectangular mesh containing marker particles. The method used to solve the finite-difference equations for each time cycle was instigated by Chorin (43) and elaborated by Viecelli (44). The method involves a simultaneous iteration of pressure and velocity components. With the position of the variables given as described in *Fig. 3*, it is possible to express the system of equations in finite-difference form, using central difference formulae in a semi-implicit way. The method is semi-implicit because all the nonlinear terms in the momentum and stress equations are written in an explicit form. To summarize the difference equations we have:

Continuity:

$$f(\bar{u}, \bar{w}) = 0 \tag{15}$$

Momentum:

$$\begin{aligned} \bar{u} &= f(u, w, \bar{\tau}_{xx}, \bar{\tau}_{xz}, \bar{P}) \\ \bar{w} &= f(u, w, \bar{\tau}_{zz}, \bar{\tau}_{xz}, \bar{P}) \end{aligned} \tag{16}$$

Constitutive Equation:

$$\begin{aligned} \bar{\tau}_{xx} &= f(\bar{u}, \bar{w}, \tau_{xx}, \tau_{xz}) \\ \bar{\tau}_{zz} &= f(\bar{u}, \bar{w}, \tau_{zz}, \tau_{xz}) \\ \bar{\tau}_{xz} &= f(\bar{u}, \bar{w}, \tau_{xx}, \tau_{zz}, \tau_{xz}) \end{aligned} \tag{17}$$

where the variables with bars are the present time variables, while the others are past time variables.

If the stresses in the momentum equations are replaced by their expressions as functions of the velocities, (*Eqs 8, 9,* and *10*) then:

Continuity:

$$f(\bar{u}, \bar{w}) = 0 \tag{18}$$

Momentum:

$$\begin{aligned} \bar{u} &= f(\bar{u}, \bar{w}, u, w, \tau_{xx}, \tau_{zz}, \tau_{xz}, \bar{P}) \\ \bar{w} &= f(\bar{u}, \bar{w}, u, w, \tau_{xx}, \tau_{zz}, \tau_{xz}, \bar{P}) \end{aligned} \tag{19}$$

The momentum equations form a system of 2N unknowns and 2N equations over the entire domain. The resulting linear system of equations can be solved by any of the conventional techniques.

Figure 4 shows the outline of the pressure cycle iteration. For each cell, the velocity divergence $D_{i,k}$ is calculated using the continuity equation. If the magnitude of $D_{i,k}$ is less than some prescribed small value, ϵ, no change in the cell velocity is necessary. However, if the magnitude of $D_{i,k}$ is larger than ϵ, then the pressure is changed and the new pressure field is used in conjunction with the momentum equations to calculate a new field of velocity.

Analysis of the Filling Stage

The filling stage is concerned with the unsteady flow of a hot non-Newtonian polymer melt into a cold cavity. The analysis has to consider unsteady-state free surface flow coupled with transient cooling. In order to describe the filling of the mold cavity mathematically, one starts from the basic equations of change (*Eqs 1* to *3*), where some terms are neglected according to a set of simplifying assumptions. The assumptions for the filling stage are the following: (a) the fluid is assumed to be viscoelastic and incompressible, (b) body forces are assumed negligible, (c) gradients in the Y-direction are negligible leading to a two-dimensional flow, and (d) the terms involving pressure in the energy equation are neglected.

The rheological viscoelastic equation used is the White-Metzner modification of the contravariant Maxwell model described in *General Approach*. Crystallization is calculated with Nakamura's non-isothermal equation. The equations of change are rewritten in terms of dimensionless variables, obtained by selecting

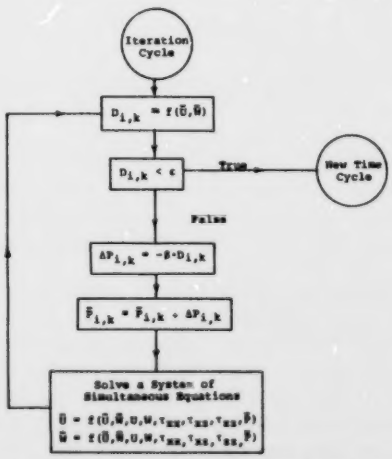

Fig. 4. Outline of the pressure cycle iteration.

a set of characteristic parameters of the system (see *Nomenclature*). All the variables used in the remaining sections are dimensionless variables.

With the above assumptions and considerations, the equations of change are reduced to the following forms:

Continuity:

$$\frac{\partial u}{\partial x} + \frac{\partial w}{\partial z} = 0 \tag{20}$$

Momentum for x and z components:

$$\frac{\partial u}{\partial t} + \frac{\partial (u)^2}{\partial x} + \frac{\partial (uw)}{\partial z} = -\frac{\partial P}{\partial x} - \frac{1}{Re}\left[\frac{\partial \tau_{xx}}{\partial x} + \frac{\partial \tau_{xz}}{\partial z}\right] \tag{21}$$

$$\frac{\partial u}{\partial t} + \frac{\partial (uw)}{\partial x} + \frac{\partial (w^2)}{\partial z} = -\frac{\partial P}{\partial z} - \frac{1}{Re}\left[\frac{\partial \tau_{xz}}{\partial x} + \frac{\partial \tau_{zz}}{\partial z}\right] \tag{22}$$

Energy Equation:

$$\frac{\partial T}{\partial t} + u\left(\frac{\partial T}{\partial x}\right) + w\left(\frac{\partial T}{\partial z}\right) = \frac{1}{RePr}\left[\frac{\partial^2 T}{\partial x^2} + \frac{\partial^2 T}{\partial z^2}\right] + \frac{(\partial k/\partial T)(T_1 - T_0)}{kRePr}\left[\left(\frac{\partial T}{\partial x}\right)^2 + \left(\frac{\partial T}{\partial z}\right)^2\right] - \frac{Br}{RePr}\left[\tau_{xx}\frac{\partial u}{\partial x} + \tau_{zz}\frac{\partial w}{\partial z} + \tau_{xz}\frac{\partial u}{\partial z} + \tau_{xz}\frac{\partial w}{\partial x}\right] \tag{23}$$

The corresponding dimensionless forms of the components of the White-Metzner equation are the following:

$$\tau_{xx} + W_s\frac{\eta}{G}\left[\frac{\partial \tau_{xx}}{\partial t} + u\frac{\partial \tau_{xx}}{\partial x} + w\frac{\partial \tau_{xx}}{\partial z} - 2\frac{\partial u}{\partial x}\tau_{xx} - 2\frac{\partial u}{\partial z}\tau_{xz}\right] = 2\frac{\partial u}{\partial x} \tag{24}$$

$$\tau_{zz} + W_s\frac{\eta}{G}\left[\frac{\partial \tau_{zz}}{\partial t} + u\frac{\partial \tau_{zz}}{\partial x} + w\frac{\partial \tau_{zz}}{\partial z} - 2\frac{\partial w}{\partial x}\tau_{xz} - 2\frac{\partial w}{\partial z}\tau_{zz}\right] = 2\frac{\partial w}{\partial z} \tag{25}$$

$$\tau_{xz} + W_s\frac{\eta}{G}\left[\frac{\partial \tau_{xz}}{\partial t} + u\frac{\partial \tau_{xz}}{\partial x} + w\frac{\partial \tau_{xz}}{\partial z} - \frac{\partial u}{\partial z}\tau_{zz} - \frac{\partial w}{\partial x}\tau_{xx}\right] = \left(\frac{\partial u}{\partial z} + \frac{\partial w}{\partial x}\right) \tag{26}$$

The Weissenberg Number, W_s, is defined in the *Nomenclature* section below.

A finite-difference representation of the above equations was written, using the field variables as described previously. However, these equations are not defined at the boundary of the system. In order to solve the system of equations to calculate the field variables everywhere on the mesh system, the variables must be defined at the boundaries. The type of boundary conditions applied depends on the type of boundary under consideration. According to the mold geometry involved in this study, we describe four kinds of boundaries, which are identified in *Fig. 5*.

(1) The centerline is a slip-free boundary which has a symmetric character. The transverse velocity component is zero at the centerline, and both the pressure and longitudinal velocity gradients in the transverse direction are zero at this line. The temperature distribution is symmetrical around $Z = 0$.

(2) At the top and the end of the mold, a no-slip rigid boundary is applied. The velocity components, both normal and tangential to the wall, vanish at the solid wall. The temperature is calculated using heat flux at the wall related to the difference between temperature at the interface and that in the fluid.

(3) The inlet velocity profile at the entrance of the mold is assumed to be that of steady, one-dimensional, fully-developed flow of a Power-Law fluid between two flat plates. The melt temperature at the entrance to the cavity is considered to be uniform.

(4) The physical principle on which the free surface boundary conditions are based is the requirement that no momentum flux may cross the free surface of the fluid. The free melt surface condition may then be expressed by (45):

$$\tau_{ij} \cdot n_j = P_e \tag{27}$$

where P_e is the external pressure applied to the fluid surface, assuming zero stress on the air side; n is the unit normal to the surface, and $\bar{\bar{\tau}}$ is the stress tensor for the incompressible fluid.

The above set of equations, coupled with the boundary conditions, was solved using the M.A.C. technique described earlier. The iteration scheme, based on a pressure iteration, was first solved for a steady-state flow problem of a Newtonian and Power-Law fluid, to evaluate convergence capabilities. The flow studied was

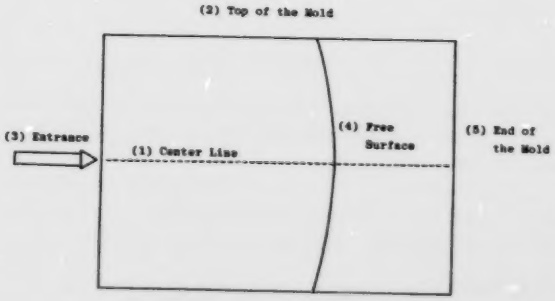

Fig. 5. Boundaries of the system.

an isothermal parallel plate pressure flow for which an analytical solution is available. The maximum relative error occurs at the point close to the wall because of the no-slip boundary condition at the wall. For a dimensionless increment of 0.1 in the thickness direction, the maximum error was 2.5 and 4.1 percent for the Newtonian and Power-Law fluids, respectively.

Analysis of the Packing Stage

After filling is completed, additional material is packed into the cavity to compensate for shrinkage during the cooling process. The increase of the density in the cavity is responsible for the rapid increase of the pressure during the packing stage. The same approach as in the case of the filling stage is employed for the analysis of the packing stage. The following assumptions are made for the mathematical analysis of the packing stage.

The conditions prevailing at the end of the filling stage are used as initial conditions for the analysis of the packing stage. After the cavity is filled, there is no more free surface flow, and the component of velocity and the pressure variations in the thickness direction are considered to be negligible. The fluid is assumed to be viscoelastic and compressible; body forces are assumed negligible. The effect of the pressure drop in the energy equation is neglected, and Nakamura's crystallization equation is used to calculate the crystallinity. Because of the important role of the density in the numerical calculations, experimental data obtained directly from the P-V-T diagram were used. Applying these assumptions to simplify the equations of change for a compressible fluid, *Eqs 1, 2,* and *3* reduce to the following dimensionless forms:

Continuity:

$$\frac{\partial \rho}{\partial t} + \frac{\partial}{\partial x}(\rho u) = 0 \tag{28}$$

Momentum:

$$\frac{\partial}{\partial t}(\rho u) + \frac{\partial}{\partial x}(\rho u^2) = -\frac{\partial P}{\partial x} - \left(\frac{\partial \tau_{xx}}{\partial x} + \frac{\partial \tau_{xz}}{\partial z}\right) \tag{29}$$

Energy:

$$\frac{\partial T}{\partial t} + u\frac{\partial T}{\partial x} = \frac{1}{RePr}\left[\frac{\partial^2 T}{\partial x^2} + \frac{\partial^2 T}{\partial z^2}\right] + \frac{(dk/dT)(T_1 - T_0)}{k\,Re\,Pr}\left[\left(\frac{\partial T}{\partial x}\right)^2 + \left(\frac{\partial T}{\partial z}\right)^{d2}\right] - \frac{Br}{RePe}\left[\tau_{xx}\frac{\partial u}{\partial x} + \tau_{xz}\frac{\partial u}{\partial z}\right] \tag{30}$$

The corresponding dimensionless forms of the components of the White-Metzner equation are the following:

$$\tau_{xx} + W_s\frac{\eta}{G}\left[\frac{\partial \tau_{xx}}{\partial t} + u\frac{\partial \tau_{xx}}{\partial x} - 2\frac{\partial u}{\partial x}\tau_{xx} - 2\frac{\partial u}{\partial z}\tau_{xz}\right] = 2\eta\frac{\partial u}{\partial x} \tag{31}$$

$$\tau_{xz} + W_s\frac{\eta}{G}\left[\frac{\partial \tau_{xz}}{\partial t} + u\frac{\partial \tau_{xx}}{\partial x}\right] = \eta\left[\frac{\partial u}{\partial z} + \frac{\partial w}{\partial x}\right] \tag{32}$$

The set of partial differential equations was solved using the M.A.C. technique described previously. The boundary conditions defined for the filling stage at the top and the end of the mold and at the centerline are applicable to the packing stage. The free surface boundary is no longer present, and the entrance boundary has to be redefined.

For the filling stage, the fluid was assumed to be incompressible. Thus, the volumetric flow rate measured in the barrel was converted to a mass flow rate and used at the entrance of the mold as a boundary condition. After the filling of the cavity is completed, the pressure will build up in the delivery channels and the cavity, causing compression of the melt throughout the system. The mass flow rate will vary from point to point. Therefore, the flow rate calculated in the barrel cannot be used as a boundary condition at the entrance of the cavity. The experimental pressure profile measured at the entrance of the cavity will be used directly to calculate the inlet velocity profile.

The set of partial differential equations, coupled with the boundary conditions, was solved using the M.A.C. technique. Because of the important role of the density in the numerical calculations, experimental data obtained directly from the P-V-T diagram were used. The same stability criterion as the one employed in the analysis of the filling stage is applicable, requiring the use of an implicit finite-difference scheme.

Analysis of the Cooling Stage

After filling and packing are completed, cooling of the plastic continues by virtue of the lower temperature of the mold. Cooling without flow continues until the plastic has reached a sufficient level of solidification. The bulk of the polymer cools very little during the filling and packing stages, but next to the molded surfaces, there will be a rapidly cooling thin skin of polymer. This produces a skin which is highly oriented. The mass of the molding starts cooling during the cooling stage, and, once it becomes frozen, no further orientation can occur. Relaxation of the stresses in the viscous melt elements requires longer than solidification, and, hence, polymer chains become frozen in their oriented configuration.

No flow takes place during the cooling stage, considerably reducing the complexity of the mathematical treatment. The equations of momentum and continuity are not required, and the energy equation is simplified by the absence of generation by viscous heating. Neglecting the effect of the pressure drop, the energy equation takes the following form:

$$\frac{\partial T}{\partial t} = \frac{1}{RePr}\left[\frac{\partial^2 T}{\partial x^2} + \frac{\partial^2 T}{\partial z^2}\right] + \frac{(dk/dT)(T_1 - T_0)}{k\,Re\,Pr}\left[\left(\frac{\partial T}{\partial x}\right)^2 + \left(\frac{\partial T}{\partial z}\right)^2\right] \quad (33)$$

Crystallization is treated using Nakamura's equation, in the same way as for the filling and packing stages. Since no flow takes place during the solidification stage, the usual significance of the dimensionless numbers *Re* and *Pr* does not apply.

The White-Metzner equation in this case is simplified to a simple Maxwellian relaxation mode. Using the Matsui-Bogue (46) theory of non-isothermal large deformation viscoelastic fluid behavior, the stresses will relax according to:

$$\tau_{xx}(t, x, z) = \tau_{xx}(O, x, z)\mathrm{EXP}\left[-\frac{1}{\lambda_{ON}}\int_o^t \frac{dt'}{a_t(T(t'))}\right] \quad (34)$$

$$\tau_{xz}(t, x, z) = \tau_{xz}(O, x, z)\mathrm{EXP}\left[-\frac{1}{\lambda_{OS}}\int_o^t \frac{dt'}{a_t(T(t'))}\right] \quad (35)$$

where λ_O is the relaxation time at zero deformation rate and at the reference temperature, and a_T is a temperature-, and, therefore, time-dependent shift factor. These two parameters were obtained experimentally, using a combination of a Rheometrics Mechanical Spectrometer and a capillary viscometer. Thus, the stress field obtained at the end of the packing stage will be relaxed according to these Maxwell equations, with a temperature shift factor obtained from the solution of the energy equation. Subscripts *S* and *N* refer to shear and normal stresses, respectively. The use of λ_0 is justified since relaxation take place at zero deformation rate during solidification.

The restriction on the time step of integration during the filling and packing stages resulting from the low Reynolds number is not applicable in the case of the cooling stage. Therefore, an explicit finite-difference scheme can be used. Because of the coupling of the energy and crystallization kinetics equations, no analytical solution can be obtained for purposes of comparison with the numerical model. In an attempt to verify the cooling and crystallization models, a simple static cooling experiment was designed. A comparison between experimental and calculated crystallization and temperature profiles was reported elsewhere (47).

Thermal boundary conditions only are required for the analysis of the cooling stage. No flux is assumed across the centerline and the entrance of the mold. At the top and end of the cavity, the temperature is considered to be the temperature of the mold.

MICROSTRUCTURE PREDICTIONS

The model presented in the previous sections can be used to evaluate the thermo-mechanical history of the resin during various stages of the injection molding process. The temperature, pressure, velocity, and stress fields experienced during the molding cycle determine the microstructure distribution and, therefore, the ultimate properties of the molded article. The model presented so far can predict the thermo-mechanical history of the resin during the processing operation. However, to predict the ultimate properties of the molded article, it is necessary to develop product quality models that relate the thermo-mechanical history to the development of microstructure, mainly crystallinity, morphology, and orientation in the molded parts, and ultimately relate the final properties of the molded articles to the distribution of microstructure.

The kinetic equation of crystallization incorporated into the heat transfer model makes it possible to follow the development of crystallinity during the three stages of the process.

Birefringence is a measure of the total molecular orientation of a system. It is defined as the difference between the principal refractive indices parallel and perpendicular to the stretch direction for a uniaxially oriented specimen. In a partially crystalline material, the velocity of light in the crystalline region will be different from that in the amorphous region. By assuming a two-phase model for a uniaxially oriented crystalline polymer, the measured birefringence is defined as (48).

$$\Delta_T n = X_c f_{CR}\Delta_C^0 + (1 - X_c) f_{AM}\Delta_{AM}^0 + \Delta_f \quad (36)$$

where X_c is the degree of crystallinity; f_{CR} and f_{AM} are the orientation functions for the crystalline and amorphous phases, respectively; Δ_{CR}^0 and Δ_{AM}^0 are the intrinsic birefringence values of the perfectly oriented crystalline and amorphous phases, respectively; Δ_f is the form birefringence.

From the crystallization kinetics model and the deformation during the flow, there is no dependable method that can be used to quantitatively determine the orientation functions of the crystalline regions. Thus, the contribution of the crystalline phase to the total birefringence cannot be estimated. On the other hand, it is possible to estimate the contribution of the amorphous phase to sample birefringence.

The orientation of the amorphous phase of the polymer can be predicted by a knowledge of

the stress field prior to solidification and by the application of stress-optical laws, whereby the birefringence can be related to the stress field through the stress optical coefficient (49).

$$n_i - n_j = C(\tau_i - \tau_j) \tag{37}$$

The principal birefringences are proportional to the differences in principal stresses, where the constant of proportionality, C, is called the stress optical coefficient. For a simple shear flow, we obtain (50):

$$\Delta n = C[(\tau_{11} - \tau_{22})^2 + 4\tau_{12}^2]^{1/2} \tag{38}$$

By coupling data regarding the time dependent stress field and the solid layer progression, it is possible to determine the frozen stresses as a function of the gapwise position. Then, *Eq 38* can be used to determine the gapwise distribution of amorphous birefringence and the amorphous orientation function can be calculated from *Eq 36*:

$$f_{am} = \Delta n/\Delta_{aM}^0 \tag{39}$$

The calculated distributions of crystallinity and orientation were used in conjunction with a two-parameter model developed by Seferis and Samuels (51) describing the mechanical properties of the oriented samples simply from a knowledge of the volume fraction of crystals and the orientation of the phases within the sample. This model was used by Moy and Kamal (52) to estimate the Young's modulus of injection molded pieces using experimental values of crystallinity and orientation functions. The equation is the following:

$$1/E_s = X_c A_{CR}(1 - f_{CR}) + (1 - X_c)A_{Am}(1 - f_{AM}) \tag{40}$$

where A_{CR} and A_{AM} are the intrinsic moduli for the crystalline and amorphous phases, respectively; and X_c is the volume fraction of the crystalline phase. An interesting finding from the work of Moy and Kamal (52) is that the noncrystalline region emerges as the controlling phase in determining the tensile modulus distribution in polyethylene injection moldings. Therefore, it is possible, as a first approximation, to estimate the tensile modulus from the distribution of amorphous orientation functions and crystallinity.

CONCLUSION

The model described in this paper has been designed to predict the thermo-mechanical history during the various stages of the injection molding process. The development of crystallinity and orientation is also considered in order to estimate the tensile modulus of the molded article.

In the second paper of this series the predictions of the model will be compared to experimental data.

ACKNOWLEDGMENT

The authors would like to acknowledge financial support from the Natural Science and Engineering Research Council of Canada, the Ministere de l'Education of the Government of Quebec, and McGill University.

REFERENCES

1. R. S. Spencer and G. D. Gilmore, *J. Coll. Sci.*, **6**, 118, (1958).
2. R. L. Ballman, T. Shusman, and H. L. Toor, *Ind. Eng Chem.*, **51**, 847, (1959).
3. R. B. Staub, *SPE J.*, 429, (April 1960).
4. D. H. Harry and R. G. Parrott, *Polym. Eng. Sci.*, **10**, 209, (1970).
5. G. Williams and H. A. Lord, *Polym. Eng. Sci.*, **15**, 553, (1975).
6. H. A. Lord and G. Williams, *Polym. Eng. Sci.*, **15**, 569, (1975).
7. P. Thienel and G. Menges, *Polym. Eng. Sci.*, **18**, 314, (1978).
8. M. R. Kamal and S. Kenig, *Polym. Eng. Sci.* **12**, 295, (1972).
9. M. R. Kamal and S. Kenig, *Polym. Eng. Sci.*, **12**, 302, (1972).
10. J. L. Berger and C. G. Gogos, *Polym. Eng. Sci.*, **13**, 102, (1973).
11. P. C. Wu, C. F. Huang, and C. G. Gogos, *Polym. Eng. Sci.*, **14**, 223 (1974).
12. J. F. Stevenson, *Polym. Eng. Sci.*, **18**, 577, (1978).
13. Y. Kuo and M. R. Kamal, *AIChE J.* **22**, 661, (1976).
14. M. R. Kamal, Y. Kuo, and P. H. Doan, *Polym. Eng. Sci.*, **15**, 863, (1975).
15. M. E. Ryan and T. S. Chung, *Polym. Eng. Sci.*, **20**, 642, (1980).
16. C. A. Hieber and S. F. Shen, *J. Non-Newt. Fluid Mech.*, **7**, 1, (1980).
17. S. F. Shen, *Int. J. Numerical Meth. Fluids*, **4**, 171, (1984).
18. H. Van Wijngaarden, J. F. Dijksman, and P. Wesseling, *J. Non-Newt. Fluid Mech.*, **11**, 175, (1982).
19. A. I. Isayev and C. A. Hieber, *Rheolog. Acta*, **19**, 168, (1980).
20. Z. Tadmor, *J. Appl. Polym. Sci.*, **18**, 1753, (1974).
21. C. F. Huang, C. G. Gogos, and L. Schmidt, 71st Annual AIChE Meeting, Paper 94, Nov. 1978.
22. K. K. Wang, *et al.*, Injection Molding Project, College of Engineering, Cornell University, Progress Report 6, Sept. 1979.
23. T. S. Chung and M. E. Ryan, *Polym. Eng. Sci.*, **21**, 271, (1981).
24. T. S. Chung and Y. Ide, *J. Appl. Polym. Sci.*, **28**, 2999, (1983).
25. R. Deterre, Thèse de Docteur Ingenieur, Universite Louis Pasteur de Strasbourg, Dec. 1984.
26. W. Dietz, *Polym. Eng. Sci.*, **13**, 1030, (1978).
27. W. Dietz, J. L. White, and E. S. Clark, *Polym. Eng. Sci.*, **18**, 53, (1978).
28. J. Greener and G. H. Pearson, *J. Rheol.*, **27**, 115, (1983).
29. G. Marruci, T. Titomanlio, and G. C. Santi, *Rheol. Acta*, **12**, 269, (1973).
30. A. I. Leonov, *Rheolog. Acta*, **15**, 85, (1976).
31. J. L. White and A. B. Metzner, *J. Appl. Polym. Sci.*, **7**, 1867, (1963).
32. S. Middleman, "Fundamentals of Polymer Processing", McGraw-Hill, New York, (1979).
33. J. A. Deiber and W. R. Schowalter, *AIChE J.*, **27**, 912, (1981).
34. G. M. Dussinberre, "Numerical Analysis of Heat Flow", McGraw-Hill, New York, (1949).
35. H. S. Carslaw and J. C. Jaeger, "Conduction of Heat in Solids", Clarendon Press, Oxford, (1959).
36. M. Avrami, *J. Chem. Physics*, **7**, 1103, (1939).

37. K. Nakamura, T. Watanabe, K. Katayama, and T. Amano, *J. Appl. Polym. Sci.*, **16**, 1077, (1972).
38. J. E. Welch, F. H. Harlow, J. P. Shannon, and B. J. Daly, "The MAC Method—A Computing Technique for Solving Viscous, Incompressible, Transient Fluid-Flow Problems Involving Free Surfaces", Los Alamos Scientific Lab., Report No. LA-3425, (1965).
39. L. W. B. Browne, "Numerical Simulation of Fluid Motion", North-Holland Publishing Company, (1978).
40. W. E. Pracht, *J. Comput. Phys.*, **7**, 46, (1971).
41. F. H. Harlow and J. E. Welch, *The Physics of Fluids*, **8**, 2182, (1965).
42. M. O. Deville, *J. Comput. Phys.*, **15**, 362, (1974).
43. A. J. Chorin, *Math. Comp.*, **22**, 745, (1968).
44. J. A. Viecelli, *J. Comput. Phys.*, **8**, 119, (1971).
45. C. W. Hirt and J. P. Shannon, *J. Comput. Phys.*, **2**, 403, (1968).
46. M. Matsui and D. C. Bogue, *Trans. Soc. Rheol.*, **21**, 133, (1977).
47. M. R. Kamal and P. G. Lafleur, *Polym. Eng. Sci.*, **24**, 692, (1984).
48. C. Chang, D. Peiffer, and R. S. Stein, *J. Polym. Sci.*, **12**, 1441, (1974).
49. Z. Tadmor and C. G. Gogos, "Principles of Polymer Processing, John Wiley and Sons, Inc., New York, (1979).
50. K. Oda, J. L. White, and E. S. Clark, *Polym. Eng. Sci.*, **18**, 53, (1978).
51. J. C. Seferis and R. J. Samuels, *Polym. Eng. Sci.*, **19**, 977, (1979).
52. H. F. Moy and M. R. Kamal, *Polym. Eng. Sci.*, **20**, 957, (1980).

NOMENCLATURE

a_t = Temperature shift factor.
A_{AM} = Intrinsic transverse modulus for the amorphous phase.
A_{CR} = Intrinsic transverse modulus for the crystalline phase.
C = Stress optical constant.
C_p = Specific heat.
E_s = Tensile Young's modulus.
f_{AM} = Orientation function for amorphous phase.
f_{CR} = Orientation function for crystalline phase.
$\vec{g}$ = Gravitational acceleration vector.
G = Modulus.
k = Thermal conductivity.
K = Consistency index.
K_A = Nakamura's rate constant.
n = Power-Law index.
n' = Avrami exponent.
P = Hydrostatic pressure.
$\vec{q}$ = Energy flux vector.
t = Time.
T = Temperature.
T_m = Melt temperature.
T_o = Cold reference temperature.
T_1 = Hot reference temperature.
u = Longitudinal velocity.
w = Transverse velocity.
x, y, z = Rectangular coordinates.
X_c = Degree of crystallinity.
Z_c = Avrami crystallization rate constant.

GREEK LETTERS

$\dot{\gamma}$ = Shear rate.
Δ = Rate of deformation tensor.
Δ^o_{AM} = Intrinsic birefringence of amorphous phase.
Δ^o_{CR} = Intrinsic birefringence of crystalline phase.
Δ_F = Form birefringence.
$\Delta_T n$ = Total birefringence.
Δ_{Hc} = Heat of crystallization per unit mass.
n = Viscosity.
λ = Relaxation time.
ρ = Density.
$\underline{\underline{\tau}}$ = Stress tensor.

DIMENSIONLESS VARIABLES AND NUMBERS

Dimensionless space variables	$X' = \frac{x}{L_c}; Z' = \frac{z}{L_c}$	
Characteristic length	L_c:	Length of the cavity
Dimensionless velocities	$U' = \frac{U}{U_c}; W' = \frac{W}{U_c}$	
Characteristic velocity	U_c:	Maximum longitudinal velocity
Dimensionless time	$t' = \frac{U_c t}{L_c}$	
Dimensionless density	$\rho' = \frac{\rho}{\rho_c}$	
Characteristic density	ρ_c:	density at 20°C
Dimensionless pressure	$P' = \frac{P}{\rho_c U_c^2}$	
Dimensionless viscosity	$K' = \frac{K}{K_c}$	
Characteristic viscosity	K_c:	Consistency power-law index
Dimensionless stress	$\tau' = \frac{\tau L_c^n}{K_c U_c^n}$	
Dimensionless rate-of-deformation	$\overset{*}{\Delta} = \frac{Lc}{Uc}\overset{*}{\Delta}$	
Reynolds Number	$Re = \frac{P_c U_c^{2-n} L_c^n}{K_c}$	
Prandtl Number	$Pr = \frac{K_c C_p L_c^{1-n}}{k U_c^{1-n}}$	
Weisenberg Number	$W_s = \frac{K_c U_c^n}{G_c L_c^n}$	
Brinkman Number	$B_r = \frac{K_c U_c^{1+n} L_c^{1-n}}{k(T_1 - T_0)}$	

A Structure-Oriented Computer Simulation of the Injection Molding of Viscoelastic Crystalline Polymers

Part II: Model Predictions and Experimental Results

M. R. KAMAL* *and* P. G. LAFLEUR**

Department of Chemical Engineering
McGill University
Montreal, Canada H3A 2A7

A theoretical model proposed for simulation of the injection molding of partially crystalline thermoplastics can predict fill time, velocity, temperature and pressure distributions, the distribution of shear and normal stresses, crystallinity, amorphous birefringence, and tensile moduli. In this paper, experimental data will be compared to the predictions of the model.

INTRODUCTION

A theoretical model has been proposed in the first part of this series (1), for simulation of the injection molding of partially crystalline thermoplastics. The model can predict fill time, velocity, temperature and pressure distributions, the distribution of shear and normal stresses, crystallinity, amorphous birefringence, and tensile moduli. In this second part, experimental data will be compared to the predictions of the model. More detailed results may be found elsewhere (2, 3).

EXPERIMENTAL

Equipment

The injection molding experiments were conducted on a Model 60-SR, 2⅓ oz. reciprocating screw injection molding machine, manufactured by Metalmec. The cavity used was a rectangular fan-gated mold cavity with the following dimensions: length = 9.1 cm, width = 6.35 cm, thickness = 0.318 cm. The cavity was equipped with three pressure transducers, two thermocouples, and a flush mounted heat flux sensor. A schematic diagram of the rectangular cavity and the positions of the measuring devices are shown in *Fig. 1*.

Material

The resin used was a high density, injection molding grade, polyethylene resin, Sclair 2908. The resin was supplied by DuPont of Canada Limited. The various properties were obtained at the Chemical Engineering Laboratories of McGill University. Shear viscosity and first normal stress difference dependence on both shear rate and temperature were obtained, for low values of shear rate, with the Rheometrics Mechanical Spectrometer (RMS) and for high shear rate with an Instron Capillary Rheometer.

The temperature dependence of the shift factor was obtained by measuring dynamic properties in oscillatory shear flow. Thermal properties, such as thermal conductivity, specific heat, PVT diagram, and crystallization kinetics data were measured experimentally for the resin studied using differential scanning calorimetry, a modified Instron Capillary Rheometer, and a specially designed thermal conductivity apparatus (4, 5).

Operating Conditions

A series of molding experiments were designed using two mold temperatures (10 and 40°C), two melt temperatures (170 and 190°C) and varying hydraulic pressures. Experiments at the four possible combinations of mold temperature and melt temperature were performed using the same settings for the pressure control valves. With the combination of the low mold and high melt temperature, the pressure settings were changed to obtain four different filling times. *Table 1* shows the different operating conditions with corresponding code names that will be used in subsequent analysis.

RESULTS AND DISCUSSION

For the mathematical simulation of the filling, packing, and cooling stages of the molding cycle, the equations of continuity, momentum, and energy, coupled with constitutive equations

* To whom all correspondence should be addressed.
** Present address: National Research Council Canada, Industrial Materials Research Institute, 75 de Mortagne Blvd., Boucherville, Quebec, Canada, H4B 6Y4.

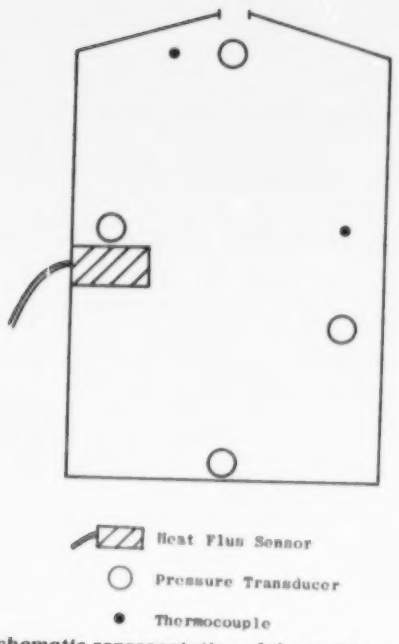

Fig. 1. Schematic representation of the mold cavity and measuring devices.

Table 1. Experimental Injection Molding Conditions.

Melt Temperature (°C)	Mold Temperature (°C)	Flow Rate (cm^3/s)	Code
170	10	18.9	LPLM
170	40	18.9	LPHM
190	10	18.9	HPLM
190	40	18.9	HPHM
190	10	22.9	HPLM1
190	10	18.9	HPLM2
190	10	13.6	HPLM3
190	10	10.4	HPLM4

Ex. LPLM Low melt-Low mold
HPHM High melt-High mold
M: Mold (temperature)
P: Polymer Melt (temperature)
L: Low
H: High

and appropriate boundary conditions described in the theoretical section, form the central core of the computer program. The solution of the finite-difference approximations is carried out in the region of the rectangular mesh containing marker particles. *Figure 2* shows the position of the cells in reference to the mold cavity. In this section, the different variables calculated by the model will be presented and, when possible, compared with experimental data.

Filling Stage

The progression of the melt front in the cavity was measured by the instantaneous response of the pressure transducers located along the cavity. Since the active diameter of the transducer is about 9 percent of the cavity length, transducer data are reported in terms of a range of values. *Figure 3* gives the position of the melt as a function of time for four cases with different flow rates and the experimental results for the two extreme cases. The good agreement between the experimental and calculated values shows the reliability of the entrance boundary conditions based on the measured flow rate.

Figure 4 contains plots of the longitudinal and transverse velocity profiles plotted against the transverse position in the thickness direction, for case HPLM2, for different positions from the entrance at the end of the filling stage. As one moves along the mold from node 2 to 10 and 20, the longitudinal velocity, U, increases at the centerline and decreases near the wall. This is due to the effect of the non-isothermal flow (combined cooling and viscous heating). The increase of viscosity near the wall is the

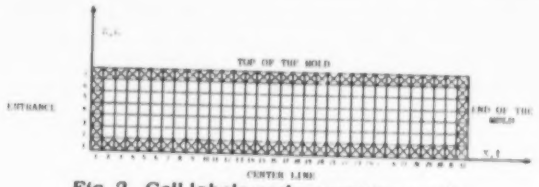

Fig. 2. Cell labels and computing mesh.

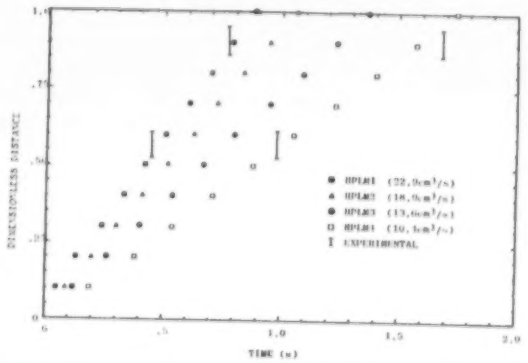

Fig. 3. Progression of the melt front at different flow rates.

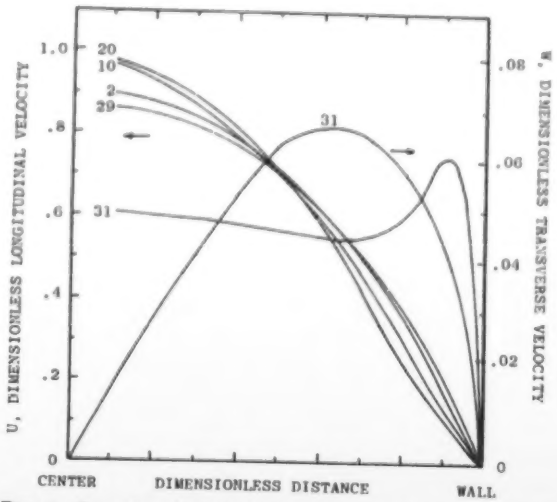

Fig. 4. Gapwise distributions of longitudinal and transverse velocity in the cavity, at the end of the filling stage, case HPLM2.

cause of the lower velocities at that point. However, because of the relatively coarse mesh system used for this analysis, the effect of cooling on the velocity near the wall is not readily discernible. It is expected that the use of finer mesh would yield such information. Near the free surface, the velocity profile flattens out and the last nodes show a rather flat velocity profile. The transverse velocity, *W*, becomes significant as the front surface is approached due to the fountain flow effect. As expected, the transverse velocity is zero at the centerline and the wall with a maximum occurring at some intermediate position. The magnitude of the velocity increases as the front surface is approached. It was found that the transverse velocity can be neglected outside of the front region representing, for our molding conditions, a distance of approximately 1.9 times the thickness of the mold. The model predictions for the effect of the injection pressure on the longitudinal velocity distributions at the center of the cavity are shown in *Fig. 5*. As expected, the model shows an increase in longitudinal velocities as the injection pressure is increased.

The pressure during the complete cycle was monitored, with the pressure transducers, at three different positions along the cavity as shown in *Fig. 1*. *Table 2* shows that the model can accurately predict the pressure required for filling at different operating conditions. The calculated pressure profiles at the end of the filling stage along the cavity are shown in *Fig. 6* for the two extreme injection pressures. The highest injection pressure is associated with consistently higher pressure along the cavity. Both cases deviate from a linear pressure drop, due to the non-isothermal flow situation. *Figure 7* shows the calculated and experimental pressure profiles during the filling stage, for case HPLM2, at the entrance and the center of the cavity. At the entrance of the mold, the model predictions are excellent. However, the estimations at the center of the mold are somewhat larger, due to the size of the transducer compared to the mesh system and also to the small difference obtained between calculated and experimental melt front positions.

Figure 8 shows the temperature *vs.* distance from the wall at varying downstream positions,

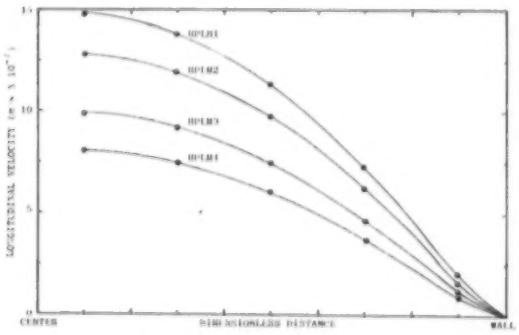

Fig. 5. Gapwise distributions of longitudinal velocity in the cavity, at the end of the filling stage, at different flow rates.

Table 2. Comparison Between Experimental and Calculated Pressure Drop During the Filling Stage.

Operating Conditions	Flow Rate (cm^3/s)	Experimental M Pa	Calculated M Pa	Relative Error %
HPLM1	22.9	7.04	7.25	3.2
HPLM2	18.9	6.83	6.67	2.3
HPLM3	13.6	5.62	5.74	2.1
HPLM4	10.4	5.41	4.96	8.3
HPHM	18.9	6.69	6.42	4.0
LPLM	18.9	7.90	8.62	8.4
LPHM	18.9	7.76	8.17	5.0

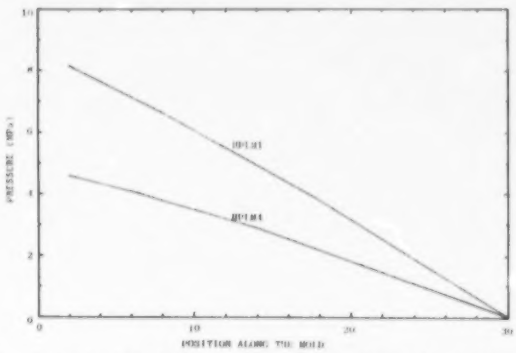

Fig. 6. Calculated pressure profiles along the cavity at the end of the filling stage.

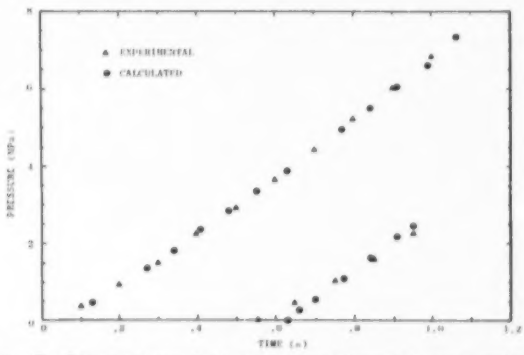

Fig. 7. Comparison between experimental and calculated pressure-time profiles during filling, case HPLM2.

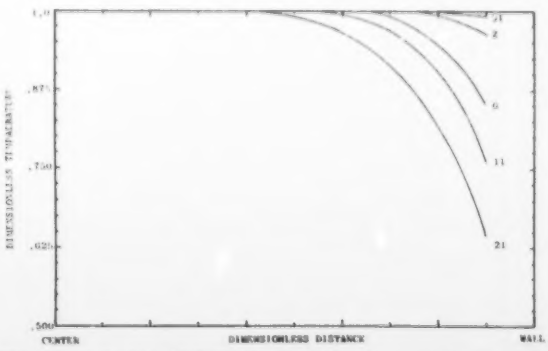

Fig. 8. Gapwise distributions of the temperature in the cavity, at the end of the filling stage, case HPLM2.

for case HPLM2. The temperature at the entrance of the mold is uniform and equal to the melt temperature. Away from the gate, a temperature profile develops, and the lowest temperatures are located at the far end of the mold. However, the temperatures increase in the melt front region. This is caused by the fountain effect, which allows hot melt to flow from the center of the mold toward the cavity wall. The resulting two-dimensional temperature profile is due to the transient filling of the mold cavity where hot polymer melt is fed in at a constant rate. The model also shows lower melt temperatures obtained by decreasing the mold temperature or decreasing the injection pressure. For the grid system used in the filling stage (5 × 30), no crystallization could be predicted at the last nodal point near the wall. The filling time being small, the thickness of the solid layer was smaller than the first node near the wall. Thus, the meshes were not fine enough to permit the calculation of crystallinity in the thin solid layer near the wall. However, it was possible to predict crystallization in a layer of 150 μ near the wall during filling when finer meshes were employed.

A knowledge of the stress field development during the injection molding cycle is essential for estimating the orientation distribution or the frozen stresses in the final product. *Figure 9* shows the distribution, in the thickness direction, of the shear and normal stress components at different positions along the cavity, at the end of the filling for case HPLM2. For the positions away from the melt front, the model predicts stress distributions similar to those obtained with steady shear flow, where the shear stress is proportional to the shear rate and the normal stress is proportional to the square of the shear rate. The shear and normal stresses are zero at the center and maximum near the wall. The temperature gradients and the viscoelastic nature of the fluid have a significant effect on the stress distributions, especially near the wall. Both the normal and shear stresses increase as the distance from the gate increases. For the four cases at different injection pressures, the model predicts a corresponding increase in the overall stress levels in the cavity. This is very important in design of mold cavities where the highest injection rate is used in order to minimize the filling time at the expense of very high stresses in the cavity.

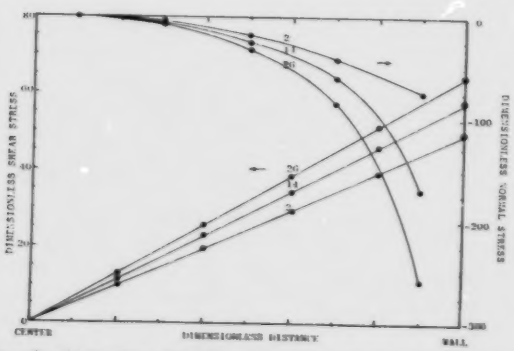

Fig. 9. Gapwise distribution of shear and normal stresses in the cavity, at the end of the filling stage, case HPLM2.

Packing Stage

After filling is completed, additional material is packed into the cavity to compensate for shrinkage during the cooling process. The model predictions for values of velocities, pressures, stresses, and temperatures are presented and compared with experimental data, when available.

In the analysis of the filling stage, the velocity of the flow front is a variable of the system. However, during the packing stage, the velocity at the end of the cavity is zero, and the compressibility or change in density is responsible for the flow in the cavity. *Figure 10* shows the velocity *vs.* distance from the wall at different positions along the cavity, after 0.05 seconds from the beginning of the packing stage, for case HPLM2. When comparing the cases with different injection pressures, the results show slightly larger velocities for the higher flow rate cases. At the beginning of the packing stage, the density is relatively low in the cavity. However, with the extra material introduced into the cavity, the density rises, thus increasing the resistance to flow. For case HPLM1, velocity profiles at the center of the mold, for various times, are shown in *Fig. 11*. The model predictions show the decreasing velocity profiles from the beginning to the end of the packing stage.

The pressure profile data obtained with the entrance pressure transducer were fitted to a high order polynomial and used as a boundary condition for the calculations of the packing stage. The model was verified by comparing the pressure reading at the center of the cavity with calculated values. For the case HPLM2, *Fig. 12* shows the pressure at the center of the cavity as a function of time during the packing process. The model predictions are consistently higher than the experimental values, and the difference at the end of the packing stage is of

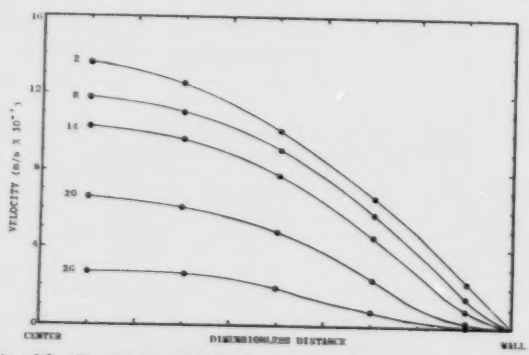

Fig. 10. Gapwise distributions of velocity in the cavity, after 0.05 sec., during the packing stage, case HPLM 2.

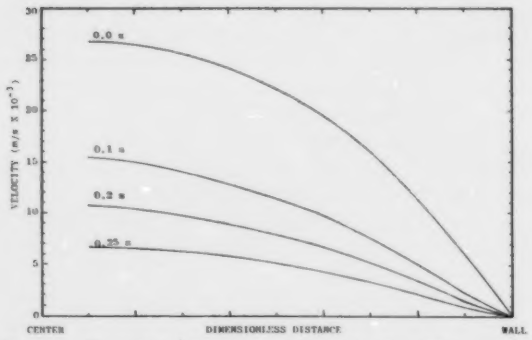

Fig. 11. Gapwise distributions of velocity at the center of the cavity, for various times during packing, case HPLM 1.

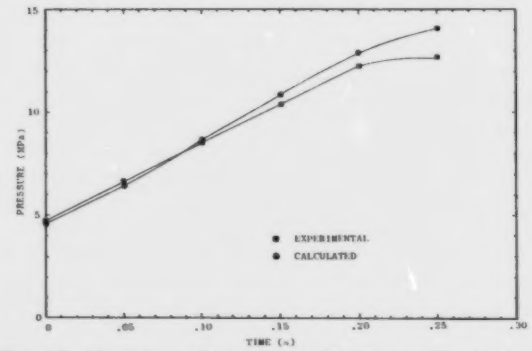

Fig. 12. Variation of pressure with time at the center of the cavity during packing, case HPLM 2.

the order of 10 to 12 percent. One of the reasons for the discrepancy is the fact that the packing stage iterative scheme is based on adjusting the pressure profile to increase the density to satisfy the continuity equation. The size of the grid system is too large and does not allow the detection or prediction of the crystallinity that is produced during the filling and packing stages close to the wall. Therefore, the model underestimates the density in this region, and more pressure is required to pack the cavity with the lower density material. These difficulties could be overcome by using a finer grid, especially near the wall.

The temperature field prevailing at the end of filling is used as the initial boundary condition for the packing stage. *Figure 13* shows the temperature *vs.* transverse distance at various positions along the cavity for case HPLM2. Cooling continues during the packing, and the temperatures are decreasing everywhere in the cavity. For all cases, no crystallization was predicted at the last nodal point near the wall. The positions away from the gate show lower temperature profiles as a result of their lower initial temperature.

Shear and normal stresses *vs.* the transverse thickness, are shown in *Fig. 14*, at different positions along the cavity at the end of the packing. The maximum shear stress profile is situated at the gate and decreases along the cavity. This is due to the decreasing transverse velocity gradients in the longitudinal direction. However, there is no definite trend in the variation of normal stresses along the cavity, because of the continuously changing longitudinal velocity gradients.

The stress field is used to determine the frozen amorphous orientation of the final article. Previous workers (6), in their analysis of the injection molding process, used the stress field at the end of the filling as the stress being relaxed during the subsequent cooling. This is the first treatment where the stresses are also calculated during the packing stage. For the case HPLM4, *Fig. 15* shows the shear and nor-

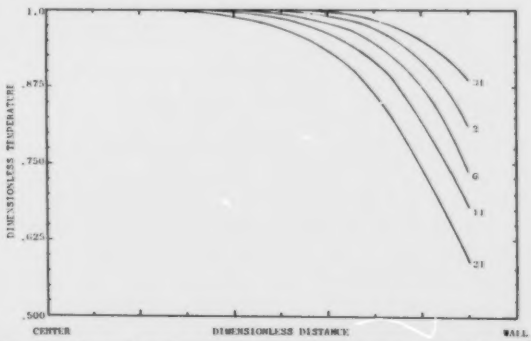

Fig. 13. Gapwise distributions of temperature in the cavity, at the end of the packing stage, case HPLM 2.

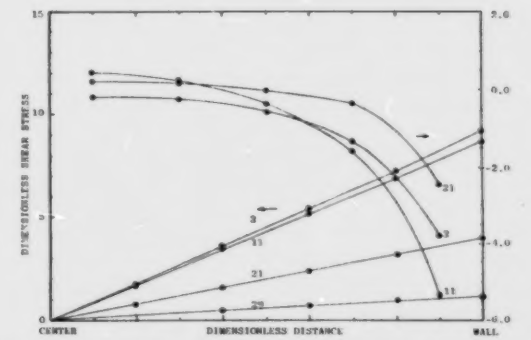

Fig. 14. Gapwise distributions of shear and normal stresses in the cavity, at the end of the packing stage, case HPLM 2.

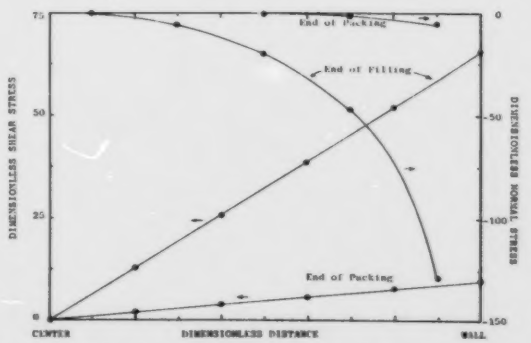

Fig. 15. Gapwise distributions of shear and normal stresses at Node 11, at the end of the filling and packing stages, case HPLM 4.

mal stresses *vs.* the transverse thickness at the nodal point # 11 in the longitudinal direction. The stresses at the end of packing are much lower than those at the end of filling, showing the kind of error induced by neglecting the analysis of the packing stage. Because of the relatively short filling and packing times and the small decrease in temperature at the first nodal point near the wall, it is not possible to see the effect of temperature near the wall on the stress relaxation.

The mass of material introduced in the cavity at various time during the packing stage is shown in *Fig. 16* for the case HPLM1. At the end of the filling, the total amount of material in the cavity was 14.6 g and an additional 0.36 g was introduced during the packing stage. This is an increase of 2.5 percent of the total mass of material.

Solidification Stage

After filling and packing are completed, cooling without flow continues until the plastic has reached a sufficient level of solidification. The cooling model allows us to calculate the crystallinity and temperature profiles using the conditions at the end of the packing as initial boundary condition. Stresses are relaxed according to the temperature field and frozen stresses are evaluated in conjunction with the position of the frozen layer.

The temperature profiles during the filling and the packing stages were not affected by the crystallization, because of the small thickness of the frozen layer developed during that relatively short time. However, the melt in the cavity will become completely solid during the cooling stage and the development of crystallinity will influence the temperature profiles. *Figure 17* shows the time variation of the gapwise distributions of temperature at the center of the cavity for case HPLM. With the developing frozen layer, it is possible to see that the shape of the temperature profiles is affected by the crystallization process (see plateaus in profiles). By selecting a constant solidification temperature from the crystallization data, the progression of the solid layer can be obtained from the temperature *vs.* time curves. The time at which the melt is completely solid in the cavity was 7 sec for the high mold temperature and 5.8 sec for the low mold temperature. However, faster cooling will influence the magnitude of the frozen stresses, as reported in the next section. A fast cooling rate is an advantage considering its effect on the cycle time. However, frozen stresses will consequently be higher, influencing the mechanical properties.

It is possible to calculate the thickness of the solid layer by two different techniques. One consists of fixing a constant temperature of crystallization based on DSC data and determining the position of the solid layer in conjunction with the temperature profiles. The other technique, based on crystallinity, consists of assuming that the melt is solid when its crystallinity reaches 50 percent of its final value. *Figure 18* shows the position of the solid layer *vs.* time at the center of the cavity for two cases with a high melt temperature and different mold temperatures. Comparing the profiles obtained using a constant temperature of crystallization demonstrates that as the mold temperature is lowered, the solidification process becomes faster. On the same figure, the two techniques for the evaluation of the solid layer thickness are compared for the case HPHM. The profile obtained on the basis of the crystallinity

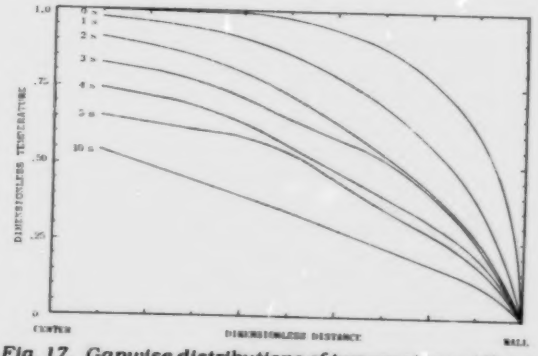

Fig. 17. Gapwise distributions of temperature at the center of the cavity, at various times during the cooling stage, case HPLM.

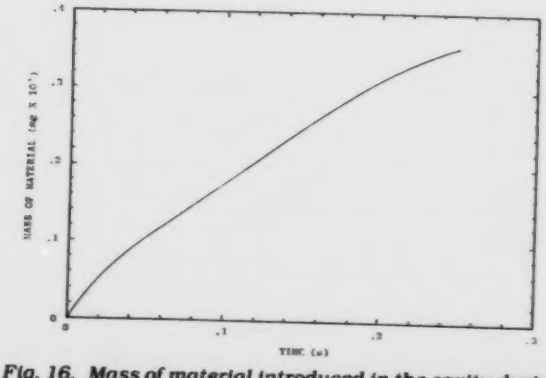

Fig. 16. Mass of material introduced in the cavity during packing, case HPLM 1.

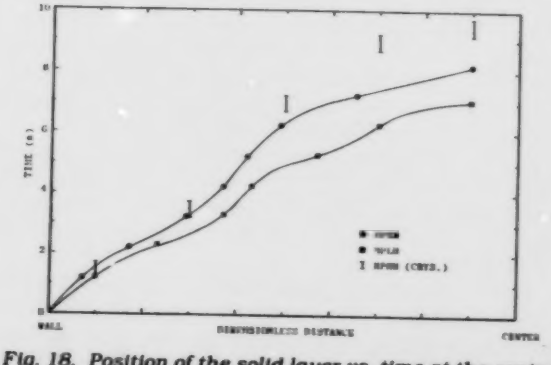

Fig. 18. Position of the solid layer vs. time at the center, comparison between cases HPHM and HPLM.

criterion gives a slower progression of the solid layer. The temperature of crystallization used to determine the ultimate crystallinity is estimated using the cooling rates prevailing during the molding process. These cooling rates are much larger than the experimental DSC scanning rates. Therefore, the estimated temperature of crystallization will be lower, resulting in a longer time before solidification.

For each case studied, it is possible, starting with the values of the shear and normal stresses prevailing at the end of packing, to calculate the variation of the stresses with time during the cooling process. *Figure 19* shows the gapwise distributions of shear and normal stress for various times during the cooling process. Relaxation of the shear stresses being ten times faster than the normal stresses, the only position, where shear stresses will not be completely relaxed after 2 sec, is near the wall, where the low temperature retards the relaxation process. Normal forces relax more slowly than shear forces, with the same phenomena occurring near the wall. Since the solid layer formed during the filling and packing stages could not be computed with the number of cells used for the analysis, it was not possible to confirm the existence of a stress maximum somewhere near the wall.

Microstructure Predictions

The predictions of the model, presented in the previous sections, elucidate the thermo-mechanical history of the resin during the various stages of the injection molding process. The temperature, pressure, velocity, and stress fields evaluated during the molding cycle determine the microstructure distribution and, therefore, the ultimate properties of the molded article. So far, we have demonstrated the utility of the model in adequately predicting the thermo-mechanical history of the resin during the processing operation. In this section, the model predictions relating the thermo-mechanical history to the development of microstructure will be presented.

The kinetic equation of crystallization incorporated into the heat transfer model makes it possible to follow the development of crystallinity, molded parts were microtomed in the thickness direction, and each section was melted using DSC to obtain its ultimate crystallinity. *Figure 20* shows a comparison between experimental and calculated crystallinity profiles for the case LPLM. For all the cases, the model predicts lower crystallinity close to the wall than in the core, because of the higher cooling rates near the wall. The calculated values show a smaller variation from the wall to the center, when compared to the experimental data. However, the model predictions are good and the maximum difference for this case is only 5 percent. It should be pointed out that larger crystallinity gradients would be obtained very close to the wall, if a finer mesh is used in that region.

The amorphous gapwise distribution of birefringence was calculated using stress-optical laws, and compared to the experimental data obtained by Moy (7) for the same cavity and molding conditions. *Figure 21* shows that, for both experimental and calculated values, the amorphous orientation is mainly due to the stress field, with a high orientation near the wall, where frozen stresses are important, and low orientation is in the core where stresses are relaxed. The method of estimating amorphous birefringence is indicated in the first part of this series. Sometimes, a maximum in birefrin-

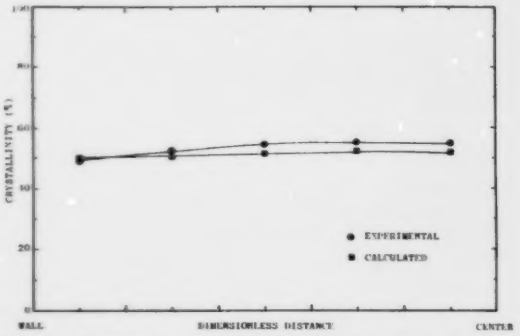

Fig. 20. Comparison between experimental and calculated crystallinity, at the center of the cavity, case LPLM.

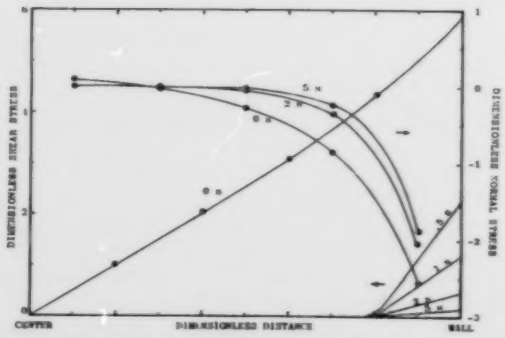

Fig. 19. Gapwise distributions of shear and normal stresses at the center of the cavity, at various times during the cooling stage, case HPHM.

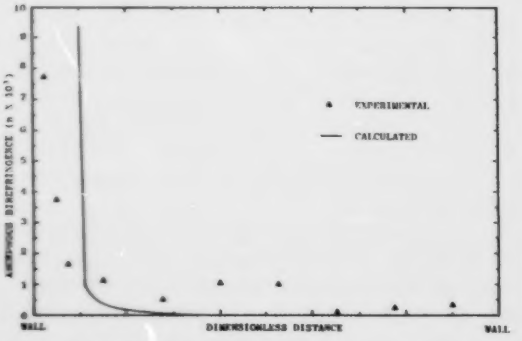

Fig. 21. Comparison between experimental and calculated amorphous birefringence at the center of the cavity, case LPHM.

gence is observed near the wall. However, this could not be confirmed, in view of the coarse mesh employed in this study.

In the theoretical section of this series, we presented a model to estimate the tensile modulus from the distribution of amorphous orientation functions and crystallinity. The estimated amorphous orientation and crystallinity were employed to predict the distribution of tensile moduli under specified molding conditions. The predicted modulus distribution is in reasonable agreement with the experimental values measured experimentally by Moy (5), as shown in *Fig. 22* for the case LPHM. The model predictions are reasonable, especially when considering the various assumptions employed (neglecting the crystalline contribution) and the error involved in the experimental measurement of modulus distributions.

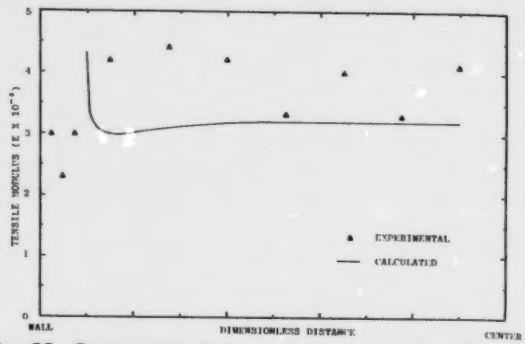

Fig. 22. Comparison between experimental and calculated tensile modulus, at the center of the cavity, case LPHM.

CONCLUSION AND OUTLOOK

The model presented for the analysis of the filling stage has shown that the predictions of the pressure variation with time are excellent at the entrance and reasonably good at the center of the cavity. The difference between the experimental and calculated position of the melt front might be responsible for the lower agreement at the center of the cavity. Predictions of velocity, temperature, and stress profiles support the assumptions of a quasi steady-state, fully-developed flow in the main part of the cavity during the filling process. For the operating conditions used in this work, the thickness of the solid layer is small compared to the size of the mesh system. Thus, no crystallization is shown during the filling stage. However, computations with a finer mesh have predicted crystallization in a layer of 150 μ thick near the wall. The existence of a fountain flow was demonstrated by the development of a transverse velocity component and the redistribution of temperature in the region of the melt front.

The sudden change of boundary conditions during packing, where pressure gradients are reduced and only the compressibility of the polymer is responsible for the flow in the cavity, results in a substantial reduction in the magnitude of the stresses. Therefore, the properties of the polymer frozen before and during the packing stage will be different due to the frozen stresses, indicating the importance of the analysis of the packing stage. Predictions of pressure distributions and variation with time are in reasonable agreement with experimental data.

During the cooling stage, no flow takes place and cooling of the polymer melt continues. Model predictions for crystallinity profiles, as well as experimental profiles, show significantly lower crystallinity near the wall than in the core. Therefore, the model is sensitive to the variation in cooling rates encountered during the process. The combined effects of the relaxation phenomena and the growth of the solid layer during the cooling stage were used to estimate the distributions of frozen stresses. These stresses were then utilized to estimate the tensile modulus of the final product. The agreement between model predictions and experimental data is reasonably good.

From this study it appears that many of the interesting phenomena occurs near the wall, where the crystallization under high cooling rates and high levels of stress is responsible for the development of different morphological zones. The same model is now being used with a larger number of cells in that critical area in an attempt to obtain a more detailed understanding of the characteristics of the molding across the section of the cavity, especially near the wall.

ACKNOWLEDGMENT

The authors would like to acknowledge financial support from the Natural Sciences and Engineering Council of Canada, the Ministere de l'Education of the Government of Quebec, and McGill University.

REFERENCES

1. P. G. Lafleur and M. R. Kamal, *Polym. Eng. Sci.*, to be published.
2. P. G. Lafleur, Ph.D. Thesis, McGill University, Montreal, Canada, 1983.
3. M. R. Kamal, E. Chu, P. G. Lafleur, and M. E. Ryan, *SPE Tech. Papers*, 31, 818 (1985).
4. S. Sourour and M. R. Kamal, *Polym. Eng. Sci.*, 16, 480 (1976).
5. R. C. Winter, M. Eng. Thesis, McGill University, Montreal, Canada, May, 1978.
6. K. K. Wang, *et al.*, "Injection Molding Project", College of Engineering, Cornell University, Progress Report, # 8.
7. H. F. Moy, Ph.D. Dissertation, McGill University, Montreal, Canada, February, 1980.

Financial Incentive of Linear Low Density Polyethylene Blends

L. A. HAMIELEC

Novacor Chemicals Ltd. 1600, 734-7 Avenue SW
Calgary, Alberta, Canada T2P 3P9

The key to successfully implementing polymer blends in end-use applications includes an understanding of performance requirements and the physical property balance of the blend, as well as the provision of financial incentive to the fabricator. The economic gain is calculated for two cases where blends were introduced to displace another material: a blend which gives higher productivity for blown film applications and a blend which allows for increased flow and a gage reduction for an injection molding application. As the resin cost usually accounts for more than seventy percent of the final product cost, the resin or blend cost affects the economic gain (if any) from the fabricator's point of view. Therefore, successful commercial implementation of a new resin or blend depends on its relative cost and benefit to other commercially available materials.

INTRODUCTION

Over the past several years, co- and terpolymerization have expanded the range of polymer properties. More recently, the concept of physically blending two or more existing polymers to obtain new products has attracted widespread interest and commercial utilization.

The high cost of developing new reactor grades is most likely the reason for the recent success of blends. Other factors impacting on the future growth of blends are:

- blends may offer a cost-effective means to fill the gap in performance of existing materials;
- blends may often improve the critical properties required for an end-use;
- blends may often result in increased revenue/sales without major expenditure or capital expansions;
- blends may often represent an easy way for commodity plastic producers to enter the lucrative specialty segment of the business.

Before 1980, some poly(vinylchloride), polypropylene, and polystyrene resins were blended commercially for commodity applications. However, it was not until the introduction of linear low density polyethylene (LLDPE) copolymers (butene, hexene, octene) that interest became focused on the modification of low density polyethylene (LDPE). In addition to the aspect of material savings, greater consideration was given to property enhancements.

This paper focuses on commercial blends of LLDPE and estimates the financial incentive from the fabricator's point of view for two commercial examples where blends were successfully introduced to displace another material. The importance of these examples is that their successful implementation was a result of the favorable cost performance of the blend over the previously used material.

MARKET APPLICATION OF BLENDS

The use of blends for commerical application requires a good understanding of performance requirements and of the parameter(s) being modified, whether it be physical, process-related or cost-related. For instance, if one sets out to control the desirable processing and end-use performance of a new blend, the following should be considered:

1. establish meaningful statistical correlations between performance and selected property indicators;
2. measure the processing or product property one is attempting to control;
3. establish where the economic limits lie.

LLDPE BLENDS

At present, more than 60 percent of LLDPE for commercial applications is blended with other polymers such as LDPE, HDPE, and EVA copolymers (*Fig. 1*). The main reason for blending is to obtain an averaging of physical properties and/or processing properties and/or material cost.

The blending of LLDPE with LDPE has gen-

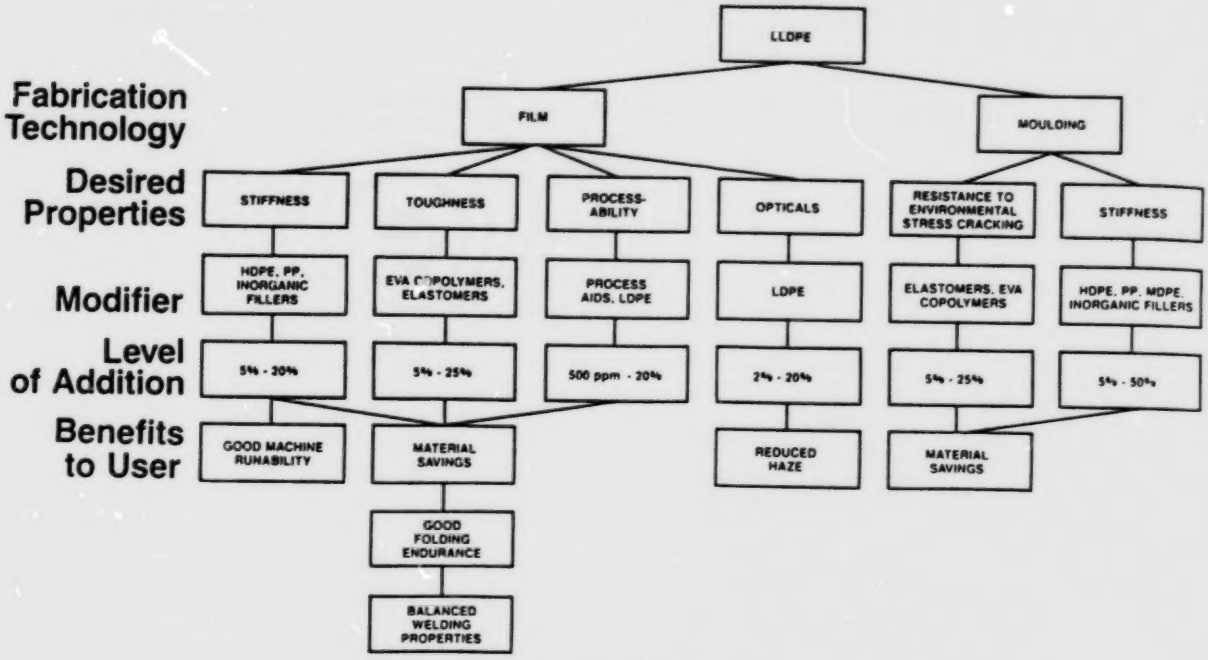

Fig. 1. LLDPE blends.

erated considerable interest in the marketplace. There are many physical and processing property differences between LLDPE and LDPE. In comparison to LDPE, LLDPE has:

- greater stiffness
- greater tensile strength
- greater elongation
- greater puncture resistance
- greater high and low temperature properties
- greater environmental stress-crack resistance
- higher energy requirements for extrusion
- easier melt drawability.

Interest in blending LLDPE with LDPE can result from a desire to obtain the melt drawability and physical property advantages of LLDPE without having to undertake the equipment modifications required for optimum LLDPE extrusion. Most film physical properties and drawdown capabilities are improved with LLDPE/LDPE blends over pure LDPE and pure LLDPE values to intermediate levels between those of the pure components. LDPE is added to LLDPE for improvements in optical and processing properties such as output rate and bubble stability, although the tear strength is reduced. Thus, LLDPE/LDPE blends are not recommended for applications demanding a high tear resistance. These applications include stretch and freezer films. Applications requiring good opticals such as bakery film, are a natural fit for LLDPE-rich blends. Various polymer processing aids, as well as LDPE, are also blended with LLDPE for improvements in processability and/or the elimination of melt fracture using conventional LDPE extrusion equipment. Conversely, LLDPE in LDPE-rich blends is used to impart hot tack and strength properties to LDPE as well as to reduce the over all resin cost.

HDPE or PP is added to LLDPE for increased stiffness as compared to pure LLDPE, which is particularly important when downgaging on film thickness. These applications include garment film, grocery sacks, merchandise bags, and refuse bags. In the case of thin film, it is necessary to find a compromise for the physical property criteria of the end-use, such as tear strength and stiffness. For example, the use of small amounts of HDPE in LLDPE cause these properties to be influenced in opposite directions; therefore, it is critical to recognize where the economic limits lie, thereby understanding the physical property criteria of the end use.

If, in a specific application, there is a certain amount of toughness in reserve, the addition of a filler can achieve material savings. On the other hand, a thinner gage can be used to realize similar savings. Downgaging on film thickness was common practice for most film applications, notably for high-volume applications such as grocery sacks and refuse bags. If the material cost is not a predominant factor, the addition of an EVA copolymer to LLDPE can be considered as a means of improving toughness.

FINANCIAL INCENTIVE OF BLENDS

Commercial implementation of blends will usually be successful if the blend is a cost-effective way to fill the gap in performance of existing materials. A conversion cost calculation is a technique which can be used to mea-

sure the relative cost performance or value-in-use of any material including blends. The conversion cost incorporates the material selling price as well as all fixed and variable manufacturing costs inherent to the fabrication process. Thus, this technique may be used in predicting the chance of success in the marketplace for the introduction of a new blend. For instance, a blend which allows for a 20 percent gage reduction for a film application may be cost effective at a maximum of $0.04 per kilogram premium over the existing material. If the incremental blend cost exceeds the above cost, then commercial implementation will likely not be successful. Therefore, successful implementation of the blend will most likely depend on the associated selling price provided by the resin supplier. Alternately, the cost performance or value-in-use of the blend should at least match (if not surpass) that which the existing material provides.

The conversion cost technique is shown below for two examples where blends were successfully used to displace another material. The sensitivity of resin selling price and extruder line size on conversion cost is also considered. All conversion cost calculations are from the fabricator's point of view.

PRODUCTIVITY GAIN FOR BLOWN FILM

Processing aids, as well as small amounts of LDPE, can be blended with LLDPE to realize a productivity gain in some blown film applications. The following example describes a blown film operation where a blend was introduced to yield a 10 percent productivity gain over the resin previously used. A film conversion cost (*FCC*) shows the cost effectiveness of the base case at 363 kilograms per h (800 pounds per h) and for an optimized case a 400 kilograms per h (880 pounds per h). The *FCC* in dollars per kilogram is calculated as

$$FCC = \frac{(FMC + VMC)}{OPR} \qquad (1)$$

where

FMC is fixed manufacturing cost in dollars per h;
VMC is variable manufacturing cost in dollars per h;
OPR is output rate in kilograms per h.

The *FMC* component includes direct labor including: supervision, maintenance of process equipment, building and offsite, general plant overhead, insurance and property taxes, and depreciation of process equipment and building and offsite. A representative *FMC* for a blown film line is $39.50 per h.

The *VMC* component includes raw materials (resin, color, concentrates, scrap, scrap credit) and utilities. A representative utility cost is $9.00 per h. With a resin selling price of $0.73 per kilogram ($0.33 per pound), the *VMC* for

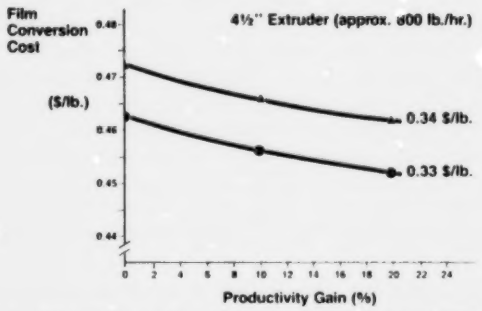

Fig. 2. Film conversion cost vs. productivity at 800 lb./hr.

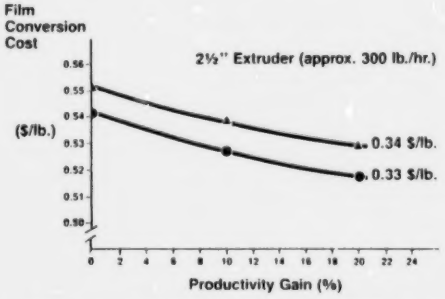

Fig. 3. Film conversion cost vs. productivity at 300 lb./hr.

the base case is approximately $329.94 per h and $362.04 per h for the optimized case (which also includes color concentrates, scrap, scrap credit).

The respective *FCC*'s are $1.02 per kilogram ($0.462 per pound) and $1.00 per kilogram ($0.456 per pound) for the base and optimal cases respectively. The resin price realized by the fabricator for both the base case and blend is the same. It is also assumed that the output rate is power and sales limited, not limited by cooling or bubble stability. The lower *FCC* for the optimal case is a result of both its lower fixed manufacturing and utility costs per pound.

An annual resin consumption of 25 million kilograms will result in a potential net savings of $500,000. A new resin or blend may shift the resin price as compared to the base case. Therefore, from the fabricator's point of view, it is important to realize the cost performance (or conversion cost) of any new resin or blend. To substantiate this, an incremental resin selling price of $0.011 per kilogram ($0.005 per pound) for the blend over the base case resin will realize a similar cost performance. A higher price for the blend would, therefore, not be commercially acceptable. *Figures 2* and *3* show how *FCC* and productivity are related for two resin selling prices.

A different cost performance relation exists for smaller-sized equipment. If the base case is for 136 kilograms per h (300 pounds per h) and the optimized case is at 150 kilograms per h

(330 pounds per h), the respective *FCC*'s are $1.19 per kilogram ($0.541 per pound) and $1.16 per kilogram ($0.528 per pound). It is clear that the benefit of an output increase is more sensitive for smaller-sized lines. For instance, an annual resin consumption of 25 million kilograms, using smaller extruders and a resin giving a 10 percent productivity gain, will result in a potential net savings of $750,000.

GAGE REDUCTION FOR INJECTION MOLDING

Many fabricators have realized improved economics through downgaging, especially in the areas of film and molding.

To show the financial incentive for gage reduction in injection molding, a part-conversion cost (*PCC*) is calculated for two cases: a base case and an optimized case using a blend which allows for 10 percent downgaging as well as 20 percent increased flow. A combination of cost-per-unit volume and cost for a given rigidity (along with resin cost, productivity, and new mold cost), forms the basis for the *PCC*. The *PCC* is calculated as

$$PCC = \frac{APW(VMC + FMC + MMC)}{OPR} \qquad (2)$$

where

APW is average part weight in kilograms per 1,000 parts;
VMC is variable manufacturing cost in dollars per h;
FMC is fixed manufacturing cost in dollars per h;
MMC is mold modification cost in dollars per h;
OPR is output rate in kilograms per h.

A typical injection molding facility with 30 16-cavity machines and a resin usage of 6.8 million kilograms (15 million pounds) per annum or 850 kilograms per h (1,875 pounds per h based on an 8,000-h production year) is considered. The output rate for the optimized case is 20 percent greater or 1,020 kilograms per h (2,250 pounds per h). The *FMC* component is assumed to be $100 per h. The *VMC* for the base case and optimized case are $841.75 and $990.10 per h respectively (including color concentrates). This assumes a utility cost of $100 per h and a resin selling price of $0.77 per kilogram ($0.35 per pound). The average part weight is 8.63 kilograms per 1,000 parts (19.0 pounds per 1,000 parts) for the base case and only 7.77 kilograms per 1,000 parts (17.0 pounds per 1,000 parts) for the optimized case. The *MMC* for the base case is zero; however, new thin-wall molds are required for the optimal case giving an *MMC* of $52.50 per h ($70,000 mold cost per machine is amortized over five years).

The *PCC* for the base case is $9.60 per 1,000 parts and only $8.70 per 1,000 parts for the optimal case. The use of the blend has resulted in improved economics, thus, the resulting payback of new, thin-wall molds is rapid and, in many cases, is realized in less than a year.

CONCLUSIONS

The use of a blend can result in cost savings for the fabricator. The magnitude of the cost savings is specific to the equipment used, the property and/or processing enhancement that the blend offers, as well as the cost of the blend.

REFERENCES

1. J. Coufal and J. Valasek. *Int. Polym. Sci. Technol.*, 9, No. 12, (1982).
2. N. K. Datta and A. W. Birley. *Plast. Rubber Process. Applications*, Vol. 3, No. 3, (1983).
3. R. S. Hagan and J. R. Thomas. *Polym. Eng. Sci.*, 14, No. 3, (1974).
4. H. Braselmann and R. H. Nurse, *Modern Plastics*, Oct. (1983).
5. T. T. Schenck, *U. S. Pat. No. 4.438.228*, (1984).
6. P. Filzek and W. Wicke. *Modification of LDPE*, *Kunstoffe*, 73, pp. 427–431, 1983).
7. J. A. Manson and L. H. Sperling, "Polymer Blends and Composites," Plenum Press, (1976).
8. D. R. Paul and S. Newman, "Polymer Blends," Academic Press, New York, (1978).

NOMENCLATURE

APW = Average part weight.
EVA = Ethylene vinyl acetate.
FCC = Film conversion cost.
FMC = Fixed manufacturing cost.
HDPE = High-density polyethylene.
LDPE = Low-density polyethylene.
LLDPE = Linear low-density polyethylene.
MDPE = Medium-density polyethylene.
MMC = Mold modification cost.
OPR = Output rate.
PCC = Part conversion cost.
PP = Polypropylene.
PPM = Parts per million.
VMC = Variable manufacturing cost.

DISCUSSION: L. HAMIELEC

M. R. KAMAL: Could you tell me what percentages of low density polyethylene your case refers to?

L. HAMIELEC: I cannot comment on some specifics. These are actual examples from some of our customers. However, in the blown film case, the substituted material was an LLDPE/LDPE blend.

M. R. KAMAL: I am asking about percentages because we know that a number of high-pressure plants are closing down. The blending technology may have economic advantages now, but a time may come when there will not be enough LDPE to go around. Therefore, the responsibility of supply should be considered.

L. HAMIELEC: A number of commodity blends including some of those with polyethylene will be displaced by single components in the future. Therefore, I do not feel that there will be an HP-LDPE shortage for blending purposes. The material of choice for a given end use will ultimately be based on its relative value in use. There are two examples where commodity blends were displaced by a single component, on which I will comment. Firstly, some blends of EVA and HP-LDPE have been displaced by pure LLDPE. Traditionally, EVA was added to HP-LDPE for improved toughness. However, more recently, the availability of LLDPE with improved strength over HP-LDPE has eliminated both the high cost of EVA and blending costs. Secondly, some HDPE/LLDPE blends have been displaced by a higher density LLDPE. HDPE was added to LLDPE for improvements in secant moduli. At present, there are LLDPE resins which will give the same benefit.

M. R. KAMAL: So you think that a day will come when there will be no need for blending, and all the required properties will be obtained by chemistry.

L. HAMIELEC: For several commodity applications, single components will likely be used. However, blends play an important role to fill the gap in the performance of existing materials before the "single component" is available. For commodity polyethylene, the advances will be in the area of co- and ter-polymerization with various alpha olefins, as well as catalyst modifications.

L. A. UTRACKI: In our symposia, we are purposely trying to cover a broad spectrum of subjects (on a given topic, be it polymer blends, composites or processing). We start with the fundamentals, thermodynamics, rheology, then processing, morphology, and finally the economics. Ms. Hamielec was very kind to accept my invitation to come and talk to us about this last key issue for commercial blends. I thank you very much for describing so clearly the everyday reality of industrial decision-making. For the researchers, it is very difficult to decide which system to work on. The savings you indicated are fractions of a cent per pound! Since the commodity market is very volatile, these are nearly impossible differences to see. Another difficulty is that, in your examples, the optimized blends had to be designed around a certain range of molecular weights and molecular weight distribution, and all these influence the final price.

PANEL AND GENERAL DISCUSSION

A. J. BOBKOWICZ: For about a year, we have had a new Plastics Institute in Canada which functions as a technology transfer agency. We do neither research nor training. We make use of resources wherever we can find them, such as this National Research Council of Canada Industrial Materials Research Institute, universities, or other R&D organizations. From meetings such as this one, we try to assess where the technology is going to be in 20 to 30 years and we evaluate projects which come to us on the basis of whether they fit in, in terms of future needs.

At this meeting we have been discussing polymer blends. This is but one factor in the new technology. Looking at the life-cycle curves, with plastics starting about forty years ago and today becoming almost a mature industry, and with a new curve for polymer blends, composites and new plastics with a special architecture, starting just a few years ago, we are looking forward to 30 to 50 years of very exciting developments in the plastics industry. There are so many items to talk about: polymer alloys and blends, high orientation and strength, specially formed materials, solid state processing, composites, conductive plastics, permeable membranes, a whole new class of materials prepared via reactive processing and, of course, the engineering plastics. All these areas can be influenced by polymer blending.

If you look back to 50 or 80 years ago, knowing what you know now, ask yourself what should you do first! Then extrapolate to the present day and you may be better prepared for the future. Asking what we should blend first and for what purpose is a question certainly worth posing at a meeting like that.

I believe that the future of polymer science will be more in the hands of physicists, material scientists, metallurgists, and engineers than those we traditionally know as chemists. In Canada, we do not make engineering materials but quite a lot of commodity resins. The polymer blending methods offer the opportunity to make use of enhancing their properties and value. Tomorrow, Ms. Hamielec will discuss the financial gains from blending of commodity resins. This is very important contribution which should illustrate how the decisions are made on technological advancement in the user-driven polymer alloys technology. If we just look at what is needed and how to solve these problems with polymer blends, we shall be on the right track.

R. D. Hoffman: In the United States there is severe pressure on commodity plastics from foreign sources. I do not think that it is possible any longer to build world-scale plants and make a profit on them. Instead, one has to tailor products to gain a premium sales price. Certainly blends are one route that has been used in the past and will continue to be used in the future.

I am not an expert who will provide you with an overview of what is happening in the U.S. plastics industry. I will, however, try to provide you with a view from my little corner of the world. There are several major university programs being conducted in the area of polymer blends. Perhaps, the best known is at the University of Massachusetts in Amherst; another is in the University of Akron Polymer Engineering Program; and still another at the Stevens Institute of Technology where Dr. Plochocki here is involved. The National Bureau of Standards has just started a joint program with General Electric and the University of Massachussetts to work on thermodynamics of polymer blends. I find that as I talk with my colleagues around the country, that certain large industrial corporations are instituting formal polymer blend research programs.

In order to elicit discussion, I will list a few areas of special interest to me personally that I believe may be important research directions. In the area of crystalline/amorphous blends, an important example is polypropylene/rubber systems and the particular problem of importance is the influence of the amorphous phase on the extent of crystallization of the crystalline component. Work in this field was done, for example by Martuscelli and coworkers in Italy (the Italian influence on the U.S. polypropylene industry is rather marked). Martuscelli demonstrated that in the presence of a rubber phase one lowers the PP melting point, and changes the nucleation and spherulitic growth rates. Some, but not all rubbers will nucleate the PP crystallization process. While the influence on the static crystallization rate has been studied to some degree, in industry, the dynamic process is the more important aspect. We somewhat understand this in a single component melt thanks to the research of White and Spruiell at the University of Tennessee. But what happens in the presence of a second phase has not been researched. Better measurement methods of dynamic crystallization must be developed in order to solve this problem. One area which would benefit immediately is melt spinning of synthetic fibers.

In crystalline/crystalline blends (example: PP with poly(butene-1)), we must consider the mutual interaction of two different crystalline regions. Citing the work of Seigmann from Israel as a starting point, he found that PP crystals tend to nucleate crystallization of PB-1, so the temperature of crystallization is increased. On the other hand, the amorphous part of PP tends to dilute the PB-1 phase and thus to reduce the total crystallinity. However, the influence of PB-1 on PP is primarily in reducing the temperature of crystallization of that polymer. Can one get any co-crystallization? For most systems, normally not. The way to force co-crystallization is

to prepare copolymers. In the poly(propylene-co-ethylene) system, there is a certain composition range in which crystallization disappears. In the poly(propylene-co-butene-1) system, crystallization is seen over the whole composition range and it seems that some co-crystallization is achieved. Can we exploit this for the development of unique products not available otherwise?

Another subject of industrial importance is concerned with rubber toughened thermosets—a subject discussed, in part this morning by Dr. Partridge in the area of rubber-toughened epoxies.

M. PIERSON: My comments concerning the European activities in polymer alloys and blends will be short for two reasons: 1) Europe is a mosaic of different people with different objectives, 2) the dominant position in Europe is taken by American not European producers. I think that you know the American products at least as well as I, so it is not necessary for me to talk about them.

Let me ask you a few questions: are the polymeric alloys important from the point of view of fundamental research? I do not know the answer. If yes, then what will be the future benefit of this to the plastics industry? Or let us start from an opposite end, are the European companies interested in specific research on alloys? If yes, what are the main problems the companies would like to have solved?

A. J. BOBKOWICZ: In Europe, the plastics research centers belong to the "Association des Directeurs des Centres Européens des Plastiques". Work in different countries is divided along some basic lines; France concentrates on understanding molecular structure, Germany—on machinery and processing, Italy—excells in design and equipment, Holland—concentrates on product, UK—on new and improved techniques, Switzerland—on refinements in testing. In short, Europe is rather a collaborative environment.

M. PIERSON: This is a good observation. In general a European company works toward improvement of: impact, fire resistance, dimensional stability in a range of temperatures, modification (i.e., either enhancement or reduction) of permeability especially for packaging, adhesion especially in reference to co-extrusion, electrical properties (e.g. development of conductive plastics), and finally speciality polymers; piezoelectric, pyroelectric, and materials designed to perform a specific role in the end-use.

The commodity resin producers in Europe are actively working, using the physical or chemical means toward development and improvement of the following alloys and blends: (1) an old ABS/PS system, (2) PP with EPR or EPDM, (3) LLDPE, LDPE or HDPE with EVA, (4) PVC with large number of modifiers like NBR, ABS, EVA, acrylics, chlorinated polyolefins, MBS, and PEBAX (PEBAX is a family of linear block polymers of polyether and polyamide with widely adjustable properties). For PVC blends, the major applications are; window frames, tubing, pipes, bottles, and packaging.

For engineering plastics, the main emphasis is on polyamides 6, 6-6, 11, and 12. Improvement in impact and permeability is sought by blending with elastomers (olefinic or acrylic) and other thermoplastics. Work on PC/PBT and PC/PEBAX is very promising.

As far as the speciality plastics are concerned, I already mentioned EVA with ter-polymers to be used especially in the field of hot melt adhesives—a very important field of development for alloys. Another group of speciality blends is in the area of fluorinated resins, where different fluorinated materials are blended together, and in the field of aromatic polyesters, especially PBT.

D. FROELICH: To start the general discussion I would like to ask a question. Apparently a lot of work is being done to improve impact resistance. Is this really the main goal for polymer blending?

J. L. WHITE: Discussions during this meeting have been prejudicial emphasizing only the thermoplastics. There has been as much work done on elastomeric blends. Automobile tire sidewall is a blend, the tread is a blend, the carcass is a blend, the liner is a blend and each of these is different, designed for a specific function. When you talk about rubber/plastic blends the perspective taken during this symposium was that plastic is the major constituent and the role of a rubber is to improve impact resistance. Often the same ingredients are used in plastic and elastomeric blends. PP with EPR is a high impact PP, but EPR with PP is a blend, with vulcanization taking place in a mixer, leading to a blend of thermoplastic and traditional elastomer with diverse applications. Blending also finds use in fiber spinning, where for example, addition of PEO changes wetting and static electricity characteristics. Certainly, blending is a way of the future. Currently there is an increasing drift toward high technology. We talked about blends suitable for automotive applications; here is a large market for polycarbonate blends. There is however a new class of polymers, also aromatic polycondensates, which are being designed for the aerospace industry. Materials such as PEEK's or with a similar structure are being blended. They will constitute a large research subject in the future.

A. J. BOBKOWICZ: The impact properties are very important, but there are other methods of achieving toughness than admixing rubber. In-

terpenetrating networks, created *in situ* layered structures, directional orientation, these are more advanced methods for toughening for the future.

L. A. UTRACKI: Today, we are very fortunate to have among us representatives of seven advanced countries of Europe and North America. We cannot discuss either all possible future technologies or all possible fields of blend application. I do not think that we have enough time, or expertise, to cover such a vast territory. However, could we please achieve some consensus regarding the future of polymer blend technology in thermoplastics? Dr. Bobkowicz, who sits on the panel representing the Canadian point of view, gives the impression that blending is not too important a technology for the Canadian plastics industry. This may or may not be true but could we clarify this point, please? A year ago, in a panel discussion such as this one today, Dr. Alim from Esso Canada expressed the opinion that in the polyethylene industry, mechanical blending to modify properties would be achieved directly in reactors by virtue of catalysts, comonomers or process adjustments. A year later, we know that some elements of this oracle are becoming a reality: in Canada there is a growing tendency to replacement of LLDPE/LDPE blends in several applications by newer hexene-based LLDPE's, in France a free-radical crosslinking of LLDPE during processing provides very advanced blend-like behavior. If this tendency continues, it seems that polyblends should be considered as a first step, a learning-stage in development of advanced materials. In short, maybe the nonvocalized opinion of Dr. Bobkowicz, regarding the lack of interest in Canadian industry (related primarily to commodity resins), is indeed based on solid economic evaluation. Can we have some clear ideas from the panelists please? The second and distinctly different question I would like to ask is what will the future of engineering polymer blends be on this and the European continent, say 10 years from now?

R. D. HOFFMAN: I could not agree more with Dr. Utracki that in the polyolefins industry there has been a trend for several years now to do blending in the reactor that is the trend in the PP industry. This obviously is a much cheaper way, if you can do it. Any time you can do your blending in the reactor and eliminate the costs of extrusion blending, the savings are obvious. But there are some morphologies, some properties (especially in semicrystalline materials) which cannot be achieved by the reactor blend technology and mechanical blending will still have its place.

M. PIERSON: I think that in commodity plastics the main reason is to lower the cost. If you do the market analysis you will soon find out if it is more economical to compound the blends outside the reactor or to keep adjusting the chemical reaction variables. I am not certain that the today verdict is out. Taking ABS as an example, in the beginning ABS was obtained by blending. Now ABS is manufactured by polymerization with phase inversion. However, the number of grades required of PE is so much larger that I am not certain if one can make a sweeping statement.

As far as the engineering resins are concerned, the reason is not so much the price as some very specific properties. These can be obtained by blending or by new types of resins. Most important is the performance of the final product. The fastest growing market is for those speciality products with a volume of 1 kt or so. I believe that the techno-economical approach and the future of commodity and engineering resins are vastly different.

A. J. BOBKOWICZ: We do not make engineering resins in Canada because of a small internal market. Blending, however, is growing very well, thank you. I think that, for us, blending technology is *very* important. There is also a new area of reaction processing toward designing in some specific properties in short runs. Here blending, reacting,and forming are taking place at the same time.

J. BLEY: Mr. Pierson, you said that in Europe the US resins are used as a standard. I disagree with you there. I am familiar with your nylons and other products you have been selling. I believe that it is not that American resin is better but rather the marketing strategy is. In Europe, resin is perfected before it sees the market. You know almost everything about the material at the moment it goes to a customer. In America, the product is brought to the market very quickly. *The follow up is important.* The performance and the applications are observed very closely and from that information the next generation of products is being produced.

D. FROELICH: I am working at a university and I would be interest to know what industry considers as an important area of work in polymer blends.

A. J. BOBKOWICZ: In the Canadian Plastics Institute we are working with as many universities and institutes as we can. Just last week a company came asking for material with a very specific requirement. Material of this type does not exist but we think that it is possible to use a specific development in one university to make it work. It is a blending technology and molecular manipulation. Tomorrow, we will have a meeting and hopefully the company will start funding a very specific advancement of a

university project which may lead to formation of a small company.

J. L. WHITE: One can refer to countries, how they can be more productive using polymer blends. But another perspective is a possibility of a small company. One could set up a company with minimal investment, say a twin-screw extruder. If you have a basic knowledge of materials you could develop your own blend systems and go into competition with larger organizations which have much higher overhead. There are many compounders which are doing that, making thermoplastic elastomers, resins of various sorts with sales of 100 million dollars a year or even less.

L. A. UTRACKI: Are you advising universities to stay away from research on commodity blends and direct their efforts toward high performance or speciality materials?

R. D. HOFFMAN: In the present economic climate, it is difficult for companies to put dollars into universities and then wait years for useable results. They would prefer to do the job inhouse. But if a university will *stake out* a research area and develop a minimal level of funding, it will eventually attract interested buyers. With the short-term outlook of much of the U.S. private sector, industrial management is not interested in funding basic research at the universities, even if it may be needed a few years down the road. This is unfortunate, since we all recognize that the university community needs stronger support, and a commitment for support from industry.

M. PIERSON: I agree with those reflections. I would like to indicate one particular area of research in polymer blend rheology and mixing; how to stabilize, or how to generate precise morphology during preparation of various blends. Rheological properties, description of mixing processes, and prediction of morphology are of utmost importance even in polyolefin blends.

L. A. UTRACKI: If you had to guess where the industrial polymer blends will be ten years from now, what would be your prediction?

A. J. BOBKOWICZ: There will be more blends, not less. There will be blends modified with fillers, foamed, thin-wall sections, speciality blends, high temperature blends containing liquid crystals, self-reinforcing blends. I believe that the future is in the polymer blend area. Definitely.

R. D. HOFFMAN: True. The key will be to develop better, less expensive blending methods, though.

M. PIERSON: I agree. I would bet on three systems: 1) mesophase liquid crystal reinforced system; 2) alloying via reaction injection molding, especially leading to IPN-type of structures; 3) technology of blending, leading to very low film permeability for packaging.

D. FROELICH: If RIM or IPN's are mentioned, that means that the domain of blending must involve both physicists and chemists.

M. PIERSON: For me, RIM is primarily an engineering problem. Chemistry is in second place. There are already materials on the market with five seconds reaction time at ambient temperature.

SI METRIC UNITS

The following list shows the names, symbols, and equivalence of the more common quantities allowed in the SI metric system. The prefixes and symbols for the more common multiple units are also shown. Neither list is complete. Full details are given by F. S. Conant, Polym. Eng. Sci., **17,** 222 (1977). A table of the more frequently needed conversion factors required to use the SI system is also shown. This journal prefers that SI metric units be employed in manuscripts submitted for publication.

Units and Symbols

Quantity	Name	Symbol	Equivalent to:
Length	metre	m	—
Time	second	s	—
	minute	min	—
	hour	h	—
Mass	kilogram	kg	—
Electric current	ampere	A	—
Plane angle	radian	rad	—
Capacity	litre	L	$10^{-3}m^3$
Frequency	hertz	Hz	s^{-1}
Force	newton	N	$m \cdot kg \cdot s^{-2}$
Pressure, Stress	pascal	Pa	$N \cdot m^{-2}$
Energy, Work, Heat	joule	J	$N \cdot m$
Power	watt	W	$J \cdot s^{-1}$
Viscosity, dynamic	pascal second	Pa·s	$N \cdot s \cdot m^{-2}$

(The following units should ***not*** be used: micron, angstrom, dyne, erg, calorie, poise, or stoke.)

Multiple Units

Prefix	Symbol	Equivalent to:
giga	G	10^9
mega	M	10^6
kilo	k	10^3
deci	d	10^{-1}
centi	c	10^{-2}
milli	m	10^{-3}
micro	μ	10^{-6}
nano	n	10^{-9}

Conversion Factors

Force: $1N = 10^5$ dynes $= 1.02 \times 10^{-1}$ kgf $= 2.248 \times 10^{-1}$ lbf.
Pressure, Stress: 1 Pa = 10 dyne $cm^{-2} = 7.5 \times 10^{-3}$ mm Hg $= 10^{-5}$ bar $= 1.02 \times 10^{-5}$ kg $cm^{-2} = 1.45 \times 10^{-4}$ psi.
Energy: 1 J $= 2.387 \times 10^{-1}$ cal.
Viscosity: 1 Pa·s = 10 poise.

INFORMATION FOR AUTHORS

Submission of original and review articles is encouraged. There is no limit on length. Three copies of the manuscript should be submitted, which should be typed, one side only, double space, with at least a 1-inch margin. Submission will be taken to imply that the paper has not been previously published, that it is not being considered elsewhere for publication, and that if accepted it will not be published elsewhere in the same form, in any language, without the consent of the editor or publisher. Authors must agree to transfer copyright to the publisher when an article is accepted for publication. Unless notified to the contrary by the authors, the publisher assumes that the act of submitting the article signifies the authors' agreement to such copyright transfer to the publisher. The journal carries a voluntary page charge. Each manuscript should include:

A separate title page, headed by a concise, meaningful title (avoid abbreviations) for the paper. This page should provide:

- The name and affiliations of each contributing author at the time the paper was prepared.
- Indicate by asterisk any changes of address for each author since article preparation.
- Acknowledgment of any prior oral presentation and original source of the material.

A separate abstract page, consisting of a single paragraph of 100–200 words to include the title and the names and addresses of the authors. Define any abbreviations for substances or methods (such as ABS, SAXS, etc.).

A list of references, on a separate page at the end of the text, numbered in order of text citation. The references are to be abbreviated in the form used in Chemical Abstracts using the names of all authors preceded by initials; see Bibliographic Guide for Editors and Authors, American Chemical Society, Washington, D.C.

- Within the text, the reference citations are typed in parentheses in line with the main copy (no superscripts or subscripts), thus:

  According to Young, et al. (1)...

- In the list of references the general style is as follows:

For periodicals:

1. S. S. Young, J. L. White, E. S. Clark and Y. Oyanogi, *Polym. Eng. Sci.*, 20, 798 (1980).

The journal name and volume are to be underlined and the year is placed in brackets. The issue number is given only when needed for identification. The article name is eliminated unless the reference is unclear without it.

For books: The title to be spelled out in full.

5. H.-G. Elias, "Macromolecules," Ch. 1, Vol. 2, Plenum Press, New York (1977). (Include the state when the city is not identifiable.)

A list of nomenclature, identifying symbols and abbreviations, commonly desirable at the end of the text. Footnotes are to be avoided.

Equations, numbered and typed in the appropriate place in the text. Where symbols cannot be typed, write them neatly in ink.

Tables, each typed on a separate page, with a heading, and numbered with arabic numerals that correspond to the order in which they are cited in the text. The tables should be inserted in the manuscript after the references and before the figures.

Figures, assembled at the end of the manuscript and preceded by a typed list of captions that explain them. Please also supply a set of original figures or sharp glossy photos thereof, on 8½ × 11 paper or attached to sheets of this size, one sheet for each figure. Each should be identified on the front edge or on the back (photographs) with the name of the first author and the figure number (e.g., Smith, Fig. 1). Originals are to be prepared with high contrast India ink and to bear uniformly stencilled notations. Line drawings and photos should be of a quality suitable for good photographic reproduction and retained legibility upon size reduction to one quarter. Manuscript transmittal letter should indicate if the figures need be returned.

Send manuscripts to:
Roger S. Porter, Editor
POLYMER ENGINEERING AND SCIENCE
% Polymer Science & Engineering
University of Massachusetts
Amherst, Massachusetts 01003

For information concerning publication dates, page charges and reprint orders contact:
Editorial Dept.
Society of Plastics Engineers
14 Fairfield Drive
Brookfield Center, Connecticut 06805

continued from front cover

63

E. BUTTA, G. LEVITA, A. MARCHETTI, and A. LAZZERI/Morphology and Mechanical Properties of ATBN/Epoxy Blends

74

S.Y. HOBBS/The Effect of Rubber Particle Size on the Impact Properties of High Impact Polystyrene (HIPS) Blends

82

A.P. PLOCHOCKI/Effect of Rheological Parameters on Phase Morphology of Polyblends: A Route to Computer Aided Design and Developments of Industrial Polyblends

92

P.G. LAFLEUR and M.R. KAMAL/A Structure-Oriented Computer Simulation of the Injection Molding of Viscoelastic Crystalline Polymers. Part I: Model With Fountain Flow, Packing, Solidification

103

M.R. KAMAL and P.G. LAFLEUR/A Structure-Oriented Computer Simulation of the Injection Molding of Viscoelastic Crystalline Polymers. Part II: Model Predictions and Experimental Results

111

L.A. HAMIELEC/Financial Incentive of Linear Low Density Polyethylene Blends

116

L.A. UTRACKI/Panel and General Discussion on the Future of Industrial Polymer Blends

Society of Plastics Engineers
14 Fairfield Drive
Brookfield Center, CT 06805